

Winter 2006

# Characterization of the spatial and temporal variability in pan-Arctic, terrestrial hydrology

Michael A. Rawlins

*University of New Hampshire, Durham*

Follow this and additional works at: <https://scholars.unh.edu/dissertation>

---

## Recommended Citation

Rawlins, Michael A., "Characterization of the spatial and temporal variability in pan-Arctic, terrestrial hydrology" (2006). *Doctoral Dissertations*. 358.

<https://scholars.unh.edu/dissertation/358>

This Dissertation is brought to you for free and open access by the Student Scholarship at University of New Hampshire Scholars' Repository. It has been accepted for inclusion in Doctoral Dissertations by an authorized administrator of University of New Hampshire Scholars' Repository. For more information, please contact [nicole.hentz@unh.edu](mailto:nicole.hentz@unh.edu).

**CHARACTERIZATION OF THE SPATIAL AND  
TEMPORAL VARIABILITY IN PAN-ARCTIC,  
TERRESTRIAL HYDROLOGY**

BY

Michael A. Rawlins

Bachelor of Science, University of Delaware, 1996

Master of Science, University of Delaware, 2001

DISSERTATION

Submitted to the University of New Hampshire  
in partial fulfillment of  
the requirements for the degree of

Doctor of Philosophy

in

Earth and Environmental Science

December 2006

UMI Number: 3241649

### INFORMATION TO USERS

The quality of this reproduction is dependent upon the quality of the copy submitted. Broken or indistinct print, colored or poor quality illustrations and photographs, print bleed-through, substandard margins, and improper alignment can adversely affect reproduction.

In the unlikely event that the author did not send a complete manuscript and there are missing pages, these will be noted. Also, if unauthorized copyright material had to be removed, a note will indicate the deletion.

**UMI**<sup>®</sup>

---

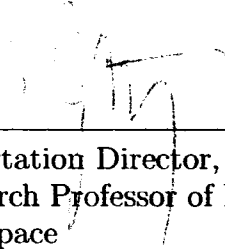
UMI Microform 3241649

Copyright 2007 by ProQuest Information and Learning Company.

All rights reserved. This microform edition is protected against unauthorized copying under Title 17, United States Code.

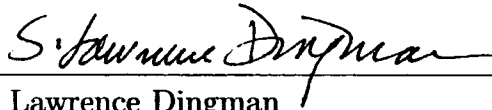
ProQuest Information and Learning Company  
300 North Zeeb Road  
P.O. Box 1346  
Ann Arbor, MI 48106-1346

This dissertation has been examined and approved.



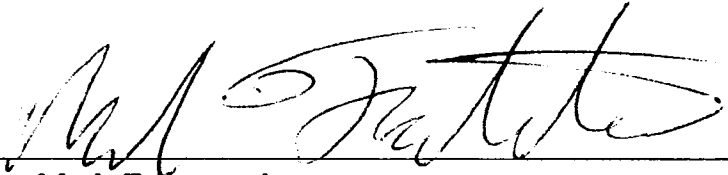
---

Dissertation Director, Dr. Charles J. Vörösmarty  
Research Professor of Earth Sciences and Earth, Oceans,  
and Space



---

Dr. S. Lawrence Dingman  
Professor Emeritus of Hydrology and Water Resources



---

Dr. Mark Fahnestock  
Research Associate Professor of Earth, Oceans, and  
Space



---

Dr. Steve Froking  
Research Associate Professor of Earth Sciences and  
Earth, Oceans, and Space



---

Dr. Ernst Linder  
Professor of Mathematics

29 November 2006

Date

## ACKNOWLEDGEMENTS

I would like to acknowledge and thank Charlie Vörösmarty for encouraging and advising me over the past several years. Dr. Vörösmarty always suggested that I think broadly, and he challenged me and to pursue interesting and exciting research. I have benefited tremendously as a result of our work together and for that I am thankful.

I thank members of the Water Systems Analysis Group including Richard Lammers, Báalazs Fekete, Alexander Shiklomanov, and Wil Wollheim. Stanley Glidden and Alexander Prusevich are thanked for their technical assistance, and Darlene Dube has been helpful in too many ways to mention here. I also thank Cort Willmott, Mark Serreze, and Kyle McDonald for the fruitful collaborations and discussions we have had over the past several years. I thank committee members Larry Dingman, Mark Fahnestock, Steve Froking, and Ernst Linder for their assistance with my dissertation studies.

This research was supported under NSF grants OPP-0094532, OPP-0230243, OPP-9818199, and OPP-9910264; NASA grants NAG5-9617, NAG5-6137, NAG5-11256, and NAG5-11750; and the ARCUS Program.

Lastly, I would like to thank my family for their love and support. A special word of thanks is reserved for my mother for encouraging me to attend college when I seemed reluctant.

# TABLE OF CONTENTS

ACKNOWLEDGEMENTS .....	iii
LIST OF TABLES .....	viii
LIST OF FIGURES .....	ix
ABSTRACT .....	xii
<b>INTRODUCTION</b>	<b>1</b>
<b>1 SIMULATING PAN-ARCTIC RUNOFF WITH A MACRO-SCALE TERRESTRIAL WATER BALANCE MODEL</b>	<b>8</b>
1.1 Hydrological Modeling .....	8
1.2 The Pan-Arctic Water Balance Model .....	11
1.3 Model Results .....	15
1.3.1 Active-layer Modeling .....	15
1.3.2 Pan-Arctic Runoff .....	18
1.4 Sensitivity Analysis .....	24
1.5 Summary and Discussion of Results .....	28

<b>2</b>	<b>REMOTE SENSING OF SNOW THAW AT THE PAN-ARCTIC SCALE USING THE SEAWINDS SCATTEROMETER</b>	<b>31</b>
2.1	Remote Sensing of Snow .....	31
2.2	Data Sources and Methods .....	36
2.2.1	Radar Backscatter .....	38
2.2.2	Hydrological Data.....	41
2.2.3	Land Surface Data .....	43
2.3	Comparison of SeaWinds-Derived Thaw Timing and Hydrological Response .....	44
2.4	Comparison of Snow Thaw Timing across the Pan-Arctic Domain .....	49
2.5	Discussion of Results .....	57
<b>3</b>	<b>EVALUATION OF TRENDS IN DERIVED SNOWFALL AND RAIN- FALL ACROSS EURASIA</b>	<b>60</b>
3.1	Changes in the Arctic Hydrological Cycle.....	60
3.2	Data and Methods .....	61
3.3	Linkages between Precipitation and Discharge.....	63
3.4	Summary of Results .....	70

<b>4</b>	<b>EFFECTS OF UNCERTAINTY IN CLIMATE INPUTS ON SIMULATED EVAPOTRANSPIRATION AND RUNOFF IN THE WESTERN ARC- TIC</b>	<b>71</b>
4.1	Introduction .....	71
4.2	Methods .....	73
4.2.1	Overview .....	73
4.2.2	Model Description .....	73
4.2.3	Input Datasets .....	74
4.2.4	Model Application and Analysis .....	78
4.3	Results .....	81
4.3.1	Simulated Evapotranspiration .....	81
4.3.2	Simulated Runoff .....	82
4.4	Discussion .....	86
4.5	Conclusions .....	90
<b>5</b>	<b>ON THE EVALUATION OF SNOW WATER EQUIVALENT ESTIMATES OVER THE TERRESTRIAL ARCTIC DRAINAGE BASIN</b>	<b>91</b>
5.1	Introduction .....	91
5.2	Data and Methods .....	93



5.3 Results.....	97
5.4 Conclusions.....	105
<b>SUMMARY</b>	<b>107</b>
<b>BIBLIOGRAPHY</b>	<b>114</b>
<b>APPENDICES</b>	<b>138</b>
<b>APPENDIX A PWBM</b>	<b>139</b>
A.1 Snow Dynamics .....	139
A.2 Soil Submodel .....	141
<b>APPENDIX B PET FUNCTIONS</b>	<b>146</b>
<b>APPENDIX C SOURCE CODE</b>	<b>148</b>

## LIST OF TABLES

1.1	Simulated long-term annual runoff . . . . .	21
3.1	Trends in annual precipitation, annual snowfall, and annual rainfall . . . . .	66
4.1	Climate data sets used in PWBM simulations . . . . .	76
4.2	Long-term mean simulated ET, runoff, and climate across the WALE domain . . . . .	76
4.3	Observed June–August ET at 2 sites in Alaska and simulated June–August ET . . . . .	78
4.4	Mean absolute difference (MAD) in simulated annual runoff as compared to observed runoff . . . . .	87
5.1	Mean February–March SWE, percent negative correlations, and minimum, maximum, and mean coefficient of determination . . . . .	102
A.1	PWBM soil texture classes and model parameters . . . . .	143

## LIST OF FIGURES

1-1	Pan-Arctic domain by sea basin boundaries . . . . .	13
1-2	Schematic of the PWBM soil zones and water fluxes in Winter/Spring and Summer . . . . .	14
1-3	Simulated active layer thickness . . . . .	16
1-4	PWBM long-term monthly runoff climatology, 1980–2001 . . . . .	19
1-5	PWBM simulated annual, long-term mean runoff for years 1980–2001 . . . . .	20
1-6	Distribution of simulated and observed annual (long-term) runoff . . . . .	23
1-7	Long-term seasonal runoff for Arctic sea basins . . . . .	24
1-8	Sensitivity of simulated annual runoff . . . . .	27
2-1	Moderate Resolution Imaging Spectroradiometer (MODIS)-derived vegetation cover . . . . .	37
2-2	Behavior of Ku-band radar backscatter with increasing snow wetness . . . . .	39
2-3	Observed basin-average runoff, model snow water content, and daily SeaWinds backscatter . . . . .	45
2-4	Comparison of hydrological event dates . . . . .	48

2-5	Primary thaw date ( $t_P$ ) for year 2000 derived from the SeaWinds backscatter .....	50
2-6	Snow water initiation date ( $t_M$ ) for year 2000 derived from the pan-Arctic Water Balance Model .....	51
2-7	Difference between PWBM snow water initiation date ( $t_M$ ) and scatterometer derived primary thaw date ( $t_P$ ) .....	52
2-8	Observed basin-average runoff, model snow water content, and daily SeaWinds backscatter for the Hanbury basin .....	53
2-9	Cumulative area histograms for $t_M - t_P$ discrepancies .....	55
2-10	Average signal to noise value ( $R$ ) grouped by percent tree cover and total 1999–2000 winter snowfall .....	56
3-1	Five-year running means of spatially averaged river discharge .....	64
3-2	Spatially averaged water equivalent of annual rainfall and snowfall .....	65
3-3	Trends in derived annual snowfall (a) and in derived annual rainfall (b), 1936–1999 .....	67
3-4	Annual total $P$ for 1972 .....	68
4-1	Annual total precipitation (upper panel) and air temperature (lower panel) across the WALE domain .....	77
4-2	Daily average relative humidity for July 2000 .....	80

4-3	PWBM simulated annual ET across the WALE domain .....	83
4-4	Simulated annual runoff across the WALE domain .....	85
4-5	Long-term mean monthly runoff across the Yukon basin .....	86
4-6	Observed and simulated annual runoff across the Yukon basin .....	87
5-1	Locations of stations used in study .....	95
5-2	Monthly total SWE and mean discharge ( $Q$ ) across the Yukon basin .....	98
5-3	Explained variance ( $R^2$ ) for pre-melt SWE and spring $Q$ comparisons .....	100
5-4	$R^2$ for PWBM simulated spring total $Q$ vs. observed spring total $Q$ .....	104

# ABSTRACT

## CHARACTERIZATION OF THE SPATIAL AND TEMPORAL VARIABILITY IN PAN-ARCTIC, TERRESTRIAL HYDROLOGY

by

Michael A. Rawlins  
University of New Hampshire, December, 2006

Arctic hydrology represents an important component of the larger global climate system, and there are signs that significant water-cycle changes, involving complex feedbacks, have occurred. This dissertation explores the methods to estimate components of the arctic hydrological cycle, the numerous biases and uncertainties associated with the techniques, and suggestions for future research needs. The studies described here focus on quantitative models and methods for predicting the spatial and temporal variability in pan-Arctic hydrology.

This dissertation discusses pan-Arctic water budgets drawn from a hydrological model which is appropriate for applications across the terrestrial Arctic. Including effects from soil-water phase changes results in increases in simulated annual runoff of 7% to 27%. A sensitivity analysis reveals that simulated runoff is far more sensitive to the time-varying climate drivers than to parameterization of the landscape. When appropriate climate data are used, the Pan-Arctic Water Balance Model (PWBM) is able to capture well the variability in seasonal river discharge at the scale of arctic sea basins.

This dissertation also demonstrated a method to estimate snowpack thaw timing from radar data. Discrepancies between thaw timing inferred from the microwave backscatter data and the hydrological model are less than one week. The backscatter signal-to-noise values are highest in areas of higher seasonal snow accumulation, low to moderate tree cover and low topographic complexity. An evaluation of snow water equivalent (SWE) estimates drawn from land surface models and microwave remote sensing data suggests that simulated SWE from a hydrological model like PWBM, when forced with appropriate climate data, is far superior to current snow mass estimate derived from passive microwave data.

Biases arising from interpolations from sparse, uneven networks can be significant. A bias of well over  $+10 \text{ mm yr}^{-1}$  was found in the early network representations of spatial precipitation across Eurasia. When examining linkages between precipitation and river discharge, these biases limit our confidence in the accuracy of historical precipitation reconstructions. This dissertation assess our current capabilities in estimating components of arctic water cycle and reducing the uncertainties in predictions of arctic climate change.

## INTRODUCTION

The terrestrial Arctic is vast and remote region which has experienced unprecedented change. The arctic water cycle is an integral component of the larger, global energy and water cycles, and alterations in the arctic system can feedback or impact global climate in ways which are not fully understood. Although the Arctic Ocean contains only 1% of the world ocean water, it receives 11% of the world runoff (Shiklomanov et al., 2000). It also has the largest contributing basin area, relative to the ocean surface area, of any of the world's oceans. Yet, despite its prominent role in the global climate system, observations of key hydrological quantities across the terrestrial arctic drainage basin have recently declined. Between 1986 and 1999, the area monitored has declined approximately 7%, from 74% to 67% of the pan-Arctic (Shiklomanov et al., 2002). This loss of information—vitally important for modeling calibration and validation efforts—seriously compromise our ability to understanding the pan-Arctic system at this critical time.

More than a century ago, scientists speculated that combustion of fossil fuels will increase the level of CO<sub>2</sub> in the atmosphere. Over the past century, mean global, surface air temperature has increased by about 0.6°C (Houghton et al., 2001). Model projections suggest an increase in global temperature, relative to 1990, of about 2°C by 2100. General circulation models (GCMs) generally agree that warming will be most pronounced across northern high latitudes during winter. Observations since 1960 confirm that warming in the Arctic has been strongest in winter and spring, amounting to as much as 2°C decade<sup>-1</sup>



for areas of greatest warming. Although the most recent warming may be attributable to multiple causes, paleoclimatic reconstructions indicate that the Arctic was warmer during the 20<sup>th</sup> century than at any time since 1600 (Overpeck et al., 1997).

Although polar amplification of global warming is a well known feature, of potentially greater importance are hydrologic changes that are likely to accompany a warmed Arctic. Recent assessments of 20<sup>th</sup>-century precipitation (Houghton et al., 1996) show that precipitation has increased by a greater percentage in the Arctic (65°N–85°N) than in any other latitudinal zone on the globe. The Arctic has become wetter as well as a warmer, suggesting an acceleration of the hydrologic cycle. Annual river discharge across the 6 largest Eurasian river basins has increased by 7% from 1936 to 1999 (Peterson et al., 2002), and there are indications that river discharge is occurring earlier in the spring in many arctic rivers (Lammers et al., 2001).

Climate change has the potential to affect arctic hydrology further through complex linkages and feedbacks. Warming air temperature has been implicated in the record sea ice minimums of the past several years. The significant downward trend of 8% decade<sup>-1</sup> since the late 1970s has led to a reduction of approximately 20% in sea ice extent in September, when the annual minimum occurs (Manabe et al., 2005). Thawing of ice-rich permafrost—a consequence of increasing air and soil temperatures—may lead to significant increases in river discharge. Simulations with the Community Land Model (CLM3) show an increase in discharge of 28% by 2100, mostly due to increases in precipitation that exceed increases in evaporation (Lawrence and Slater, 2005). Approximately 15% of the increase, however, is attributed to contributions from thawing permafrost. These increases in river discharge

may lead to a freshening of the Arctic Ocean, reduction of the North Atlantic Deep Water formation, and a slowing of the Atlantic thermohaline circulation (Broecker, 1997).

Current climate models are unable to capture sufficiently the spatial and temporal dynamics in pan-Arctic hydrology (Waliser et al., 2005). Most state-of-the-art climate models significantly overestimate the snow mass across the Northern Hemisphere, particularly in spring (Roesch, 2006). Regional climate models (RCMs) or offline land-surface models (LSMs) run at higher spatial scales may offer improvements over GCMs. However, since they are usually driven by a GCM, water balances predicted by RCMs and LSMs may not be much better. On the other hand, hydrological models—data-rich and suitably physically based—currently offer the best tools for estimating arctic water budgets at small to medium scales. Although simple bucket models (Robock et al., 1995) have performed comparably to complex biosphere models, the equations used are often empirical, which limits their use in simulations involving future climate scenarios. The desire to implement physically-based algorithms is challenged by the lack of input data required to parameterize the relevant model equations. Moreover, hydrological models and LSMs are more sensitive to climate-driven perturbations than to the chosen biotic surface parameters (Beringer et al., 2002; Federer et al., 2003). Understanding the degree of complexity in model structure necessary to obtain reasonable water budget predictions is central to our goal of developing a predictive capability in arctic change studies.

Across the terrestrial Arctic, *in situ* snow depth observations are biased toward populated areas and lower elevations, and gauge undercatch can be severe (Groisman et al., 1991; Yang et al., 2005). Remote sensing techniques offer the potential to overcome many of the challenges in direct monitoring across remote arctic lands. Evapotranspiration has been

estimated using the Moderate Resolution Imaging Spectroradiometer (MODIS) instrument (Nishida et al., 2003). Low spatial resolution, high temporal revisit microwave radiometers and scatterometers are well-suited for quantifying the timing of landscape freeze/thaw state (Kimball et al., 2001; McDonald et al., 2004).

Among all hydrological quantities, estimation of snow mass currently has the best potential from a remote-sensing perspective. A critical component of the arctic hydrological cycle, seasonal snow cover stores large amounts of energy and provides the principle source of freshwater in many arctic communities (White et al., 2004). Snow cover is involved in many feedbacks (Randall, 1994), the most critical being the surface albedo feedback (Hall, 2004). Remote sensing of snow mass at microwave wavelengths can be achieved without the limitations of optical-infrared sensors such as MODIS. Passive microwave sensors such as the Special Sensor Microwave Imager (SSM/I) have proven particularly useful for retrieving information on snowpack water storage (Armstrong and Brodzik, 2001; Derksen et al., 2003). Snowpack thaw timing can be inferred from passive radiometers and from active instruments (eg., SeaWinds on NASA QuikScat). Uncertainties in snow water equivalent (SWE) and snow thaw timing estimates arise due to the integration of many different terrain and land cover features into a single grid-cell brightness temperature value. These sub-pixel-scale features include grain size variability, high-density snow layers or ice lenses, and a significant lake cover fraction (Rees et al., 2006). Filling the gap in snow observations with remotely sensed data is dependent on a better understanding of regional biases due to landcover effects.

The primary objective of this study is to evaluate our current ability to characterize the arctic terrestrial hydrological cycle. The following research objectives help achieve this goal:

- To modify an existing hydrological model for application to the pan-Arctic basin
- To estimate the timing in landscape thaw from remote sensing data
- To understand the driving mechanisms behind observed hydrological changes

By assembling the requisite input data, a hydrological model, and remote sensing fields, the main objectives of this study can be addressed through a series of specific research questions:

1. What is the spatial and temporal distribution of runoff across the pan-Arctic drainage basin
2. What is the effect of incorporating soil freeze/thaw processes in a hydrological model?  
Are the effects on simulated runoff due to climate driver data more important than differences due to specification of landscape properties?
3. How do uncertainties and errors in model forcing data affect simulated water budgets?
4. Can remote sensing provide information about landscape thaw timing sufficient to improve hydrological forecast and biogeochemical modeling of the Arctic? What are the primary influences on thaw timing estimates across the pan-Arctic basin?

5. Have changes in precipitation played a prominent role in the observed discharge trends across Eurasia? How does the sparse observing network impact our ability to monitor the region?
6. Are current SWE estimates derived from passive microwave observations able to capture the spatial and temporal variability in pan-Arctic SWE? Are SWE estimates derived from a suitable hydrological model superior at this time?

This dissertation is organized into five chapters. The first chapter describes the development, coding, and testing of a version of the Water Balance Model (WBM, Vörösmarty et al., 1996) suitable for simulations across the pan-Arctic drainage basin. Details of a new soil moisture phase-change submodel—added to more accurately represent the daily changes to soil liquid and solid water fractions—are also presented. Results of a sensitivity experiment illustrate the most important model components for simulating the arctic water cycle. A version of this chapter was published in the journal *Hydrological Processes* (Rawlins et al., 2003) in 2003.

The second chapter presents an evaluation pan-Arctic snow thaw timing estimates which are derived from the SeaWinds instrument. Timing of thaw inferred from SeaWinds backscatter is compared with observed river discharge and runoff from the hydrological model described in Chapter 1. An examination of landscape factors which influence the backscatter signal provides information on the applicability of this instrument for monitoring the timing of landscape thaw at the pan-Arctic scale. This study was published in the *Journal of Hydrology* (Rawlins et al., 2004) in 2005.

The third chapter examines the role of precipitation in the observed discharge trends across Eurasia. Several recent studies (Ye et al., 1998; Frey and Smith, 2003; McClelland et al., 2004) suggest that increased precipitation is the most plausible source for the discharge anomaly. In this study, trends in both annual snowfall and rainfall—derived from common precipitation data sets—is examined and compared with the discharge trends. The effect of changing station networks on trends drawn from common gridded data sets is also explored. A version of this study was published in *Geophysical Research Letters* (Rawlins et al., 2006) in 2006.

The fourth chapter describes how several configurations of climate driver and potential evapotranspiration function affect simulated water budgets. This study also examines several biases in common climate data sets and how these uncertainties propagate through the simulated water budgets. Identifying these biases is important given known problems in commonly-used, large-scale precipitation data sets. Results from this study were published in the journal *Earth Interactions* (Rawlins et al., 2005) in 2006.

The fifth chapter presents a method for evaluating SWE data through the use of monthly river discharge data. Comparisons of agreements between river discharge and snow mass drawn from (i) the hydrological model described in Chapter 1, (ii) another land surface model, and (iii) SSM/I data are presented. The study also explores the linkages between precipitation input to the landscape and the freshwater flux through the basin. A journal article submitted to a special issue of *Hydrological Processes* (Rawlins et al., 2005) focusing on work presented at the 63<sup>rd</sup> Eastern Snow Conference has been accepted for publication.

# CHAPTER 1

## SIMULATING PAN-ARCTIC RUNOFF WITH A MACRO-SCALE TERRESTRIAL WATER BALANCE MODEL

### 1.1 Hydrological Modeling

Global-change scenarios have predicted significant positive increases in surface air temperature, with the greatest increases expected to occur in the Arctic (Manabe et al., 1991; Nicholls et al., 1996). Although much speculation surrounds the causes, feedbacks, and uncertainty in Arctic environmental change, a large body of evidence suggests that major changes have already occurred (Serreze et al., 2000; Vörösmarty et al., 2001). Increases in surface air temperature over the next several decades may lead to significant changes in permafrost active-layer thickness (Anisimov et al., 1997). Thawing of permafrost-rich soils can dramatically alter landscape patterns, with a potential to release water and carbon stored in soils (Hinzman and Kane, 1992; Waelbroeck et al., 1997). Given the linkages between Arctic hydrology and numerous geophysical systems over a wide range of scales, along with recent evidence of significant change (Chapman and Walsh, 1993; Groisman et al., 1994; Oechel et al., 1993; SEARCH SCC, 2001), the mechanisms underlying major hydrological processes across the Pan-Arctic deserve considerable attention. Large variations in river-

ine exports to the Arctic Ocean have the potential to alter global ocean and atmospheric circulations (Broecker, 1997; Schiller et al., 1997) as well as oceanic net carbon storage (Anderson et al., 1998). Major changes in runoff and freshwater export can also affect the biogeochemistry of Arctic aquatic ecosystems (Holmes et al., 2000; Wolheim et al., 2001). And although it contains only 1 % of the world ocean water, the Arctic Ocean receives 11 % of the global river runoff (Shiklomanov, 1998).

Models that simulate water budgets at continental and global scales have been widely used in hydrology and earth science research (Roads et al., 1994; Vörösmarty et al., 1998; Nijssen et al., 2001). Mintz and Walker (1993) applied a simple bucket model to derive global fields of monthly soil moisture. Pitman et al. (1999) employed a land surface model to estimate the effects of frozen soil moisture parameterizations on simulated runoff. A hydrology model was used to evaluate the water budgets of climate model simulations (Maurer et al., 2001), revealing significant biases in the climate model fields. A similar overprediction of evapotranspiration and underprediction of runoff from a climate model land-surface scheme was found across the Yenisei, Lena, and Amur basins in Asia (Arora, 2001). Improvement in global estimates of river discharge were obtained using a new method to determine runoff calibration parameters (Nijssen et al., 2001). Given the lack of observed river discharge data across large portions of the Pan-Arctic basin (Shiklomanov et al., 2002; Lammers et al., 2001), hydrological models which adequately capture the Arctic water cycle are needed to provide accurate benchmarks and aid in environmental change studies. Further, given the significant bias in runoff generated by current GCMs (Walsh et al., 1998), accurate time series of simulated seasonal runoff routed through a Simulated Topological



Network (STN) (Vörösmarty et al., 2000a; Vörösmarty et al., 2000b) offers the potential to improve freshwater forcing in coupled ocean models.

Thawing and freezing of Arctic soils is affected by many factors, with soil surface temperature, vegetation, and soil moisture among the more significant (Zhang and Stamnes, 1998). Soil texture and slope/aspect also strongly influence active-layer dynamics, which can vary considerably over short lateral distances. Indeed, differences in end-of-season mean thaw depths up to 50 % have been found when comparing two sites even in close (< 10 km) proximity (Nelson et al., 1997).

Investigations of active-layer thickness (ALT) have traditionally been performed through field studies at point locations (Romanovsky and Osterkamp, 1995; Zhang et al., 1996). Given the difficulty in compiling spatially coherent data sets of key input drivers, few studies have been conducted to model seasonal active-layer changes at the regional scale. Anisimov et al. (1997) applied a semi-empirical method to calculate the depth of seasonal freezing and thawing using annual air temperature, snowcover, vegetation, soil moisture, and thermal conductivity parameterizations. More complicated models, which simulate heat flow and phase change, have been used to investigate the sensitivity of soil thermal processes to air temperature, seasonal snow cover, and soil moisture (Zhang and Stamnes, 1998). Although detailed models are helpful in understanding the effects of climatic and landscape factors, simple models may be useful in estimating changes in ALT, particularly for large-scale applications. The Stefan solution to the differential equation of heat transfer with phase change under constant conditions (e.g. Lunardini, 1981) shows that ALT progresses as the square root of time. This approach has been applied across the Kuparuk basin (2100 km<sup>2</sup>) in northern Alaska (Nelson et al., 1997). Klene et al. (2001) found that incorporating the

effects of vegetation on soil temperatures could improve this method. In addition to the difficulty in compiling accurate input data sets to model soil thawing and freezing, a lack of empirical observations for validation of simulated estimates presents a further challenge for Pan-Arctic applications (Vörösmarty et al., 2001).

Our focus in this paper is the estimation of runoff across the Pan-Arctic drainage basin for the period 1980-2001. A simple sub-model for estimating phase changes in soil moisture is described and evaluated by comparing model-estimated active-layer thickness to field measurements from several locations in Alaska. Model simulated runoff is then presented and compared to observed data. Sensitivity of simulated runoff to variations in climate inputs and model parameterization are also investigated to identify the most sensitive model requirements.

## 1.2 The Pan-Arctic Water Balance Model

Large-scale numerical models which simulate the hydrologic cycle have recently been developed to characterize moisture fluxes and storage across diverse landscapes (Nijssen et al., 2001; Zhuang et al., 2001). A modified version of the water balance model (WBM) (Vörösmarty et al., 1996; Vörösmarty et al., 1998) was applied across the Pan-Arctic to study the spatial and temporal variability of the high-latitude terrestrial water cycle, with significant changes incorporated into this version—henceforth referred to as the Pan-Arctic Water Balance Model (PWBM)—detailed in the Appendix A.

Models which simulate water and energy balance at fine vertical resolution within the soil have been developed and show promise in estimating soil thermal regimes (Zhuang et al.,

2001) as well as water balance (Bruland et al., 2001) in Arctic regions. Simple “bucket” models, however, have been shown to perform comparably to complex biosphere models in estimating soil moisture (Robock et al., 1995). A fundamental premise in the development and modification of the PWBM is that for large-scale spatial applications there are severe limitations in basic data quality needed to parameterize and drive a hydrological model (e.g., precipitation, soil properties, vegetation characteristics such as leaf area and rooting depth), so developing a simple, suitably-scaled model is appropriate. The model should balance physically-based simulations of hydrological processes with the practical limits of soil and vegetation parameterizations and meteorological drivers. To this end, PWBM is data-rich, suitably physically based, and well scaled to the challenges of water budget estimation over the Pan-Arctic. Our model does not explicitly simulate glacier accumulation and melt. Therefore, runoff for areas dominated by glaciers and ice fields are expected to have substantial error.

In this study, estimates of snow water equivalent, soil ice and water stores, along with fluxes such as evaporation, evapotranspiration, and runoff are made with the PWBM at explicit daily time steps across the Pan-Arctic drainage basin, defined as all land areas draining to the Arctic Ocean in Russia and Canada, as well as Hudson Bay and the Bering Sea (Figure 1-1). The PWBM requires spatial data sets of vegetation cover, plant rooting depth, soil texture, soil depth, and soil carbon content. Gridded fields of daily air temperature and precipitation drive the PWBM. Input data (parameter fields, air temperature, and precipitation) and model output is gridded at 25 km resolution on the Lambert Azimuthal equal area EASE-Grid (NSIDC, 1995; Brodzik and Knowles, 2002). A total of 39,926 EASE-Grid pixels defines the Pan-Arctic drainage basin, which extends as far south as 45°N in

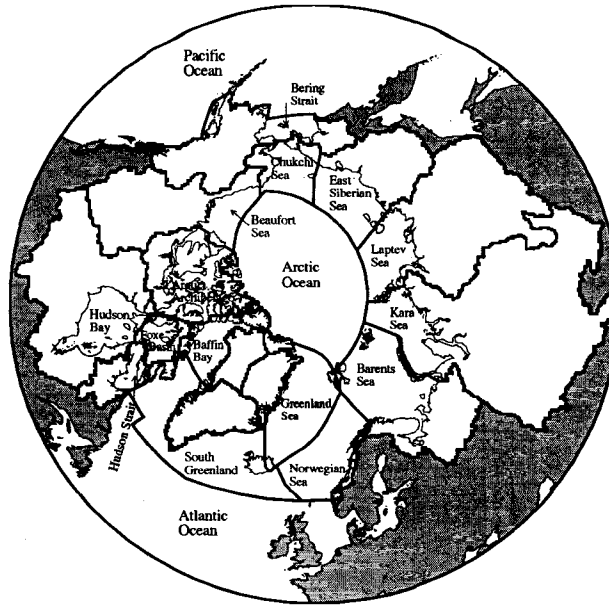


Figure 1-1: Pan-Arctic domain by sea basin boundaries. Basin boundaries are derived from a digital river network at 30 minute grid cell resolution.

southern Canada (Nelson Basin) and southern Siberia (Ob Basin). Air temperature and precipitation inputs are derived from the National Center for Environmental Prediction (NCEP) reanalysis project (Kalnay et al., 1996; Uppala et al., 2000). The NCEP-NCAR reanalysis constitutes a retrospective record of numerical weather prediction (NWP) analysis and forecasts, with the added advantage of being constantly updated with minimal (1 month) time lag. Six-hourly NCEP data are aggregated to daily means and interpolated to the 25 km EASE-Grid using a statistical downscaling approach (Serreze et al., 2002). Usage of data sets for vegetation cover (Mellilo et al., 1993), soil texture (Food and Agriculture Organization/UNESCO, 1995), and rooting depth is based on the methodologies originally reported in Vörösmarty et al. (1989). Data for soil organic content were obtained from the Oak Ridge National Laboratory (ORNL) (Global Soil Data Task, 2000).

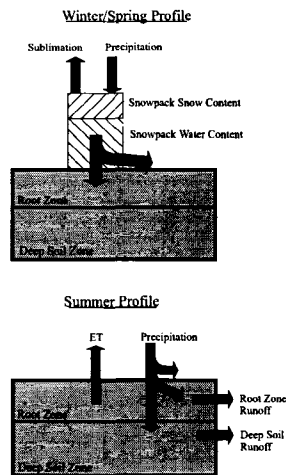


Figure 1-2: Schematic of the PWBM soil zones and water fluxes in Winter/Spring and Summer. Root Zone represents the spatially-variable vegetation rooting depth. Water in root and deep soil zones can be all frozen, partially frozen, or all liquid. In some locations/cells, the deep zone never fully thaws and in others, it never fully freezes.(Modified from (Holden, 1999)).

PWBM has two soil layers, a root zone that gains water from infiltration and loses water via evapotranspiration and horizontal and vertical drainage, and a deep zone that gains water via root zone vertical drainage and loses water via horizontal drainage (Figure 1-2). Seasonal changes in soil water/ice content are an important component of Arctic hydrology (Woo, 1998), so specification of phase changes in soil moisture is a key component of the PWBM. Soil liquid water and ice contents of each soil layer are calculated in a submodel referred to as the Thaw-Freeze Model (TFM). Because PWBM does not simulate vertical heterogeneity within either soil layer, it does not explicitly track the depth of thawing or freezing, but instead uses the Stefan solution to update daily changes in the amount of liquid and frozen water of each soil layer. The sign of the daily thaw/freeze increment determines the exchange of water and ice within each layer. Details of the TFM are presented in Appendix A.

## 1.3 Model Results

### 1.3.1 Active-layer Modeling

To evaluate the efficacy of the Stefan solution, simulated active-layer estimates from the two-layer TFM (equations A.4 and A.5) within the PWBM framework are examined. Simulated active-layer development (for a single grid located in northern Alaska) progresses from the organic layer (depth = 23 cm) to mineral soil through the warm season (Figure 1-3a). This Figure also shows the effect of soil moisture variability. After 600°C-days had accumulated, ALT for this grid was 38.4 cm for 1999 (drier) and 42.9 cm for 1996 (wetter) conditions, with the variation attributed to differences in thermal conductivity of wet and dry soils. For the purposes of comparison to data in Zhang (1997), a linear regression model fit through the estimates in Figure 1-3a reveals a rate of change approximated by  $ALT = 0.058 \text{ DDT}$  ( $r = 0.99$ ), where DDT is accumulation of degree days of thawing (°C-day). Zhang et al. (1997) examined 17 observation at 3 locations across northern Alaska (1987-1992), and found  $ALT = 0.046 \text{ DDT}$  ( $r = 0.75$ ), a difference of 1.2 mm per 10°C-days from the TFM estimates.

The Stefan solution to heat transfer with phase change in one dimension (vertical) provides a simple estimate of ALT (Lunardini, 1981). Nelson et al. (1997) used an empirical ALT similar to the Stefan solution to determine ALT estimates within ~6cm of observed values. Here we compare gridded estimates from the two-layer Stefan solution (in the TFM) to a set of observed data from the Circumpolar Active Layer Monitoring network (CALM) (Brown et al., 2000). Various sampling strategies are represented in the CALM data set, with maximum summer ALT determined as an average of samples across relatively small areas (10 m lattice within a 100 m<sup>2</sup> area) as well as larger sampling designs (100 m lattice

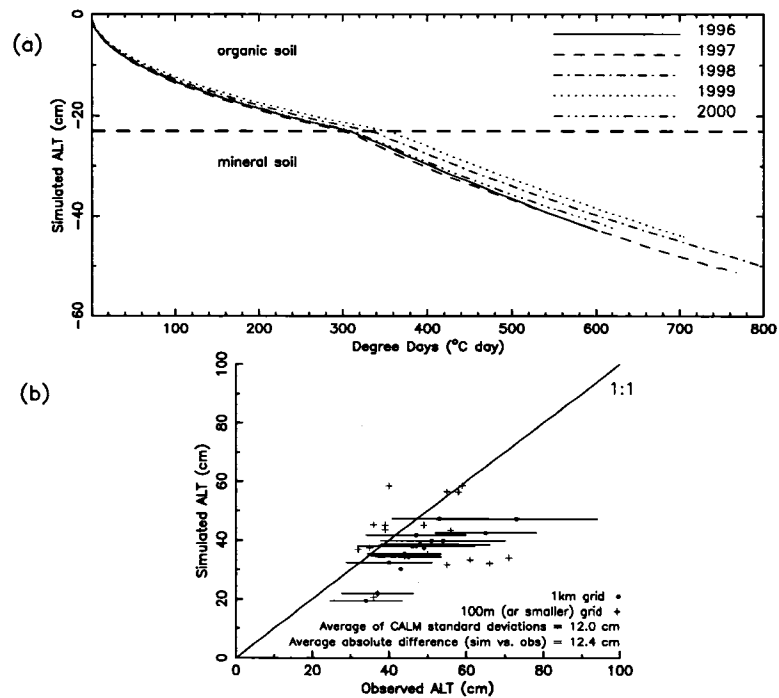


Figure 1-3: Simulated active layer thickness (ALT) as a function of degree days for one EASE-Grid over North Slope, AK (a); and model predicted active-layer thickness vs. CALM observed depth (b). Horizontal lines in lower panel represent one standard deviation on each side of observed ALT for the  $1 \text{ km}^2$  CALM sites.

within a 1 km<sup>2</sup> area) in some locations. Simulated ALT values on the 25 km EASE-Grid encompassing each CALM validation site are compared to the maximum summer CALM ALT for 27 sites in Alaska (years 1999 and 2000). Specifically, we use the TFM model value for the day on which the CALM estimate was made. Model estimates are generally within one standard deviation of the observed value (Figure 1-3b). A bias (underestimation) in simulated ALT is evident, which is likely attributable, in part, to a bias in the air temperature field that is adjusted to 25 km grid mean elevation, which is higher, and thus cooler, than CALM site elevation in most cases (data not shown). It should be noted that the CALM value used in each comparison represents a single point sample within the 625 km<sup>2</sup> EASE-Grid and grid-to-point comparisons are known to create interpretation problems (Blöschl and Sivapalan, 1995; Klene et al., 2001; Vörösmarty et al., 1998). And although an increasing number of CALM sites have begun to employ a gridded sampling design, the use of observed active-layer thickness estimates made from a single observation should be undertaken with caution (Brown et al., 2000). Nonetheless, the average absolute error of the TFM model versus observations is 12.4 cm (observed data range 32 cm to 72 cm), while the average standard deviation of samples from the 1 km<sup>2</sup> grids (100 m lattice) is 12.0 cm. Given the variance in the observed data, TFM estimates are within the variability seen in these field samples. Improvements in ALT estimates using the Stefan solution in this manner have been achieved using higher resolution data sets across the Kuparuk basin in Alaska (Klene et al., 2001). Although there is no apparent bias between the comparisons with the 1 km<sup>2</sup> CALM sites and those from smaller areas, there is evidence that the 100 m spacing is unable to resolve the variability in ALT at upland (North Slope, AK) sites (Nelson et al., 1999).



### 1.3.2 Pan-Arctic Runoff

To estimate runoff over the Pan-Arctic drainage basin, the PWBM was used to simulate the water cycle at daily time steps for each EASE-Grid across the domain. The model was run with inputs of air temperature and precipitation for the year 1980, repeated for 50 years to stabilize soil moisture content, followed by a transient run for the years 1980-2001. Climatologies of monthly total runoff (Figure 1-4) show the progression of the annual pattern of runoff, from the spring snowmelt pulse, to low flow conditions, to freeze-up. Monthly runoff is relatively low across much of the terrestrial Arctic in winter with the exception of coastal western Canada and southern Alaska. Snowmelt contributes to higher runoff across Eurasia in April. Runoff increases in both magnitude and extent during May in both hemispheres. The most northern areas of Eurasia see the snowmelt driven runoff peak in June. In a general sense, this peak runoff progresses northward toward the Arctic Ocean through spring in central Eurasia, indicative of seasonal changes in surface air temperature. Summer rainfall then contributes to runoff through summer, however, higher evapotranspiration tends to produce relatively dry conditions. The water cycle in fall and winter is dominated by snowpack accumulation and low runoff amounts.

Simulated long-term annual runoff (1980-2001) is highest across southern Alaska, coastal Norway, and Iceland. Higher runoffs are also found across southern parts of Canada in the Nelson basin and the Eurasian part of Russian. Lower runoffs are evident across the Canadian archipelago and Siberia (Figure 1-5). Runoffs exceeding  $400 \text{ mm year}^{-1}$  are noted across northeastern Canada and southern Alaska. Simulated long-term annual runoff across the largest Arctic drainage basins is approximately  $100$  to  $180 \text{ mm year}^{-1}$  (Table 1.1). More

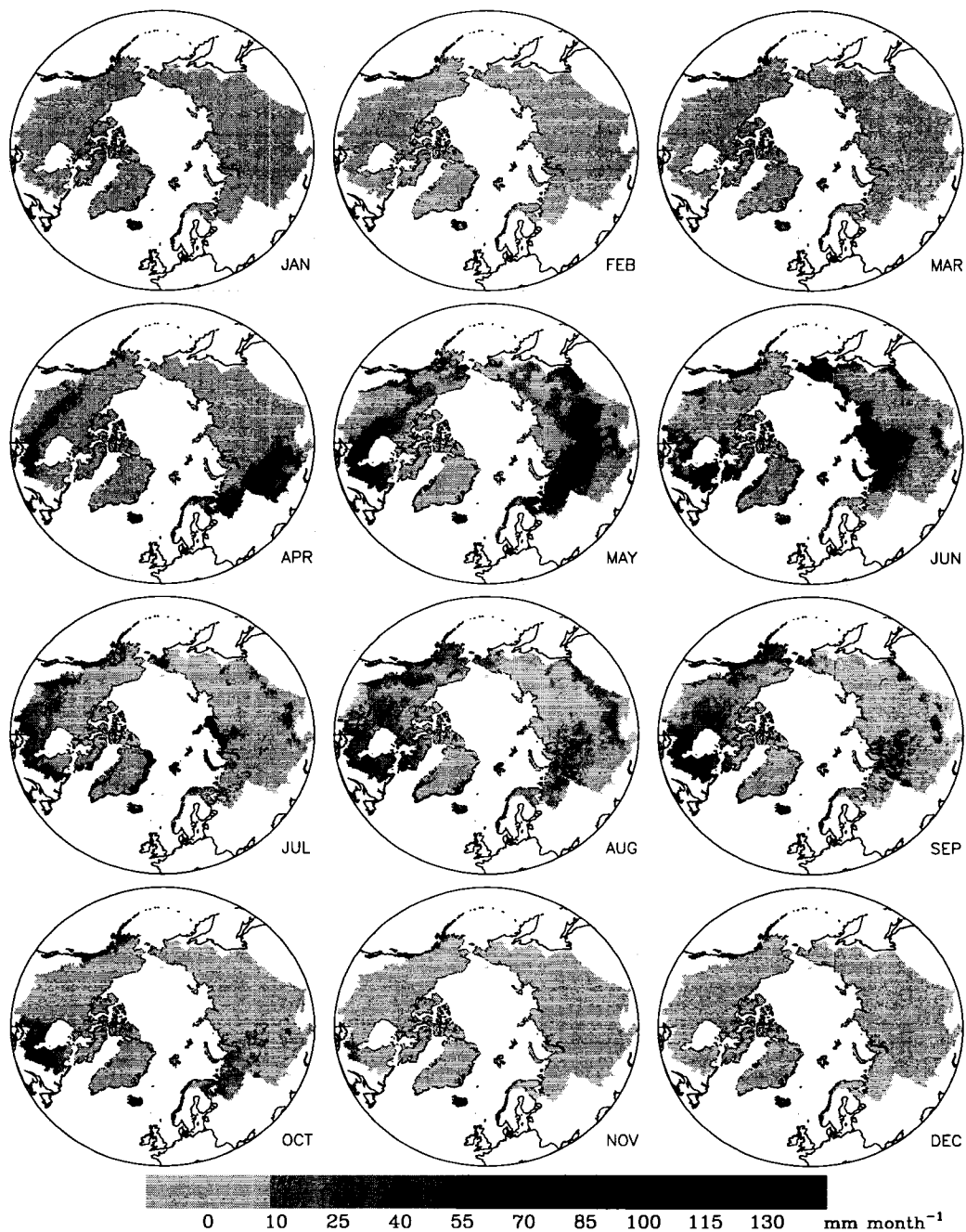


Figure 1-4: PWBM long-term monthly runoff climatology 1980–2001. This figure includes runoff for southern Alaska, which is not part of the Pan-Arctic drainage per se. Grids with zero runoff for the month are shaded in blue. Runoff for areas with glaciers should be interpreted with caution, as the PWBM does not model glacier accumulation and melt/ablation.



River Basin	Basin Size <sup>a</sup> (km <sup>2</sup> )	Gaged Area <sup>b</sup> (km <sup>2</sup> )	Simulated Annual Runoff <sup>c</sup> (mm year <sup>-1</sup> )
Ob	2,994,238	2,965,100	180
Yenisei	2,537,404	2,452,300	170
Lena	2,460,742	2,460,000	100
Mackenzie	1,783,972	1,769,200	150
Yukon	833,232	831,391	120
Nelson	1,106,578	1,050,300	160

Sea Basin	Contributing Area <sup>a</sup> (km <sup>2</sup> )	Gaged Area <sup>b</sup> (km <sup>2</sup> )	Simulated Annual Runoff <sup>c</sup> (mm year <sup>-1</sup> )
Arctic Archipelago	1,134,856	209,270	40
Hudson Bay	3,304,025	2,613,320	270
Barents Sea	1,322,741	984,830	300
Hudson Strait	468,050	285,480	410
Beaufort Sea	2,139,635	1,860,100	130
South Greenland	1,174,444	10,800	250
Bering Strait	1,205,234	1,010,940	170
Kara Sea	6,631,308	5,159,700	200
Chukchi Sea	282,143	56,160	190
Laptev Sea	3,639,584	3,232,480	100
East Siberian Sea	1,329,025	941,500	90
Pan-Arctic <sup>d</sup>	22,611,659	16,460,080	180

Table 1.1: Simulated long-term annual runoff for selected Arctic drainage basins and terrestrial runoff integrated across basins draining to selected Arctic Ocean sea basins.

<sup>a</sup>Total area for river or sea basin on the EASE-Grid (NSIDC, 1995)

<sup>b</sup>Area captured by observed gaging stations (Lammers et al., 2001).

<sup>c</sup>Annual runoffs in Table represent an integration across all EASE grids in a given basin.

<sup>d</sup>The Pan-Arctic value represents the spatially-averaged runoff for all land areas draining to the Arctic Ocean in Russia, Canada, and Alaska, as well as Hudson Bay and the northern Bering Sea.

negligible. Mean values of the simulated and observed runoff distributions for precipitation between 300–900 mm (80 % of total samples) are comparable (Figure 1-6). PWBM simulated runoff is conservative (does not exceed precipitation) and the residual of precipitation minus runoff represents modeled evapotranspiration. Observed runoff, however, exceeds the inter-station-area precipitation in some regions, implying either considerable interbasin groundwater transfers or significant problems with the spatial precipitation and/or runoff data (Vörösmarty et al., 1998; Fekete et al., 1999).

Simulated and observed runoffs are further compared by aggregating to long-term seasonal runoff for each Arctic sea basin. Seasonal runoff represents the total stock of freshwater which contributes to the sea basin's seasonal riverine input. Here we compare the integrated runoff across all EASE grids in a given basin to the observed runoff over the monitored portion of that basin. Although underestimates are again more common than overestimates, good correlation is evident ( $r = 0.84$ , Figure 1-7). The PWBM runoff estimates are near zero in winter, and underestimate most observed basin values. This is likely due to several factors, including groundwater inputs that do not freeze in winter, and lags in water transport that generate winter flow (observed at gaging stations) from fall runoff. For some basins, the monitored area is only a small fraction of the total basin (Table 1.1), which could introduce a bias into the observed runoff, evidence that the decline in river discharge monitoring across both North America and Asia (Shiklomanov et al., 2002) complicates our model verification efforts.

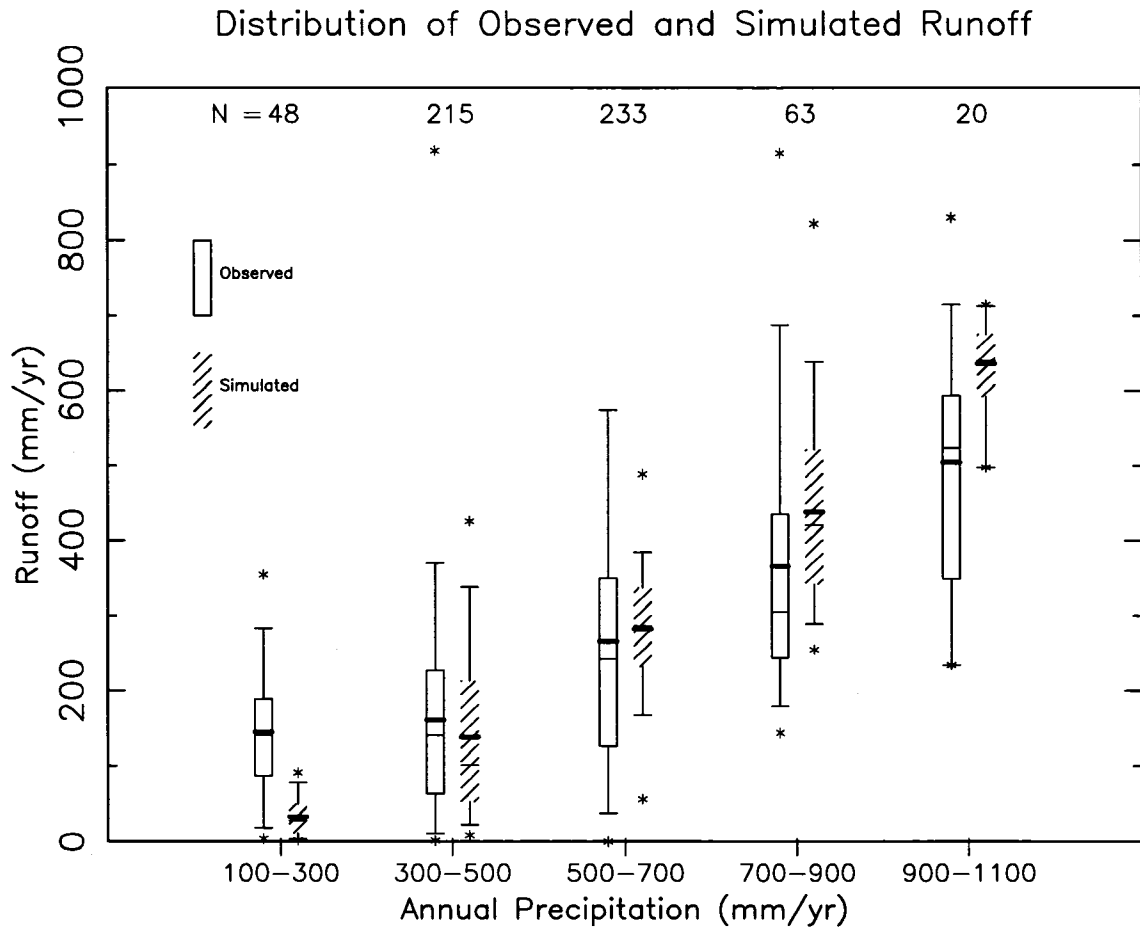


Figure 1-6: Distribution of simulated and observed annual (long-term) runoff at (n=579) inter-station areas for groupings of annual long-term precipitation. The top and bottom of each box are the 25th and 75th percentiles, respectively. Boxplot whiskers represent the 5th and 95th percentiles. The spatial mean is the thick line and the median is the thin line. Maximum and minimum runoff for each distribution is marked with an asterisk. The number of observed and simulated runoffs in each grouping is listed along the top of the Figure. Maximum value of observed runoff for 500–700 precipitation is 1915 mm and is not plotted. Note that in all bins except 900–1100 mm yr<sup>-1</sup>, the maximum observed runoff is greater than annual precipitation.

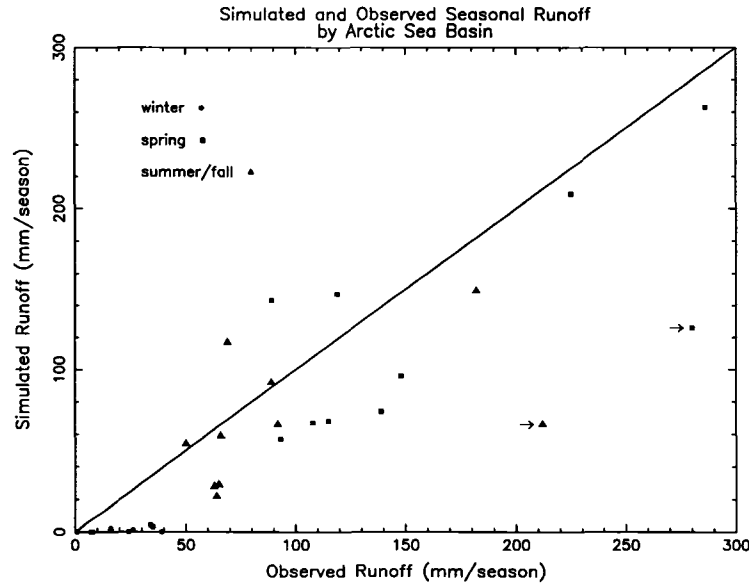


Figure 1-7: Long-term seasonal runoff for Arctic sea basins. Winter is December, January, February, March; spring is April, May, June, July; summer/fall is August, September, October, November.

## 1.4 Sensitivity Analysis

Biogeophysical characteristics such as plant rooting depth, organic-layer thickness, and soil texture affect water flow paths and are integral factors in hydrological models. In addition, climate data (precipitation and air temperature) are essential inputs with both spatial and temporal variations and uncertainties. Precipitation and air temperature data for the Arctic, however, are more poorly resolved (owing to the the sparsity of meteorological stations), relative to other parts of the world. In addition to being undersampled, biases in Arctic precipitation records are known to be large, particularly at higher latitudes. Underestimates of 20-25 % (Karl et al., 1993) and 10-140 % (Yang et al., 1998) have been determined across North America and at 10 locations in Alaska, respectively. Substantial gage undercatch across the Arctic has also been estimated by applying a hydrological model (Fekete et al.,

1999). Although NCEP reanalysis data have been adjusted for measurement biases (Serreze et al., 2002), some uncertainty in the model input can be assumed. Comparison of daily gridded NCEP air temperatures in summer with observed meteorological data yielded absolute differences from 1.6°C for an Arctic continental location and 6.6°C at a coastal site. In general, NCEP air temperatures are consistently cooler than the station observations throughout summer.

To investigate the sensitivity of the PWBM to model parameterizations and climate inputs, long-term annual runoff (1980–2001) was compared against the long-term annual runoff produced in a series of model perturbations runs. The following perturbation experiments were performed: (i) model organic-layer depths were halved [0.5x Org] and (ii) doubled [2x Org]; (iii) vegetation rooting depths were halved [0.5x RD] and (iv) doubled [2x RD]; (v) soil field capacity was increased by 0.05 cm<sup>3</sup>/cm<sup>3</sup> of pore space [FC + 25 %]; (vi) horizontal and downward water flux from rooting zone (Figure 1-2) was increased to 40 % (from 20 %) of water over field capacity [RF = 40%]; (vii) TFM submodel was not applied [No TFM]; (viii) summer air temperatures were increased by 4°C [T + 4°C] and (ix) daily precipitation was increased by 25 % [P + 25 %]. The control run represents our best estimate of annual runoff (e.g., Figure 1-5) (with associated error characteristics as discussed above) using available fields of soil characteristics, NCEP-derived air temperature and precipitation, and the TFM-generated active-layer behavior. Comparisons were examined for the Yukon, Nelson, MacKenzie, Ob, Yenisei, and Lena River basins. Differences between the control and sensitivity runs also were determined for the entire Pan-Arctic basin.

Of the nine sensitivity experiments performed, an increase in precipitation produces the most significant changes in basin-average runoff. Adding 25 % to each daily precipitation



occurrence increases Arctic-wide and basin runoff well over 50 % (Figure 1-8), as additional precipitation is more likely to be diverted to runoff than evapotranspiration. Bias in precipitation inputs has been noted as a primary source of error in other large-scale hydrology models (Nijssen et al., 2001).

Increasing daily summer air temperatures by 4°C also has a significant effect (albeit smaller than precipitation) across much of the Pan-Arctic. Annual runoff is reduced by more than 20 % across the Yukon, Lena, and Nelson basins (Figure 1-8). Warmer air temperatures result in higher rates of evapotranspiration (Equation A.1), enhanced development of the active layer each spring/summer, an increased water holding capacity (which allows for more evapotranspiration) and, therefore, less runoff. The larger changes across the Yukon and Lena basins are expected considering the greater extent of permafrost conditions in these areas, relative to the other basins. A similar mechanism and magnitude of effect occurs when the TFM sub-model is not used, effectively neglecting the seasonal thawing and freezing (i.e., changes to water-holding capacity) of Arctic soils. In this case, the absence of a shallow active-layer in late spring and early summer results in higher infiltration and summer evaporation, with a resultant reduction in annual runoff of 7 % for the Yenisei basin (least effect) to 27 % for the Yukon basin (greatest effect). This result is consistent with a recent investigation of soil frost effects on catchment runoff, which found that ignoring soil frost tends to decrease total runoff (Stähli et al., 2001). However, two recent studies have questioned the importance of modeling soil ice for runoff estimation in forested environs (Nyberg et al., 2001) and at large basin scales (Pitman et al., 1999).

As opposed to the perturbations to climate inputs (and the TFM), changes to other model parameterizations result in relatively smaller changes (generally < 15 %) in annual

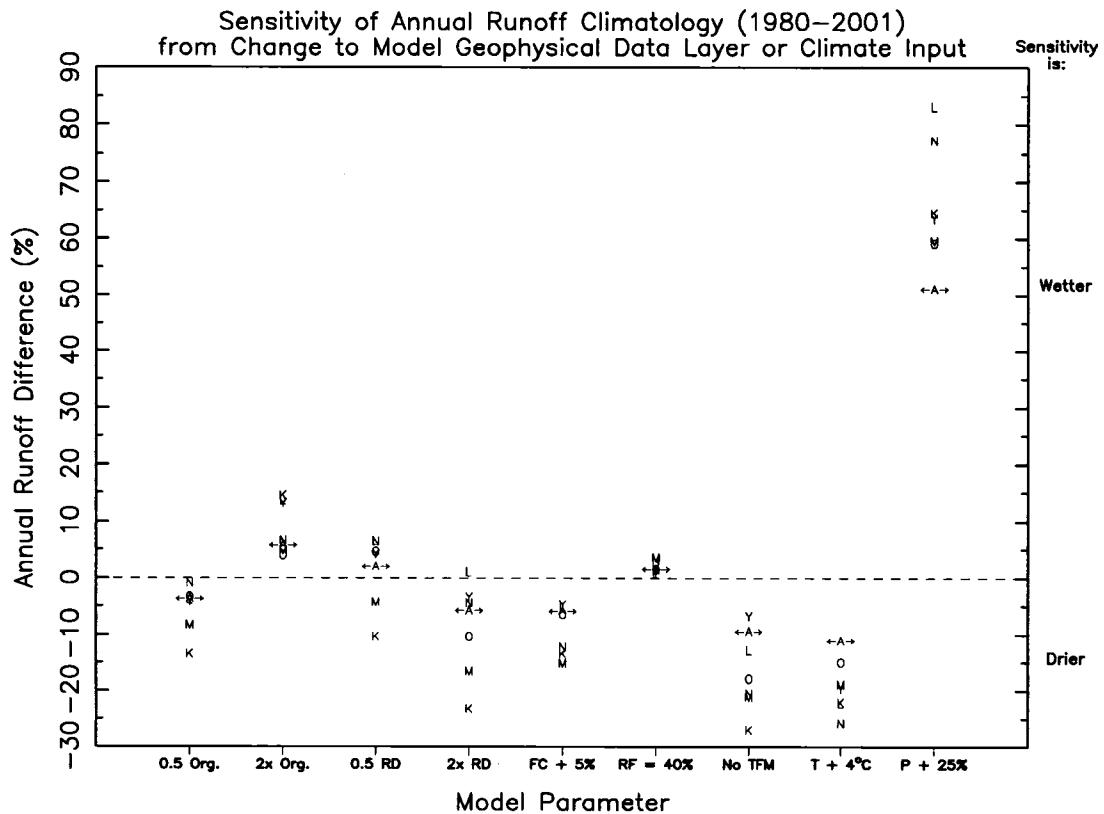


Figure 1-8: Sensitivity of simulated annual runoff to various alterations of input parameters. Relative percent differences are defined by  $\Delta RO = (RO_c - RO_p) / RO_c * 100\%$  where  $\Delta RO$  is the relative difference in percent,  $RO_c$  is the 1980–2001 runoff climatology, and  $RO_p$  is the 1980–2001 runoff climatology for perturbation or sensitivity run. Basins in analysis are O = Ob, Y = Yenisei, L = Lena, M = Mackenzie, N = Nelson, K = Yukon, ←A→ = Pan-Arctic. Perturbation experiments are as follows: model organic-layer depths are halved [0.5x Org], doubled [2x Org], vegetation rooting depths are halved [0.5x RD], and doubled [2x RD], soil field capacity is increased by 0.05 cm<sup>3</sup>/cm<sup>3</sup> of pore space [FC + 25%], horizontal and downward water flux from rooting zone is increased to 40% (from 20%) [RF = 40%], TFM submodel is not applied [No TFM], summer air temperatures are increased by 4°C [T + 4°C], and daily precipitation is increased by 25% [P + 25%].

runoff. Reducing organic layer depths enhances active-layer development, reducing runoff (Figure 1-8). A doubling of rooting depths, (as well as an increase in field capacity) also increases soil water-holding capacity, which lowers runoff. Runoff changes are negligible when the flux from the rooting zone is increased. These differences from the control runoff are significantly less than the standard deviation in annual runoff, further emphasizing the relatively small impact of these model parameterization compared to the climate inputs.

## 1.5 Summary and Discussion of Results

A comprehensive understanding of Arctic hydrological systems has become important in light of recent evidence of the region's environmental changes. Given the linkages involving water and carbon in terrestrial landscapes, the atmosphere and oceans, quantifying the Arctic water cycle at continental scales allows us to establish baseline conditions and explore changes predicted to occur (SEARCH SCC, 2001). River discharge is highly undersampled across many of the higher latitudes in the Pan-Arctic drainage basin. With recent closures to a number of observed discharge monitoring stations (Shiklomanov et al., 2002), modeling efforts which simulate runoff and freshwater flux to the Arctic Ocean can provide the requisite inputs to ocean models in lieu of observed data.

A Pan-Arctic Water Balance Model (PWBM) has been developed and applied to estimate the water cycle at daily time steps for the 25 million km<sup>2</sup> land area of the Pan-Arctic drainage basin for the period 1980–2001. Phase changes in soil moisture were simulated with the Thaw-Freeze Model (TFM). These linked models utilize spatial fields of vegetation rooting depth, organic-layer depth, and soil textures, and are driven with climate data from

the NCEP reanalysis project. These spatial data sets are of varying quality, and many regions are severely undersampled in all variables. Nonetheless, their compilation and analysis provides a framework for evaluating consistencies between data sets (eg. runoff and precipitation) as well as a means for simulating the hydrological cycle.

Active-layer thicknesses generated with the TFM were compared with observed data from the Circumpolar Active Layer Monitoring (CALM) network. Simulated end-of-season active-layer thickness was generally within the range of variability seen in the observed data; model biases were 12.4 cm, while the average standard deviation of the observed CALM estimates is 12.0 cm. In large-scale studies of this nature, observed data validation sites, even 1 km<sup>2</sup> grid sampling, represent point estimates within the larger (625 km<sup>2</sup>) PWBM grid. Considerable variability exist at this scale in all biophysical parameters, including seasonal n-factors, with soil-surface degree-day sums varying up to 100 % within 1-ha plots (Klene et al., 2001). Although simulated maximum summer ALT estimates are generally within the variability observed in the field samples, our interest centers on the day-to-day changes in active layer development used to determine phase changes of soil water. Recent studies (Anisimov et al., 1997; Klene et al., 2001) have suggested that improvements in active-layer simulation are dependent on the development of more spatially coherent data sets of air temperature, vegetation, and soil moisture.

Simulated monthly runoff is relatively low during winter when precipitation accumulates as snow. A spring melt pulse is evident in a south-to-north progression across the Arctic basin, with the majority of runoff occurring between the months of April–June. Annual long-term runoff is highest across coastal western Canada, northeastern Canada and west central Eurasia. Lowest annual runoffs are seen across the Canadian archipelago and

Siberia. Simulated long-term annual runoff is less variable than observed runoff, and is highly correlated with precipitation. Good correspondence was found when comparing simulated and observed seasonal runoff at individual Arctic sea basins ( $r = 0.84$ ). This suggests that the PWBM has the potential to provide the seasonal (temporal) variations in freshwater discharge to ocean circulation models. Our sensitivity analyses show this model to be strongly influenced by climate drivers as well as the absence or presence of modeled active-layer changes, and that uncertainties in parameters such as rooting depth and organic layer thickness may be less problematic. As important as model development, it is essential for the research community to work to improve spatial data sets for fundamental biophysical variables and climatic drivers, and to maintain and expand river gaging in the Pan-Arctic to provide more complete data sets for model evaluation. Simulation of the Arctic water cycle is notably influenced by specification of active-layer changes. This finding suggests that modeling and analyses which depend on hydrological drivers such as ocean circulation, coastal processes, ecosystem biogeochemistry, and climate models will benefit from incorporation of thawing and freezing of Arctic soils. Gridded runoff fields are available from the Water Systems Analysis Group, University of New Hampshire (<http://wsag.unh.edu>).

## CHAPTER 2

# REMOTE SENSING OF SNOW THAW AT THE PAN-ARCTIC SCALE USING THE SEAWINDS SCATTEROMETER

### 2.1 Remote Sensing of Snow

The climate and hydrological cycle of the Arctic have undergone rapid change in recent decades (Serreze et al., 2000). Among the changes are increased winter air temperatures (Chapman and Walsh, 1993; Rawlins and Willmott, 2003; Robeson, 2004), reduced snow cover (Serreze et al., 2000), warming of permafrost (Osterkamp and Romanovsky, 1999; Romanovsky et al., 2002), increased runoff and river discharge (Peterson et al., 2002), and reduced extent of sea ice cover (Serreze et al., 2002; Rothrock et al., 2003). These significant changes are occurring over large spatial domains. The combination of remoteness and extreme climate have led to a relatively low density of ground-based hydrological and meteorological observation stations. This sparse network hinders the development of strong baseline hydrological and meteorological time series data, the ability to detect change occurring across large regions, and the search for strong explanatory relationships linking the changing components of the arctic hydroclimatic system. Satellite-borne remote sensing can provide large spatial coverage at high temporal resolution, and thus may be able to

contribute to our ability to observe and understand the pan-Arctic system. The expanded use of remotely sensed data has recently been cited as a vital component in the study of Arctic environmental change (Vörösmarty et al., 2001).

Satellite-borne microwave radars provide year-round all-weather capability for monitoring high latitude ecosystems. Wide-swath coverage provided by current scatterometer instruments ( $\sim 1800$  km for SeaWinds at  $\sim 25$  km spatial resolution) allows observations of the polar regions at sub-daily timescales. Combined with their day/night measurement capability, and high sensitivity to the freeze/thaw state of water within the landscape, these instruments offer distinct advantages over optical and near-IR sensors for monitoring hydrologic processes across the pan-Arctic land mass.

Microwave backscatter is sensitive to structural and dielectric properties of water and vegetation in the scanned swath (Elachi, 1987). Short wavelength radar such as the current  $K_u$  band SeaWinds scatterometer (wavelength = 2.2 cm; frequency = 13.4 GHz) and the earlier NASA scatterometer (NSCAT; 2.1 cm; 14 GHz), can exhibit significant diffuse or volume scattering from dry snow (Raney, 1998; Ulaby et al., 1986) and thus should be able to monitor seasonal snow cover at large scales (Nghiem and Tsai, 2001). At snow thaw, the ripening snow will contain a significant quantity of liquid water (with a very high dielectric constant), surface scattering will dominate the microwave interaction with the snow, and backscatter should decrease dramatically. It is likely that the lowest backscatter signals occur on days when the landscape surface element (resolution is an ellipse of roughly  $37 \times 25$  km) has near-continuous, very wet snow cover (Nghiem and Tsai, 2001).

Nghiem and Tsai (2001) compared winter 1996–1997, weekly-averaged NSCAT backscatter data, binned to 25 km resolution, to a northern hemisphere, weekly 2° resolution snow cover data set based on optical remote sensing data (Northern Hemisphere Snow Cover Data, 1999), and to maps of snow-cover class (tundra, taiga, prairie, alpine, maritime, and ephemeral). They concluded that K<sub>u</sub>-band backscatter was insensitive to vegetation cover across the taiga/tundra zone, and that backscatter dropped rapidly at snow thaw, as inferred both from hemispheric snow-cover and from weather station data from three sites in Alaska, three sites in Canada, and five sites in Siberia.

Wiseman (2000a) examined 8 years of ERS scatterometer (C-band; 5.3 GHz; 5.5 cm) data for a spring thaw signal in Siberia. Data were averaged to 3-days, and the spatial resolution was approximately 50 × 50 km. The thaw detection algorithm used an intermediate threshold based on local mean backscatter for winter and summer. He found that the onset of thaw varied locally by about one month over 1992–1999, that it took about 4 months for the thaw signal to move from the southern part of the study region (50°N) to the northern part (75°N), and that onset of thaw correlated well with the geographical variability of air temperature. Wiseman (2000b) also studied the Greenland snow thaw signal with ERS scatterometer data over this same period. Thaw detection was based on a backscatter offset of 3 dB from a winter (November–March) mean, corresponding to a 7 cm layer of snow having an 0.5 % liquid water content, based on a modeling analysis by Winebrenner et al. (1994). He found a strong correlation between annually integrated positive air temperature and an annually integrated backscatter offset. In the 1992–1999 ERS scatterometer record, Wiseman (2000b) found a 3-fold range in the thaw extent on Greenland.



Hillard et al. (2003) compared spatial patterns of spring thaw signals from NSCAT (active between 15 September 1996 and 29 June 1997) with simulated snow surface temperature and liquid water content from the Variable Infiltration Capacity (VIC) hydrological model (Liang et al., 1994), driven by station meteorological data (maximum and minimum air temperature and precipitation) at daily time resolution for the Upper Mississippi Basin and the BOREAS study region in central Canada. They found that only occasionally was there a similar spatial pattern in their maps of simulated snow liquid water content and scatterometer backscatter. They attributed this lack of correlation to time of day of NSCAT overpass (10:00 am and 10:00 pm, not optimal times for maximum and minimum snow liquid water content), interference from vegetation cover, and signal noise. However, their approach did not employ temporal change detection schemes to classify freeze-thaw events. Such schemes have been shown to provide effective detection of springtime thaw onset and subsequent thaw-freeze cycles when applied to active and passive microwave remote sensing data (Kimball et al., 2004a, 2004b; McDonald et al., 2004). Using scatterometer estimated freeze-thaw as an additional driver for the VIC model improved simulations only slightly in the Upper Mississippi Basin, which has a high-density network of meteorological stations providing daily driving data for the model, allowing little opportunity for improvement utilizing the 25 km resolution scatterometer data.

Kimball et al. (2004a) developed a temporal change detection algorithm for identifying springtime thaw across a 1-million km<sup>2</sup> region in central Canada, using daily scatterometer backscatter data from the earlier NSCAT instrument. During spring (defined as 1 March–31 May in their analysis), initial and final thaw dates were identified as the first and last days when the daily mean backscatter was 2.9 dB below the average backscatter of the five

previous days. They also defined a day of primary thaw as the day with the lowest (i.e., most negative) daily backscatter difference of the spring period. These thaw dates were compared to daily meteorological data from 31 field stations, and were within 1 day of mean daily air temperature transitions from frozen ( $T_{\text{avg}} \leq 0^{\circ}\text{C}$ ) to non-frozen ( $T_{\text{avg}} > 0^{\circ}\text{C}$ ) conditions 97% of the time for initial and primary thaw, and 84% of the time for final thaw.

Kimball et al., (2004b) used a similar algorithm with 2000 and 2001 SeaWinds data to determine the timing and length of growing season across a North American latitudinal transect of boreal and subalpine evergreen forest stands. In this case, minimum radar backscatter thresholds were first determined as the absolute value of twice the standard deviation of daily radar backscatter differences from a moving window average of the previous 5-day period during fall (1 September–30 November) and spring (1 March–31 May). For each study site, significant positive and negative daily radar backscatter differences were identified as those exceeding prescribed thresholds. They then identified the date of the final significant backscatter difference in spring as a surrogate for the date of growing season initiation, and the date of the initial significant backscatter difference in fall as a surrogate for the date of growing season cessation. Site growing season initiation and cessation were determined from site measurements of the first and last days of the calendar year when the evergreen trees show significant trunk (xylem) sap flow and canopy net daily  $\text{CO}_2$  uptake. Scatterometer-derived dates and independent ground measurements of growing season onset and length were correlated, with a mean difference of about  $\pm 5$  days.

In this study we compare the timing of spring 2000 snow thaw determined from the SeaWinds backscatter data with daily discharge observations across 52 small (5000–10,000  $\text{km}^2$ )

basins in Canada and Alaska. Our analysis then expands to the entire pan-Arctic drainage basin, where we compare the scatterometer-derived thaw timing with timing of daily simulated snow water content from the pan-Arctic Water Balance Model (PWBM) (Rawlins et al., 2003). Landscape and climatic factors that influence the radar backscatter temporal response and the agreement in thaw timing between the remotely sensed (scatterometer), observed (discharge), and modeled (PWBM snow content) data are explored. SeaWinds scatterometer data are evaluated here to better understand the potential benefits as well as the limitations of using microwave scatterometer data in the study of high-latitude hydrology.

## 2.2 Data Sources and Methods

Timing of snow thaw is derived from daily SeaWinds backscatter time series, daily river discharge data, and model simulated daily snow water content during spring of 2000. The spatial data is gridded to a  $25 \times 25$  km Lambert Azimuthal equal area EASE-Grid (NSIDC, 1995; Brodzik and Knowles, 2002). Our large-scale analysis encompasses the pan-Arctic drainage basin, which extends as far south as  $45^\circ\text{N}$  in southern Canada and southern Siberia (Figure 2-1). Given a lack of seasonal snow thaw, regions of permanent ice are excluded from our analysis. Areas with insufficient model snow water (described below) are also eliminated. The resulting 32,896 grid points ( $\sim 21$  million  $\text{km}^2$ ) are used to compare the estimates of snow thaw timing for 2000. To compare timing of thaw from the radar, river discharge, and model snowwater data, we identify a year-day (DOY) in each time series that marks the exceedence of a critical threshold indicative of thaw and/or subsequent runoff.

**Land Cover Fractions from MODIS  
0.5 km Product Aggregated to EASE-Grid**

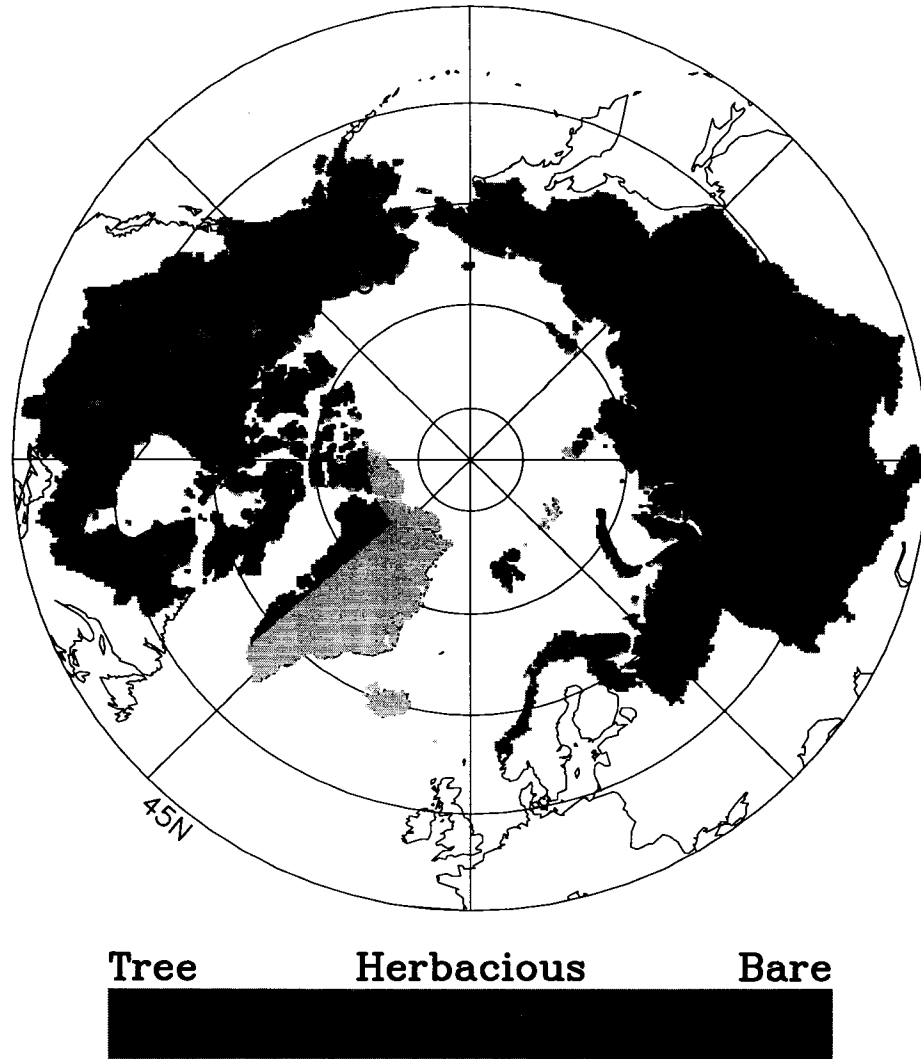


Figure 2-1: Moderate Resolution Imaging Spectroradiometer (MODIS)-derived vegetation cover (Hansen et al., 2003) across the pan-Arctic drainage basin. Colored regions show land areas which drain northward to the Arctic Ocean. MODIS cover fractions of tree, herbaceous, and bare ground sum to 100% and are shown following aggregation to the 25 km EASE-Grid. Each grid is colored with red, green, and blue intensities representing fractions of tree, herbaceous, and bare ground, respectively. Circles locate the 52 study basins (5000–10000 km<sup>2</sup>) with observed daily hydrographic data used in this study. Grids with missing MODIS data are shaded in gray.

### 2.2.1 Radar Backscatter

The SeaWinds scatterometer was launched onboard the QuikSCAT satellite on June 19, 1999 as a follow-on instrument to the NSCAT sensor, and continues to operate into 2004. The SeaWinds instrument consists of a rotating, pencil-beam antenna, which provides contiguous measurement swaths of 1400km (inner-beam) and 1800km (outer-beam), coverage of approximately 70 % of the Earth on a daily basis and 90 % global coverage every 2 days. Overlapping orbit tracks at higher latitudes improve SeaWinds temporal coverage, providing multiple backscatter measurements each day for much of the pan-Arctic land mass. We are thus able to partition the daily measurements by ascending and descending node tracks, while maintaining daily observations for each node. Ascending node data correspond to early morning observations ( $\sim$ 6:00 am equator crossing time) and descending node data correspond to late-day observations ( $\sim$ 6:00 pm equator crossing time). The instrument has mean incidence angles of  $54^\circ$  (outer-beam) and  $46^\circ$  (inner-beam) and a spatial resolution ranging from approximately 37 x 25-km ("egg" data) to 6 x 25-km ("slice" data). The SeaWinds scatterometer transmits at a frequency of 13.4 GHz (2.1 cm wavelength). Surface backscatter measurements have a 0.25 dB relative accuracy (King and Greenstone, 1999). In addition to landscape factors, backscatter from active radar systems is strongly affected by the dielectric properties of a snow (Elachi, 1987). High microwave frequencies (i.e. shorter microwave wavelengths) are best suited for observing snow processes owing to the increased scattering albedo for snow observed at these wavelengths (e.g. Ulaby et al., 1986; Raney, 1998). As water transitions from a solid to a liquid phase, its dielectric properties change significantly (Kraszewski, 1996), giving rise to a dynamic response in the surface backscatter as the snow thaws, though the magnitude of the backscatter response is

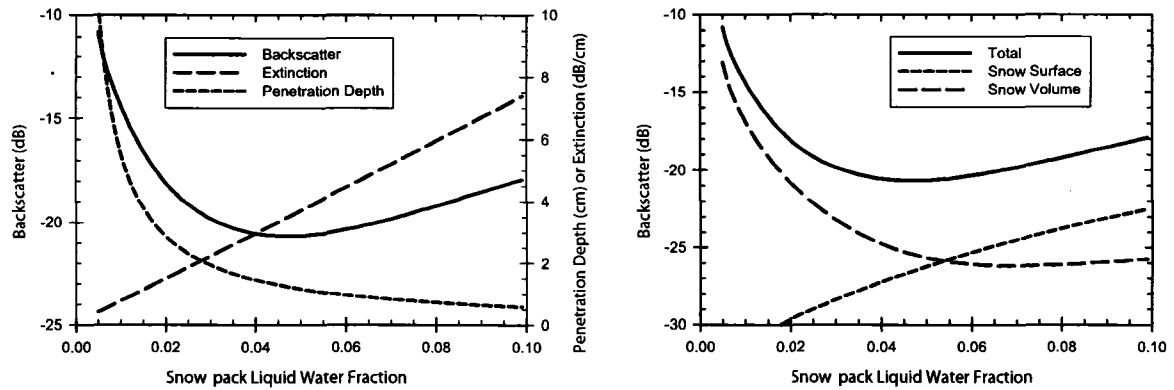


Figure 2-2: Behavior of Ku-band radar backscatter with increasing snow wetness derived using a radiative transfer radar backscatter model for a wet snow (Shi and Dozier, 1995). The model was applied at Ku-band and an incidence angle of 54 degrees, corresponding to the parameters of the QuikSCAT data applied in this study.

dependent on sensor wavelength, polarization and surface heterogeneity (Ulaby et al., 1986; Waring et al., 1995). At Ku-band, the effect of snow cover on backscatter is significant (Nghiem and Tsai, 2001). Figure 2-2 illustrates the response of Ku-band radar backscatter to increasing snow wetness as predicted with a radar backscatter model applied to a pure, wet snow (Shi and Dozier, 1995). For illustrative purposes, this theoretical snow was assigned properties of the type found in tundra landscapes (Sturm et al., 1995). For dry snow, extinction of the radar energy is small. Increases in the fractional content of liquid water in the snow result in increasing extinction, and a corresponding decrease in the radar signal penetration. This leads to a diminishing contribution of diffuse (volume) scatter to the total backscatter signal, and an increase in the scattering from the snow surface. At Ku-band, backscatter thus exhibits a marked decrease with the thaw onset. This effect is readily apparent for snow-covered tundra with little or no exposed vegetation. The magnitude of this decrease will diminish in more complex, heterogeneous landscapes where other landscape constituents affect the backscatter.

Snow thaw at each EASE-Grid cell is determined by an algorithm which identifies the temporal backscatter response in reference to background frozen conditions. Although the backscatter signal is affected by water phase transitions over the entire landscape surface element (snowcover, lakes, glaciers), we refer to the process as “snow thaw”, as lakes and glaciers make up a small fraction in each scan swath. Snow thaw events are characterized by significant daily departures (negative) from a 30 day running mean backscatter. We identify the timing of thaw based on the time-series daily ascending node data utilizing a moving window classifier. For each EASE-Grid cell, a five-day moving window is then applied to the daily ascending node measurements to produce a running five-day mean backscatter. To determine critical thaw events, each daily value is compared to the previous five-day mean. We define the primary thaw date ( $t_P$ ) as the day between DOY 60 and 182 for which the decrease in daily backscatter from the five-day mean is a maximum. More explicitly, we define the threshold

$$\delta = \overline{\sigma_5^0}(t - 5 \leq t_0 \leq t - 1) - \sigma^0(t) \quad (2.1)$$

where  $\overline{\sigma_5^0}(t - 5 \leq t_0 \leq t - 1)$  is the five day mean ascending node backscatter computed over the five day moving window preceding day ( $t$ ), and  $\sigma^0(t)$  is the ascending node backscatter for day  $t$  immediately following the five-day window. The primary thaw day ( $t_P$ ) corresponds to the day  $60 \leq t \leq 182$  where  $\delta$  is a maximum. This thaw detection algorithm is used to define  $t_P$  for year 2000 across all EASE-Grid cells defining the pan-Arctic drainage basin. Since river discharge is an integration of physical processes across a given watershed,  $t_P$  for each of the 52 basins is taken as the average of all EASE-Grid  $t_P$  within the

basin. Basin extent is determined from a digital river network developed specifically for high latitude research.

### 2.2.2 Hydrological Data

Observed daily river discharges for year 2000 are a subset of daily and monthly records for the Arctic (Lammers et al., 2001; Shiklomanov et al., 2002). Basins with a drainage area between 5,000 and 10,000 km<sup>2</sup>, were selected, since delays in thawed snow water reaching the gage at the basin outlet are known to occur in relatively larger basins. A total of 55 basin represented in R-ArcticNET have daily discharge records in 2000; all are in North America. Of these, 3 were removed from our analysis; one due to discrepancies in gage metadata for basin characteristics and two due to the known presence of impoundments. Each basin is defined by 8–16 EASE-Grid cells.

At high latitudes, thawing of the winter snow contributes the majority of freshwater input to river systems and, eventually, the Arctic Ocean (Kane, 1997; Shiklomanov et al., 2000). As with the SeaWinds backscatter data, a thresholding scheme was employed to identify a snow thaw signal in the daily discharge data; ie., the time of significant change in the discharge ( $Q$ ) time series. For each of the 52 study basins, the day of year in 2000 marking the snow thaw discharge pulse ( $t_Q$ ) is the day when  $Q$  reaches a critical threshold  $Q'$ ,

$$Q' = [(Q_{max} - \bar{Q}) \times \omega_Q] + \bar{Q} \quad (2.2)$$

where  $Q_{max}$  is the maximum daily discharge rate during January–June (m<sup>3</sup> s<sup>-1</sup>),  $\bar{Q}$  is January–February average daily discharge rate (m<sup>3</sup> s<sup>-1</sup>), and  $\omega_Q$  is the fraction defining



a critical exceedence (unitless). This algorithm is constrained to identify the critical exceedence following the seasonal (January–June) discharge minimum. For ten study basins with zero or missing discharge during January–February,  $\bar{Q}$  becomes the average March  $Q$ . We chose  $\omega_Q = 0.1$  to determine  $t_Q$  in this study. This thaw detection algorithm is not calibrated to the respective basin discharge. Rather, the algorithms for determining SeaWinds-based snow thaw (equation 2.1) and basin discharge increase (equation 2.2) were independently chosen based on our understanding of the processes controlling backscatter temporal response and subsequent discharge increase.

Observed daily discharge data provide a key measure of spring thaw timing to evaluate the SeaWinds backscatter. Daily discharge data, however, are available for only a fraction of the pan-Arctic basin. Therefore we use snow liquid water content from the pan-Arctic Water Balance Model (PWBM) (Rawlins et al., 2003). The PWBM is driven by climate time series (precipitation and air temperature) from the National Center for Environmental Prediction (NCEP) reanalysis project (Kalnay et al., 1996; Uppala et al., 2000), along with gridded fields of plant rooting depth (Vörösmarty et al., 1989) and soil characteristics of texture (Food and Agriculture Organization/UNESCO, 1995) and organic content (Global Soil Data Task, 2000). The NCEP/NCAR Reanalysis (NRR) Project is an effort to reanalyze historical data using state-of-the-art models. Reanalysis provides a modern depiction of the atmospheric hydrological budget using the Medium Range Forecasting (MRF) spectral model and the operational NCEP spectral statistical interpolation (SSI, Parish and Derber 1992). Input and output data sets, like the scatterometer data, are gridded on the 25 km EASE-Grid across the pan-Arctic basin, and the model is run at an explicit daily time step for the year 2000. Estimates of PWBM winter 1999–2000 snowfall are determined using

air temperatures from NCEP and rescaled NNR precipitation products. Six-hourly NNR precipitation forecasts (at  $2^\circ \times 2^\circ$  resolution) are aggregated to daily means and interpolated to the 25 km resolution EASE-Grid using a statistical downscaling approach based on a probability transformation (Serreze et al., 2003b). Precipitation occurring on days with a mean surface air temperature of  $\leq -1^\circ\text{C}$  is considered snow and is accumulated from October through May to estimate total winter snowfall as snow water equivalent (*SWE*, mm). PWBM snow thaw is driven by NNR air temperature in a simple temperature index method (Willmott et al., 1985). From the snow liquid water content we define date of snowwater initiation ( $t_M$ ) as the DOY when snow water is greater than zero for three consecutive days.

### 2.2.3 Land Surface Data

Continuous fields of land cover fraction from the Moderate Resolution Imaging Spectroradiometer (MODIS) 0.5 km vegetation continuous field data set (Hansen et al., 2003) were aggregated to the pan-Arctic EASE-Grid. The MODIS land cover data set is an annual representation of tree, herbaceous, and bare ground cover for the period November 2000 to November 2001. Continuous fields of vegetation fraction offer better representation than discrete classifications in areas of high spatial heterogeneity. The three cover fractions sum to 100 %, and the 0.5 km MODIS grid cells were aggregated to the EASE-Grid (Figure 2-1) using spatial averaging. Given a high degree of uncertainty in the backscatter temporal response across ice, a data set which depicts the distribution and properties of permafrost and ground ice in the Northern Hemisphere (Brown et al., 1998) is used to mask these regions from our statistical analysis. Elevation and elevation standard deviation estimates

are scaled to the EASE-Grid from the GTOPO30 data set (Gesch et al., 1999; USGS EROS Data Center, 1996). High variations in regional elevation or “topographic complexity” is determined by calculating the standard deviation of 5 minute GTOPO30 digital elevation model (DEM) elevations within each EASE-Grid cell.

### 2.3 Comparison of SeaWinds-Derived Thaw Timing and Hydrological Response

Methods described in section 2.2 were used to estimate timing of snow thaw inferred from the SeaWinds scatterometer ( $t_P$ ), observed discharge ( $t_Q$ ), and PWBM simulated snow liquid water content ( $t_M$ ) for each of the 52 study basins. River discharge is converted to a basin-averaged runoff depth (per unit area) by dividing a basin’s discharge by the basin area (Lammers et al., 2001). Across the Kugaruk basin (Figure 2-3a), a stable early season backscatter signal precedes a large signal decrease ( $\sim 8$  dB) during snow thaw. PWBM snow water increase is well timed with the scatterometer response. Observed runoff increases soon thereafter. As opposed to the stable winter and large signal decrease seen across the Kugaruk, the Murray basin (mountainous, forested) experienced several backscatter decreases near DOY 50 (mid February), 62 (early March), 80-90 (late March), and DOY  $\sim 110$  (mid April) (Figure 2-3b). Model snow water increases are noted for the latter 3 events, resulting in a basin average  $t_M = \text{DOY } 101$ . Although the time series is quite dissimilar from the backscatter signal across the Kugaruk, basin-average values for  $t_P$  and  $t_M$  are nearly coincident. Observed basin runoff lags snow thaw in this region by  $\sim 10$  days. The Whitemud basin in southern Manitoba, Canada experienced low snowfall and runoff

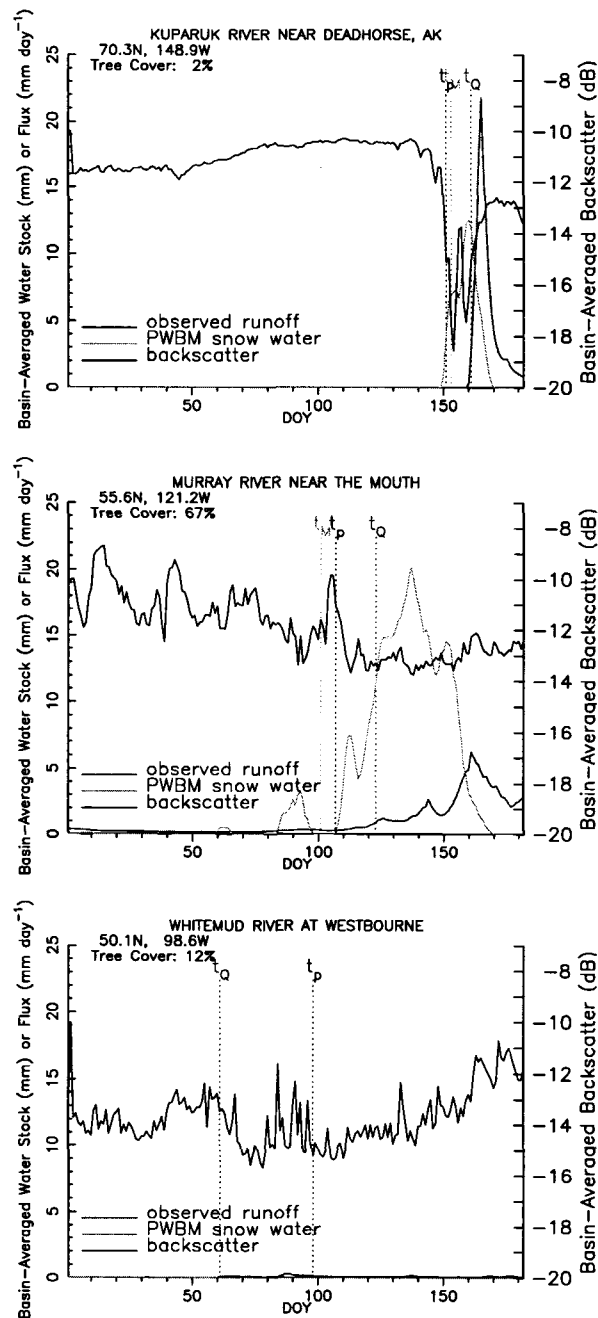


Figure 2-3: Observed basin-average runoff, model snow water content, and daily SeaWinds backscatter for three of the 52 study basins, the Kuparuk (a), Murray (b), and Whitemud (c) basins. Dotted vertical lines mark dates of snow thaw-driven discharge increase ( $t_Q$ ), model snow water initiation ( $t_M$ ), and scatterometer-derived primary thaw ( $t_P$ )

during the first half of 2000 (Figure 2-3c). Snow water initiation date ( $t_M$ ) is undefined across this basin, as relatively shallow snowcover is lost primarily through sublimation, with little or no simulated snow liquid water content. The backscatter signal lacks a stable winter signature and strong response during thaw which is noted in regions with continuous, ample snowcover (eg, Kuparuk River basin, figure 2-3a). Although the signal response is fairly confused, possible thaw events near days 65 and 90 are reflected in both the SeaWinds backscatter and observed runoff. Across the Kuparuk, Murray, and, to some extent, the Whitemud basin, decreases in backscatter correlate with the PWBM snow water content, which is strongly influenced by the simulated air temperatures. This agrees with the results of Wiseman (2000a) who found that the onset of scatterometer-derived thaw was correlated with air temperature and snow cover.

Our analysis here focuses on timing of scatterometer-derived primary thaw and basin runoff increase across a wide range of North American climate and landscape zones. This comparison is based on the assumption that thaw observed by the SeaWinds scatterometer has an effect on the local streamflow measured by the discharge gage. In order to represent an amount of discharge attributed to snow thaw, a snow runoff index ( $snowRO$ ) is defined  $snowRO = RO_S - 3 RO_W$ , where  $RO_S$  is total basin-average runoff from January–June and  $RO_W$  is total January–February runoff, all in mm for a given river basin. A large positive value of  $snowRO$  indicates proportionally more of the basin’s river discharge occurs after February and therefore is more likely to be the result of snow thaw. Abundant snow is an important factor in the backscatter response, since the lowest backscatter values are likely to occur when the basin has an extensive, wet snow. Thin or inhomogeneous snow will compromise the determination of thaw timing. In addition, discharge increases are not

always dominated by snow thaw processes. Across the 52 study basins, correspondence between  $t_P$  and  $t_Q$  is best for later thawing basins (Figure 2-4a). Across the 52 basins, the mean absolute difference ( $MAD = \frac{1}{52} \sum_{i=1}^{52} |t_Q - t_P|$ ) is 21.5 days ( $r = 0.45$ ). The mean bias ( $MB = \frac{1}{52} \sum_{i=1}^{52} t_Q - t_P$ ) is 6.1 days. Poorer agreement is evident for the basins where discharge increase occurs earliest ( $t_Q < 73$ ). Agreement between  $t_P$  and  $t_M$  ( $MAD = 14.1$  days,  $r = 0.75$ ) is comparable to the  $t_P, t_Q$  relationship.  $MB$  for the  $t_P$  and  $t_M$  comparison is only  $-2.2$  days. Sensitivity to the choice of  $\omega_Q$  is not substantial. Defining  $\omega_Q = 0.1$  results in  $r = 0.50$  and  $MAD = 19.2$  days. For  $\omega_Q = 0.15$ ,  $r = 0.41$  and  $MAD = 24$  days. Discrepancies are lower across basins with moderate–high *snowRO* index (Figure 2-4b). The discrepancy or difference between the two dates is largely a result of lags in snow thaw at the soil surface reaching the river system. Although the study basin sizes have been minimized to eliminate longer travel times, a bias between snow thaw and observed discharge increase is expected. Lags such as damming of snow thaw runoff has been shown to cause delays in streamflow increases during spring at high latitudes (eg, Hinzman and Kane, 1991). Since  $t_P$  and  $t_M$  are determined for the same process, the bias ( $-2.1$  days) is lower. Considerable discrepancies are found for the basins with the lower *snowRO* index. These larger discrepancies may result from errors in the scatterometer snow thaw identification as well as deficiencies in the discharge algorithm for the driest basins. For example, the thresholding scheme to identify  $t_Q$  (Equation 2.2) is unable to capture discharge/runoff increases across the basins with variable winter flow and small increases during spring. Large negative discrepancies occur predominately across the basins with lower tree cover (Figure 2-4c), many of which are drier prairie basins with low *snowRO* (open circles in Figure 2-4c). Good agreement is noted for moderate (20–50%) tree cover,

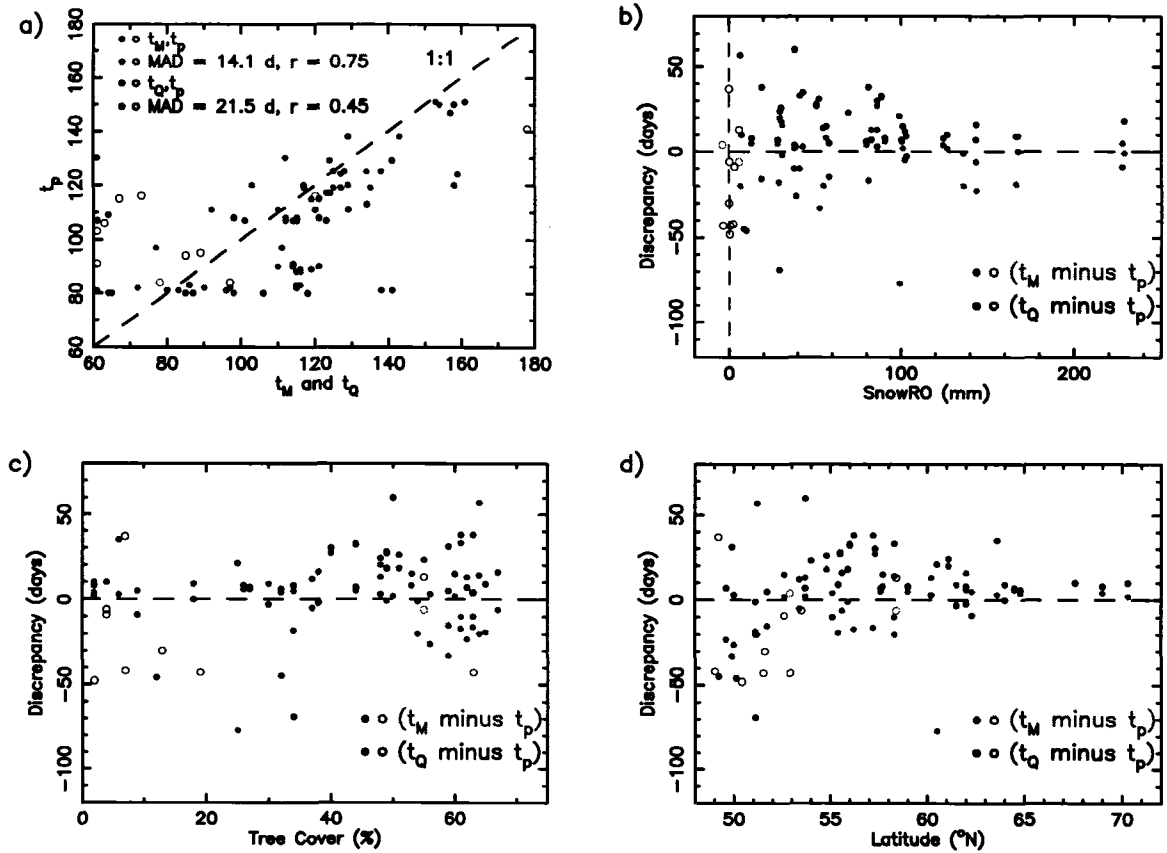


Figure 2-4: Comparison of hydrological event dates ( $t_Q$ ,  $t_M$ ) and scatterometer-derived thaw date ( $t_P$ ) for the 52 study basins with observed discharge data. Comparisons between  $t_Q$  and  $t_P$  are in black.  $t_P$  vs.  $t_M$  relations are shown in red. Open circles in (a–d) identify the 10 basins with the lowest snow thaw runoff values. Discrepancies ( $t_Q - T_P$ ,  $t_Q - T_P$ ) are expressed as a function of snow thaw-driven runoff (b), MODIS fractional tree cover (c), and latitude (d).

with the largest positive discrepancies for basins with highest tree cover. Higher latitude sites have lower discrepancies (Figure 2-4d). This is intuitively expected, as high latitude basins with frozen soils during thaw season have a lower soil infiltration capacity, causing a quicker streamflow response following snow thaw.

## 2.4 Comparison of Snow Thaw Timing across the Pan-Arctic Domain

Given a lack of observed daily discharge data across much of the pan-Arctic drainage basin, we make use of the relatively good correspondence between scatterometer thaw timing ( $t_P$ ) and timing from the PWBM snow water content ( $t_M$ )—determined across the 52 study basins with observed discharge—to examine the spatial pattern of the pan-Arctic discrepancies ( $t_M - t_P$ ). Across the pan-Arctic basin, a spatially-coherent pattern in  $t_P$  is evident (Figure 2-5). Areas of permanent ice (shown in gray) are excluded from the large-scale statistical analysis. Across Canada, a noticeable gradient exists where the boreal forest transitions to high-latitude tundra. Across the prairies,  $t_P \geq 160$  are suspiciously late. Snow thaw occurs earliest in the boreal forest ( $t_P \sim 80$ ) in Canada and western Eurasia, while thaw progresses in a general south to north pattern across the entire pan-Arctic. High elevations in eastern Asia are well resolved, with thaw occurring 7–10 days later than the surrounding lowlands. High spatial variations are noted in the boreal forest and mountainous areas in central Eurasia.

The spatial pattern in  $t_M$  (Figure 2-6) is, in general, similar to the pattern in  $t_P$ . In addition to regions of permanent ice, areas lacking three consecutive days of PWBM snow water (shaded in yellow) are eliminated from the statistical analysis. In contrast to  $t_P$  patterns, the  $t_M$  field is more smooth, lacking the high spatial variations (speckled pattern) across much of the Arctic. This result is attributable to coarse NNR climate inputs (derived from sparse weather stations) driving the PWBM model. High spatial variations in  $t_P$  across central Eurasia arise from the effects of tree cover and elevation variations on the backscatter



## Date of Primary Thaw in 2000 from SeaWinds

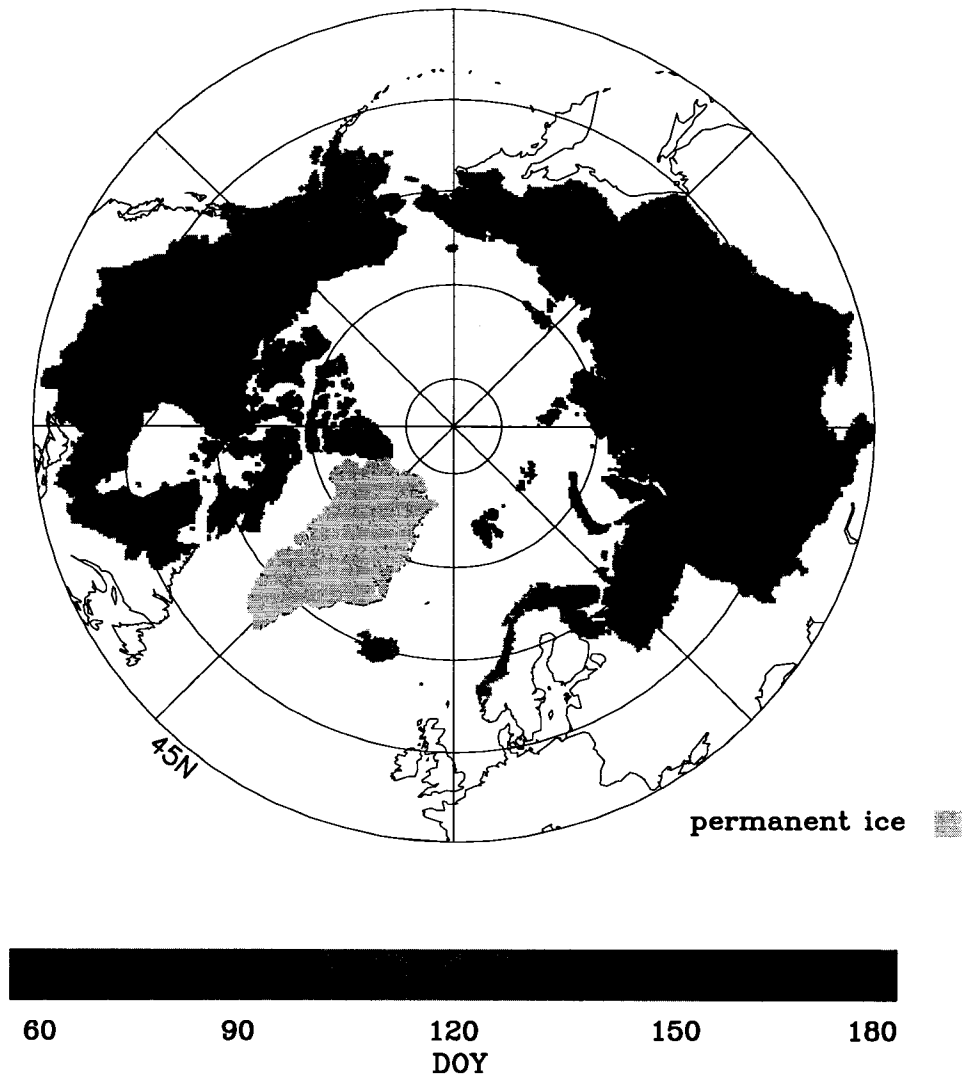


Figure 2-5: Primary thaw date ( $t_P$ ) derived from the SeaWinds scatterometer for year 2000. A moving window algorithm is used to determine timing of final thaw from SeaWinds ascending pass data at each EASE-Grid cell of the pan-Arctic drainage basin (see text for details). Grid cells across Greenland and other areas of permanent ice are masked in gray due to the limited presence of snow thaw.

## Date of Snowmelt Initiation in 2000 from PWBM

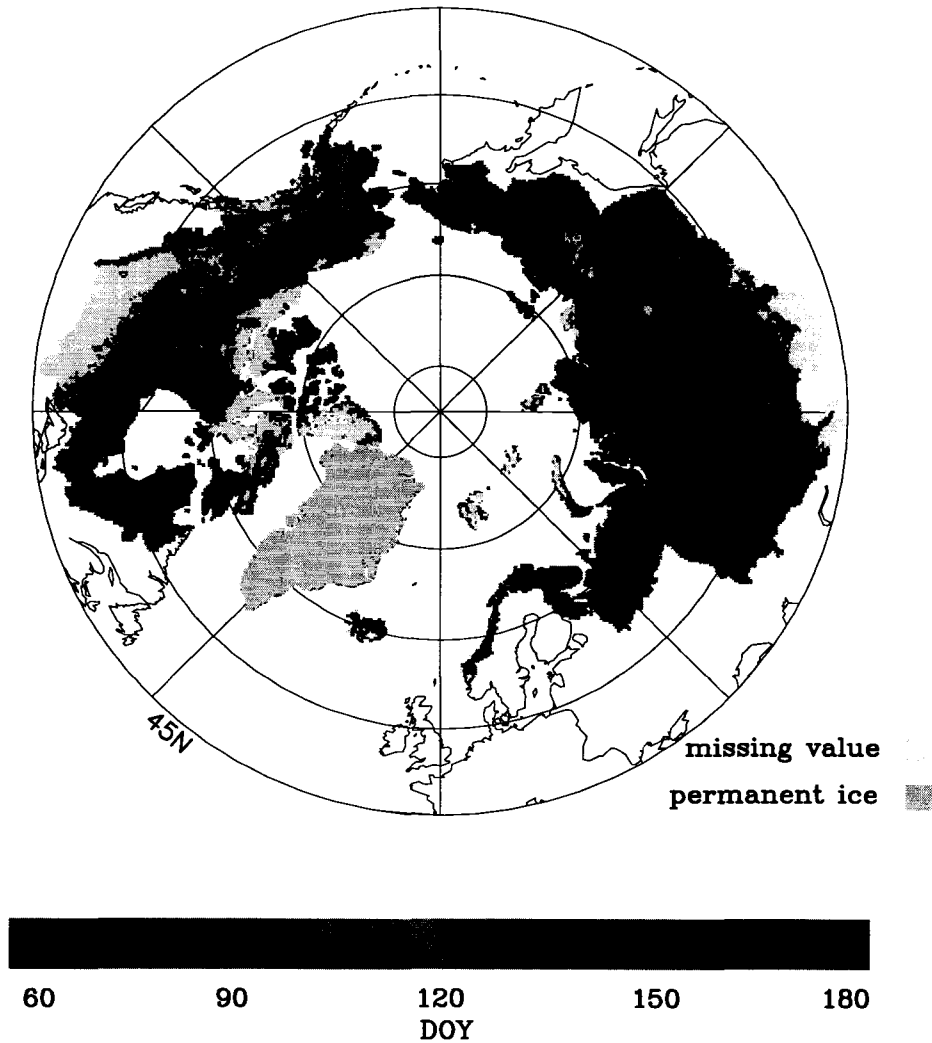


Figure 2-6: Snow water initiation date ( $t_M$ ) for year 2000 derived from the pan-Arctic Water Balance Model (PWBM) (Rawlins et al., 2003). Gray shading masks regions of permanent ice and yellow shows grid cells where  $t_M$  is undefined, i.e., PWBM snow water is never  $> 0$  mm for 3 consecutive days during spring 2000. Gray and yellow regions are excluded in our statistical analysis. These regions generally have low total 1999-2000 snowfall, additionally limiting both our analysis and the SeaWinds backscatter response.

## Difference Between PWBM Snowmelt Initiation Date and Scatterometer-Derived Primary Thaw Date

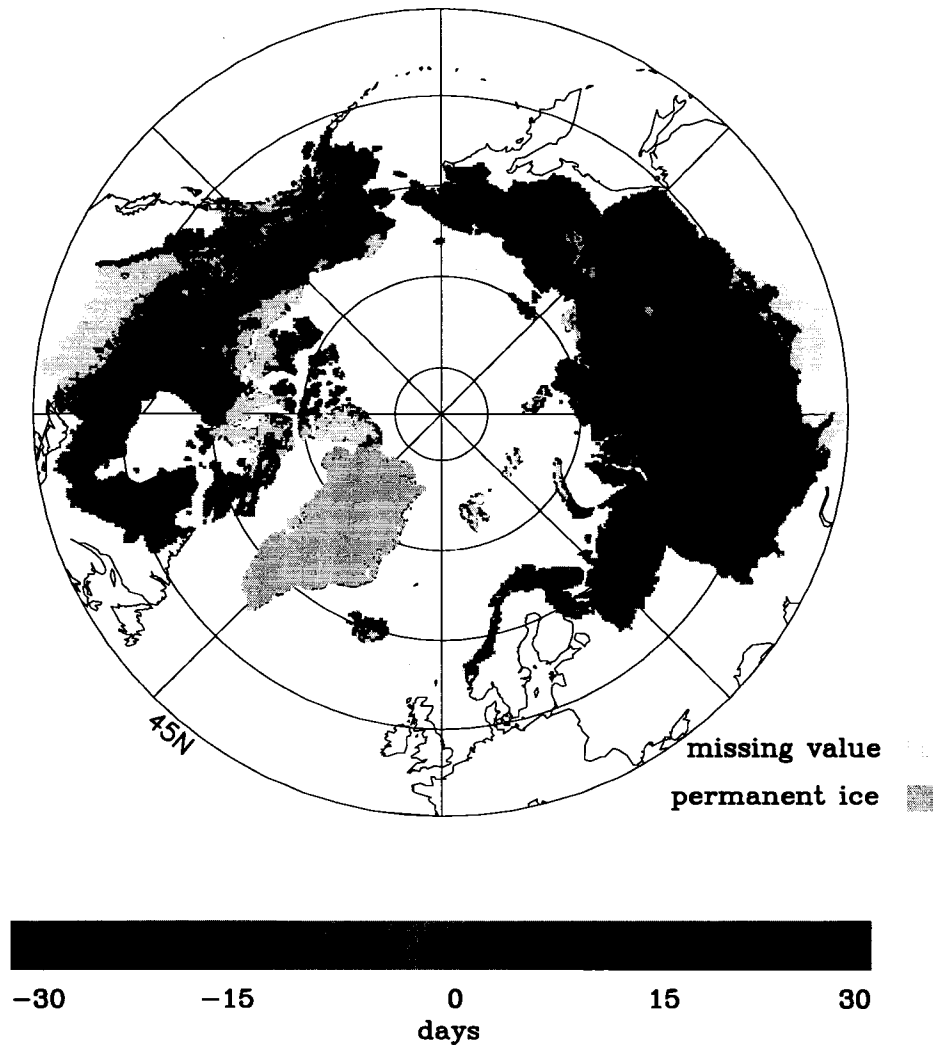


Figure 2-7: Difference between PWBM snow water initiation date ( $t_M$ ) and scatterometer derived primary thaw date ( $t_P$ ) for 2000 across the pan-Arctic drainage basin. Gray and yellow grids are excluded from statistical analysis (see Figure 2-6). Areas with large (MAD > 15 days) differences are characterized by several thaw events throughout spring, and are largely due to identification of two thaw events ( $t_M$  for one event,  $t_P$  for another) separated by 2-3 weeks.

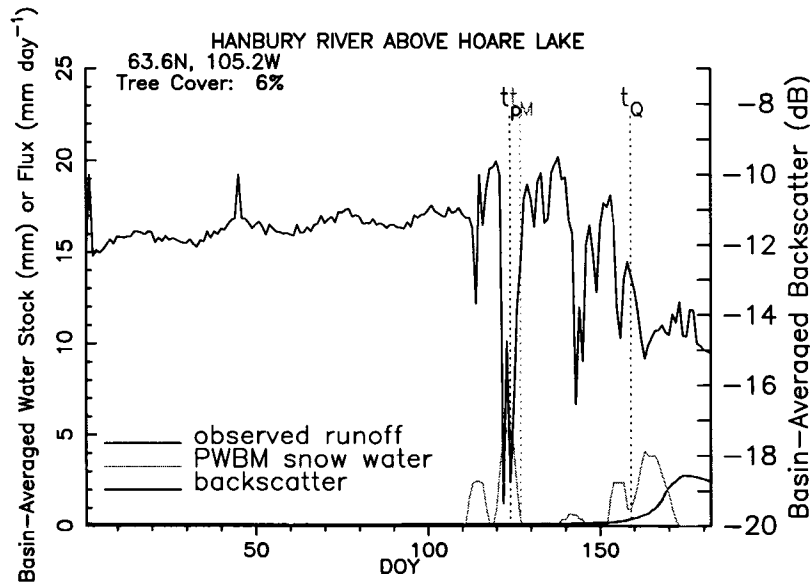


Figure 2-8: Observed basin-average runoff, model snow water content, and daily SeaWinds backscatter for the Hanbury basin. This basin experienced significant thawing near DOY 126 and 141, with a final basin thaw close to DOY 155.

response. Along coastal sections,  $t_M$  tends to occur early due to the wet maritime climate and frequent early spring freeze/thaw conditions. Best agreement between  $t_M$  and  $t_P$  is found across the tundra of central and northwestern North America, eastern Russia, and eastern Siberia (Figure 2-7). Large negative discrepancies dominate the coastal locations—southern Alaska, across Iceland and Norway. Across the pan-Arctic basin, 49.4% of the grid cells have discrepancies of less than one week. The spatially averaged mean absolute difference ( $MAD$ ) is 11.7 days across Eurasia and 15.1 days over North America. Mean biases ( $MB$ ) are low across Eurasia (1.2 days) and North America ( $-3.1$  days) regions. Larger discrepancies ( $MAD > 15$  days) tend to occur in regions which experienced two or three distinct thaw events during spring of 2000. For example, the nature of large discrepancies can be illustrated by examining the scatterometer and hydrographic data across the Hanbury River basin in central Canada (Figure 2-8).

Although the algorithms for identifying  $t_P$  (equation 2.1) and  $t_M$  both identify primary thaw near DOY 126, the scatterometer response in neighboring grid cells results in  $t_P$  (primary thaw) being defined as the second thaw event near DOY 141. Based on the observed discharge data, final snow ablation across the Hunbury basin and nearby regions may in fact occur shortly after DOY 150. The majority of large discrepancies across the pan-Arctic arise under similar conditions; multiple thaw-freeze events are captured by the  $t_P$  (for one event) and  $t_M$  (a second event) algorithms. Nonetheless, approximately 60% of the discrepancies ( $t_M - t_P$  at each EASE-Grid) are between  $\pm 10$  days (Figure 2-9). Over 15% of the pan-Arctic annual runoff occurs at grids with discrepancies in excess of  $-15$  days (primarily coastal regions). This leads to approximately 60% of the annual runoff occurring at grids cells with discrepancies between  $-22$  and  $10$  days. Thus, the wet coastal locations tend to decrease the correspondence (ie., spatial statistics) between PWBM snow thaw- and scatterometer-derived estimates of pan-Arctic snow thaw timing. Grid cells encompassing over half of the 21 million  $\text{km}^2$  area analyzed have discrepancies of less than 1 week (inset of Figure 2-9).

Landcover effects on the backscatter signal can be explored by defining a signal-to-noise value ( $R$ , unitless). We use the maximum decrease in daily backscatter from the five-day mean (used to obtain  $t_P$ , equation 2.1) for signal, with noise defined as the average absolute deviation of daily backscatter (December 1999–February 2000) from the backscatter running 5-day mean. Areas with stable snow cover seen by repeated instrument scans are expected to have low backscatter variability during Dec–Feb (see Figure 2-3a). Values of  $R$  are strongly correlated with tree cover, seasonal snowfall, and topographic complexity across the pan-Arctic, excluding Greenland. Across relatively flat regions (Figure 2-10a), the

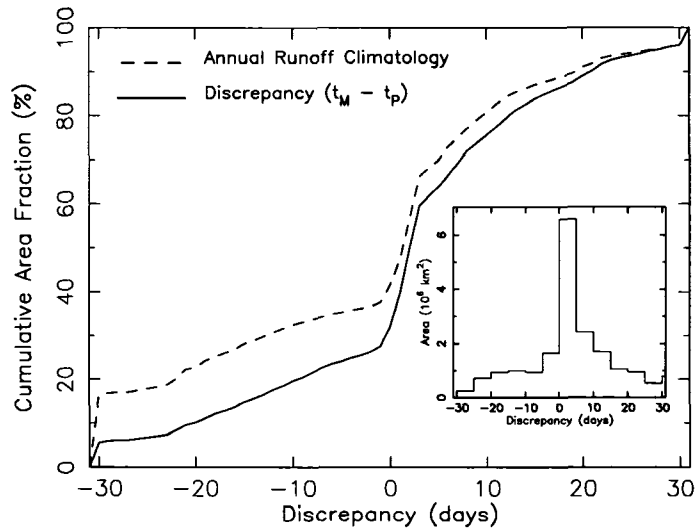


Figure 2-9: Cumulative area histograms for  $t_M - t_P$  discrepancies (solid line) and annual runoff climatology (dashed line). Curves are generated by summing the area for ordered discrepancies from least to greatest across all 32,896 analyzed grid cells (Figure 2-7). Histogram of total area for discrepancies is shown in inset.

largest  $R$  values occur with low tree cover and moderate–high snowfall. Strong correlations are also noted for moderately complex topography (Figure 2-10b). Regions with the highest topographic complexity generally have low  $R$  values for all tree cover/snowfall classes (Figure 2-10c). High snowfall in this group occur in grid cells across southeast Alaska, a region dominated by a highly variable maritime polar climate and high topographic complexity. Grid cells for Alaska in this group (snowfall > 1000 mm) do not drain directly to the Arctic Ocean. Wet winter storms along with frequent thaw events cause relatively high backscatter variability during winter and spring, leading to lower  $R$  values. For southeastern Alaska and similar regions, variable snow cover across opposing slopes, the presence of permanent ice and glaciers, and a highly dynamic, maritime winter/spring precipitation regime adversely affect our ability to extract a single, consistent radar backscatter spring thaw response.

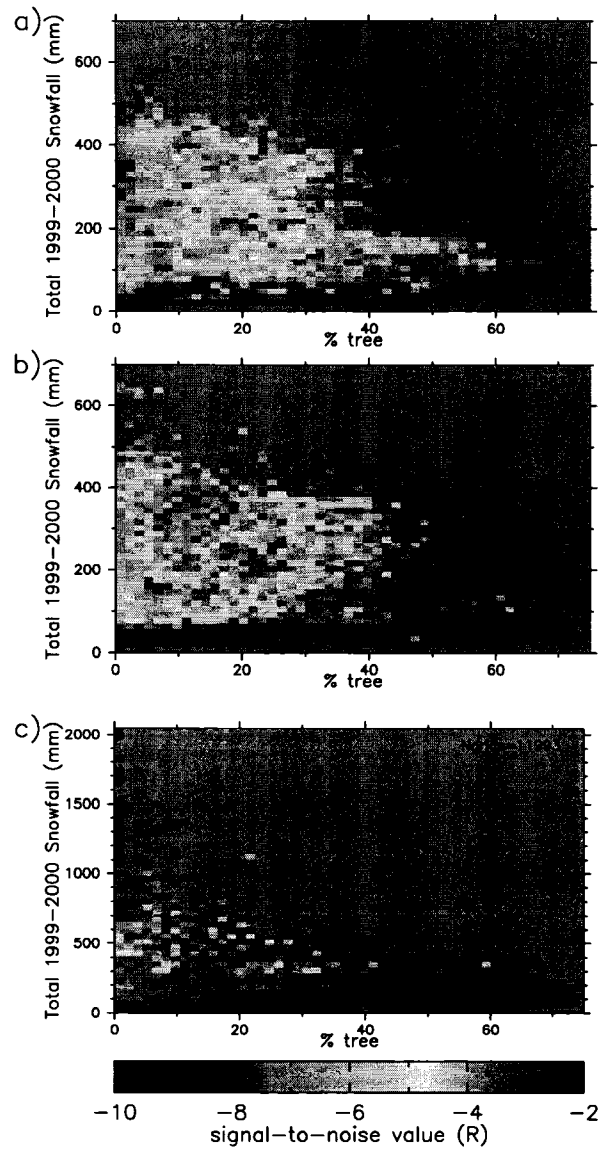


Figure 2-10: Average signal to noise value ( $R$ ) grouped by percent tree cover and total 1999–2000 winter snowfall for (a) low (elevation standard deviation  $\leq 14.8$  m), (b) moderate ( $14.8 \text{ m} < \text{elevation standard deviation} \leq 52.2$  m), and (c) high (elevation standard deviation  $> 52.2$  m) topographic complexity.  $R = \delta_{max} - \sigma_{DJF}$ , where  $\delta_{max}$  is the maximum daily backscatter departure from previous 5-day backscatter average (Equation 2.1) and  $\sigma_{DJF}$  is the average absolute deviation of daily backscatter (December 1999–February 2000) from the running 5-day mean. Plotted values are the average of all data in the two-dimensional tree cover/snowfall bin. The horizontal dotted line in (c) represents the extent of ordinate in (a) and (b).

## 2.5 Discussion of Results

Approaches to estimating spring snow thaw at regional and continental scales are usually dependent on meteorological data (air temperature, precipitation, radiation) from a network of stations which, one assumes, can resolve the complex spatial variations in thaw. Across the pan-Arctic drainage basin, meteorological station density is sparse, which introduces a degree of uncertainty in thaw estimates. Timing of spring snow thaw inferred from the SeaWinds scatterometer was compared to timing from two hydrological measures at 52 basins (5,000–10,000 km<sup>2</sup>) in Canada and Alaska to evaluate the correspondence between timing estimates from the remotely sensed, observed, and modeled data.

Agreement between timing of discharge increase ( $t_Q$ ) and scatterometer-derived thaw date ( $t_P$ ), determined as mean absolute deviation ( $MAD$ ), averages 21.5 days ( $r = 0.45$ ). The mean bias  $MB$  is 6.1 days. The  $MAD$  is not unexpected given delays in snow thaw reaching stream systems which are known to occur, but difficult to model. Future studies which use field snow thaw snow water equivalent and snow thaw timing information will be useful in further evaluating the discrepancies presented here. The  $MAD$  between PWBM snow water initiation ( $t_M$ ) and  $t_P$  are lower (14.1 days,  $r = 0.75$ ), since  $t_M$  and  $t_P$  are identifying the same process (snow thaw) which should precede the spring increase in discharge. Both comparisons show good correlations for basins with moderate to high runoff attributed to snow thaw. Individual discrepancies tend to be higher for more heavily forested watersheds (tree cover > 50%) and the dry prairie basins. The correspondence between  $t_Q$  and  $t_P$  (and  $t_M$ ,  $t_P$ ) is best for high latitude basins. A critical component of our comparisons using  $t_Q$  involves the assumed presence of a measured hydrographic re-



sponse to snow thaw. The analysis here included several watersheds with low snow amounts and small discharge increases in spring. These relatively low river flows introduce a degree of error in our identification of discharge increase. Moreover, in many areas, particularly along warmer southerly margins and maritime regions of the pan-Arctic, our assumption of a single major snow thaw and discharge event in spring may not be valid. These areas tend to exhibit frequent snow thaw and discharge responses during winter and early spring from periodic warming events. The timing of  $t_Q$  and  $t_P$  across many regions suggest lags in the discharge increase following snow thaw, with shorter delays in high-latitude basins and longer lags to the south. Lags in the discharge response to snow thaw are expected due to known delays such as snow damming and lags in groundwater transport. Lags in timing are also related to differences in the infiltration capacity of permafrost and seasonally frozen soils. Future studies in specific moderate-sized watersheds involving scatterometer-derived timing of snow thaw could be useful in understanding the spatial pattern of lags between snow thaw and hydrological response as well as the factors contributing to the delays in snow thaw reaching Arctic river systems.

Good agreement between  $t_M$  and  $t_P$  across the 52 North American basins provide the motivation for expanding our analysis to the entire pan-Arctic drainage basin. Of the 32,896 analyzed grid cells almost half (49.4%) have  $t_M - t_P$  discrepancies of less than one week. Correspondence is slightly better across the Eurasia ( $MAD = 11.7$  days) as opposed to North America (15.1 days). Biases across both Eurasia and North America are low; 1.2 and  $-3.1$  days, respectively. Agreement between  $t_M$  and  $t_P$  is generally higher across tundra regions and lower along coastal margins. Larger discrepancies are primarily due to the identification of two separate thaw events by the  $t_M$  and  $t_P$  algorithms. That is, regions

with higher discrepancies tend to be characterized by multiple thaw events through spring of 2000 and our algorithms selected different events. A majority of the  $t_M - t_P$  discrepancies are within  $\pm 10$  days.

Although signal-to-noise values are highest for regions of low tree cover, low topographic complexity, and high winter snowfall, the spatial pattern of discrepancies in timing is influenced by climatic type (eg, the presence of multiple spring freeze/thaw cycles) as well as landscape factors. Our analysis show that the best correspondence occurs at high latitude interior basins, areas which are most lacking in meteorological observation stations. Results of this study suggest that the SeaWinds backscatter is correlated with observed discharge (given lags between snow thaw and hydrographic response) and model simulated snow thaw. Further studies are needed to determine if active radar instruments will be more useful for estimating spatial patterns of thaw than a absolute data of thaw. Research focusing on the influence of geophysical factors on radar response are also warranted. Although not studied here, future studies examining thaw timing from passive microwave time series may prove useful for trend analysis of pan-Arctic snow thaw timing.

## CHAPTER 3

# EVALUATION OF TRENDS IN DERIVED SNOWFALL AND RAINFALL ACROSS EURASIA

### 3.1 Changes in the Arctic Hydrological Cycle

Changes are occurring in the Arctic climate and hydrological cycles (Serreze et al., 2000; Peterson et al., 2002). Increasing winter-average air temperatures (Rawlins and Willmott, 2003), reductions in sea-ice thickness and extent (Serreze et al., 2003b), and a significant increase in river discharge of  $0.22 \text{ mm yr}^{-1}$  from 1936–1999 across Eurasia (Peterson et al., 2002) have been documented. River discharge increases have the potential to impact global climate through alterations in the oceanic thermohaline circulation (Rahmstorf, 1995; Broecker, 1997). Warming is predicted to enhance atmospheric moisture storage resulting in increased net precipitation, since precipitation increases will likely exceed evaporative losses (ACIA, 2005).

With the potential for increased net freshwater input to the terrestrial Arctic, precipitation emerges as a likely source for the observed discharge trend. In a study of the possible effects of dams, melting of permafrost, and fires on river discharge, McClelland et al. (2004) suggested that increased precipitation is the most plausible source for the observed discharge trend. Annual total precipitation, however, has generally decreased across the three largest

Eurasian basins since 1936 (Berezovskaya et al., 2004). Given this apparent disagreement between precipitation and river discharge, analysis of changes in seasonal precipitation is relevant to our understanding of the discharge trends. Indeed, increases in spring runoff across the Yenisey basin in central Eurasia during the period 1960–1999 have been linked with an increase in winter precipitation and earlier snowmelt (Serreze et al., 2003a). Acknowledging the challenges in deriving climate change signals from a sparse network of observations which contain numerous uncertainties, our study analyzes seasonal precipitation drawn from historical station data to better understand the role of precipitation in the river discharge increases from Eurasia.

## 3.2 Data and Methods

Monthly station precipitation ( $P$ ) time series are taken from NCDC’s Dataset 9813, “Daily and Sub-daily Precipitation for the Former USSR” (National Climatic Data Center, 2005), which originated at the Russian Institute for Hydrometeorological Information-World Data Center of the Federal Service for Hydrometeorology and Environmental Monitoring, Obninsk, Russian Federation. Precipitation records in this archive (hereinafter TD9813) contain adjustments to account for wetting losses i.e. moisture on the gauge walls, changes in gauge type and observing practices, and wind-induced errors (see TD9813 documentation and references therein). Among these inconsistencies, the undercatch errors due to aerodynamic effects of wind are generally greatest, particularly in winter (Table 1, Groisman et al., 1991). Bias due to change in gauge type are also significant, while wetting losses are typically smallest. Biases adjustments are vital in order to accurately ascertain “true”

changes in precipitation over time (Yang et al., 2005; Forland and Hanssen-Bauer, 2000). We also use monthly  $P$  and air temperature ( $T$ ) data from the Willmott–Matsuura (WM) archive (Willmott and Matsuura, 2001) and from CRU v2.0 data (Mitchell et al., 2004). Monthly  $P$  from TD9813 were interpolated to the 25 km×25 km EASE-Grid using inverse-distance-weighted interpolation. CRU  $T$  and  $P$  at  $0.5^\circ \times 0.5^\circ$  resolution were sampled at each EASE-Grid. In contrast to the new TD9813 archive, CRU and WM data contain no adjustments for biases in the precipitation records. Spatial aggregations of the gridded data are made across the 6 largest Eurasian river basins; the *Severnaya Divina*, *Pechora*, *Ob*, *Yenisey*, *Lena*, and *Kolyma*. Annual snowfall (water equivalent) at each grid is calculated by examining  $T$  each month to estimate the fraction of monthly  $P$  as snowfall, and then summing those monthly snowfall amounts over the year. The ratio ( $R$ ) of monthly snowfall to total monthly  $P$  is:  $R = [1.0 + 1.61 \cdot (1.35)^T]^{-1}$ , where  $T$  is the monthly mean in  $^\circ\text{C}$  and  $0 \leq R \leq 1$  (Legates and Willmott, 1990a). This function was derived using a logistic curve fit to monthly data and has a reported mean absolute deviation of  $0.06 \text{ mm month}^{-1}$ . Annual rainfall in a given year is total from the monthly amounts using  $P \cdot (1 - R)$ . River discharge ( $Q$ ) records are drawn from an updated version of R-ArcticNET (Lammers et al., 2001).

Slope and significance from ordinary least squares regression are computed for spatially averaged annual rainfall across the Eurasian basin and for rainfall/snowfall at each EASE-grid over the region. A change-point regression method (Draper and Smith, 1981; Müller et al., 1994) was applied for annual snowfall integrated over the Eurasian basin given the shape of the time series. This method determines optimal mid-series change-points by minimizing the sum of squared residuals of all possible change-point regressions. Serial

autocorrelation was assessed graphically by plotting autocorrelation functions and numerically by calculating Durbin-Watson test statistics. Temporal correlations were not found at a 5% significance level.

Potential biases in spatial  $P$  induced when gridding from irregular station networks was estimated by attempting to recreate total precipitation in 1972 using the available station networks each year from 1936–1999. In 1972 the station network was most dense, with 1549 and 341 stations having complete records across the former USSR and within the Eurasian basin, respectively. Starting from the 1972 station network, we sampled annual  $P$  at only those stations in operation each year for 1936, 1937...1999. Those subsets of station  $P$  were then interpolated to the grids prior to spatial averaging across the Eurasian basin.

### 3.3 Linkages between Precipitation and Discharge

A significant correlation ( $p < 0.01$ ) is noted among all three precipitation time series for the Eurasian basin (Figure 3-1). Annual precipitation is also correlated with annual discharge ( $p \sim 0.05$  for TD9813), although the Pearson's correlation coefficient is low ( $r = 0.26, 0.41, 0.35$ , for TD9813, CRU, and WM respectively.) Correlations are not expected to be high given year-to-year changes in water storage over the landscape. The correlation over the period 1936-1970, however, is 0.55, 0.56, and 0.53, respectively. Thereafter, annual discharge increases yet precipitation declines. Discharge/precipitation ( $Q/P$ ) ratios are highest between 1970-1990 (inset Figure 3-1).

Estimating snowfall increases over northern lands is important, since snowmelt there occurs on frozen soils with low infiltration rates. A relatively small fraction of this water

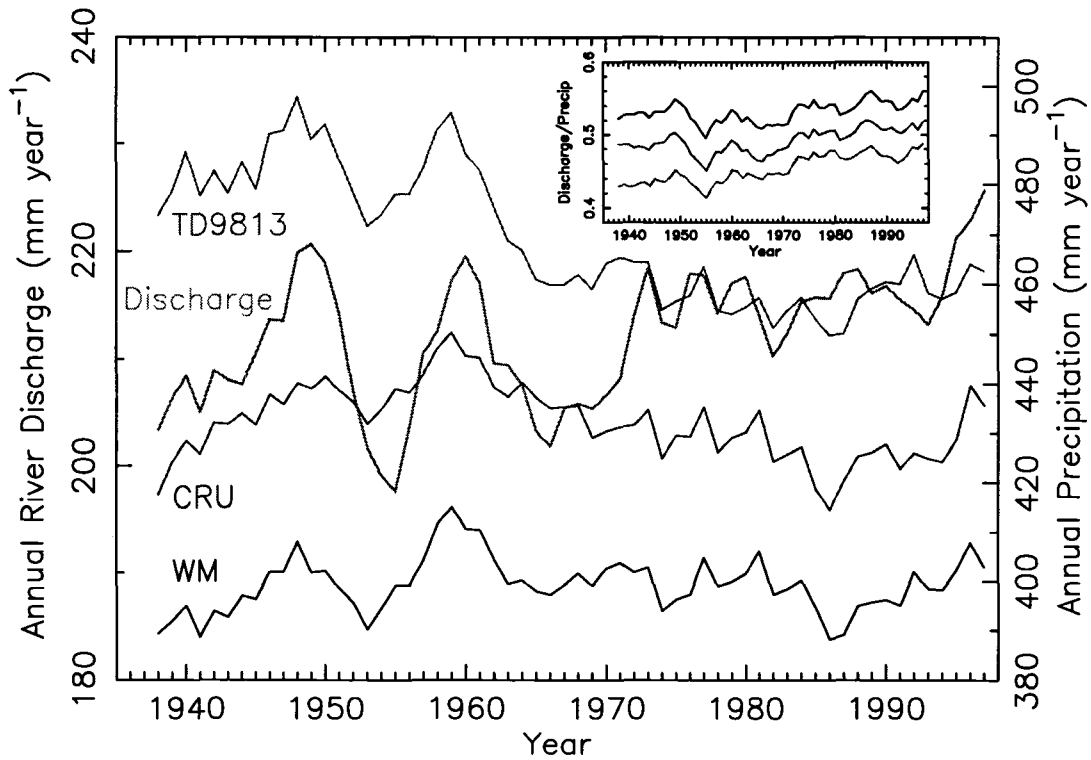


Figure 3-1: Five-year running means of spatially averaged river discharge ( $Q$ ,  $\text{mm yr}^{-1}$ ) and precipitation ( $P$ ,  $\text{mm yr}^{-1}$ ) across the 6 largest Eurasian river basins from 1936–1999. Inset shows the ratio of annual discharge to annual precipitation.

will evaporate and a larger proportion will run off. The ratio of runoff volume to snowmelt volume was found to have averaged 34% greater than the ratio for cumulative summer runoff and rainfall (Kane et al., 2003). Precipitation occurring during summer undergoes considerably more recycling to the atmosphere and contributes more to soil recharge. It has been estimated that approximately 25% of July precipitation across northern Eurasia is of local origin (Serreze et al., 2003a), i.e., associated with the recycling of water vapor within the domain.

Annual snowfall derived from TD9813 precipitation exhibits a strongly significant increase ( $0.75 \text{ mm yr}^{-1}$ ) until the late 1950s followed by a moderately significant decrease

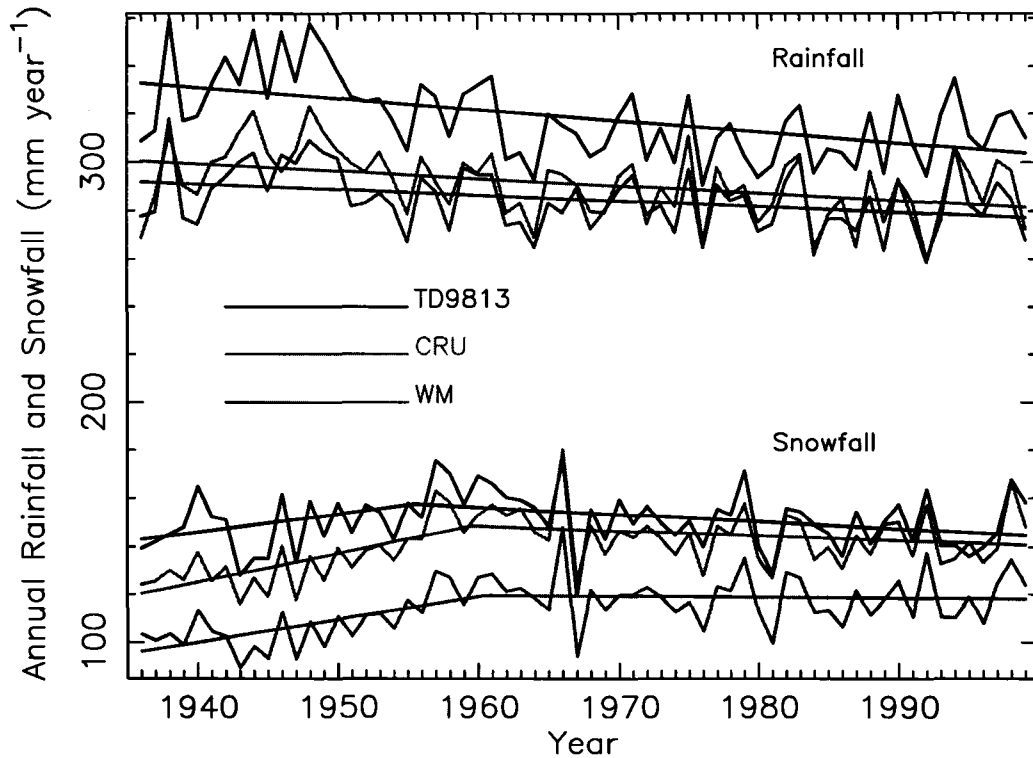


Figure 3-2: Spatially averaged water equivalent of annual rainfall and snowfall across the 6 largest Eurasian basins. Snowfall is derived using monthly gridded  $P$  data from TD9813, CRU, and WM datasets. Annual rainfall is computed using  $1 - R$ .

( $-0.30 \text{ mm yr}^{-1}$ ) thereafter (Figure 3-2, Table 3.1). Strongly significant early increases (1.19, 0.96) are also noted for derived snowfall from CRU and WM, with insignificant decreases during the latter period. No significant change is noted in snowfall derived from TD9813 over the entire 1936–1999 period. The early snowfall increases derived from CRU and WM precipitation are likely influenced by change in gauge type during the 1948–1953 period (Groisman et al., 1991), and homogenization of the station records would tend to reduce the early trends. Such bias adjustments likely make the TD9813 data more representative of the true precipitation changes over time. It should also be noted that means and trends from CRU and WM are remarkably similar, despite differing methods used to grid



	Ann. P	Ann. Snowfall			Ann. Rainfall
Data Set	Trend (mm yr <sup>-1</sup> )	Trend1 (mm yr <sup>-1</sup> )	Trend2 (mm yr <sup>-1</sup> )	Change-point (year)	Trend (mm yr <sup>-1</sup> )
TD9813	-0.49**	0.75**	-0.30*	1955.5	-0.46**
CRU	-0.06	1.19**	-0.20	1960.5	-0.30**
WM	0.07	0.96**	-0.04	1959.5	-0.23**

Table 3.1: Trends in annual precipitation, annual snowfall, and annual rainfall derived from TD9813, WM, and CRU  $P$  for 1936–1999. Trend1 and Trend2 are the change-point regression slopes for the early and late periods, respectively (see Figure 2a). Trends significant at  $p < 0.01$  and  $p < 0.05$  are indicated by \*\* and \*, respectively.

the station data. Spatially, positive local trends drawn from the entire 1936–1999 period are noted primarily across north-central Eurasia, while negative trends occur across eastern Siberia (Figure 3-3a). These increases in derived snowfall are consistent with positive trends in winter  $P$  (4–13% decade<sup>-1</sup>) across western Siberia (Frey and Smith, 2003) and snow depth across most of northern Russia (Ye et al., 1998). The geography of the snowfall changes is important to note, since they occur primarily across colder, northerly regions where soils have a limited capacity for infiltration during snowmelt.

Consistent decreases in spatially averaged rainfall over the entire Eurasian basin have occurred (Figure 3-2). The magnitude of the rainfall decrease is greater than the snowfall increase (Table 3.1), consistent with the reported (Berezovskaya et al., 2004) decline in total precipitation. Rainfall decreases are greatest across north-central Eurasia (Figure 3-3b), the area where positive snowfall trends are noted. A positive trend in 500 hPa height anomalies across much of northern Eurasia between 1960–1999 (Serreze et al., 2003a) may be linked with the rainfall decrease during that time.

Biases arising when interpolating from spatially uneven networks can be significant (Willmott et al., 1994). Station networks across Eurasia, for example, give rise to an

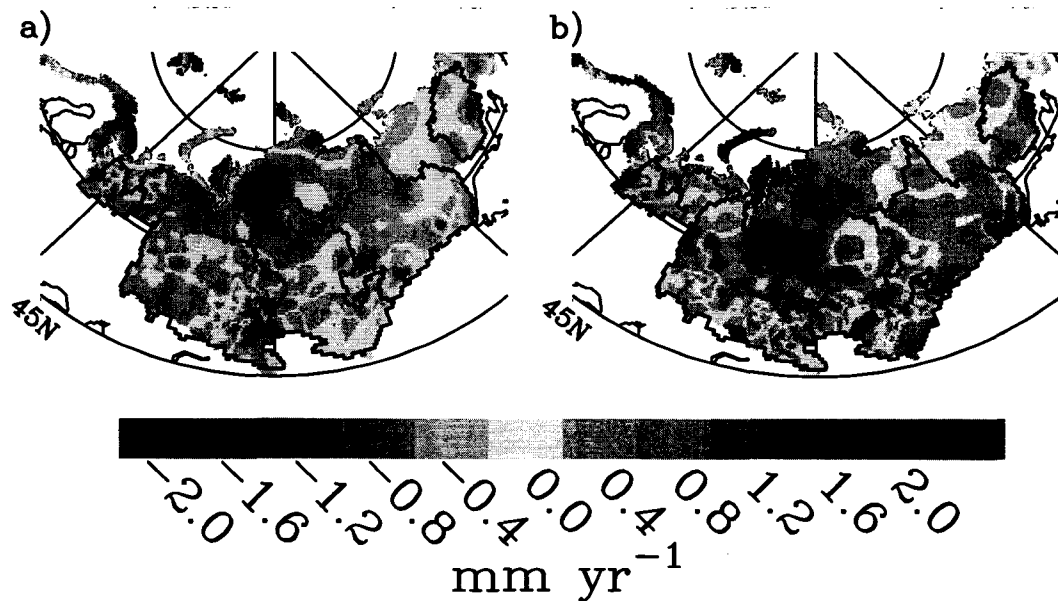


Figure 3-3: Trends in derived annual snowfall (a) and in derived annual rainfall (b) (1936–1999) from TD9813  $P$  at each  $25 \times 25$  km EASE-Grid cell encompassing the 6 largest Eurasian basins. Shaded areas are part of the larger pan-Arctic drainage basin of Eurasia. Spatially averaged values presented in this study (see Figures 1, 2, and 4) represent integrations across the 6 basins (west to east: *Severnaya Divina*, *Pechora*, *Ob*, *Yenisey*, *Lena*, *Kolyma*) outlined in bold.

overestimation of annual precipitation during earlier years (Figure 3-4). Early networks originated in the south and gradually expanded northward. Although true precipitation derived from the best Arctic networks is difficult, if not impossible, to know with certainty, we estimate a bias of well over +10 mm in the early network representations of spatial precipitation. A similar bias is noted when alternate base years are used. For assessments of continental-scale precipitation aggregations, early station networks essentially over-represent precipitation due to their uneven spatial arrangement.

Spatially, the bias assumed when interpolating from the sparse network is complex. For example, both overestimates and underestimates are noted when attempting to recreate 1972 annual  $P$  from the 1936 station network. Interestingly, some of the largest overesti-

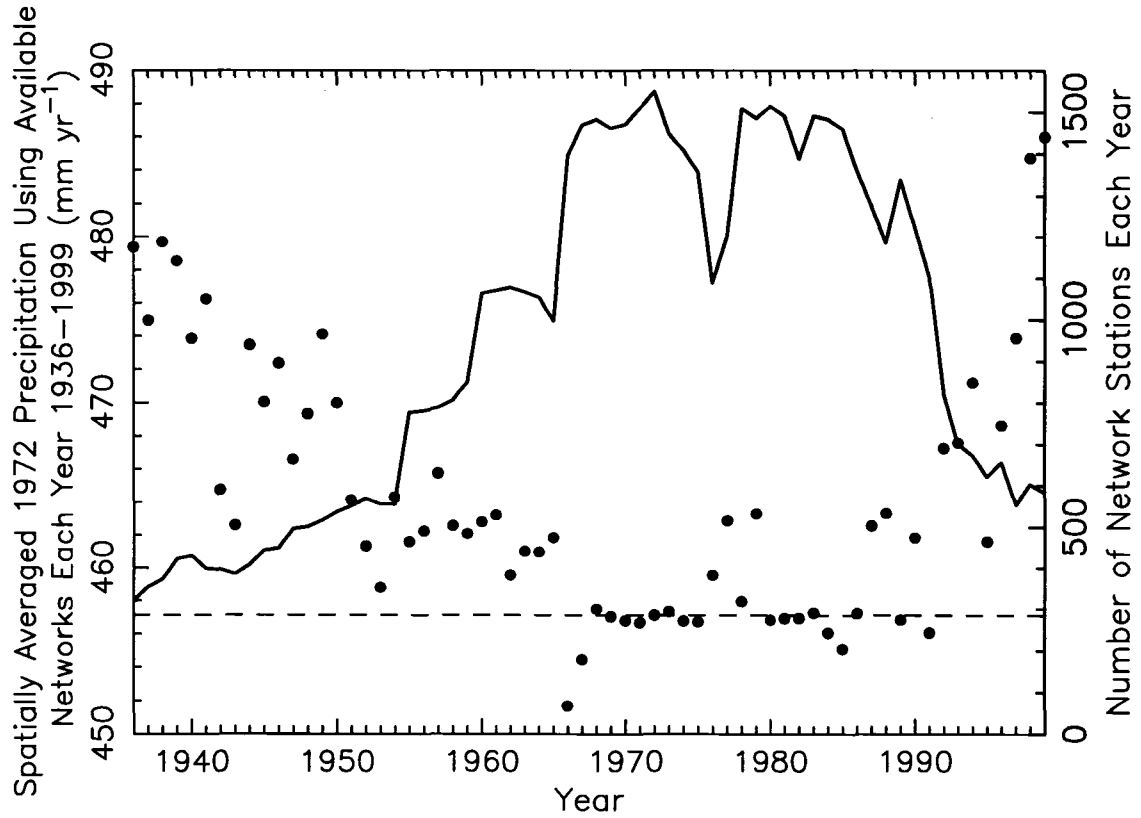


Figure 3-4: Annual total  $P$  for 1972 (dots) interpolated and spatially averaged from each yearly station network. The dashed line represents spatially averaged  $P$  for 1972, a year with the highest number of stations in the network between 1936–1999. The number of stations each year (solid line, right axis) mirrors the yearly network estimates of 1972 total precipitation, represented by the dash line.

mates are in the far northern part of Eurasia. A further examination of the bias magnitudes was performed by choosing different years other than 1972 as the baseline network. For example when 1970 or 1974 is used as the baseline network, the patterns in the spatially averaged bias are similar to those obtained when the baseline network is the configuration from 1972 (see above). Thus it is reasonable to assume that 1972 network is appropriate for deriving these bias “scenarios”.

Biases at grid locations (and for each year used to subset the 1972 network) were used to adjust the TD9813 monthly P estimates. The bias determined from annual P was evenly distributed and applied across the monthly P using the fraction of each month’s P to the annual P total. Thus, if May P at a grid was 10% of the annual P at that grid, 10% of the annual bias was applied to May P. Following adjustment of the precipitation fields, a new time series of spatially averaged P across the Eurasian pan-Arctic was produced. The slope of the linear least squares trend line fit to the new adjusted P is  $-0.37 \text{ mm yr}^{-2}$  vs.  $-0.49 \text{ mm yr}^{-2}$  computed from the default TD9813 curve. The trend in discharge is  $0.22 \text{ mm yr}^{-2}$ .

The adjusted P fields were used in PWBM simulations, and simulated runoff was compared with observed gauge records across the Eurasian pan-Arctic and the 6 basins individually. Simulated runoff from PWBM runs using the original, default P data was used for the comparisons. Surprisingly, the goodness of fit (simulated vs. observed runoff) decreases when new adjusted P data are used to drive PWBM. For aggregate simulated runoff across the entire Eurasian pan-Arctic, the Pearson correlation coefficient (R) decreases from 0.41 to 0.37 (default vs. new adjusted).

### 3.4 Summary of Results

Annual precipitation across the Eurasian basin drawn from the gridded data are correlated with observed river discharge over the period 1936–1999. Annual discharge has become a larger fraction of total precipitation during this time. Annual snowfall derived from the new bias-adjusted TD9813 precipitation data set exhibits a highly statistically significant increase until the late 1950s and a moderately significant decrease thereafter. Annual rainfall has declined significantly. Interpolations from the uneven, early station networks result in a biased depiction of spatially averaged precipitation, meaning that real local snowfall increases over the region were likely greater, and the rainfall decreases were possibly less, than the changes determined from analysis of gridded data sets such as CRU and WM. While we believe that our partitioning of rainfall and snowfall contains no systematic bias, the method itself is crude, and we emphasize that the computed trends depend on the quality interpolations from sparse precipitation and air temperature observations. Although our study suggests that increased cold season precipitation may be a significant driver of the discharge change, inherent biases in early meteorological networks and uncertainties in the historical precipitation observations render this finding intriguing, yet inconclusive.

## CHAPTER 4

# EFFECTS OF UNCERTAINTY IN CLIMATE INPUTS ON SIMULATED EVAPOTRANSPIRATION AND RUNOFF IN THE WESTERN ARCTIC

### 4.1 Introduction

Changes are occurring to high latitude environments with further alteration likely under several global change scenarios. Responses in the arctic environment may include alterations to the landscape and in water fluxes and stores. While conceptual water balance models have proved useful in assessing contemporary hydrological conditions and in modeling future states, general circulation models have not proved accurate enough to close water budgets in hydrological applications. Precipitation simulated in GCMs tends to be overestimated and seasonal dynamics are often inaccurate (Kite and Haberlandt, 1999; Töyrä et al., 2005). Hydrological models which account for phase changes in soil water (Rawlins et al., 2003; Su et al., 2005) have recently been adopted in hopes of improving simulated water budgets across high-latitude regions.

Water budget models are dependent on accurate inputs of air temperature and especially precipitation in order to adequately depict the spatial and temporal dynamics of Arctic wa-

ter fluxes. Deficiencies leading to biases in model input data can significantly impact the usefulness of the data for climate change research and other efforts to solve environmental problems. In a sensitivity experiment, an arctic hydrological model was more sensitive to changes in daily precipitation than in the prescribed land surface parameterizations (Rawlins et al., 2003). Uncertainties in precipitation data used to drive hydrological models are a particular problem in the Arctic where gauge undercatch is often substantial. Precipitation underestimates of 20 to 25% have been determined across North America (Karl et al., 1993), while biases of 80 to 120% (in winter) have been estimated for the terrestrial Arctic north of 45°N (Yang et al., 2005). In regions where precipitation exceeded potential evapotranspiration (PET), uncertainty in precipitation translated to an uncertainty in simulated runoff of roughly similar magnitude (Fekete et al., 2004). In order to better understand the effect of data biases and uncertainties on simulated water budgets, we perform a series of model simulations using three climate drivers and three methods for estimating PET across the Western Arctic Linkage Experiment (WALE) domain. Goals of the WALE project include identification of uncertainties in regional hydrology and carbon estimates with respect to uncertainties in (i) driving data sets and (ii) among different models. The present paper focuses on how the limitations and uncertainties in 3 climate data sets affect our ability to accurately simulate water budgets across the terrestrial Arctic. Additional details of the WALE project can be found in (McGuire, 2005).

## 4.2 Methods

### 4.2.1 Overview

A series of simulations using three climate drivers and three methods for estimating PET (nine model runs) were made for the period 1980–2001 with a hydrological model (subsection 4.2.2). We use commonly available data sets (subsection 4.2.3) to judge the impact of climate on the simulated water budgets. PET is estimated using the Hamon method (Hamon, 1963) (equation B.1 in Appendix B), the surface-dependent Penman-Monteith method (PM) (Monteith, 1965) (equation B.2 in Appendix B), and the PM method with adjusted vapor pressure data, described in section 4.2.4. Details of the simulations to produce the nine scenarios and the comparisons with observed evapotranspiration (ET) and runoff are described in subsection 4.2.4.

### 4.2.2 Model Description

We use the Pan-Arctic Water Balance Model (PWBM, Rawlins et al., 2003) to simulate runoff and ET at an implicit daily time step across the Western Arctic Linkage Experiment (WALE) domain. This hydrological model uses gridded fields of plant rooting depth, soil characteristics (texture, organic content), vegetation, and is driven with daily time series of precipitation and air temperature. The PWBM incorporates a soil organic layer and a soil moisture phase-change submodel which partitions water to solid and liquid amounts. Spatial fields of air temperature, vegetation, and soil characteristics provide the inputs to the thaw/freeze submodel. A detailed description of the model was provided in Rawlins et al. (2003). Simulations in the present study were performed on the Equal-Area Scalable



Earth Grid (EASE-Grid) at a resolution of  $25 \text{ km} \times 25 \text{ km}$  across 3511 grid cells which define the domain. The WALE domain encompasses Alaska and the upper headwaters of the Yukon basin in northwestern Canada. Simulations are performed over the period 1980–2001.

### 4.2.3 Input Datasets

Water budget simulations are made using three climate driver data sets. We use precipitation and air temperature from the NCEP/NCAR reanalysis project (NNR) (Kistler et al., 2001), hereinafter referred to as NCEP1. We also use precipitation data (NCEP2) which represents an improvement to the standard NNR fields through application of a statistical downscaling approach based on a probability transformation for precipitation (Serreze et al., 2003b). The NCEP2 air temperature grids are derived from NNR data using a method which accounts for elevation effects. The third climate driver set is the Willmott-Matsuura archive (Willmott and Matsuura, 2001), hereinafter referred to as WM. The WM archive was produced using the Global Historical Climatology Network (GHCN) version 2 data (Vose et al., 1992) and Legates and Willmott's (Legates and Willmott, 1990a; Legates and Willmott, 1990b) station records of monthly and annual air temperature and total precipitation. WM climate data are available through year 2000. Table 4.1 summarizes the climate data sets used in the PWBM simulations. Mean annual precipitation across the WALE domain is highest for NCEP1 ( $650 \text{ mm yr}^{-1}$ ) and lowest for the WM archive ( $510 \text{ mm yr}^{-1}$ , Figure 4-1, Table 4.2). A significant problem with the NCEP reanalysis model is a severe over-simulation of summer precipitation over land areas due to excessive convective precipitation (Serreze and Hurst, 2000). The statistical method used to create the NCEP2

precipitation reduces this bias, and the NCEP2 precipitation average ( $580 \text{ mm yr}^{-1}$ ) falls between the excessive NCEP1 data and the unadjusted WM data (Figure 4-1).

Land cover is defined from a new 1 km resolution vegetation classification for Alaska that prescribes fractional cover for 6 vegetation types in each  $25 \text{ km} \times 25 \text{ km}$  EASE-Grid cell. Two AVHRR-based land cover classifications for Alaska (Fleming, 1997) and Canada (Cihlar and Beaubien, 1998) were merged and aggregated into five major vegetation types using an expert model (Calef et al., 2005). The cover types are black spruce, white spruce, deciduous forest, tundra, coastal forest, and bare ground (encompasses areas of rock and ice). With 1991 as the base year, transient land cover was interpolated backward and forward for 1950 to 2000 using a hierarchical logistic regression approach, the historic fire record, and ecological knowledge on succession. Tundra vegetation comprises the majority (55%) of the WALE domain, with coniferous forest (black spruce, white spruce, and coastal forest) second most prevalent. The same parameter specifications are used for these coniferous forest grids in the PWBM runs. Across the Yukon basin, tundra again is dominant, with slightly more coniferous forest (39%) than the entire WALE domain contains (22%). For a given climate driver and PET method configuration, the PWBM was run separately for each land cover type over the 1980–2001 period. A 50-year spinup was first performed to stabilize model soil moisture. Runoff and ET for each grid cell is a weighted average of runoff or ET across each land cover type in the grid. We use this “mosaic” of ET or runoff in the analysis to follow. Simulated ET is the total water loss from the surface, which includes transpiration from plants, evaporation from soils, and sublimation from snow.

Data Set	Precipitation	Air Temperature	Vapor Pressure
NCEP1	NNR	NNR	NNR/NNR <sup>c</sup>
NCEP2	NNR <sup>a</sup>	NNR <sup>b</sup>	NNR <sup>c</sup>
WM	WM	WM	NNR <sup>c</sup>

Table 4.1: Climate data sets used in PWBM simulations and original source for precipitation, air temperature, and vapor pressure data used in the model runs. NNR is the NCEP–NCAR reanalysis (NNR). NNR<sup>a</sup> indicates NNR data adjusted by methods in Serreze et al. (2003); NNR<sup>b</sup> is NNR adjusted for effects of elevation on air temperature interpolations; and NNR<sup>c</sup> denotes NNR vapor pressures which are reduced by the difference with CRU vapor pressure data.

Data Set	Climate (mm yr <sup>-1</sup> , °C)			ET (mm yr <sup>-1</sup> )			Runoff (mm yr <sup>-1</sup> )		
	P	T <sub>A</sub>	T <sub>S</sub>	Hamon	PM	PM*	Hamon	PM	PM*
NCEP1	650	-6.9	9.2	267	115	146	366	504	474
NCEP2	580	-5.8	9.7	263	116	143	296	443	418
WM	510	-3.8	12.5	275	112	139	243	403	373

Table 4.2: Long-term mean simulated ET, runoff, and climate across the WALE domain from the three climate drivers and three PET methods. P is mean annual precipitation (mm yr<sup>-1</sup>); T<sub>A</sub> and T<sub>S</sub> are mean annual and summer (JJA) air temperature, respectively. PET methods (described in section 4.2.4) are: Hamon method (Hamon, 1963) (equation B.2 in Appendix B), the Penman-Monteith method (PM) (Monteith, 1965) (equation B.2 in Appendix B), and the PM method with adjusted vapor pressure data (PM\*). Averages for ET are taken from the time series in Figure 4-3, and runoff averages are derived from time series in Figure 4-4.

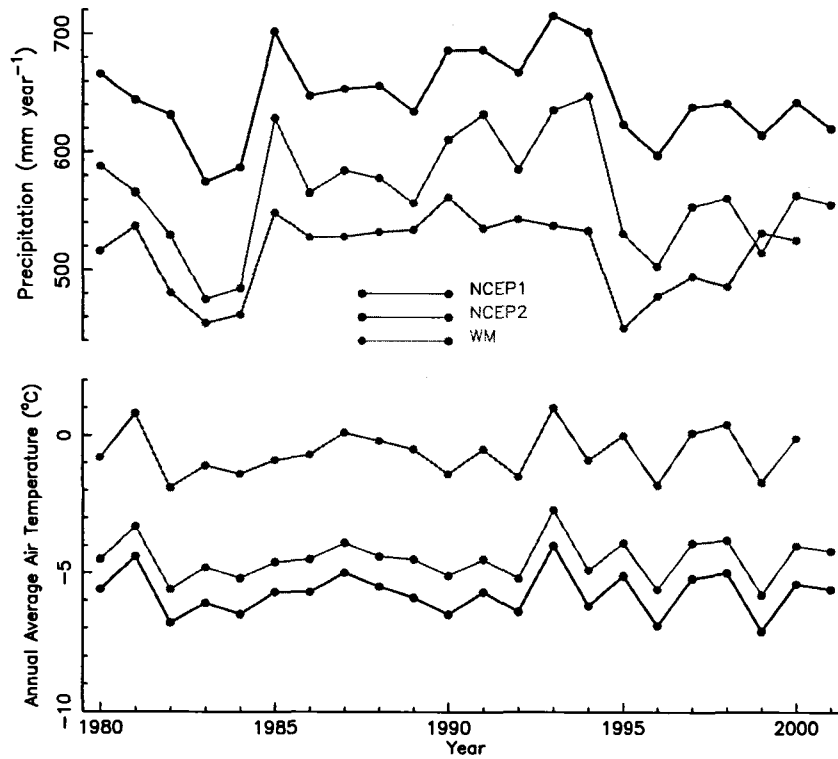


Figure 4-1: Annual total precipitation (upper panel) and mean annual air temperature (lower panel) across the WALE domain for the years 1980–2001. Precipitation and air temperatures are drawn from NCEP/NCAR reanalysis (NCEP1) (Kistler et al., 2001), a version based on a statistical downscaling (Serreze et al., 2003b) of the NCEP/NCAR reanalysis (NCEP2), and the Willmott-Matsuura archive (Willmott and Matsuura, 2001) (WM).

Location	ET (mm season <sup>-1</sup> )				Period
	Obs	Hamon	PM	PM*	
Council	97	93	81	81	6/18/99–8/22/99
Delta Junction	178	142	55	61	6/1/02–8/31/02

Table 4.3: Observed June–August ET at 2 sites in Alaska and simulated June–August ET for 25×25 km EASE-Grid in which site is located. Simulated ET is taken from model runs using the Hamon method, the Penman-Monteith method (PM), and the adjusted PM method (PM\*). For each PET method we averaged simulated ET over the three climate driver (NCEP1, NCEP2, and WM) runs. Eddy covariance measurements of latent heat were reported for Council (64.8°N , 163.7°W) (Beringer et al., 2005) and Delta Junction (63.9°N , 145.7°W) (Liu et al., 2005). Observations were taken from June–August 1999 at Council and from June–August 2002 at Delta Junction.

#### 4.2.4 Model Application and Analysis

Simulated water fluxes of runoff and ET were evaluated and compared with observed data where available. We use discharge data from the downstream site (Pilot Station) on the Yukon River for comparison with the simulated runoff across the Yukon basin. Observed ET data are drawn from 2 sites across Alaska (Table 4.3). We compare PWBM simulated summer total (June–August) ET at the grid cell in which the observed site is located with the observed value, which was measured using flux towers eddy covariance measurements (Beringer et al., 2005; Liu et al., 2005).

Within the PWBM simulated PET was estimated using the relatively simple Hamon function (Hamon, 1963) (equation B.1 in Appendix B), a physically-based, surface-dependent combination approach (Penman-Monteith, PM) (Monteith, 1965) (equation B.2 in Appendix B); and the PM method forced with adjusted vapor pressure data. These adjustments were made after problems were identified with the NNR humidity data. The Hamon method falls into a class known as reference-surface PET methods, i.e., methods

which produce evaporation that would result from a specific land surface known as a reference crop. In contrast, the PM approach is known as a surface-dependent PET method, i.e., it produces the evaporation which would occur from any of a variety of designated land surfaces. In the PM method, parameterizations for quantities such as leaf conductance and aerodynamic resistance are a function of the landcover type as described by Federer et al. (1996). Aerodynamic resistances are taken from the neutral wind profile equation. Net radiation time series from the NNR data set are used in the PM approach. We chose the Penman-Monteith method since it was found to be the least biased of 11 methods applied over the conterminous US (Vörösmarty et al., 1998). Our analysis focuses on simulated runoff and ET obtained from a model run using a specific combination of climate driver and PET method. Although we mention PET method when discussing model implementation, analysis of model output is restricted to simulated ET, which is distinguished from PET through limitations imposed by soil water deficit within the model run. Vapor pressure data required for the PM function are not available from the NCEP2 and WM data sets, and we use those from the NNR project in all simulations involving the PM PET method.

Surface-dependent PET functions such as PM use air temperature, vapor pressure data and other climate drivers to estimate the potential flux of water from vegetated surfaces. Observed meteorological station data for several sites in Alaska were compared with relative humidities derived from NNR vapor pressure and air temperatures. Mean daily air temperature and dew point at the sites for year 2000 were taken from stations in the Global Summary of the Day (SOD) database distributed by the National Climatic Data Center. Relative humidities derived from NNR data are near 100% during summer, while lower values and greater variability are present in the station data (Figure 4-2). High humidities

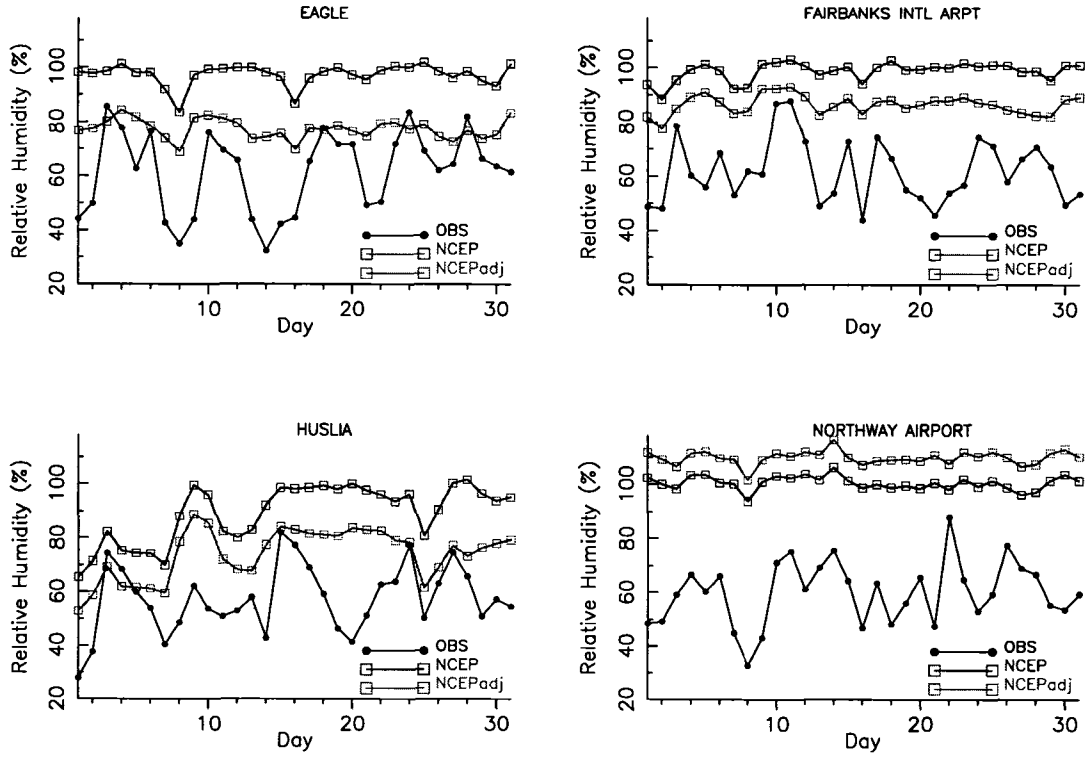


Figure 4-2: Daily average relative humidity for July 2000 derived from NCEP-NCAR reanalysis vapor pressure (VP) data (NCEP), reanalysis VP adjusted using CRU monthly VP (NCEPadj), and from air temperature and dewpoint in the Summary of the Day data set (OBS).

are consistent with excessive surface evaporation rates in the NNR, a problem which may be related to excessive soil moisture and solar radiation during summer in the reanalysis data (Serreze and Hurst, 2000).

In order to better understand the effect of NNR moisture biases, gridded vapor pressures from the University of East Anglia's Climate Research Unit (CRU; <http://www.cru.uea.ac.uk>) are used to adjust the NNR vapor pressure data at each EASE-grid cell. The CRU data are monthly averages, and the adjustment to the gridded NNR daily vapor pressure data is

$$VP_D = VP_{NNR} - (VP_M - VP_{CRU}) \quad (4.1)$$

where  $VP_D$  are the adjusted daily NNR vapor pressures (kPa) at the EASE-grid,  $VP_{NNR}$  is the daily NNR vapor pressure,  $VP_M$  is monthly average vapor pressure from NNR, and  $VP_{CRU}$  is monthly CRU vapor pressure. CRU vapor pressures are generally lower than NNR values across most of interior Alaska, while similar vapor pressures occur across coastal regions. These adjusted  $VP_D$  values are used in a third suite of PWBM simulations involving each climate driver set. We refer to the PET method for these simulations as the “adjusted PM method” (PM\* in Tables 2,3,4). When the adjusted NNR vapor pressures ( $VP_D$ ) are used, simulated ET increases an average of 30 mm yr<sup>-1</sup> over the default PM configuration (Table 4.2).

## 4.3 Results

### 4.3.1 Simulated Evapotranspiration

Comparisons between simulated and observed ET rates illustrate the effect of biases in the vapor pressure data. Table 4.3 shows observed ET along with the average simulated ET for the Hamon, PM, and adjusted PM PET methods, where the average for each PET method is calculated across the three climate driver simulations. At the coastal tundra site (Council), small differences (no greater than 16 mm summer<sup>-1</sup>) in ET are noted. Indeed, differences between NNR and CRU vapor pressures across coastal regions are small; therefore, simulated ET using the default and the adjusted vapor pressures, for the Council grid cell, are identical (81 mm season<sup>-1</sup>). At interior site (Delta Junction) greater differences are evident. Simulations using the PM method lead to ET rates much lower than observed



values. When the adjusted vapor pressures are used, ET increases 6 mm summer<sup>-1</sup> for the Delta Junction grid cell.

Across the WALE domain, low NNR-derived vapor pressure deficits cause reduced PET and ET rates. For the three climate driver simulations, the ET average (1980–2001) when using PM is 113 mm yr<sup>-1</sup>, whereas the simulations using Hamon are over 100% higher, averaging 268 mm yr<sup>-1</sup> (Figure 4-3a). ET rates when PM method is used are less than half of the Hamon ET values. Differences in annual ET when PM is used are also relatively small, averaging 115, 116, and 112 mm yr<sup>-1</sup> for NCEP1, NCEP2, and WM climate (Table 4.2). Long-term mean monthly ET is 15–20 mm month<sup>-1</sup> lower for PM method vs. Hamon (Figure 4-3b). For NCEP2 climate, simulated ET from the adjusted PM method is 23% higher than the ET rates from the model run using default PM PET method (Figure 4-3c, Table 4.2), while the Hamon method again is approximately 100% higher. These comparisons illustrate well the underestimation of ET in simulations using the default PM method and NNR vapor pressures.

### 4.3.2 Simulated Runoff

Differences between the climate data inputs as well as the NNR humidity anomaly are evident in PWBM runoff simulations. Annual runoff is highest when NCEP1 data are used and lowest with WM. Long-term mean simulated runoff across the WALE domain averages 366, 296, and 243 mm yr<sup>-1</sup> from the NCEP1, NCEP2, and WM simulations respectively (Table 4.2). Correlation between NCEP1 and NCEP2 runoff is 0.92—which is expected, whereas the correlation between NCEP2 and WM is 0.55 (Figure 4-4a). When the PM method is used, runoff averages 504, 443, and 403 mm yr<sup>-1</sup>, respectively. Correlations

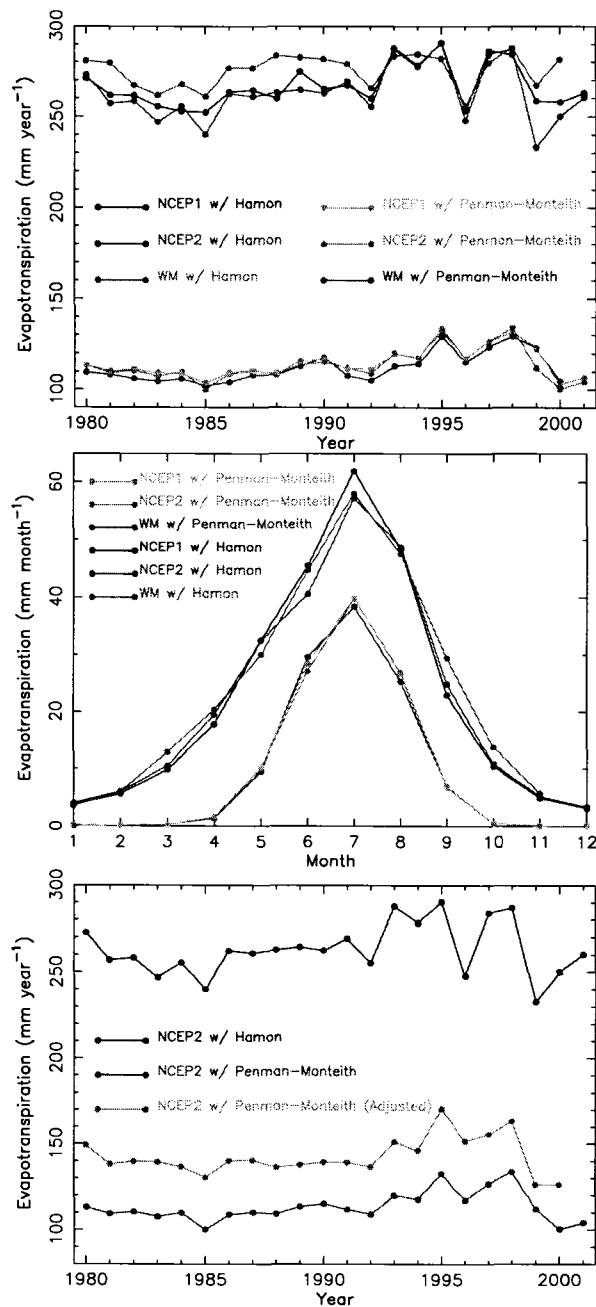


Figure 4-3: PWBM simulated annual ET across the WALE domain for the period 1980–2001. In Figures 4-3, 4-4, and 4-5, NCEP1 indicates climate data from NNR, NCEP2 is the modified NNR data set from Serreze et al. (2003) and WM are simulations using Willmott and Matsuura data. (a) Annual totals of ET from the 3 climate drivers and Hamon and PM PET for 1980–2001. (b) Monthly climatology from the standard simulation runs. (c) Annual ET from simulations with NCEP2 climate and Hamon, PM, and adjusted PM PET methods

here are 0.92 (NCEP1/NCEP2) and 0.21 (NCEP2/WM) (Figure 4-4b). Although less well correlated in time, the NCEP2 and WM climate data produce runoff of similar magnitude. Differences between runoff from simulations using NCEP2 or WM climate and Hamon PET (Figure 4-4a) are attributable, in part, to colder air temperatures (lower ET → higher runoff) in the NCEP2 data set (Figure 4-1). Use of the NCEP1 climate data results in the highest runoff, WM climate inputs produce the lowest runoff, and all three simulations using the PM PET method show higher runoff than the model runs using Hamon. Runoff from the NCEP1 simulations is 13–24% higher than NCEP2 runoff depending on PET method (Table 4.2), since incorporation of observed data reduces the excessive NCEP1 precipitation. Arctic precipitation in the NNR has been shown to be systematically too high (particularly in summer ) due mostly to excessive convective precipitation (Serreze and Hurst, 2000). When the adjusted PM method is used to account for the vapor pressure bias, simulated runoff decreases by 25–30 mm yr<sup>-1</sup> or 6–7%.

Runoff from simulations using the PM method show a higher snow melt peak than those using Hamon (Figure 4-5). Observed runoff (i.e., discharge measured at the downstream site) lags the simulated melt peak by one month in all simulations. This is expected, as snowmelt-driven runoff from upstream areas often takes several weeks to reach the downstream gauge in large basins. Simulated runoff is less than observed (underestimate) for NCEP2 and WM climate with the Hamon function (Table 4.4). The PM method generates excess runoff for each climate driver, a result of higher vapor pressure and low simulated ET. Adjusting the NNR vapor pressures lowers runoff (7–13%). Across the Yukon River basin generally good agreement between simulated and observed runoff is noted; simulated runoff differs from the observed by 7% for the NCEP2 and WM climate drivers when the

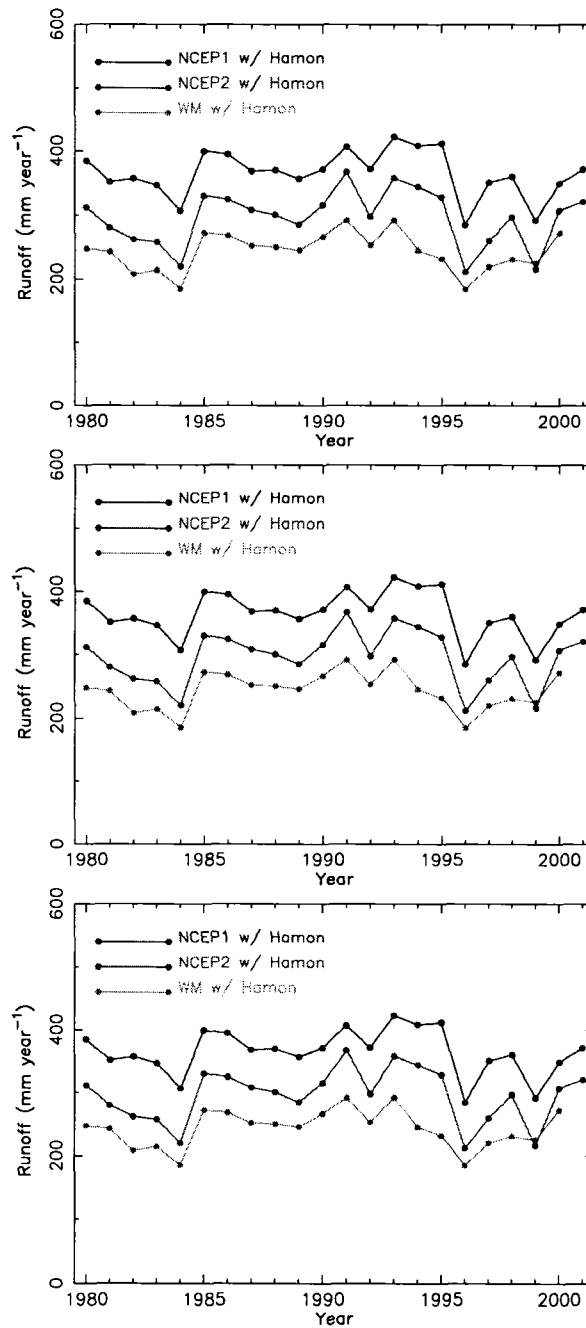


Figure 4-4: Simulated annual runoff across the WALE domain for 1980-2001. (a) Three climate driver simulations using Hamon method for PET. (b) Simulations using PM method. (c) NCEP2 climate together with each PET method.

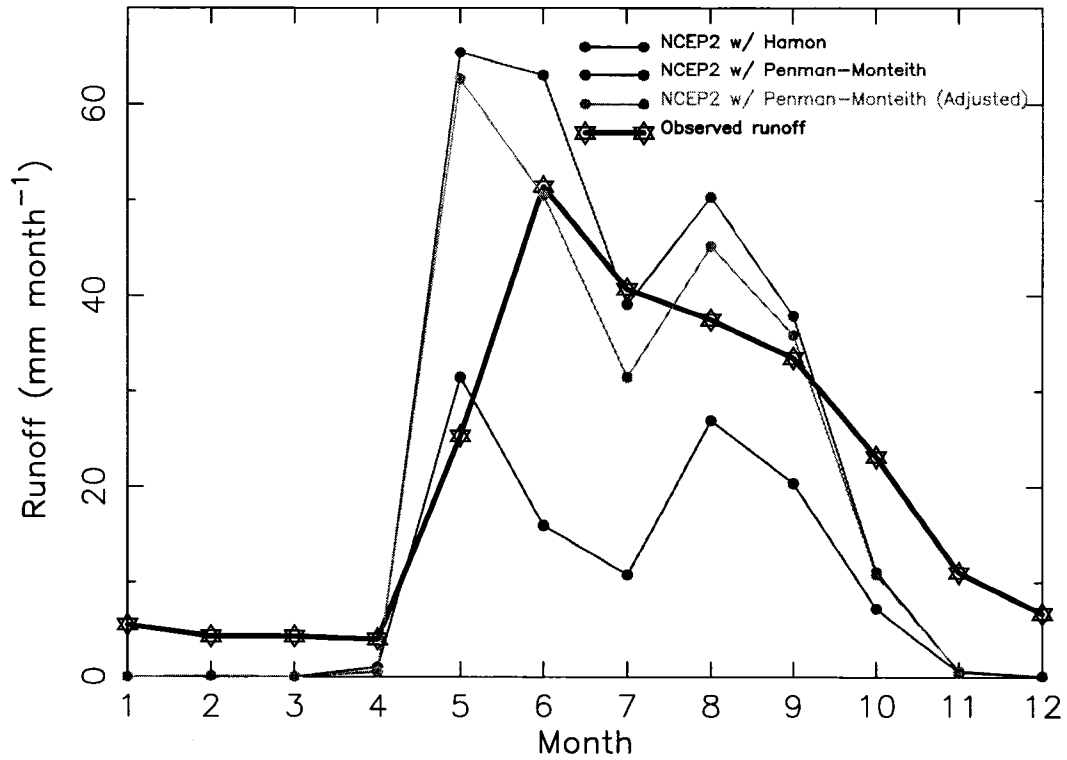


Figure 4-5: Long-term mean monthly runoff across the Yukon basin simulated for the period 1980–2001. Observed runoff is discharge as a unit depth across the Yukon river basin. Simulated runoff taken from model runs using the NCEP2 climate with each of the PET methods.

adjusted PM PET method is used (Figure 4-6). Runoff generated with NCEP1 climate exceeds observed values regardless of the PET method used. The average MAD is 200, 60, and 70 mm yr<sup>-1</sup> for NCEP1, NCEP2, and WM climate, respectively.

#### 4.4 Discussion

Model simulations of evapotranspiration across forested interior regions are more strongly affected by synoptic weather conditions (e.g. vapor pressure deficits) than tundra locations. This is expected, as transpiration is the dominant source of water loss in forested regions

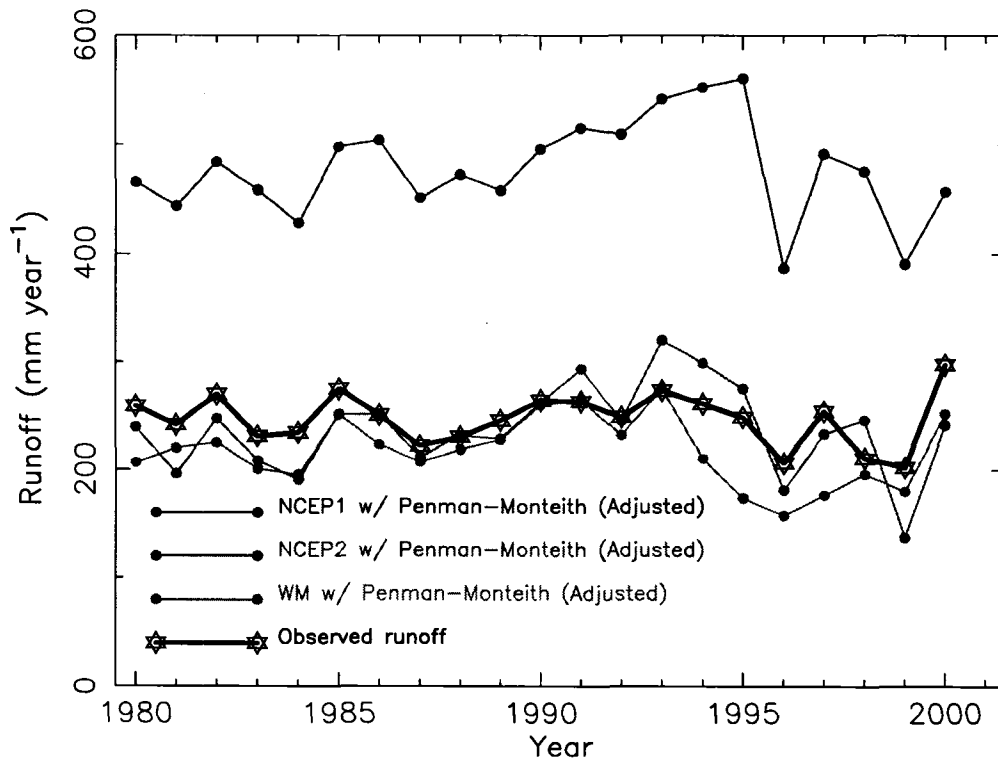


Figure 4-6: Observed and simulated annual runoff across the Yukon basin 1980–2000. Simulated runoff is drawn from model runs using each climate driver along with adjusted PM PET method.

Data Set	MAD (mm yr <sup>-1</sup> )			Average
	Hamon	PM	PM*	
NCEP1	110 ↑	260 ↑	230 ↑	200
NCEP2	130 ↓	30 ↑	30 ↓	60
WM	170 ↓	20 ↑	30 ↓	70
Average	137	103	93	–

Table 4.4: Mean absolute difference (MAD) in simulated annual runoff as compared to observed runoff across the Yukon basin.  $MAD = \frac{1}{22} \sum_{i=1}^{22} |R_s - R_o|$ , where  $R_s$  is the simulated annual runoff,  $R_o$  is the observed, and MAD is in mm yr<sup>-1</sup>. Using signed differences, overestimation ( $\sum_{i=1}^{22} R_s - R_o > 0$ ) is indicated with ↑, and underestimation ( $\sum_{i=1}^{22} R_s - R_o < 0$ ) shown with ↓.

(soil evaporation is dominant in tundra locations), and synoptic controls such as vapor pressure deficit are an important driver in these areas (Beringer et al., 2005). Feedbacks between radiation, precipitation, and soil moisture in the NNR affect the near surface moisture amounts (Serreze and Hurst, 2000). The relatively high vapor pressures result in small vapor pressure deficits, which tend to reduce ET rates when used in land surface and hydrologic models. Modeled ET rates in simulations using Hamon PET method more closely match observed ET values across interior regions of Alaska. Downwelling shortwave fluxes in the NNR are also reportedly too high (Serreze and Hurst, 2000). As opposed to the effect of elevated vapor pressure (leads to reduced ET), the biased radiation data (used in the PM PET method) would tend to increase estimated ET rates, and reduce runoff. ET rates for the PM and Hamon simulations converge toward observed values along coastal regions where evaporation from tundra vegetation dominates the surface ET flux. When the PM PET method is used, differences between simulated and observed ET at Delta Junction (forest site) suggest that greater uncertainties in simulated budgets are likely across these forest regions. Comparisons with the observed values also show that ET estimated in model runs using the Hamon PET method represent an upper bound on simulated ET rates, with lower rates when the PM method is chosen.

Monthly climatologies of simulated ET from PM are nearly identical across the three climate drivers. Differences in ET from simulations using the PM and Hamon methods are largely due to low vapor pressure deficits which drive the surface-dependent PM PET method. Simulated ET rates across the WALE domain are strongly influenced by both the vapor pressure data and the PET method chosen, with less effect from differences in

precipitation data. A thorough evaluation of model simulated ET fluxes is hampered by the paucity of observed, high-latitude ET measurements.

Simulated annual runoff show substantial variations between model runs, with long-term means strongly dependent on which climate driver and PET function is implemented. When the PM method is used, lower ET leads to increased soil moisture storage and higher runoff estimates. The highest mean runoff (from NCEP1 climate with PM PET) is double the lowest runoff rate (WM climate with Hamon PET). Simulations using the raw NNR climate drivers (NCEP1) result in the highest runoff independent of PET function. This is due to higher summer precipitation in the NNR data. The WM climate data—which is produced from observed station records—generates the lowest runoff, as expected, since the WM archive does not incorporate precipitation gauge corrections. Precipitation in the NCEP2 data set was produced through downscaling of the NCEP1 data based on observed data; therefore, NCEP2-derived water fluxes represent a combination of Arctic reanalysis and observed climate. Model simulations with the PM method generate runoff which exceeds the observed Yukon runoff due to low ET rates. Using the adjusted vapor pressure data lowers runoff across the WALE and Yukon domains. Across all PET methods, average *MAD* for NCEP1 climate is a factor of 3 greater than *MAD* for NCEP2 or WM due to excessive precipitation in the NCEP-NCAR reanalysis.

Although good correspondence with observed runoff is noted for NCEP2 and WM climate with adjusted PM PET method, the accuracy of these precipitation data—the most important variable for Arctic hydrological models—cannot be verified. Adjustment for biases such as gauge undercatch would likely significantly change simulated water fluxes.



Other sources of climate data such as the new ERA-40 reanalysis may prove useful in improving closure of water budgets across the WALE region.

## 4.5 Conclusions

Three climate drivers and three methods for estimating PET were used in simulations with a water budget model to better understand our ability to simulate arctic water balances across the western arctic. High surface vapor pressures in the NNR tend to limit modeled PM PET and result in PWBM-simulated ET rates that are less than half the rates found when the Hamon PET function is used. Differences in precipitation have much less influence on simulated ET rates than do the vapor pressure inputs and type of model PET method used. High simulated runoff noted in simulations driven by NCEP1 climate reflects the excessive precipitation in the NNR. More modest runoff rates are noted in simulations using NCEP2 precipitation—a combination of atmospheric reanalysis and station observations. Agreement between simulated and observed runoff to within 7% occurs with NCEP2 and WM climate drivers when the adjusted PM PET method is used. We find that simulations of arctic evapotranspiration and runoff are strongly dependent on the quality of time series data used to drive the model. These results suggest that closure of simulated water budgets across arctic regions is strongly dependant on thorough evaluations of model requirements, potential biases in climatic data sets, and comparisons with observed data where available.

**CHAPTER 5**

**ON THE EVALUATION OF SNOW WATER  
EQUIVALENT ESTIMATES OVER THE TERRESTRIAL  
ARCTIC DRAINAGE BASIN**

**5.1 Introduction**

Winter snow storage and its subsequent melt are integral components of the climate system. Much remains unknown regarding the magnitudes and interannual variations of this key feature of the arctic water and energy cycles. Across large parts of the terrestrial Arctic direct snow observations are unavailable, and this lack of information limits our ability to monitor a region which is exhibiting signs of change (Peterson et al., 2002; Vörösmarty et al., 2001). Yet, amid declines in Pan-Arctic station observations (Shiklomanov et al., 2002), a growing number of models and remote sensing data are being brought to bear for studying the arctic hydrological cycle. Retrospective analysis or “reanalysis” of the atmospheric state such as the National Centers for Environmental Prediction (NCEP) and the National Center for Atmospheric Research (NCAR) Reanalysis Project (Kalnay et al., 1996) provide benchmark, temporally-consistent data sets for water cycle studies. Remote sensing techniques offer the potential for more complete coverage at regional scales (Derksen et al., 2003; McDonald et al., 2004).

High quality estimates of snow storage and melt can be used to validate the behavior of hydrological models and GCMs, which have difficulty reproducing solid precipitation dynamics (Waliser et al., 2005). Snow cover and snow water equivalent (SWE) estimates are also needed for climate change analysis and flood prediction studies. Approximately 8000 (daily) snow depth observations were analyzed to create monthly snow depth and SWE climatologies for North America (Brown et al., 2003) for use in evaluating Atmospheric Model Intercomparison Project II (AMIP II) snow cover simulations. Comparisons of continental-scale snow parameters with river discharge time series are useful to improving our understanding of the role of snow accumulation and melt in runoff generation processes. Yang et al. (2002), examining the snow-discharge relationship, noted a weak correlation ( $R = 0.14$  to  $0.27$ ) between winter precipitation (a proxy for snow thickness) and streamflow between May and July across the Lena river basin in Siberia. Across the Ob basin, winter snow depth derived from Special Sensor Microwave Imager (SSM/I) agrees well with runoff in June ( $R=0.61$ ), with lower correlations for comparisons using May or July discharge (Grippa et al., 2005). Strong links have been reported between end-of-winter SWE and spring/early summer river discharge in the Churchill River and Chesterfield Inlet Basins of Northern Canada (Déry et al., 2005). Frappart et al. (2006) recently compared snow mass derived from SSM/I data and three land surface models with snow solutions derived from GRACE geoid data. GRACE (Gravity Recovery and Climate Experiment) is a geodesy mission to quantify the terrestrial hydrological cycle through measurements of Earth's gravity field. They found that GRACE solutions correlate well with the high-latitude zones of strong accumulation of snow at the seasonal scale.

To better understand the agreement between SWE and observed river discharge, we examine comparisons of their year-to-year changes across 179 river basins over the period 1988–2000. Gridded SWE estimates across the Pan-Arctic drainage basin are taken from both satellite microwave data and land surface model estimates. The objective of our study is to evaluate several common SWE data sets using monthly discharge for watersheds across the terrestrial arctic basin.

## 5.2 Data and Methods

Spatial, gridded estimates of monthly SWE and discharge for river basins across the Pan-Arctic were analyzed for the period 1988–2000. Monthly SWE is drawn from the analysis scheme described by Brown et al. (2003) and archived at the Canadian Cryospheric Information Network (CCIN, <http://www.ccin.ca>); from simulations using the Pan-Arctic Water Balance Model (PWBM) (Rawlins et al., 2003); from snowpack water storage in the Land Dynamics Model (LaD) (Milly and Shmakin, 2002); and from SSM/I brightness temperatures (Armstrong and Brodzik, 1995; Armstrong et al., 2006). PWBM uses gridded fields of plant rooting depth, soil characteristics (texture, organic content), vegetation, and is driven with daily time series of climate (precipitation ( $P$ ) and air temperature ( $T$ )) variables. Monthly PWBM SWE is obtained from model runs using  $P$  and  $T$  from 3 different sources (i) ERA-40 (ECMWF, 2002), (ii) NCEP-NCAR Reanalysis (NNR) (Kalnay et al., 1996), (iii) Willmott-Matsuura (WM) (Willmott and Matsuura, 2001). We refer to these SWE estimates as PWBM/ERA-40, PWBM/NNR, and PWBM/WM, respectively. The NNR  $P$  data have been adjusted based on a statistical downscaling approach (Serreze et al.,

2003b). Implemented in an effort to minimize biases through the use of observed  $P$  data, this method involved (1) interpolation of observed monthly totals from available station records with bias adjustments and (2) disaggregation of the monthly totals to daily totals, making use of daily  $P$  forecasts from the NCEP/NCAR Reanalysis. PWBM simulations were performed on the  $25 \times 25$  km Equal Area Scalable Earth Grid (EASE-Grid) (Brodzik and Knowles, 2002). The LaD has previously been found to explain half of the interannual variance of the runoff/precipitation ratio of 44 major river basins (Shmakin et al., 2002). In a study of SWE derived from GRACE and from three LSMs, LaD estimates most closely matched those from GRACE, with a good correspondence at seasonal time scales (Frappart et al., 2006). Our analysis also includes SWE ( $0.25^\circ$  resolution for years 1988-1997) from the analysis scheme described by Brown et al. (2003) and archived at the Canadian Cryospheric Information Network (CCIN, <http://www.ccin.ca>). LaD SWE at  $1^\circ$  resolution was mapped to the EASE-Grid using inverse-distance weighted interpolation, while CCIN SWE was aggregated to the EASE-Grid using the average of all  $0.25^\circ$  grids falling within each EASE-Grid cell. The PWBM-, LaD-, and SSM/I-derived SWE estimates are Pan-Arctic in nature, ie. defined at all 39,926 EASE-Grid cells encompassing the Pan-Arctic drainage basin (Figure 5-1). CCIN SWE are available across EASE-Grid cells over North America only.

Passive microwave radiances from SSM/I—aboard the Defense Meteorological Satellite Program satellite series since 1987—have been used to produce maps of SWE across large regions (Armstrong and Brodzik, 2001; Armstrong and Brodzik, 2002; Derksen et al., 2003; Goita et al., 2003). Monthly SWE estimated from SSM/I radiances for the period 1988–1999 (on the EASE-Grid) were acquired from the US National Snow and Ice Data Center (M. J.

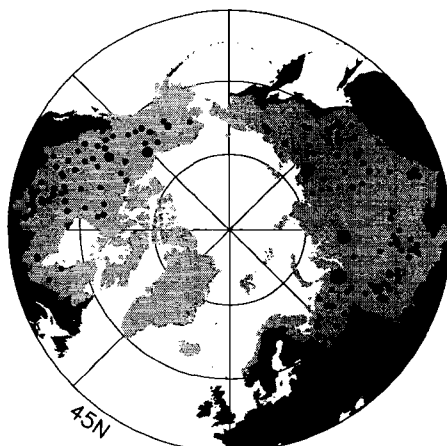


Figure 5-1: Locations of stations used in study. Pan-Arctic land mass (north of 45°N, dark gray), the arctic drainage basin (light gray), and locations of 179 river basins are shown. Dot sizes are scaled by basin area. A total of 39,926 EASE-Grid cells comprise the approximately 25 million km<sup>2</sup> drainage basin. Areas for the 179 river basins range from 20,000 km<sup>2</sup> to 486,000 km<sup>2</sup>.

Brodzik, personal communication, March 2, 2004) and are archived under the ArcticRIMS project (<http://RIMS.unh.edu>). The snow depth algorithm (Armstrong and Brodzik, 2001) is: snow depth (cm) = 1.59 \* [( $T_{19H} - 6$ ) - ( $T_{37H} - 1$ )], where  $T_{19H}$  is the brightness temperature at 19 GHz and  $T_{37H}$  is the brightness temperature at 37 GHz. Water equivalent is obtained from the product of snow depth and density.

Our analysis involves the use of what we term “pre-melt” SWE (the average of February and March monthly SWE) and spring total  $Q$  (the total discharge flow over the months April–June). We chose an average of two months of SWE over one month (or maximal monthly) to better represent mid-winter conditions. The SWE and  $Q$  time series are prewhitened to remove any trends prior to the covariance analysis. The  $Q$  records are drawn from an updated version of R-ArcticNET (Lammers et al., 2001). Although SWE

estimates are available for more recent years, our analysis here ends in 2000 due to a lack of more recent river discharge data for river basins across Eurasia. Alternate comparisons using SWE and  $Q$  which vary depending thaw timing derived from SSM/I data, and by simulated snowmelt, are described in the Results section. In this study, all SWE data sets have valid data at each grid defining the Pan-Arctic drainage basin. For each of the 179 river basins, pre-melt SWE is then determined as an average over all EASE-Grid cells defining the respective the basin.

Satellite-borne remote sensing at microwave wavelengths can be used to monitor landscape freeze/thaw state (Ulaby et al., 1986; Way et al., 1997; Frohling et al., 1999; Kimball et al., 2001). A step edge detection scheme applied to SSM/I brightness temperatures (McDonald et al., 2004) was used to identify the predominant springtime thaw transition event for each EASE-Grid cell. As with SWE, we derived a basin average date of thaw by averaging thaw event dates across the basin grid cells. Snow thaw across arctic basins often can occur over a period of weeks or months. Therefore, for large watersheds, our timing estimates derived from SSM/I brightness temperatures must be interpreted with caution. Nonetheless they provide a general approximation of the timing in landscape thaw for use in estimating pre-melt SWE and spring  $Q$ . As an illustration, monthly river discharge, SWE, and thaw date for the Yukon basin are shown in Figure 5-2a-d).

A simulated topological network (Vörösmarty et al., 2000a), recently implemented at 6 minute resolution, defines river basins over the approximately 25 million km<sup>2</sup> of the Pan-Arctic basin. The degree to which SWE and  $Q$  covary over the period 1988-2000 is evaluated using the coefficient of determination,  $R^2$  (squared correlation). Throughout our analysis we assume a significance level of 0.05 (5%) as the cutoff to determine whether a given SWE

vs.  $Q$  comparison is statistically significant, and not due to chance. For a sample size of 13 years this corresponds to  $R^2 \geq 0.22$ .

### 5.3 Results

Interannual variability in basin averaged, pre-melt SWE is compared with spring  $Q$  for 179 basins over the period 1988–2000. With the exception of SWE derived from SSM/I data, interannual variability in pre-melt SWE agrees well with spring  $Q$  variability across the Yukon basin in Alaska (Figure 5-2). Variability in basin SWE from the CCIN analysis scheme explains nearly 75% of the variability in spring  $Q$ . When reanalysis data drives the PWBM (PWBM/ERA-40 or PWBM/NNR), pre-melt SWE explains well over 50% of the variability in spring  $Q$ . Across the Yukon basin, the greater SWE variability and magnitude (among all SWE products) is noted for LaD SWE, along with a lower  $R^2$  (Figure 5-2c–d). Basin averaged SWE derived from SSM/I, however, shows little interannual variability and relatively low magnitude. For snow packs above 100 mm, the bias in SWE estimated from Scanning Multichannel Microwave Radiometer (SMMR) data was shown to be linearly related to the snow pack mass, with root-mean-square errors approaching 150 mm (Dong et al., 2005).

In contrast to the result over the Yukon basin, strong agreements in pre-melt SWE and spring  $Q$  variability are not noted across many of the study basins. Although  $R^2$ s for a majority of the North American basins are significant (mean values between 0.26 and 0.36, Table 1), agreements across eastern Eurasia are generally low (Figure 5-3, Table 1). Of the comparisons involving SWE from PWBM, more than half (130 of 231) are significant. Mean



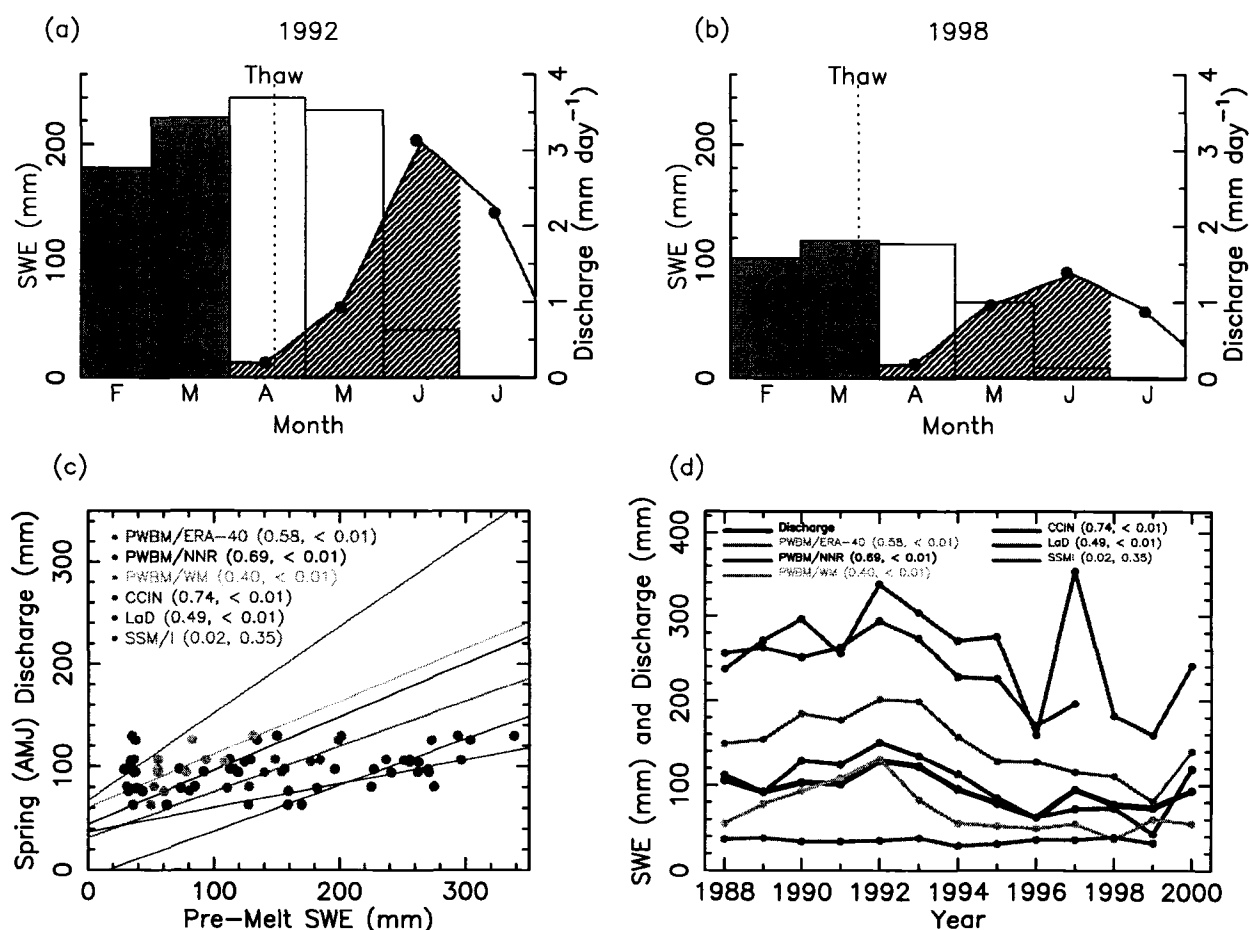


Figure 5-2: Monthly total SWE and mean discharge ( $Q$ ) across the Yukon basin for (a) 1992, a year with relatively high SWE and  $Q$ , and (b) 1998, a year with low SWE and  $Q$  totals. Vertical bars show SWE— in this case from PWBM driven with ERA-40 data (PWBM/ERA-40). February and March SWE values (in mm, gray bars here) are averaged to give “pre-melt” SWE in this study. April–June SWE are depicted by white bars. Spring  $Q$  (in mm day<sup>-1</sup>, monthly values indicated by dots at middle of month) is the integration of the monthly  $Q$  for April through June (hatched area), and is used for comparisons with the pre-melt SWE. A “thaw date” (marked Thaw) estimated from SSM/I data are used in alternate  $Q$  integrations. (c) Scatterplot of pre-melt SWE from each data set, for years 1988-2000. The best fit line based on linear least squares regression is shown. (d) Time series of SWE and  $Q$ . Statistics ( $R^2$  and associated  $p$ -value) for each covariance comparison are shown in parenthesis.

$R^2$ s from comparisons using the PWBM are comparable to those involving CCIN SWE estimates, which were developed using observed snow depth observations (Brown et al., 2003). Across all basins analyzed, the highest proportion of negative correlations (very poor agreement) and lowest overall  $R^2$  are associated with SSM/I SWE. The algorithm used to produce these estimates, like many of the early passive-microwave SWE algorithms, tends to underestimate SWE in forested regions. Models which account for the differing influences on the microwave signature have shown promise in reducing errors in forested regions (Goita et al., 2003). The best agreements involving SSM/I SWE are found across the prairies of south-central Canada. This is expected, as the SSM/I SWE algorithm was developed for application across the non-forested prairie provinces of Canada.

Comparisons using SWE from the PWBM simulations (PWBM/ERA-40, PWBM/NNR, and PWBM/WM), produce similar  $R^2$  values across each region, with mean value by region ranging from 0.15 to 0.36. Given that water budget models like PWBM are most sensitive to time-varying climatic inputs (Rawlins et al., 2003), small differences in  $R^2$  among these SWE estimates suggest similar spatial and temporal variability among the underlying precipitation data. Basin  $R^2$ s obtained from comparisons using LaD SWE are comparable with those from the comparisons using PWBM SWE across North America, while lower correlations are noted for Eurasia. Mean  $R^2$ s are higher across eastern Eurasia (east of longitude 90°E) as compared with western Eurasia. The better agreement across Siberia is likely attributable to the higher fraction of precipitation which falls as snow and the higher discharge/precipitation ratios across the colder east. When the PWBM is driven with precipitation data from a new gauge-corrected archive for the former USSR (“Daily and Sub-daily Precipitation for the Former USSR”) (National Climatic Data Center, 2005),

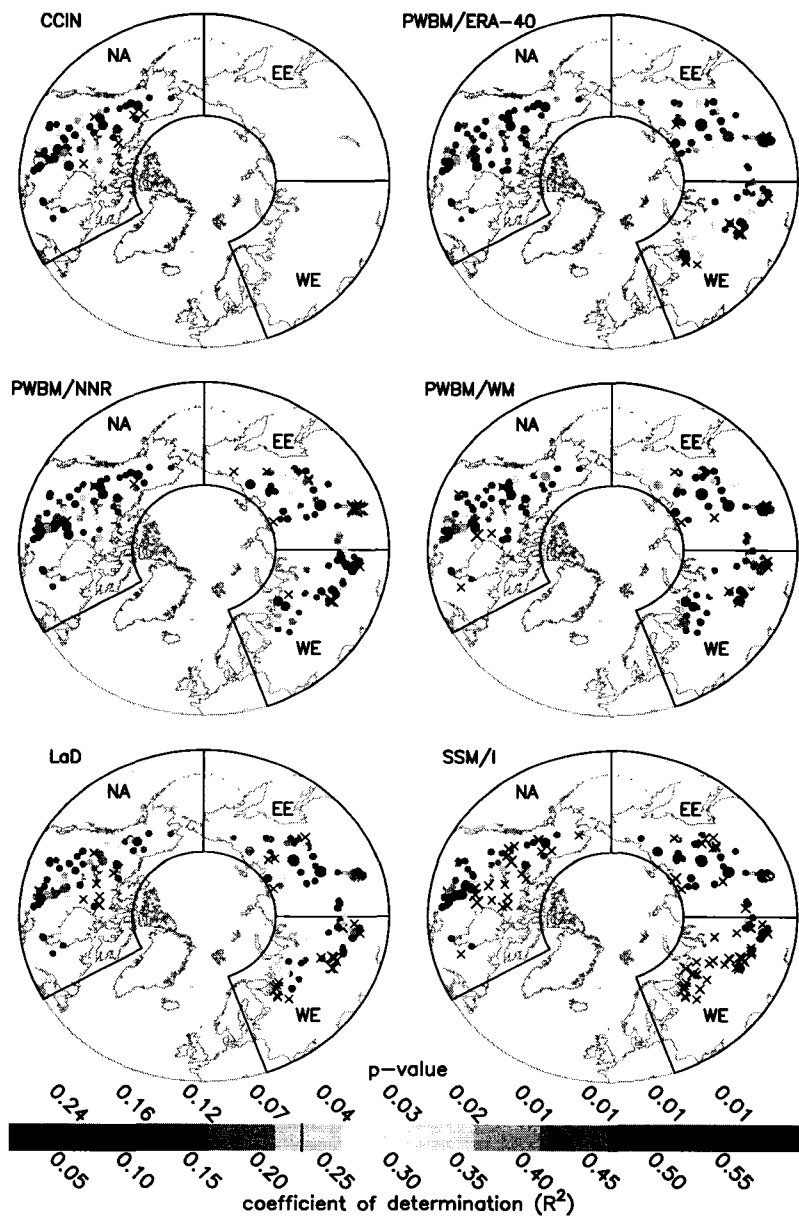


Figure 5-3: Explained variance ( $R^2$ ) for pre-melt SWE and spring  $Q$  comparisons (1988–2000) at the 179 river basins and for the 6 SWE products. SWE is taken from the CCIN SWE analysis; PWBM simulations driven by ERA-40, NNR and WM; LaD model; and SSM/I data. The 'X's mark basins with a negative correlation. Average  $R^2$  values across all basins, North America (NA), western Eurasia (WE), and eastern Eurasia (EE) are shown in Table 1. The vertical line in colorbar is level ( $R^2 = 0.22$ ) at which  $R^2$  is significant at 5% level. P-values associated with each  $R^2$  interval are shown above the colorbar. Note that  $p < 0.01$  for all  $R^2 \geq 0.40$ .

basin  $R^2$ s are generally no higher (figure not shown). This suggests that precipitation-gauge undercatch is not a significant influence on the computed SWE vs.  $Q$  agreements.

Snowmelt and subsequent rises in river  $Q$  begins in southerly regions of the terrestrial arctic and progresses northward each spring. Comparisons of winter SWE storage and  $Q$  over a fixed interval (e.g. April–June) are complicated when inputs from rainfall are significant, or a large fraction of the snowmelt occurs outside of the April–June period. A more meaningful comparison of SWE and river  $Q$  would be restricted to that fraction of  $Q$  which is attributable to the melting of snow. For example, simulated spring  $Q$  from PWBM—driven by ERA-40 data—explains a much higher proportion of observed spring  $Q$  than does the pre-melt SWE across the study basins (Figure 5-4, Table 1). The correspondence between simulated and observed spring  $Q$  suggests the model—to some degree—is accounting for processes connecting the snowpack and spring river flow, e.g. sublimation, rainfall, and soil infiltration.

To better understand the covariance between SWE and  $Q$ , alternate comparisons were made using PWBM/ERA-40 monthly SWE and an estimate of when thaw is assumed to have occurred. The month of thaw ( $TM$ , with  $TM - 1$ , and  $TM + 1$  indicating the month preceding and postceding the thaw month, respectively) was determined with a step edge detection scheme applied to SSM/I brightness temperatures (McDonald et al., 2004). Then,  $SWE_{TM}$  becomes monthly basin SWE during  $TM$  (or  $TM - 1$ ), and  $Q_{TM}$  is discharge in month  $TM$ . These alternate comparisons (across all 179 basins) are defined (a)  $SWE_{TM}$  vs. spring  $Q$ , (b)  $SWE_{TM-1}$  vs. spring  $Q$ , (c)  $SWE_{TM-1}$  vs.  $Q_{TM+1}$ , (d)  $SWE_{TM-1}$  vs.  $Q_{TM+1,2}$ .  $R^2$ s are highest for alternate comparison (b), which compared SWE in the month before thaw ( $TM - 1$ ) with spring (April–June)  $Q$  (Table 1). Yet, despite the fact that the

SWE Data	Feb-Mar SWE (mm)	% neg.	Min, Max, and Mean Coefficient of Variation, $R^2$			
			All	North Am.	W. Eurasia	E. Eurasia
CCIN	N/A	15.6	N/A	0.00, 0.87, 0.35	N/A	N/A
PWBM/ERA-40	103	8.5	0.00, 0.91, 0.28	0.00, 0.91, 0.36	0.00, 0.45, 0.15	0.00, 0.66, 0.27
PWBM/NNR	109	12.6	0.00, 0.87, 0.25	0.00, 0.87, 0.33	0.00, 0.56, 0.15	0.00, 0.71, 0.23
PWBM/WM	109	11.9	0.00, 0.91, 0.26	0.00, 0.91, 0.33	0.00, 0.75, 0.22	0.00, 0.53, 0.17
LaD	144	20.1	0.00, 0.83, 0.24	0.00, 0.83, 0.33	0.00, 0.49, 0.12	0.00, 0.69, 0.16
SSM/I	80	72.1	0.00, 0.76, 0.20	0.00, 0.76, 0.26	0.00, 0.40, 0.10	0.00, 0.57, 0.14
SimRO	103	5.3	0.00, 0.92, 0.46	0.01, 0.91, 0.44	0.00, 0.79, 0.35	0.05, 0.92, 0.57
PWBM/ERA-40 <sup>a</sup>	103	10.0	0.00, 0.80, 0.27	0.00, 0.80, 0.33	0.00, 0.61, 0.22	0.00, 0.64, 0.22
PWBM/ERA-40 <sup>b</sup>	103	18.7	0.00, 0.93, 0.34	0.00, 0.93, 0.37	0.00, 0.86, 0.38	0.00, 0.70, 0.26
PWBM/ERA-40 <sup>c</sup>	103	10.0	0.00, 0.80, 0.27	0.00, 0.80, 0.33	0.00, 0.61, 0.22	0.00, 0.64, 0.22
PWBM/ERA-40 <sup>d</sup>	103	10.0	0.00, 0.80, 0.27	0.00, 0.80, 0.33	0.00, 0.61, 0.22	0.00, 0.64, 0.22
PWBM/ERA-40 <sup>e</sup>	103	22.8	0.00, 0.76, 0.25	0.00, 0.76, 0.35	0.00, 0.28, 0.12	0.00, 0.58, 0.19

Table 5.1: Mean February-March SWE, percent negative correlations, and minimum, maximum, and mean coefficient of determination ( $R^2$ ) from the pre-melt SWE and spring  $Q$  comparisons. SWE (mm) is taken from data sets described in Data and Methods and shown in Figure 5-3. Percentage of negative correlations, and mean explained variance is also tabulated for simulated spring  $Q$  vs. observed spring  $Q$  (row SimRO), where simulated  $Q$  is from PWBM/ERA-40 model simulation. Mean February-March SWE is averaged across the terrestrial arctic basin, excluding Greenland. Individual  $R^2$  values for each study basin (shown in Figure 5-3) are averaged (excluding negative correlations) over all 179 river basins (All), and the basins across North America, western Eurasia, and eastern Eurasia, with the latter two separated by the 90°E meridian. Mean  $R^2$  for CCIN SWE are determined for North American sector only. PWBM/ERA-40<sup>a-e</sup> represent the alternate comparisons, defined in Results section.

mean  $R^2$  across western Eurasia improves from 0.15 (using default PWBM/ERA-40) to 0.38 (alternate comparison b), little difference is noted with the remaining alternate comparisons and other regions.

Lastly, we scaled spring  $Q$  using a factor  $S$ , where  $S = \text{PWBM monthly snow melt-runoff ratio}$ , with  $0 < S < 1$ . Then, snowmelt  $Q$  each month is  $Q_s = Q \cdot S$ . Each occurrence of  $Q_s$  was then summed resulting in a total  $Q_S$  each spring, for each basin. Using  $Q_S$  in place of the default  $Q$  (and PWBM/ERA-40 SWE), we note a decrease in agreement across eastern Eurasia, with no change across most of the domain. And although SWE from simulations with ERA-40, in general, explains more than a third of the variation in  $Q$ , a large proportion of the interannual variability is not due to SWE variability. When considering these results, it is interesting to note that Lammers et al. (2006) recently found that annual simulated discharge across Alaska (drawn from three separate models) was in poor agreement with observed discharge data between 1980–2001. Better agreements across northwestern North America, eastern Eurasia (EE in Figure 5-3), and parts of western Eurasia (WE) in this study are attributable to relatively higher snowfall rates and a greater interannual variability in spring discharge (Figure 5-4b). Conversely, the region of eastern Eurasia with numerous negative correlations is characterized by low spring discharge variability. Delays in snowmelt water reaching river systems, which can be significant (Hinzman and Kane, 1991), are likely an additional influence on these reported correlations. For large arctic basins, comparisons between snow storage and discharge volume are complicated by the large temporal variation in basin thaw and the delays in snowmelt water reaching the gauge. More meaningful comparisons between spatial SWE and river discharge are possible through the use of hydrograph separation to partition discharge into overland and baseflow

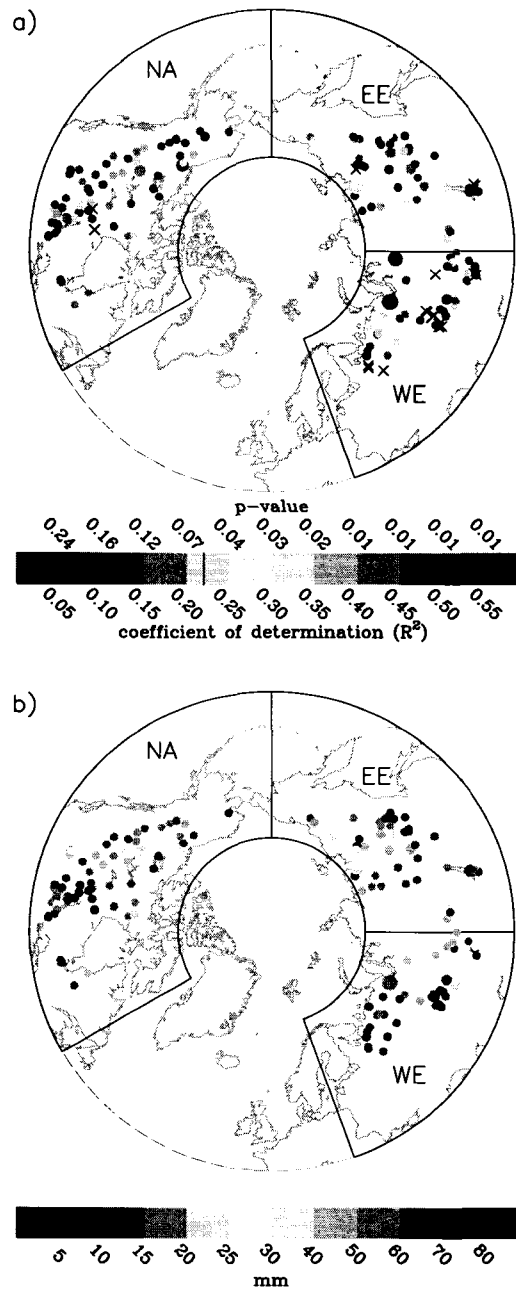


Figure 5-4: (a)  $R^2$  for PWBM simulated spring total  $Q$  vs. observed spring total  $Q$ . The vertical line in colorbar is level at which  $R^2$  is significant. Minimum, maximum, and mean  $R^2$ s across all basins, North America (NA), western Eurasia (WE), and eastern Eurasia (EE) are shown in Table 1. The 'X's mark basins with a negative correlation. (b) Standard deviation of spring (April–June) discharge for the period 1988–2000.

components. This, however, requires the use of daily discharge data which are more limited for the Pan-Arctic region.

## 5.4 Conclusions

In our comparisons of interannual variations in pre-melt SWE and spring  $Q$ ,  $R^2$  values are highest (mean of 0.25 to 0.28 over all basins) when PWBM is driven by ERA-40, NNR or WM climate data. Similar agreements are noted when SWE from the observed data analysis scheme are used, which suggests that the hydrological model is capturing as much variability in the spring flow as does the observed SWE scheme. Average  $R^2$  determined from the SSM/I SWE and spring  $Q$  comparisons are generally low, and a sizable majority (over 72%) of these correlations are negative. The low variability and magnitude is likely related to saturation of the SSM/I algorithm at high SWE values. Continued development of new regional schemes which account for microwave emission from forests should improve large-scale SWE estimates. Poor agreements among all SWE products—particularly across parts of western Eurasia—are noted in areas with low discharge variability. Pre-screening to eliminate basins with low flow or insufficient variability would likely improve the SWE vs.  $Q$  agreements.

Results of the covariance analysis using alternate temporal integrations to derive pre-melt SWE (or  $Q$ ) suggest that our choice of a fixed interval for spring, ie. April–June, is not the primary cause of the relatively low  $R^2$ s. Furthermore, we conclude that much of the interannual variability in river discharge must be influenced by factors other than basin SWE storage variations. The unexplained variability is likely due to a combination of



effects from physical processes (sublimation, infiltration) and errors in spatial SWE. Relatively good agreement between simulated and observed spring  $Q$  suggests that hydrological models can be useful in understanding the SWE-to- $Q$  linkages. Our results provide a benchmark of the relationship between the solid precipitation input and spring discharge flux, and demonstrate that hydrological models driven with reanalysis data can provide SWE estimates sufficient for use in validation of remote-sensing and GCM SWE fields. Additional studies using daily discharge data to better quantify snowmelt runoff will further facilitate SWE product evaluations and the understanding of linkages in arctic hydrological system.

## SUMMARY

This dissertation was undertaken in an effort to improve our understanding of the behavior of the Arctic system, specifically the hydroclimatology of the pan-Arctic drainage basin. A sparse and declining observational network limits our ability to improve quantitative models of the arctic system. A key development resulting from this study was a hydrological model (the Pan-Arctic Water Balance Model, PWBM) appropriate for simulations of the arctic hydrological cycle. The studies described here examined several data sets developed specifically to provide better estimates of climate drivers used to force the model. This dissertation examined our ability to monitor elements of the arctic hydrological, discussed limitations in common modeling approaches and remote sensing data sets, and offered suggestions for future studies.

As described in Chapter 1, the PWBM has been modified to include a scheme for simulating changes in freezing and thawing of water in the soil. PWBM-generated maximum summer active-layer thickness estimates differed from observed values by approximately  $1\sigma$ . Thus the model captured spatial variations in thaw depth to within the variability seen in observed data. Seasonal and permanent frost reduces infiltration into soils and severely limits the amount of water that can be stored. Simulating this process results in higher (10–25%) runoff as compared to simulations with the soil freeze/thaw submodel disabled. Processes involving groundwater are represented in the lowest soil layer, and no inter-grid connectivity is currently implemented. With recent research suggesting that groundwater

contributions to discharge during winter may be changing, improvements in simulation of winter discharge are likely with the implementation of more physically-based soil and groundwater algorithms.

Although good agreement was noted between simulated and observed long-term seasonal runoff to the 10 arctic sea basins, budget closure at the basin scale remains a problem. Simulated annual runoff is most sensitive to changes in climate driver data—precipitation and air temperature—while less effect is noted when other model parameters are altered. It is clear that improvements in the performance of conceptual and quantitative hydrological models will be achieved best with the use of more accurate time-varying climate forcings, rather than from more detailed specification of landscape attributes. Although the merits of model complexity were not fully tested here, comparisons between the BROOK90 and WBM (Federer et al., 2003) suggest that more detailed physical parameterizations do not increase model performance. A declining observational network limits the usefulness of spatial fields derived from point observations, while inaccuracies in satellite precipitation retrievals preclude their use at this time. Therefore, climate data from the NCEP-NCAR reanalysis (or the more recent ERA-40 reanalysis), when adjusted based on observed data (Serreze et al., 2003b), currently offer the best forcings for model simulations.

The analysis of snow thaw timing shows that, for much of the pan-Arctic, backscatter from SeaWinds offers the potential for monitoring high-latitude snow thaw at spatial scales appropriate for pan-Arctic applications. The study described a method to estimate the spatial and temporal dynamics of daily landscape freeze/thaw determined from low spatial resolution, high frequency (Ku-band) backscatter data. Daily river discharge for some 52 basins was used to represent observed landscape thaw. For nearly half of the pan-

Arctic grid cells analyzed, timing of snow thaw from SeaWinds data differed from timing noted in PWBM by less than one week. Scattering of the microwave signal is sensitive to other surface properties than snow and ground. Not surprisingly, the most unambiguous backscatter response in this study is noted across regions with (i) high snow accumulation, (ii) low to moderate tree cover and (iii) low topographic complexity.

Given that algorithms used to estimate snow thaw timing have not been tested under a wide variation of snow cover properties, land cover and terrain conditions, future validation studies will depend upon the collection of consistent and reliable ground truth hydrological measurements across a wide range of arctic landscapes. A paucity of daily river discharge observations across the arctic basin (Shiklomanov et al., 2002) hinders these efforts. To be useful for large-scale hydrological applications, remote sensing thaw timing estimates must account for the partitioning of freeze-thaw over different regions with highly variable landscape attributes. Unanswered in this study is the question of precisely how thaw timing information can be used to constrain hydrological and ecological processes models. Development of novel assimilation techniques which incorporate thaw timing estimates in model simulations may prove useful. Predictions of flood timing, for example, could be improved using the backscatter signal across large regions which lack observed meteorological stations.

This dissertation also explores whether observed increases in freshwater discharge from Eurasia (1936–1999) are attributable to changes in precipitation seasonality. As Earth's climate warms, the rate of water exchange in the land-atmosphere-ocean system is expected to increase. This analysis was motivated under the premise that high-latitude precipitation and, consequently, river runoff, is expected to increase under a warmed climate. Increases

in snowfall over the pan-Arctic may be particularly important since snowmelt there occurs on frozen soils with low infiltration rates (Kane and Stein, 1983; Stähli et al., 2001).

Analysis of the precipitation and discharge data revealed that annual discharge has become a larger fraction of total precipitation over the region during the period 1936–1999. Although basin-averaged rainfall has declined significantly, no significant change was noted in basin snowfall over the entire period. Significant snowfall increases were noted, however, across north-central Eurasia where soils have a limited capacity for infiltration during snowmelt. In addition, this study described the bias likely to occur when interpolating from point observations to a regular grid, which is due primarily to changes in station locations over time. Although the results, and those from other recent studies (Ye et al., 1998; Frey and Smith, 2003), suggest that increased cold season precipitation may be a significant driver of the discharge change, biases in early meteorological networks preclude a confident assessment of the precipitation-discharge linkages. However, the analysis of the effects of changing station network configurations indicates that real local snowfall increases over the region were likely greater, and the rainfall decreases were possibly less, than the changes determined from analysis of gridded data sets such as CRU and WM. Future studies related to the sharp decline in rainfall—which is consistent with projections of a general drying over most mid-latitude continental interiors—should focus on biological effects (increased risk of fires, changes to soil carbon stores) and human impacts. Reconstructing historical fields of arctic precipitation, to within tolerances required to properly address the discharge increase, may not be possible. However, by restricting evaluations to more recent decades, and through the use of “temporally-consistent” precipitation estimates available from arctic

reanalysis, more useful examinations of precipitation-discharge trends and other linkages in the land-atmosphere-ocean system can be made.

Issues surrounding our ability to simulate arctic water budgets were explored in a sensitivity study by forcing the PWBM (in 9 separate simulation runs) with three common climate data sets and three methods of estimating potential evapotranspiration (PET). Evaluations of simulated water budgets are important in developing a capability to predict and understand future changes in the arctic system. Biases in NCEP-NCAR reanalysis precipitation and vapor pressure—related to model convective feedbacks involving precipitation, radiation, and soil moisture (Serreze and Hurst, 2000)—cause an excess of simulated runoff. When precipitation from interpolations of station data, or from adjusted NCEP-NCAR reanalysis data are used, budget closure to within 7% is noted across the Yukon basin in Alaska. Runoff differences due to specification of landcover type are an order of magnitude smaller than differences due to biases in precipitation or in choice of PET function used. Validation of simulated water budgets in this manner helps to ensure that high-quality, robust model results are available for comparisons with observed data expected to be gathered during upcoming International Polar Year (IPY) campaign of 2007–2008.

The final chapter of this dissertation focused on the use of common gridded SWE data sets to understand linkages in the land-atmosphere system. Comparisons of SWE drawn from land surface models and microwave remote sensing with measured river discharge reveal that basin-averaged SWE prior to snowmelt explains a relatively small (yet statistically significant) fraction of interannual variability in spring (April–June) discharge. Much of the interannual variability in river discharge, therefore, must be influenced by factors other than basin SWE storage variations, such as sublimation and infiltration into the soil.

Variability and magnitude in SWE derived from SSM/I data are considerably lower than the variability and magnitude in SWE drawn from the land surface models, and generally poor agreement is noted between SSM/I SWE and spring discharge. To produce their global SWE product, Armstrong and Brodzik (2001) applied a single snow depth algorithm over the entire globe. Physically-based models (Wiesmann and Mätzler, 1998) which take into account the different contributions to the measured microwave radiation can improve spatial estimates of SWE. Development of new regional schemes which define the relationship between lake ice, snow cover, and microwave brightness temperature at the scale of satellite passive microwave observations are needed to improve large-scale SWE estimates. The next step in this research will be to compare new SWE estimates from the Advanced Microwave Scanning Radiometer (AMSR-E) instrument with river discharge data. A subset of the gauge records, from stations which have sufficient interannual variability, will be used for future comparisons, as low interannual variability impedes our ability to understand the SWE-discharge linkages.

Research plans involving the PWBM include simulations of future hydrological conditions driven with climate inputs drawn from IPCC scenarios. Model updates which help account for human influences on the water cycle are needed to improve regional simulations, particularly for areas where arctic populations have significant interaction with water resources. The addition of relatively simple routines to account for hydrological characteristics of mosses and other surface organic material should improve water budget simulations, particularly those with a changing vegetation structure. Impacts to arctic hydrology under climate change are the next focus of research involving the PWBM. This research will in-

volve accounting for the effects of impoundments, irrigation, groundwater withdrawals, and other anthropogenic effects.

Remote sensing of the arctic hydrosphere is in its infancy. Yet, the low density of *in situ* hydrometeorological observations, as well as problems with the use of optical sensors, make satellite-borne active and passive microwave observations promising options for monitoring of the arctic environment. Although addressed only briefly here, there is much potential for improvements in deriving snow mass budgets from remote sensing. Assessment of regional uncertainties will help to improve our understanding of a critical component in many high-latitude feedback processes. This dissertation and other similar efforts are important steps in our understanding of arctic change and the uncertainties inherent in projections of future change.



## BIBLIOGRAPHY

- ACIA (2005). Arctic Climate Impact Assessment. Cambridge University Press.
- Anderson, L. G., Olsson, K., and Chieriei, M. (1998). A carbon budget for the Arctic Ocean. *Global Biogeochem. Cycles*, 12:455–465.
- Anisimov, O. A., Shiklomanov, N. I., and Nelson, F. E. (1997). Effects of global warming on permafrost and active-layer thickness: Results from transient general circulation models. *Global and Planetary Change*, 15:61–77.
- Armstrong, R. L. and Brodzik, M. J. (1995). An earth-gridded SSM/I data set for cryospheric studies and global change monitoring. *Advances in Space Research*, 16(10):155–163.
- Armstrong, R. L. and Brodzik, M. J. (2001). Recent Northern Hemisphere snow extent: a comparison of data derived from visible and microwave sensors. *Geophys. Res. Lett.*, 28(19):3673–3676.
- Armstrong, R. L. and Brodzik, M. J. (2002). Hemispheric-scale comparison and evaluation of passive-microwave snow algorithms. *Annals of Glaciology*, 34(1):38–44.
- Armstrong, R. L., Knowles, K. W., Brodzik, M. J., and Hardman, M. A. (2006). DMSP SSM/I Pathfinder daily EASE-Grid brightness temperatures. Technical report, National Snow and Ice Center. CDROM, Boulder, CO, USA. <http://nsidc.org/data/nsidc-0032.html>.

- Arora, V. K. (2001). Assessment of simulated water balance for continental-scale river basins in an AMIP 2 simulation. *J. Geophys. Res.*, 106(D16):14827–14842.
- Berezovskaya, S., Yang, D., and Kane, D. L. (2004). Compatibility analysis of precipitation and runoff trends over the large siberian watersheds,. *Geophys. Res. Lett.* L21502, doi:10.1029/2004GL021277.
- Beringer, J., Chapin III, F. S., Thompson, C. D., and McGuire, A. D. (2005). Surface energy exchanges along a tundra-forest transition and feedbacks to climate. *Agric. For. Meteorol.*, 131:143–161.
- Beringer, J., McIlwaine, S., Lynch, A. H., Chapin III, F. S., and Bonan, G. B. (2002). The use of a reduced form model to assess the sensitivity of a land surface model to biotic surface parameters. *Clim. Dynam.*, 19:455–466.
- Blöschl, G. and Sivapalan, M. (1995). Scale issues in hydrological monitoring: A review. *Hydrol. Processes*, 9:251–290.
- Brodzik, M. J. (2004). personal communication, 2 March, 2004.
- Brodzik, M. J. and Knowles, K. (2002). EASE-Grid: A versatile set of equal-area projections and grids. in M. Goodchild (Ed.) *Discrete Global Grids*. Santa Barbara, CA, USA: National Center for Geographic Information and Analysis.
- Broecker, W. S. (1997). Thermohaline circulation, the Achilles heel of our climate system: Will man-made CO<sub>2</sub> upset the current balance? *Science*, 278:1582–1588.
- Brown, J., Hinkel, K. M., and Nelson, F. E. (2000). The Circumpolar Active Layer Monitoring (CALM) program. *Polar Geography*, 24(3):165–258.

- Brown, J., Jr., O. J. F., Heginbottom, J. A., and Melnikov, E. S. (1998). Circum-Arctic map of permafrost and ground-ice conditions. Technical report, National Snow and Ice Data Center/World Data Center for Glaciology. Digital Media.
- Brown, R. D., Brasnett, B., and Robinson, D. (2003). Gridded North American monthly snow depth and snow water equivalent for GCM evaluation. *Atmosphere-Ocean*, 41(1):1-14.
- Bruland, O., Maréchal, D., Sand, K., and Killingtveit, Å. (2001). Energy and water balance studies of a snow cover during snowmelt period at a high Arctic site. *Theor. Appl. Clim.*, 70:53-63.
- Calef, M. P., McGuire, A. D., Epstein, H. E., Rupp, T. S., and Shugart, H. H. (2005). Analysis of vegetation distribution in interior Alaska and sensitivity to climate change using a logistic regression approach. *Journal of Biogeography*, 32(5). Page 863, doi:10.1111/j.1365-2699.2004.01185.x.
- Chapman, W. L. and Walsh, J. E. (1993). Recent variations of sea ice and air temperature in high latitudes. *Bull. Am. Meteorol. Soc.*, 74(1):33-47.
- Cihlar, J. and Beaubien, J. (1998). Land cover of Canada Version 1.1. Special Publication, NBIOME Project. Produced by the Canada Centre for Remote Sensing and the Canadian Forest Service, Natural Resources Canada. Available on CDROM from the Canada Centre for Remote Sensing, Ottawa, Ontario. [http://www.ccrs.nrcan.gc.ca/optic/map\\_e.php](http://www.ccrs.nrcan.gc.ca/optic/map_e.php).

- Derksen, C., Walker, A., LeDrew, E., and Goodison, B. (2003). Combining SMMR and SSM/I data for time series analysis of central North American snow water equivalent. *J. Hydrometeorol.*, 4(2):304–316.
- Déry, S. J., Sheffield, J., and Wood, E. F. (2005). Connectivity between Eurasian snow cover extent and Canadian snow water equivalent and river discharge. *J. Geophys. Res.*, 110(D23). D23106, doi:10.1029/2005JD006173.
- Dong, J., Walker, J. P., and Houser, P. R. (2005). Factors affecting remotely sensed snow water equivalent uncertainty. *Remote Sens. Environ.*, 97:68–82.
- Draper, N. R. and Smith, H. (1981). *Applied Regression Analysis*. New York: John Wiley and Sons.
- Elachi, C. (1987). *Introduction to the Physics and Techniques of Remote Sensing*. John Wiley and Sons, New York.
- European Centre for Medium Range Weather Forecasts (ECMWF) (2002). ERA-40 Project Report Series. 3. Workshop on Re-analysis, 5-9 November 2001. Technical report, European Centre for Medium Range Weather Forecasts. 443 pp.
- Federer, C. A., Fekete, B. M., and Vörösmarty, C. J. (2003). Sensitivity of annual evaporation to soil and root properties in two models of contrasting complexity. *J. Hydrometeorol.*, 4(6):1276–1290.
- Federer, C. A. and Lash, D. (1978). Brook: A hydrologic simulation model for eastern forests. Technical report, University of New Hampshire Water Resources Research Center *Research Report* No. 19.

- Federer, C. A., Vörösmarty, C. J., and Fekete, B. M. (1996). Intercomparison of methods for calculating potential evaporation in regional and global water balance models. *Water Resour. Res.*, 32(7):2315–2321.
- Fekete, B. M., Vörösmarty, C. J., and Grabs, W. (1999). Global composite runoff fields based on observed river discharge and simulated water balance. Technical report, WMO Global Runoff Data Center Report #22, Koblenz, Germany.
- Fekete, B. M., Vörösmarty, C. J., Roads, J. O., and Willmott, C. J. (2004). Uncertainties in precipitation and their impacts on runoff estimates. *J. Clim.*, 17:294–304.
- Fleming, M. D. (1997). A statewide vegetation map of Alaska using phenological classification of AVHRR data. In *Proceedings of the Second circumpolar Arctic vegetation mapping workshop and the CAVM-North America workshop*, pages 25–26. Boulder, Colorado, USA.
- Food and Agriculture Organization/UNESCO (1995). Digital Soil Map of the World and Derived Properties, version 3.5, November, 1995. Original scale 1:5,000000, UNESCO, Paris, France.
- Forland, E. J. and Hanssen-Bauer, I. (2000). Increased precipitation in the Norwegian Arctic: True or false. *Clim. Change*, 46(4):485–509. doi:10.1023/A:1005613304674.
- Frappart, F., Ramillien, G., Biancamaria, S., Mognard, N. M., and Cazenave, A. (2006). Evolution of high-latitude snow mass derived from the GRACE gravimetry mission (2002–2004). *Geophys. Res. Lett.*, 33. L02501, doi:10.10292005GL024778.

- Frey, K. E. and Smith, L. C. (2003). Recent temperature and precipitation increases in West Siberia and their association with the Arctic Oscillation. *Polar Research*, 22(2):287–300.
- Frolking, S., McDonald, K. C., Kimball, J., Way, J. B., Zimmermann, R., and Running, S. W. (1999). Using the space-borne NASA scatterometer (NSCAT) to determine the frozen and thawed seasons of a boreal landscape. *J. Geophys. Res.*, 104(D22):27,895–27,907.
- Gesch, D. L., Verdin, K. L., and Greenlee, S. K. (1999). New land surface digital elevation model covers the Earth. *EOS Trans. AGU*, 80(6):69–70.
- Global Soil Data Task (2000). Global gridded surfaces of selected soil characteristics (IGBP-DIS). Available from the ORNL Distributed Active Archive Center, Oak Ridge National Laboratory, Oak Ridge, Tennessee, USA.
- Goita, K., Walker, A. E., and Goodison, B. E. (2003). Algorithm development for the estimation of snow water equivalent in the boreal forest using passive microwave data. *Int. J. Remote Sens.*, 24(5):1097–1102.
- Grippa, M., Mognard, N., and Toana, T. L. (2005). Comparison between the interannual variability of snow parameters derived from SSM/I and the Ob river discharge. *Remote Sens. Environ.*, 98:35–44.
- Groisman, P. Y., Karl, T. R., and Knight, T. W. (1994). Observed impact of snow cover on the heat balance and the rise of continental spring temperatures. *Science*, 263:198–200.

- Groisman, P. Y., Koknaeva, V. V., Belokrylova, T. A., and Karl, T. R. (1991). Overcoming biases of precipitation measurement: A history of the USSR experience. *Bull. Am. Meteorol. Soc.*, 72(11):1725–1733.
- Hall, A. (2004). The role of surface albedo feedback in climate. *J. Clim.*, 17:1550–1568.
- Hamon, W. R. (1963). Computation of direct runoff amounts from storm rainfall. *Int. Assoc. Sci. Hydrol. Publ.*, 63:52–62.
- Hansen, M., DeFries, R., Townshend, J., Carroll, M., Dimiceli, C., and Sohlberg, R. (2003). Global percent tree cover at a spatial resolution of 500 meters: First results of the MODIS vegetation continuous fields algorithm. *Earth Interactions*, 7(10):1–15.
- Hillard, U., Sridhar, V., Lettenmaier, D. P., and McDonald, K. C. (2003). Assessing snowmelt dynamics with NASA scatterometer (NSCAT) data and a hydrologic process model. *Remote Sens. Environ.*, 86:52–69.
- Hinzman, L. D. and Kane, D. L. (1991). Snow hydrology of a headwater Arctic basin 2. Conceptual analysis and computer modeling. *Water Resour. Res.*, 27(6):1111–1121.
- Hinzman, L. D. and Kane, D. L. (1992). Potential response of an Arctic watershed during a period of global warming. *J. Geophys. Res.*, 97:2811–2820.
- Holden, J. B. (1999). A permafrost-based water balance model. Master's thesis, University of New Hampshire (Dept. of Earth Sciences).
- Holmes, R. M., Peterson, B. J., Gordeev, V. V., Zhulidov, A. V., Maybeck, M., Lammers, R. B., and Vörösmarty, C. J. (2000). Flux of nutrients from Russian rivers to the Arctic

Ocean: Can we establish a baseline against which to judge future change. *Water Resour. Res.*, 36(8):2309–2320.

Houghton, J. T., Ding, Y., Griggs, D. J., Noguer, M., van der Linden, P. J., and Xiaosu, D. (2001). *Climate Change 2001: The Scientific Basis. Third Assessment Report. IPCC Working Group I*. Cambridge University Press. Cambridge, United Kingdom.

Houghton, J. T., Filho, L. G. M., Callandar, B. A., Harris, N., Kattenberg, A., and Maskell, K. (1996). *Climate Change 1995: The Science of Climate Change. Contribution of Working Group I to the Second Assessment of the Intergovernmental Panel on Climate Change*. Cambridge University Press. Cambridge, United Kingdom, 572 pp.

Jumikis, A. R. (1997). *Thermal Geotechnics*. Rutgers Univ. Press. New Brunswick, NJ, 375 pp.

Kalnay, E., Kanamitsu, M., Kistler, R., Collins, W., Deaven, D., Gandin, L., Iredell, M., Saha, S., White, G., Woolen, J., Zhu, Y., Chelliah, M., Ebisuzaki, W., Higgins, W., Janowiak, J., Ropelewski, K. C., Wang, J., Leetma, A., Reynolds, R., Jenne, R., and Joseph, D. (1996). The NCEP/NCAR 40-year reanalysis project. *Bull. Am. Meteorol. Soc.*, 77:437–471.

Kane, D. L. (1997). *Global Change and Arctic Terrestrial Ecosystems, Ecol. Stud.*, volume 124, chapter The Impact of Arctic hydrologic perturbations on Arctic ecosystems induced by climate change, pages 63–81. Springer-Verlag, New York.

Kane, D. L., McNamara, J. P., Yang, D., Olsson, P. Q., and Gieck, R. E. (2003). An extreme rainfall/runoff event in Arctic Alaska. *J. Hydrometeorol.*, 4(6):1220–1228.



- Kane, D. L. and Stein, J. (1983). Water movement into seasonally frozen soils. *Water Resour. Res.*, 19:1547–1557.
- Karl, T. R., Groisman, P. Y., Knight, R. W., and Heim, R. R. (1993). Recent variations of snow cover and snowfall in North America and their relation to precipitation and temperature variations. *J. Clim.*, 6:1327–1344.
- Kimball, J. S., McDonald, K. C., Frohling, S., and Running, S. W. (2004a). Radar remote sensing of the spring thaw transition across a boreal landscape. *Remote Sens. Environ.*, 89:163–175.
- Kimball, J. S., McDonald, K. C., Frohling, S., and Running, S. W. (2004b). Satellite radar remote sensing of seasonal growing seasons for boreal and subalpine evergreen forests. *Remote Sens. Environ.*, 90:243–258.
- Kimball, J. S., McDonald, K. C., Keyser, A. R., Frohling, S., and Running, S. W. (2001). Application of the NASA scatterometer (NSCAT) for determining the daily frozen and nonfrozen landscape of Alaska. *Remote Sens. Environ.*, 75:113–126.
- King, M. D. and Greenstone, R. (1999). *1999 EOS Reference Handbook: A Guide to NASA's Earth Science Enterprise and the Earth Observing System*. NASA Goddard Space Flight Center, Greenbelt, Maryland. NASA document NP-1999-08-134-GSFC 361 pp.
- Kistler, R., Kalnay, E., Collins, W., Saha, S., White, G., Woolen, J., Chelliah, M., Ebisuzaki, W., Kanamitsu, M., Kousky, V., van den Dool, H., Jenne, R., and Fiorino, M. (2001). The NCEP-NCAR 50-year reanalysis: Monthly means CD-ROM and documentation. *Bull. Am. Meteorol. Soc.*, 82:247–267.

- Kite, G. W. and Haberlandt, U. (1999). Atmospheric model data for macroscale hydrology. *J. Hydrol.*, 217:303–313.
- Klene, A. E., Nelson, F. E., Shiklomanov, N. I., and Hinkel, K. M. (2001). The N-factor in natural landscapes: Variability of air and soil-surface temperatures, Kuparuk River basin, Alaska, U.S.A. *Arctic, Antarctic and Alpine Research*, 33(2):140–148.
- Kraszewski, A. (1996). *Microwave Aquametry: Electromagnetic Wave Interaction with Water-Containing Materials*. IEEE Press. 484 pp.
- Lammers, R. B., Rawlins, M., McGuire, D., Clein, J., Kimball, J., and Wu, W. (2006). Water budget closure over the western arctic and Yukon river basin - a model inter-comparison. *Earth Interactions*. in preparation.
- Lammers, R. B., Shiklomanov, A. I., Vörösmarty, C. J., Fekete, B. M., and Peterson, B. J. (2001). Assessment of contemporary Arctic river runoff based on observational discharge records. *J. Geophys. Res.*, 106(D4):3321–3334.
- Lawrence, D. M. and Slater, A. G. (2005). A projection of severe near-surface permafrost degradation during the 21st century. *Geophys. Res. Lett.* doi:10.1029/2005GL025080.
- Legates, D. R. and Willmott, C. J. (1990a). Mean seasonal and spatial variability in gauge-corrected global precipitation. *Int. J. Climatol.*, 10:111–133.
- Legates, D. R. and Willmott, C. J. (1990b). Mean seasonal and spatial variability in global surface air temperature. *Theor. Appl. Clim.*, 41:11–21.

- Liang, X., Lettenmaier, D. P., Wood, E. F., and Burges, S. J. (1994). A simple hydrologically based model of land surface water and energy fluxes for general circulation models. *J. Geophys. Res.*, 99:14415–14428.
- Liu, H., Randerson, J. T., Lindfors, J., and Chapin III, F. S. (2005). Changes in the surface energy budget after fire in boreal ecosystems of interior Alaska: An annual perspective. *J. Geophys. Res.* D13101,doi:10.1029/2004JD005158.
- Lunardini, V. J. (1978). Theory of N-factor and correlation of data. In *Proceedings of the Third International Conference on Permafrost*, volume 1, pages 40–46. National Council of Canada, Ottawa.
- Lunardini, V. J. (1981). *Heat Transfer in Cold Climates*. Van Nostrand Reinhold, New York. 731 pp.
- Manabe, S., Stouffer, R. J., Spelman, M. J., and Bryan, K. (1991). Transient responses of a coupled ocean-atmosphere model to gradual changes of atmospheric CO<sub>2</sub>. Part I: Annual mean response. *J. Clim.*, 4:785–817.
- Manabe, W., Stroeve, J., Fetterer, F., and Knowles, K. (2005). Reductions in Arctic sea ice cover no longer limited to summer. *Geophys. Res. Lett.*, 86:326–327.
- Maurer, E. P., O'Donnell, G. M., Lettenmaier, D. P., and Roads, J. O. (2001). Evaluation of the land surface water budget in NCEP/NCAR and NCEP/DOE Reanalysis using an off-line hydrological model. *J. Geophys. Res.*, 106(D16):17841–17862.

- McClelland, J. W., Holmes, R. M., Peterson, B. J., and Stieglitz, M. (2004). Increasing river discharge in the Eurasian Arctic: Consideration of dams, permafrost thaw, and fires as potential agents of change. *J. Geophys. Res.*, 109. D18102, doi:10.1029/2004JD004583.
- McDonald, K. C., Kimball, J. S., Njoku, E., Zimmermann, R., and Zhao, M. (2004). Variability in springtime thaw in the terrestrial high latitudes: Monitoring a major control on biospheric assimilation of atmospheric CO<sub>2</sub> with spaceborne microwave remote sensing. *Earth Interactions*, 7:1–23.
- McGuire, A. D. (2005). Western Arctic Linkage Experiment (WALE): Background, objectives, results, and conclusions. *Earth Interactions*. in review.
- Mellilo, J. M., McGuire, D. A., Kicklighter, D. W., Moore III, B., Vörösmarty, C. J., and Schloss, A. L. (1993). Global climate change and terrestrial net primary production. *Nature*, 363:234–240.
- Milly, P. C. D. and Shmakin, A. B. (2002). Global modeling of land water and energy balances: I. The Land Dynamics (LaD) model. *J. Hydrometeorol.*, 3:283–299.
- Mintz, Y. and Walker, G. K. (1993). Global fields of soil moisture and land surface evapotranspiration derived from observed precipitation and surface air temperature. *J. Appl. Meteorol.*, 32:1305–1334.
- Mitchell, T. D., Carter, T. R., Jones, P. D., Hulme, M., and New, M. (2004). A comprehensive set of high-resolution grids of monthly climate for Europe and the globe: the observed record (1901–2000) and 16 scenarios (2001–2100). Technical report, Tyndall Centre for Climate Change Research. available online at: <http://www.cru.uea.ac.uk/>.

- Monteith, J. L. (1965). Evaporation and environment. In *The State and Movement of Water in Living Organisms*, pages 205–233. Cambridge University Press, Cambridge UK. Proc. 19th Symposium of the Society of Experimental Biology.
- Müller, H. G., Carlstein, E., and Siegmund, D. (1994). Change-point Problems. *Institute of Mathematical Statistics Lecture Notes and Monograph Series*, 23.
- National Climatic Data Center (2005). Daily and Sub-daily Precipitation for the Former USSR. Technical report. Available from National Geophysical Data Center, <http://www.ncdc.noaa.gov/oa/documentlibrary/surface-doc.html9813>.
- Nelson, F. E., Shiklomanov, N. I., and Mueller, G. R. (1999). Variability of active-layer thickness at multiple spatial scale, North-central Alaska, U.S.A. *Arctic, Antarctic and Alpine Research*, 11(2):179–186.
- Nelson, F. E., Shiklomanov, N. I., Mueller, G. R., Hinkel, K. M., Walker, D. A., and Bockheim, J. G. (1997). Estimating active-layer thickness over a large region: Kuparuk River basin, Alaska, U.S.A. *Arct. Alp. Res.*, 29:367–378.
- Nghiem, S. V. and Tsai, W. Y. (2001). Global snow cover monitoring with spaceborne  $K_u$ -band scatterometer. *IEEE Trans. Geosci. Rem. Sens.*, 39:2118–2134.
- Nicholls, N., Gruza, G. V., Jouzel, J., Karl, T. R., Ogallo, L. A., and Parker, D. E. (1996). *Climate Change 1995, The Science of Climate Change*, chapter Observed Climate Variability and Change, pages 133–192. Cambridge University Press. Intergovernmental Panel on Climate Change, Contribution of Working Group I to the Second Assessment Report of the Intergovernmental Panel on Climate Change in J. T. Houghton, J. T., Meira Filho, L. G., Callander, B. A., Harris, N., Kattenburg, A., and Maskell, K. (eds.).

- Nijssen, B., O'Donnell, G. M., Lettenmaier, D. P., Lohmann, D., and Wood, E. F. (2001). Predicting the discharge of global rivers. *J. Clim.*, 14:3307–3323.
- Nishida, K., Nemani, R. R., Running, S. W., and Glassy, J. (2003). An operational remote sensing algorithm of land surface evaporation. *J. Geophys. Res.*, 108(D9). doi: 10.1029/2002JD002062.
- Northern Hemisphere Snow Cover Data (1999). Northern hemisphere snow cover data, operational 89x89 northern hemisphere snow cover data 1973–present. Technical report.
- NSIDC (1995). The Equal-Area Scalable Grid. Technical report, National Snow and Ice Data Center. <http://nsidc.org/data/ease/index.html>.
- Nyberg, L., Stähli, M., Mellander, P. E., and Bishop, K. H. (2001). Soil frost effects on soil water and runoff dynamics along a boreal transect: 1. Field investigations. *Hydrol. Processes*, 15:909–926.
- Oechel, W. C., Hastings, S. J., Vourlitis, G., Jenkins, M., Riechers, G., and Grulke, N. (1993). Recent change of Arctic tundra ecosystems from a net carbon sink to a source. *Nature*, 361:520–523.
- Osterkamp, T. E. and Romanovsky, V. E. (1999). Evidence for warming and thawing of discontinuous permafrost in alaska. *Permafrost and Periglacial Processes*, 10(1):17–37.
- Overpeck, J., Hughen, K., Hardy, D., Bradley, R., Case, R., Douglas, M., Finney, B., Gajewski, K., Jacoby, G., Jennings, A., Lamoureux, S., Lasca, A., MacDonald, G., Moore, J., Retelle, M., Smith, S., Wolfe, A., and Zielinski, G. (1997). Arctic environmental change of the last four centuries. *Science*, 278:1251–1256.

- Parish, D. F. and Derber, J. C. (1992). The National Meteorological Center's spectral statistical interpolation analysis system. *Mon. Wea. Rev.*, 120:1747–1763.
- Peterson, B. J., Holmes, R. M., McClelland, J. W., Vörösmarty, C. J., Lammers, R. B., Shiklomanov, A. I., Shiklomanov, I. A., and Rahmstorf, S. (2002). Increasing river discharge to the Arctic Ocean. *Science*, 298:2171–2173.
- Pitman, A. J., Slater, A. G., Desborough, C. E., and Zhao, M. (1999). Uncertainty in the simulation of runoff due to the parameterization of frozen soil moisture using the global soil moisture project methodology. *J. Geophys. Res.*, 104(D14):16879–16888.
- Rahmstorf, S. (1995). Bifurcations of the Atlantic thermohaline circulation in response to changes in the hydrological cycle. *Nature*, 378:145–149.
- Randall, D. (1994). Analysis of snow feedbacks in 14 general circulation models. *J. Geophys. Res.*, 99:20757–20771.
- Raney, K. R. (1998). *Radar Fundamentals: Technical Perspective*, volume 2 of *Principles and Applications of Imaging Radar*. John Wiley and Sons Inc, New York. F. M. Henderson and A. J. Lewis, Eds.
- Rawlins, M. A., Lammers, R. B., Froking, S., Fekete, B. M., and Vörösmarty, C. J. (2003). Simulating pan-Arctic runoff with a macro-scale terrestrial water balance model. *Hydrological Processes*, 17:2521–2539.
- Rawlins, M. A., Lammers, R. B., Froking, S., and Vörösmarty, C. J. (2005). Effects of uncertainty in climate inputs on simulated evapotranspiration and runoff in the western arctic. *Earth Interactions*. in revision.

- Rawlins, M. A., McDonald, K. C., Froking, S., Lammers, R. B., Fahnestock, M., Kimball, J. S., and Vörösmarty, C. J. (2004). Remote sensing of snow thaw at the pan-arctic scale using the seawinds scatterometer. *J. Hydrol.* in press.
- Rawlins, M. A. and Willmott, C. J. (2003). Winter air-temperature change across the terrestrial Arctic, 1961–1990. *Arctic, Antarctic and Alpine Research*, 35(4):530–537.
- Rawlins, M. A., Willmott, C. J., Shiklomanov, A., Linder, E., Froking, S., Lammers, R. B., and Vörösmarty, C. J. (2006). Evaluation of trends in derived snowfall and rainfall across eurasia and linkages with discharge to the arctic ocean. *Geophys. Res. Lett.*, 33. L07403, doi:10.1029/2005GL025231.
- Rees, A., Derksen, C., English, M., Walker, A., and Duguay, C. (2006). Uncertainty in snow mass retrievals from satellite passive microwave data in lake-rich high-latitude environments. *Hydrol. Processes*, 20:1019–1022.
- Roads, J. O., Chen, S. C., Guetter, A., and Georgakakos, K. (1994). Large-scale aspects of the United States hydrologic cycle. *Bull. Am. Meteorol. Soc.*, 75:1589–1610.
- Robeson, S. M. (2004). Trends in time-varying percentiles of daily minimum and maximum air temperature over North America. *Geophys. Res. Lett.*, 31. doi:10.1029/2003GL019019.
- Robock, A., Vinnikov, K. Y., and Schlosser, C. A. (1995). Use of midlatitude soil moisture and meteorological observations to validate soil moisture simulations with biosphere bucket models. *J. Clim.*, 8:15–35.



- Roesch, A. (2006). Evaluation of surface albedo and snow cover in AR4 coupled climate models. *Geophys. Res. Lett.*, 111. doi:10.1029/2005JD006473.
- Romanovsky, V., Burgess, M., Smith, S., Yoshikawa, K., and Brown, J. (2002). Permafrost temperature records: Indicators of climate change. *EOS Trans. AGU*, 83(50):589–594.
- Romanovsky, V. E. and Osterkamp, T. E. (1995). Interannual variations of the thermal regime of the active layer and near-surface permafrost in northern alaska. *Permafrost and Periglacial Processes*, 6:313–335.
- Rothrock, D. A., Zhang, J., and Yu, Y. (2003). The arctic ice thickness anomaly of the 1990s: A consistent view from observations and models. *J. Geophys. Res.*, 108(C3):3083. doi:10.1029/2001JC001208.
- Schiller, A., Mikolajewicz, U., and Voss, R. (1997). The stability of the North Atlantic thermohaline circulation in a coupled ocean-atmosphere general circulation model. *Clim. Dynam.*, 13:325–347.
- SEARCH SCC (2001). SEARCH: Study of Environmental Arctic Change, Science Plan. Technical report, Seattle, Polar Science Center, University of Washington. Available at: <http://psc.apl.washington.edu/search>.
- Serreze, M. C., Clark, M. P., and Bromwich, D. H. (2003a). Large-scale hydroclimatology of the terrestrial Arctic drainage system. *J. Geophys. Res.*, 108(D2).
- Serreze, M. C., Clark, M. P., Bromwich, D. H., Etringer, A. J., Zhang, T., and Lammers, R. (2003b). Monitoring precipitation over the Arctic terrestrial drainage system: Data

- requirements, shortcomings, and applications of atmospheric reanalysis. *J. Hydrometeorol.*, 4(2):387–407.
- Serreze, M. C. and Hurst, C. M. (2000). Representation of mean Arctic precipitation from NCEP–NCAR and ERA Reanalysis. *J. Hydrometeorol.*, 4:387–407.
- Serreze, M. C., Maslanik, J. A., Scambos, T. A., Fetterer, F., and Stroeve, J. (2002). A record minimum sea ice cover in the Arctic Ocean for summer 2002. *Geophys. Res. Lett.*, 30:110. doi:10.1029/2002GL016406.
- Serreze, M. C., Walsh, J. E., Chapin III, F. S., Osterkamp, T., Dyurgerov, M., Romanovsky, V., Oechel, W. C., Morison, J., Zhang, T., and Barry, R. (2000). Observational evidence of recent change in the northern high-latitude environment. *Clim. Change*, 46:159–207.
- Shi, J. and Dozier, J. (1995). Inferring snow wetness using c-band data from SIR-C's polarimetric synthetic aperture radar. *IEEE Trans. Geoscience and Remote Sensing*, 34(4):905–914.
- Shiklomanov, A. I., Lammers, R. B., and Vörösmarty, C. J. (2002). Widespread decline in hydrological monitoring threatens Pan-Arctic research. *EOS Trans. AGU*, 83(2):13–17.
- Shiklomanov, I. A. (1998). A comprehensive assessment of the freshwater resources of the world: Assessment of water resources and availability in the world. Technical report, WMO, UNDP, UNED, FAO, UNESCO, World Bank, WHO, UNIDO, SEI. Published by WMO, Geneva, 88 p.
- Shiklomanov, I. A., Shiklomanov, A. I., Lammers, R. B., Peterson, B. J., and Vörösmarty, C. J. (2000). *The dynamics of river water inflow to the Arctic Ocean*, pages 281–296.

- Kluwer Academic Press, Dordrecht. in *The Freshwater Budget of the Arctic Ocean*, edited by E.I Lewis, et al.
- Shmakin, A. B., Milly, P. C. D., and Dunne, K. (2002). Global modeling of land water and energy balances. part III: Interannual variability. *J. Hydrometeorol.*, 3(3):311–321.
- Stähli, M., Nyberg, L., Mellander, P. E., Jamison, P. E., and Bishop, K. H. (2001). Soil frost effects on soil water and runoff dynamics along a boreal transect: 1. simulations. *Hydrol. Processes*, 15:927–941.
- Sturm, M. J., Holmgren, J., and Liston, G. E. (1995). A seasonal snow cover classification system for local to global applications. *J. Clim.*, 8(5):1261–1283.
- Su, F., Adam, J. C., Bowling, L. C., and Lettenmaier, D. P. (2005). Streamflow simulations of the terrestrial Arctic domain. *J. Geophys. Res.*, 110. D08112, doi:10.1029/2004JD005518.
- Töyrä, J., Pietroniro, A., and Bonsal, B. (2005). Evaluation of GCM simulated climate over the Canadian prairie provinces. *Canadian Water Resources Journal*, 30(3):245–262.
- Ulaby, F. T., Moore, R. K., and Fung, A. K. (1986). *Microwave Remote Sensing: Active and Passive, Vol. III – Volume Scattering and Emission Theory, Advanced Systems and Applications*. Artec House Inc., Dedham, MA.
- Uppala, S., Gibson, J. K., Fiorino, M., Hernandez, A., Kallberg, P., Li, X., Onogi, K., and Saarinen, S. (2000). ECMWF Second Generation Reanalysis. In *Proceedings of the Second WCRP International Conference on Reanalysis*. pages 9–13. WMO/TD-No. 985.

- USGS EROS Data Center (1996). Global 30 arc second elevation data set GTOPO30.  
<http://edcwww.cr.usgs.gov/landdaac/gtopo30/README.html>.
- van Wijk, W. R. and de Vries, D. A. (1963). *Physics of Plant Environment*. van Wijk WR (ed.). North Holland: Amsterdam; 102–143.
- Vörösmarty, C. J., Federer, C. A., and Schloss, A. L. (1998). Potential evapotranspiration functions compared on US watersheds: Possible implications for global-scale water balance and terrestrial ecosystem modeling. *J. Hydrol.*, 207:147–169.
- Vörösmarty, C. J., Fekete, B. M., Maybeck, M., and Lammers, R. B. (2000a). Geomorphometric attributes of the global system of rivers at 30-min spatial resolution. *J. Hydrol.*, 237:17–39.
- Vörösmarty, C. J., Fekete, B. M., Maybeck, M., and Lammers, R. B. (2000b). Global system of rivers: Its role in organizing continental land mass and defining land-to-ocean linkages. *Global Biogeochem. Cycles*, 14:599–621.
- Vörösmarty, C. J., Hinzman, L. D., Peterson, B. J., Bromwich, D. H., Hamilton, L. C., Morrison, J., Romanovsky, V. E., Sturm, M., and Webb, R. S. (2001). The hydrologic cycle and its role in arctic and global environmental change: A rationale and strategy for synthesis study. Technical report, Fairbanks, AK: Arctic Research Consortium of the U.S.
- Vörösmarty, C. J., Moore III, B., Grace, A. L., Gildea, M. P., Melillo, J. M., Peterson, B. J., Rastetter, E. B., and Steudler, P. A. (1989). Continental scale models of water balance and fluvial transport: An application to South America. *Global Biogeochem. Cycles*, 3(3):241–265.

- Vörösmarty, C. J., Willmott, C. J., Choudhury, B. J., Schloss, A. L., Streans, T. K., Robeson, S. M., and Dorman, T. J. (1996). Analyzing the discharge regime of a large tropical river through remote sensing, ground-based climatic data and modeling. *Water Resour. Res.*, 32:3137–3150.
- Vose, R. S., Schmoyer, R. L., Steurer, P. M., Peterson, T. C., Heim, R., Karl, T. R., and Eischeid, J. (1992). The global historical climatology network: long-term monthly temperature, precipitation, sea level pressure, and station pressure data. ORNL/CDIAC-53, NDP-041. Technical report, Carbon Dioxide Information Analysis Center, Oak Ridge National Laboratory, Oak Ridge, Tennessee.
- Waelbroeck, C., Monfray, P., Oechel, W. C., Hastings, S., and Vourlitis, G. (1997). The impact of permafrost thawing on the carbon dynamics of tundra. *Geophys. Res. Lett.*, 24:229–232.
- Waliser, D. E., Waliser, S. E., Seo, K., and Enjoku, E. (2005). Evaluation and climate change projections of the global hydrological cycle in IPCC AR4 model simulations. In *Eos Trans. AGU*, volume 86. Fall Meet. Suppl., Abstract H51I-07.
- Walsh, J. E., Kattsov, V., Portis, D., and Meleshko, V. (1998). Arctic precipitation and evaporation. *J. Clim.*, 11:72–87.
- Waring, R. H., Way, J. B., Hunt, E. R., Morrissey, L., Ranson, K. J., Weishampel, J. F., Oren, R., and Franklin, S. E. (1995). Imaging radar for ecosystem studies. *Bioscience*, 45(10):715–723.

- Way, J. B., Zimmermann, R., Rignot, E., McDonald, K., and Oren, R. (1997). Winter and spring thaw as observed with imaging radar at BOREAS. *J. Geophys. Res.*, 102(D24):29673–29684.
- White, D. M., Alessa, L., Hinzman, L., and Schweitzer, P. (2004). The impact of hydrologic and climatic change on domestic water supplies in the Arctic. In *Cold Regions Engineering and Construction Conference*. Alberta, Canada.
- Wiesmann, A. and Mätzler, C. (1998). Microwave emission model of layered snowpacks. *Remote Sens. Environ.*, 70:307–316.
- Willmott, C. J. and Matsuura, K. (2001). Arctic terrestrial air temperature and precipitation: Monthly and annual time series (1930–2000) version 1. available online at: <http://climate.geog.udel.edu/~climate/>.
- Willmott, C. J., Robeson, S. M., and Feddema, J. J. (1994). Estimating continental and terrestrial precipitation averages from raingauge networks. *Int. J. Climatol.*, 14:403–414.
- Willmott, C. J., Rowe, C. J., and Mintz, Y. (1985). Climatology of the terrestrial seasonal water cycle. *J. Clim.*, 5:589–606.
- Winebrenner, D. P., Nelson, E. D., Colony, R., and West, R. (1994). Observation of melt onset on multiyear Arctic sea ice using the ERS-1 synthetic aperture radar. *J. Geophys. Res.*, 99:22425–22441.
- Wismann, V. (2000a). Monitoring of seasonal thawing in siberia with ERS scatterometer data. *IEEE Trans. Geosci. Rem. Sens.*, 38:1804–1809.

- Wismann, V. (2000b). Monitoring of seasonal thawing on greenland with ERS scatterometer data. *IEEE Trans. Geosci. Rem. Sens.*, 38:1821–1826.
- Wolheim, W. M., Peterson, B. J., Deegan, L. A., Hobbie, J. E., Hooker, B., Bowden, W. B., Edwardson, K. J., Arscott, D. B., Hershey, A. E., and Finlay, J. (2001). Influence of stream size on ammonium and suspended particulate nitrogen processing. *Limnol. Oceanogr.*, 46(1):1–13.
- Woo, M. K. (1998). Arctic snow cover information for hydrological investigations at various scales. *Nordic Hydrology*, 29:245–266.
- Yang, D., Goodison, B. E., Ishida, S., and Benson, C. S. (1998). Adjustment of daily precipitation data at 10 stations in Alaska: Application of World Meteorological Organization intercomparison results. *Water Resour. Res.*, 34(2):241–256.
- Yang, D., Kane, D., Zhang, Z., Legates, D., and Goodison, B. (2005). Bias corrections of long-term (1973–2004) daily precipitation data over the northern regions. *Geophys. Res. Lett.*, 32. doi:10.1029/2005GL024057.
- Yang, D., Kane, D. L., and Hinzman, L. D. (2002). Siberian Lena River hydrologic regime and recent change. *J. Geophys. Res.*, 107(D23). 4694, doi:10.1029/2002JD002542.
- Ye, H., Cho, H. R., and Gustafson, P. E. (1998). The changes in Russian winter snow accumulation during 1936–1383 and its spatial patterns. *J. Clim.*, 11(5):856–863.
- Zhang, T., Osterkamp, T. E., and Stamnes, K. (1996). Some characteristics of the climate in northern Alaska. *Arct. Alp. Res.*, 28(4):509–518.

- Zhang, T., Osterkamp, T. E., and Stamnes, K. (1997). Effects of climate on the active layer and permafrost on the North Slope of Alaska, U.S.A. *Permafrost and Periglacial Processes*, 8:45–67.
- Zhang, T. and Stamnes, K. (1998). Impact of climatic factors on the active-layer and permafrost at Barrow Alaska. *Permafrost and Periglacial Processes*, 9:229–246.
- Zhuang, Q., Romanovsky, V. E., and McGuire, A. D. (2001). Incorporation of a permafrost model into a large-scale ecosystem model: Evaluation of temporal and spatial scaling issues in simulating soil thermal dynamics. *J. Geophys. Res.*, 106(D24):33,649–33,670.



## **APPENDICES**

## APPENDIX A

### PAN-ARCTIC WATER BALANCE MODEL

The Pan-Arctic Water Balance Model (PWBM) is a daily explicit hydrologic model, whereas the Water Balance Model (WBM) contains an optimized soil moisture routine and is run using monthly inputs and a quasi-daily, statistically-equivalent daily time step (Vörösmarty et al., 1998). The significant changes to the original algorithms which comprise the PWBM are described below.

#### A.1 Snow Dynamics

Daily precipitation for each grid is partitioned into either rain or snow based on a daily air temperature threshold of 0°C. The simulated snowpack contains both a solid (frozen) and liquid portion, providing a total model value for snow water equivalent (SWE). Sublimation from the frozen snow is determined through a simple function (Hamon, 1963), which allows for a small amount of sublimation at air temperatures below freezing. The function is

$$E_t = 715.5 \Lambda e * (T_t) / (T_t + 273.2) \quad (\text{A.1})$$

where  $E_t$  is sublimation (or potential evapotranspiration when snow is absent) ( $\text{mm day}^{-1}$ ),  $\Lambda$  is daylength (fraction of day), and  $e^*(T_t)$  is daily saturated vapor pressure (kPa) at temperature  $T_t$  ( $^{\circ}\text{C}$ ).

Daily snowmelt, a function of rainfall and/or air temperature, is

$$M_t = f_v \cdot (2.63 + 2.55 T_t + 0.0912 T_t P_t) \quad (\text{A.2})$$

where  $M_t$  is snowmelt ( $\text{mm day}^{-1}$ ),  $f_v$  is a vegetation factor that accounts for the differential absorption of radiation for different landcover types (dimensionless, range 0.4 to 1.0) (Federer and Lash, 1978),  $T_t$  represents daily air temperature ( $^{\circ}\text{C}$ ) and  $P_t$  is precipitation ( $\text{mm day}^{-1}$ ), all on day  $t$  (Willmott et al., 1985). Snowmelt and/or rainfall contributes to the liquid portion of the snowpack. Damming of snowmelt runoff is a complex process which delays the timing of streamflow during spring (Hinzman and Kane, 1991). In the PWBM, the snowpack is assumed to retain liquid water until this liquid content exceeds 80% of the snowpack frozen portion's water equivalent ( $SW E_t$ ), whereupon a fraction (60%) of the snowpack liquid water is released to the soil surface. The value of 80% represents all processes of delay to release of liquid water within the  $625 \text{ km}^2$  grid cell. This process is determined through

$$AW_t = \begin{cases} SW_t \gamma, & SW_t \geq \sigma SW E_t \\ 0, & \text{otherwise} \end{cases} \quad (\text{A.3})$$

where  $AW_t$  is water made available to the soil surface ( $\text{mm day}^{-1}$ ),  $SW_t$  is the snowpack liquid water content (mm),  $SW E_t$  is snowpack frozen water content (mm),  $\gamma$  is the per-

centage of  $SW_t$  released from snowpack (0.6 or 60 % day<sup>-1</sup>), and  $\sigma$  is the critical threshold (80 %).

## A.2 Soil Submodel

Daily changes in the PWBM soil liquid water and ice content are made by using gridded fields of soil properties and daily air temperature and the Stefan solution to heat transfer with phase change in a uniform semi-infinite medium (Lunardini, 1981), defined

$$z(t) = \sqrt{\frac{2k(nDDT(t))}{w\rho L}} \quad (\text{A.4})$$

where  $z_t$  is the depth of the phase change boundary (m),  $k$  is the soil thermal conductivity above the phase change boundary ( $\text{J m}^{-1} \text{C}^{-1} \text{d}^{-1}$ ),  $n$  is the  $n$ -factor, relating integrated air temperature to integrated soil-surface temperature (Lunardini, 1978) (dimensionless),  $DDT(t)$  is the accumulated degree days of thaw (or freeze) ( $^{\circ}\text{C}\text{-day}$ ),  $w$  is the soil water content at the phase change boundary ( $\text{kg kg}^{-1}$  dry soil),  $\rho$  is the soil bulk density ( $\text{kg m}^{-3}$ ), and  $L$  is the latent heat of fusion of water ( $\text{J kg}^{-1}$ ). Our implementation of Equation A.4 within the TFM includes an assumption of saturation at the interface between thawed and frozen soils. Although used frequently in engineering applications involving paved surfaces, few scientific studies have estimated spatially-variable  $n$ -factors across large areas. A constant value of 0.8 was assigned for all EASE-Grids, which represents an average  $n$ -factor across several vegetative classes determined using multiply observations of air and soil-surface temperatures at sites in northern Alaska (Klene et al., 2001).

Organic soils have very different thermal properties than mineral soils (van Wijk and de Vries, 1963), , and since many soils in the Pan-Arctic have a surface organic layer, we used the two-layered-soil Stefan solution (Jumikis, 1997). If the freeze/thaw depth calculation is within the surface layer, Equation A.4 applies with organic soil thermal properties ( $k_o$ ,  $w_o$ , and,  $\rho_o$ ), otherwise the depth is given (after Jumikins, 1977) by,

$$z(t) = z_o \left(1 - \frac{k_m}{k_o}\right) + \sqrt{\left(z_o \frac{k_m}{k_o}\right)^2 - \left(z_o^2 \frac{k_m w_o \rho_o}{k_o w_m \rho_m}\right) - \frac{2 k_m n DDT(t)}{w_m \rho_m L}} \quad (\text{A.5})$$

where the subscript  $o$  refers to organic soil properties and the subscript  $m$  refers to mineral soil properties. Soil thermal conductivity for organic ( $k_o$ ,  $\text{J m}^{-1} \text{C}^{-1} \text{d}^{-1}$ ) and mineral ( $k_m$ ,  $\text{J m}^{-1} \text{C}^{-1} \text{d}^{-1}$ ) soils is a function of soil moisture and soil texture (Table A.1). Organic-layer thickness was estimated by assuming half of the total soil organic matter (Global Soil Data Task, 2000) is in the surface organic layer, with a bulk density of  $100 \text{ kg m}^{-3}$ . Organic-layer thicknesses across the Pan-Arctic range from 0.10 to 0.70 m, with a Pan-Arctic mean of 0.22 m.

Daily soil conductivity ( $k_o$  and  $k_m$ ) for each grid cell is obtained by using the PWBM-generated soil moisture and linearly interpolating between conductivity associated with two of the three moisture classes; dry (soil moisture  $\sim 0\%$ ), wet (50%) and saturated (100%) (Table A.1).

Soil moisture (water and ice) is determined from interactions between the changing active layer thickness, snowmelt and/or rainfall, and evapotranspiration. Runoff occurs when (i) soil moisture exceeds field capacity or (ii) snowmelt and/or rainfall exceeds a predefined critical value (described below). While changes in soil water content have a

Texture	porosity	field capacity	wilting point	bulk density	thermal conductivity (Saturated, Wet, Dry) *
	cm <sup>3</sup> /cm <sup>3</sup>	cm <sup>3</sup> /cm <sup>3</sup>	cm <sup>3</sup> /cm <sup>3</sup>	g/cm <sup>3</sup>	cal cm <sup>-1</sup> s <sup>-1</sup> °C <sup>-1</sup>
Coarse	0.39	0.05	0.04	1.6	5.2, 4.2, 0.7
Coarse+med.	0.43	0.14	0.05	1.5	4.8, 3.8, 0.7
Medium	0.45	0.24	0.09	1.44	4.3, 3.3, 0.6
Coarse+fine	0.45	0.24	0.09	1.44	4.3, 3.3, 0.6
Coarse+med.+fine	0.45	0.24	0.09	1.44	4.3, 3.3, 0.6
Medium+fine	0.48	0.32	0.17	1.35	3.9, 2.9, 0.6
Fine	0.53	0.35	0.22	1.21	3.8, 2.8, 0.6
Organic	0.92	0.5	0.1	0.1	1.2, 0.7, 0.14

Table A.1: PWBM soil texture classes and model parameters. \* Data from Van Wijk and de Vries (1963).

significant effect on ALT, variations in seasonal snow cover have a relatively slight impact (Zhang and Stamnes, 1998). The PWBM accounts for the insulating effects of snowcover through a delay to soil thawing in spring when model snowcover is present.

Change in active-layer thickness (ALT) is used to determine the amount of water which changes phase (melt or freeze) on a daily basis. Soil ice (water) which melts (freezes) is also dependent on the relative saturation of the zone. The amount of ice that melts (freezes) is thus

$$L_t = \Delta z_t R_t \quad (\text{A.6})$$

where  $L_t$  is melt (freeze) ( $\text{mm day}^{-1}$ ) on day  $t$ ,  $\Delta z_t$  is the increase (decrease) in active-layer thickness ( $\text{mm day}^{-1}$ ) on day  $t$ , and  $R_t$  is the relative saturation of the zone (0 to 1). Relative saturation is defined

$$R_t = \frac{I_{t-1} + W_{t-1}}{SD} \quad (\text{A.7})$$

where  $I_{t-1}$  is soil ice (mm) and  $W_{t-1}$  is soil water (mm), both from the previous day, and  $SD$  is the total pore space of the soil layer (mm). If  $\Delta z_t > 0$ , ice is melted. Liquid water is converted to ice when  $\Delta z_t < 0$ . This algorithm is used to change the phase of water in the deep soil layer when all water has been converted in the overlying root zone.

Daily snow drainage and/or rainfall infiltrates the root zone to recharge soil moisture storage to a maximum of  $12 \text{ mm day}^{-1}$ . Surface inputs (snow drainage and rain) greater than this threshold contribute to runoff. Soil recharge is defined

$$R_w = IW \cdot F_w \cdot \frac{W}{W + I} \quad (\text{A.8})$$

where  $R_w$  is recharge ( $\text{mm day}^{-1}$ ) to the soil reservoir of water,  $IW$  represents water infiltrating the soil ( $\text{mm day}^{-1}$ ),  $W$  is root zone soil water (mm), and  $I$  is root zone ice content (mm). The remaining fraction of infiltration water contributes to soil ice storage.

The upper soil (root) zone loses water through evapotranspiration, lateral movement, and vertical drainage to the deep soil zone. Potential evapotranspiration (PE) is estimated with the Hamon function (Hamon, 1963) (Equation A.1). Vegetation is assumed to utilize soil moisture at the potential rate when soil water  $\geq$  field capacity. In times of moisture stress, evapotranspiration is a fraction of the potential rate, and is determined through a soil-retention function (Vörösmarty et al., 1989). The field capacity for each layer is

$$FC_r = (SD_r - I_r) \alpha \quad (\text{A.9})$$

where  $FC_r$  is field capacity in the root zone (mm),  $SD_r$  is pore space (mm),  $I_r$  is ice content (mm), and  $\alpha$  is field capacity (%) (Table A.1). Water draining vertically is proportioned into liquid water and ice in the deep zone

$$d_w = B \frac{W_d}{W_d + W_i} \quad (\text{A.10})$$

where  $d_w$  (mm) is the vertical flux per day which contributes to water in the deep zone,  $B$  is the excess water from the root zone (mm),  $W_d$  is water in the deep zone (mm), and  $W_i$  is ice in the deep zone (mm). The contribution to deep zone ice,  $d_i$  (mm), is

$$d_i = B \frac{W_i}{W_d + W_i} \quad (\text{A.11})$$



## APPENDIX B

### PET FUNCTIONS USED IN PWBM

Hamon as given by *Hamon* (1963)

$$PE_r = 715.5 \Lambda e^*(T_m)/(T_m + 273.2) \quad (\text{B.1})$$

Penman-Monteith (PM) as given by *Monteith* (1965) ( $R_n = R_n - S$  with  $S = 0$ )

$$c_t L_v \rho_w PE_s = \frac{\Delta R_n + c_p \rho D_a / r_a}{\Delta + \gamma + \gamma (r_c / r_a)} \quad (\text{B.2})$$

$c_p$  heat capacity of air,  $1005 \text{ J kg}^{-1} \text{ K}^{-1}$

$c_t$  conversion constant,  $0.01157 \text{ W m d, MJ}^{-1} \text{ mm}^{-1}$

$D_a$  vapor pressure deficit in air,  $\text{kPa}$ ,  $e^*(T_a) - e_a$

$e^*(T)$  saturated vapor pressure at temperature  $T$ ,  $\text{kPa}$

$L_v$  latent heat of vaporization,  $2448.0 \text{ MJ/m}^2$

$PE_r$  reference-surface potential evapotranspiration,  $\text{mm/d}$

$PE_s$  surface-dependent potential evapotranspiration,  $\text{mm/d}$

$r_a$  aerodynamic resistance, s/m

$r_c$  surface or canopy resistance, s/m

$R_n$  net radiation above the surface, W/m<sup>2</sup>

$T_m$  mean air temperature for day, °C

$z_a$  reference height, m

$\gamma$  psychrometer constant, 0.067 kPa/K

$\Delta$  rate of change of vapor pressure with temperature, kPa/K

$\Lambda$  daylength, days

$\rho$  density of air, 1.234 kg/m<sup>3</sup>

$\rho_w$  density of water, 1.0 Mg/m<sup>3</sup>

## APPENDIX C

### PWBM SOURCE CODE

```
program wbm

implicit none

integer narray,nbasins,ncells,kyr,iyrindex,inum
parameter (narray=39926,nbasins=7645)
real r_lat,r_lon,rlat(narray),rlon(narray)
integer length1,length2,length3,length4,length5,length6,imon
integer length7,length8,length9,ispinupyr,ispinupday,lengthout
integer i,j,k,l,m,mm,n,icell,irec,ii,jj,ntime,ibad,julday
integer iindx(narray),jindx(narray),id,ibasin,idrains,k1,k2,k3,iyr
integer ihave_basinout,init,nspinup,intrnl_bas,idryriv,idata
integer ifrstyr,ilstyr,ifrstmon,iday,ndays,nmons,ivegcov,imoday1
integer ntotdays,ivegetation(narray),n_days,isoilclass,iwrite
integer igetcell,ithawflag(narray),navs,ichosen,ioutput,iflag
integer ntemp_point,nthawdays(narray),ihave_basin(nbasins)
integer fallflag(narray),springflag(narray),iphase
integer ifrstfrz(narray),iseason(narray),iaccumulate(narray)
integer ndegdays_summed(narray),monlastday(12),lastday
integer ioutyr1,ioutmon1,ioutyr2,ioutmon2,idailyout(50)
integer monthlyout(50),ievapfunc,inewveg1(narray,120)
integer iwetland(narray)
parameter(igetcell=2256,navs=10)
dimension ihave_basinout(narray),intrnl_bas(79),idryriv(narray)
dimension id(narray+1),ibasin(narray),idrains(narray),imoday1(12)
data imoday1 / 0, 31, 59, 90, 120, 151, 181, 212, 243, 273,
$                               304, 334 /
data monlastday /31, 28, 31, 30, 31, 30, 31, 31, 30, 31, 30, 31/
real*8 evap,totwat,sum,km_per_mm,globe_cloud,rmissing,totjunk
real*8 total_initial_water,total_land_water,effective_e,pr0_new
real*8 wa1,wa2,dwa,et,h_d,q,qs,pr0,precip,prain,psnow,sum2ocean
real*8 tminvals,tmaxvals,vaporvals,windvals,radvals,wetlandstore
real*8 tmin,tmax,vaporpress,windsp,radnet,years,wetlandstoreprev
```

```

real*8 rootwatprev,rootwat,ds,rootwater,wg1,wg2,dg,wg,xg,xr
real*8 deepwatprev,deepwat,rooticeprev,rootice,rootices
real*8 deepwater,deepiceprev,deepice,deepices,sum_deepices
real*8 ro,ro1,ro2,wr1,wr2,dr,wr,da,db1,db2,wt,d3,d3s,disch,area
real*8 wsnw1,wsnw2,wsnow,temp,tair,tsnow_cutoff,potent_et
real*8 FL,sheat,rLAI,wetlandwat,sum_wetlandstore
real*8 sum_p,sum_wsnow,sum_rootwater,sum_deepwater,sum_wr,sum_et
real*8 check,sum_intrnl,basin_outlet,sum2ocean_alltime,total
real*8 snowpk1,snowpk2,snowpack,sum_snowpk,snowretain,snowrelease
real*8 avail_wat,snow_subl,snowpet,sum_snowsubl,PminusE,snowmelt
real*8 surf_evap,evap_unmet,sum_surfevap,rad_2_melt,rad_melt
real*8 temp_array(3,narray),sum2,tavg,sum_rootices,sum_runoff
real*8 soildepth(narray),sumtair2(narray),soilconduct,soildensity
real*8 rootdepth(narray),soilwatvolume,root_excess,deep_excess
real*8 root_depth,fieldcapacity,depthout,sumprecip
real*8 soil_depth,soilwatvol,grndwatvol,basin_av,root2deep
real*8 overlandR0,rootbaseflow,deepbaseflow,initialstate
real*8 sumtair(narray),soilporosity,wiltingpoint,infiltration
real*8 field_capac(narray),soil_porosity(narray),zfrzmax(narray)
real*8 abs_sumtair,wilt_point(narray),zthawmax(narray)
real*8 rootbaseflowfact,deepbaseflowfact,diff,sumro,sumatocean
real*8 sumtair_prev,sumpet,sumsnow,sumsubl,sumavailwat,sumsurfevap
real*8 sumrunoff,sumriver,sumet,summerthaw,active_layer
real*8 bulkdensity,thermcondwet,thermcondsat,thermconddry
real*8 bulk_dens,therm_conddry,therm_condwet,therm_condsat
real*8 therm_condpeatdry,therm_condpeatwet,therm_condpeatsat
real*8 therm_condpeat,peatdensity,soilcarbon,activelayer,sumbas
real*8 active_layer_prev,basin_area(nbasins),varjunk
real*8 conduct_av,conduct_sum,conductpeat_av,conductpeat_sum
real*8 depth_space(narray),depth_phys(narray),depth_space_prev
real*8 depth_phys_prev,rootwat1(narray,31),thawfreezeD1(narray,31)
real*8 rootice1(narray,31),deepwat1(narray,31),deepice1(narray,31)
real*8 runoff1(narray,31),evap1(narray,31),snowwateq1(narray,31)
real*8 monthrutoff(narray,12),monthevap(narray,12)
real*8 monthrootwat(narray,12),monthrootice(narray,12)
real*8 monthdeepwat(narray,12),monthdeepice(narray,12)
real*8 monthswe(narray,12),monthroot2deep(narray,12),pfactor(12)
real*8 monthsub(narray,12),snowice(narray,31),snowwater(narray,31)
real*8 snowmelt1(narray,31),monthmeltwat(narray,12)
real snow4pet,pmdayf,sngl_lai,sngl_snow,sngl_FL,sngl_wind,sngl_rad
real sngl_tair,sngl_vap,sngl_sheat,sngl_tmax,sngl_tmin
real sngl_lat,sngl_lon,laivals,lai
dimension evap(31,narray),basin_outlet(narray),temp(31,narray)
dimension pr0(31,narray),wsnow(narray),snowpack(narray)
dimension tminvals(31,narray),tmaxvals(31,narray)
dimension vaporvals(31,narray),windvals(31,narray)

```

```

dimension radvals(31,narray),laivals(12,31,narray)
dimension disch(0:narray),ro(narray),qs(narray),deepwater(narray)
dimension rootwater(narray),wg(narray),wr(narray),d3s(narray)
dimension rootices(narray),deepices(narray),summerthaw(narray)
dimension bulk_dens(narray),therm_condwet(narray)
dimension therm_conddry(narray),therm_condsat(narray)
dimension soilcarbon(narray),activelayer(31,narray)
dimension active_layer(narray),initialstate(nbasins)
dimension basin_av(nav,nbasins),sumbas(nav,nbasins)
dimension conductpeat_sum(narray),conduct_sum(narray)
dimension pr0_new(31,narray),wetlandwat(narray)
character header*60,datestring*7,datestring2*11,fmt*40
character*100 path1,path2,path3,name1,name2,name3,yrstring*4
character*100 path4,path5,path6,name4,name5,name6
character*100 path7,path8,path9,name7,name8,name9
character tname(900)*100,pname(900)*100,thawname(900)*100
character tmaxname(900)*100,tminname(900)*100,vaporname(900)*100
character windname(900)*100,radname(900)*100,lainame(200)*100
character ename(900)*100,runoffname*60,fname*80,domain_file*100
character*100 rootfile,carbonfile,temvegfile,soiltextfile
character*100 spinupfile,prcppath,tempopath,altpath,outpath
character*100 tmaxpath,tminpath,vaporpath,windpath,radpath,laipath
character yearchk*4,yearstr*4,homedir*100,str1*120,str2*200
character headerPfile*20,headerTfile*20
logical read_evapdat,read_thawdat,printflag,ctrl_thaw,no_thaw
logical read_penmandat
data read_evapdat,read_thawdat,ctrl_thaw,no_thaw
$      /.false.,.false.,.false.,.false./

```

C DEFINE CONSTANTS

```

km_per_mm=1.0d-6

```

C OPEN CONTROL FILE AND READ RECORDS

```

call getenv('HOME', homedir)
inum = index(homedir, ' ') - 1
OPEN(11,FILE='pwbm.initialize.txt')
READ (11,'(a100)') str1
length1 = index (str1, ' ') - 1
domain_file = str1(1:length1)
READ (11,'(a100)') str1
length1 = index (str1, ' ') - 1
rootfile = str1(1:length1)
READ (11,'(a100)') str1
length1 = index (str1, ' ') - 1
carbonfile = str1(1:length1)
READ (11,'(a100)') str1

```

```

length1 = index (str1, ' ') - 1
temvegfile = str1(1:length1)
READ (11,'(a100)') str1
length1 = index (str1, ' ') - 1
soiltextfile = str1(1:length1)
READ (11,'(a100)') str1
length1 = index (str1, ' ') - 1
spinupfile = str1(1:length1)
length2 = index (str1, 'spinup.') - 1
READ (11,'(a100)') str1
length1 = index (str1, ' ') - 1
prcpath = str1(1:length1)
READ (11,'(a100)') str1
length1 = index (str1, ' ') - 1
temppath = str1(1:length1)
READ (11,'(a100)') str1
length1 = index (str1, ' ') - 1
altpath = str1(1:length1)
READ (11,'(a100)') str1
lengthout = index (str1, ' ') - 1
outpath = str1(1:lengthout)

```

c Read path names for time series used to get Penman-Monteith PET

```

READ (11,'(a100)') str1
length1 = index (str1, ' ') - 1
tmaxpath = str1(1:length1)
READ (11,'(a100)') str1
length1 = index (str1, ' ') - 1
tminpath = str1(1:length1)
READ (11,'(a100)') str1
length1 = index (str1, ' ') - 1
vaporpath = str1(1:length1)
READ (11,'(a100)') str1
length1 = index (str1, ' ') - 1
windpath = str1(1:length1)
READ (11,'(a100)') str1
length1 = index (str1, ' ') - 1
radpath = str1(1:length1)
READ (11,'(a100)') str1
length1 = index (str1, ' ') - 1
laipath = str1(1:length1)

READ (11,*) ! read blank line in init file
READ (11,*) area
READ (11,*) peatdensity
c print*, 'Peat', peatdensity

```

```

READ (11,*) therm_condpeatdry,therm_condpeatwet,therm_condpeatsat
c   print*, 'Conduct',therm_condpeatdry,therm_condpeatwet,
c   $       therm_condpeatsat
READ (11,*) tsnow_cutoff
c   print*, 'Snow cutoff', tsnow_cutoff
READ (11,*) snowretain
c   print*, snowretain
READ (11,*) snowrelease
c   print*, snowrelease
READ (11,*) infiltration
c   print*, infiltration
READ (11,*) rootbaseflowfact,deepbaseflowfact
c   print*, rootbaseflowfact,deepbaseflowfact
READ (11,*) ievapfunc
c   print*, ievapfunc
READ (11,*) nspinup
c   print*, nspinup

READ (11,*)                               ! read blank line in itit file
READ (11,*) pfactor(1)
READ (11,*) pfactor(2)
READ (11,*) pfactor(3)
READ (11,*) pfactor(4)
READ (11,*) pfactor(5)
READ (11,*) pfactor(6)
READ (11,*) pfactor(7)
READ (11,*) pfactor(8)
READ (11,*) pfactor(9)
READ (11,*) pfactor(10)
READ (11,*) pfactor(11)
READ (11,*) pfactor(12)

READ (11,*)                               ! read blank line in init file
READ (11,*) ifrstyr
READ (11,*) ilstyr
READ (11,*) ioutyr1,ioutmon1
READ (11,*) ioutyr2,ioutmon2
READ (11,*) idailyout(1)
READ (11,*) idailyout(2)
READ (11,*) idailyout(3)
READ (11,*) idailyout(4)
READ (11,*) idailyout(5)
READ (11,*) idailyout(6)
READ (11,*) idailyout(7)
READ (11,*) idailyout(8)
READ (11,*) idailyout(9)

```

```

READ (11,*) idailyout(10)
READ (11,*) monthlyout(1)
READ (11,*) monthlyout(2)
READ (11,*) monthlyout(3)
READ (11,*) monthlyout(4)
READ (11,*) monthlyout(5)
READ (11,*) monthlyout(6)
READ (11,*) monthlyout(7)

write(yearchk,'(i4)') ifrstyr
if (yearchk .ne. spinupfile(length2+8:length2+11)) then
  write(6,*)
  $'** ERROR: mismatched spinup file and first year of simulation **'
  print*, ifrstyr, yearchk, spinupfile(length2+8:length2+11)
  stop
endif

if (ievapfunc .ge. 2) then
  read_penmandat = .true.
else
  read_penmandat = .false.
endif

c Get precipitation and air temperature filename string to use in
c output file headers.
  length1 = index (prcppath, ' ') - 1
  do i = length1, length1-100, -1
    if (prcppath(i:i) .eq. '/') then
      headerPfile = prcppath(i+1:length1-1)
      goto 222
    endif
  enddo
222 length1 = index (temppath, ' ') - 1
  do i = length1, length1-100, -1
    if (temppath(i:i) .eq. '/') then
      headerTfile = temppath(i+1:length1-1)
      goto 333
    endif
  enddo
333 continue

  open (unit=14,file=domain_file)
c   open (unit=14,file='ease_drainage.txt')
c   open (unit=14,file='ease_drainage.txt.subset')

c Read drainage cell information from table.  Indices for

```



c latitude and longitude are read in from file. j is for lat, i for  
 c lon. They are not used in model. Fill arrays for basin info.

```

    read(14,*) header          ! skipping header/label
    do icell=1, 100000
      read (14,16,end=99) id(icell), jindx(icell), iindx(icell),
    $      r_lat, r_lon, ibasin(icell), idrain2(icell)
16  format (i6,2i5,2f9.4,2i6)
      rlat(icell) = r_lat
      rlon(icell) = r_lon
c    write(*,16) id(icell), jindx(icell), iindx(icell),
c    $      r_lat, r_lon, ibasin(icell), idrain2(icell)
    enddo
99  ncells = icell - 1
    print*, ncells, ' Arctic Basin records read'

```

c Initialize all disch(grid#) to zero. grid ID # went from 62242 to 4446  
 c for previous geographic grid. Now go from 1 to 39926 for EASE drainage

```

    do m=0, ncells          ! grid ID # go from 1 to 39926
      disch(m) = 0.0d0
    enddo
    do m=1, ncells          ! previously had 6267 basin outlet. Now all
      ihave_basinout(m) = 0 ! are outlets with current EASE basin file
      basin_outlet(m) = 0.0d0
    enddo

```

c Sum up basin areas for each basin in domain. Then calculate the basin  
 c area for each of the basins. Also determine which numbers (1-nbasins) are  
 c designated as a basin. For example, Ob is 5 and Yenisei is 7, but  
 c numbers 3, 4, and 6 (and more) are not associated with a particular basin.

```

    do m = 1, nbasins
      basin_area(m) = 0.0d0
      ihave_basin(m) = 0
      initialstate(m) = 0.0d0      ! initial state variables for each basin
    enddo
    do icell = 1, ncells          ! next line sums area for each basin
      basin_area(ibasins(icell)) = basin_area(ibasins(icell)) + area
      if (basin_area(ibasins(icell)) .gt. 0.0d0)
    $      ihave_basin(ibasins(icell)) = 1 ! flag numbers for basins
    enddo

```

c Read in cell ids for "internal basin"; those that drain nowhere.  
 c Will account for this water in water balance calculations.

```

c    open(16,file='arctic.internalbasins.txt')

```

```

c      do i=1, 79
c          read(16,*) intrnl_bas(i)
c      enddo

      k=0
      precip=0.0d0
      q=0.0d0
      d3=0.0d0
      xr=0.0d0
      xg=0.0d0
      da=0.0d0
      et=0.0d0
      da=0.0d0
      dg=0.0d0
      dr=0.0d0
      ds=0.0d0
      sum_intrnl=0.0d0
      sum2ocean=0.0d0
      sum2ocean_alltime=0.0d0
      sumatocean = 0.0d0
      total_initial_water = 0.0d0
      globe_cloud=0.0d0          ! setting the global cloud water content
      totjunk = 0.0d0

c  Initialize arrays and fill array with rootdepth and maxthawdepth from file
c  Limit root/soil zone to 60% of the maxthawdepth that was calculated
c  from Stephan solution.  Read in initial soil and ground water storage,
c  snowpack, and snow water.
c  Also read soil texture from file and call lookup.f to get soil porosity,
c  fieldcapacity, and wilting point.  Convert root and max thaw depths to
c  their water equivalent based on soil porosity.  Also open file of
c  soil carbon data.

      print*, '*****'
c      print*, 'global cloud set to zero'
c      print*, ' '
      print*, '*****'
      open(50,file=rootfile)
      open(51,file=temvegfile)
      read(51,*) years
      kyr = int(years)
      varjunk = years - real(kyr)
      mm = (ilstyr - ifrstyr) + 1 !run years from frst and lst yr of init file
c      if (kyr.gt.1.and.kyr.ne.mm)stop 'Mismatch in run years & veg file'
      if (varjunk .gt. 0.01) stop 'years of vegetation read as real num'
      if (kyr .lt. 10) write(fmt, '(2f10.4,i3)')

```

```

    if (kyr .ge. 10 .and. kyr .lt. 100)
$       write(fmt, '(2f10.4, ', i2, ', ', i3, ')') kyr
    if (kyr .ge. 100) write(fmt, '(2f10.4, ', i3, ', ', i3, ')') kyr
    print*, 'Reading ', kyr, ' annual values of vegetation from file'
c     print*, years, kyr, varjunk
c     open(52, file='spinup.1980.output') !output from model spinup
    open(52, file=spinupfile)
    open(53, file=soiltextfile) ! soil textures at gridcells
    open(54, file=carbonfile)
    open(55, file=homedir(1:inum)//'/Model/wetlands.dat')
    read(52, *) ! read header
    do icell = 1, ncells
        read(50, *) r_lat, r_lon, rootdepth(icell), soildepth(icell)
c         if (icell.eq.igetcell) print*, rootdepth(icell), soildepth(icell)
20        format(20x, 3f8.2, 2i3)
c         print*, rootdepth(icell), soildepth(icell)
        if (rootdepth(icell) .eq. 0.0d0) rootdepth(icell) = 50.0d0
c         rootdepth(icell) = rootdepth(icell) * 2.0d0
c         soildepth(icell) = soildepth(icell) * 2.0d0
        if (rootdepth(icell) .gt. soildepth(icell)) then !adjust if rootdepth
            rootdepth(icell) = soildepth(icell) * 0.80d0 ! is < max soildepth
c            write(95, *) rlat(icell), rlon(icell), rootdepth(icell)
        endif
        if (soildepth(icell)-rootdepth(icell) .lt. 50.0d0) ! adjust if deep
$         soildepth(icell) = rootdepth(icell) + 50.0d0 ! capacity is small

c         read(51, *) r_lat, r_lon, ivegitation(icell)
        read(51, fmt) r_lat, r_lon, (inewveg1(icell, j), j=1, kyr)
        if (kyr .eq. 1) then
            do nn = 1, 120 ! 120 is dimension of inewveg1(ngrid, 120)
                mm = inewveg1(icell, 1)
                inewveg1(icell, nn) = inewveg1(icell, 1)
c                write(88, *) inewveg1(icell, 1)
            enddo
        endif

        read(52, 21) rootwat, rootice, deepwat, deepice, wetlandstore,
$         snowpk1, wsnw1, wr1, sumtair(icell), depth_phys(icell),
$         depth_space(icell), conduct_sum(icell),
$         conductpeat_sum(icell), ndegdays_summed(icell),
$         izeason(icell), iaccumulate(icell)
c         print*, rootwat, rootice, deepwat, deepice, wetlandstore

c         write(94, 23) icell, rlat(icell), rlon(icell), depth_phys(icell)
23        format(i5, 2f10.4, f8.1)
21        format(11x, 13f16.8, i6, 2i2)

```

22       format(i5,2i3,8f8.2,i2)

```
c Handle conversion of soil carbon content to depth in mm
  read(53,*) r_lat, r_lon, isoilclass
c   isoilclass = 2                               ! set all soils to 'medium'
  read(54,*) r_lat, r_lon, soilcarbon(icell)
  soilcarbon(icell) = soilcarbon(icell) * 10.0d0       ! in mm
c   soilcarbon(icell) = soilcarbon(icell) * 5.0d0       ! set C to half
c   soilcarbon(icell) = soilcarbon(icell) * 20.0d0      ! set C to twice
c   write(96,*) soilcarbon(icell) / 10.
  read(55,*) r_lat, r_lon, iwetland(icell)

c Look up soil characteristics for given soil class. Convert units for soil
c variables. Also set some array values.
c
  call lookup(isoilclass,soilporosity,fieldcapacity,
$   wiltingpoint,bulkdensity,thermcondwet,thermcondsat,
$   thermconddry)
c   fieldcapacity = fieldcapacity + 0.05d0   ! increase field capacity
  rootdepth(icell) = rootdepth(icell) * soilporosity
  soildepth(icell) = soildepth(icell) * soilporosity
  field_capac(icell) = fieldcapacity / soilporosity
  wilt_point(icell) = wiltingpoint / soilporosity
  soil_porosity(icell) = soilporosity
  bulk_dens(icell) = bulkdensity
  therm_conddry(icell) = thermconddry
  therm_condwet(icell) = thermcondwet
  therm_condsat(icell) = thermcondsat
c   write(97,'(f8.1)') (rootdepth(icell) * field_capac(icell) -
c   $   rootdepth(icell) * wilt_point(icell)) / 10.

c Ensure that deep ice does not exceed deep capacity. This should not
c happen after spinup has run!!!
  root_excess = (rootwat+rootice) - rootdepth(icell)
  deep_excess = (deepwat+deepice) -
$   (soildepth(icell)-rootdepth(icell))
  if (root_excess .gt. 1.0d-1) then
c   print*, 'Warning: Water+ice in rootzone > rootdepth on grid',
c   $   icell
  rootice = rootdepth(icell) * 0.5
  rootwat = 0.
  endif
  if (deep_excess .gt. 1.0d-1) then
c   print*, 'Warning: Water+ice in deepzone > deepdepth on grid',
```

```

c      $                                                    icell
      deepice = (soildepth(icell) - rootdepth(icell)) * 0.5
      deepwat = 0.
      endif

c Place each initial value in a spatial array.
      wsnow(icell)=wsnw1
      snowpack(icell)=snowpk1
      rootwater(icell)=rootwat
      deepwater(icell)=deepwat
      rootices(icell)=rootice
      deepices(icell)=deepice
      wetlandwat(icell)=wetlandstore
      ro(icell)=0.0d0
      wr(icell)=wr1
      d3s(icell)=0.0d0

      ! next block sets initial water in input state variables
      total_initial_water = total_initial_water +
$      snowpk1*km_per_mm*area + wsnw1*km_per_mm*area +
$      rootwat*km_per_mm*area + rootice*km_per_mm*area +
$      deepwat*km_per_mm*area + deepice*km_per_mm*area +
$      wetlandstore*km_per_mm*area + wr1

      initialstate(ibasin(icell)) = initialstate(ibasin(icell)) +
$      (snowpk1+wsnw1+rootwat+rootice+deepwat+deepice+wetlandstore) *
$      km_per_mm*area

      enddo
444 total_initial_water = total_initial_water + globe_cloud

c Create a list of input file names. These files will be opened
c by a read subroutine. Must be same number of temp and prcp files.
c NOT READING EVAP FILES AT THIS TIME.

      path1 = prcppath
      path2 = temppath
      path3 = altpath
      path4 = tmaxpath
      path5 = tminpath
      path6 = vaporpath
      path7 = windpath
      path8 = radpath
      path9 = laipath

      length1 = index (path1, ' ') - 1

```

```

length2 = index (path2, ' ') - 1
length3 = index (path3, ' ') - 1
length4 = index (path4, ' ') - 1
length5 = index (path5, ' ') - 1
length6 = index (path6, ' ') - 1
length7 = index (path7, ' ') - 1
length8 = index (path8, ' ') - 1
length9 = index (path9, ' ') - 1

ii=0
c   ifrstyr = 1980
c   ilstyr = 2001
   ifrstmon = 1
   do i=ifrstyr, ilstyr
     yrindex = (i - ifrstyr + 1)
     write(yrstring, '(i4)') i
     lainame(iyrindex) = path9(1:length9)//yrstring//'.txt'
     do j=ifrstmon, 12
       ii=ii+1
       write(datestring, '(i4,','.',i2.2)') i, j
       pname(ii) =
$     path1(1:length1)//datestring//'.txt'
       tname(ii) =
$     path2(1:length2)//datestring//'.txt'
       thawname(ii) =
$     path3(1:length3)//datestring//'.txt'
       tmaxname(ii) =
$     path4(1:length4)//datestring//'.txt'
       tminname(ii) =
$     path5(1:length5)//datestring//'.txt'
       vaporname(ii) =
$     path6(1:length6)//datestring//'.txt'
       windname(ii) =
$     path7(1:length7)//datestring//'.txt'
       radname(ii) =
$     path8(1:length8)//datestring//'.txt'

       enddo
     enddo
98   nmons = ii

c   Start outmost loop for spinup.  NEED TO EDIT *NOSPIN* Wraps around time loop
c   Inner loop processes water balance at gridcells.

   ispinupday = 365
   if (mod(ifrstyr,4) .eq. 0) ispinupday = 366

```

```

ntotdays=0
do init = 1, nspinup+1 ! a "spinup" loop around the time loop
                        ! usually won't use in this time series program

iyr = ifrstyr
imon = ifrstmon
rmissing=-9999.00d0 ! missing value code for input data

do k=1, nmons
  iyrindex = (iyr - ifrstyr + 1) ! iyr incremented @ bottom of mon loop
c Fill arrays to missing...will fill them with values below.
  if (imon.eq.2.or.imon.eq.4.or.imon.eq.6.or.imon.eq.9.or.
$   imon.eq.11) then

    do icell=1, ncells
      do iday=1, 31
        evap1(icell,iday) = -9999.
        runoff1(icell,iday) = -9999.
        snowwateq1(icell,iday) = -9999.
        rootwat1(icell,iday) = -9999.
        rootice1(icell,iday) = -9999. ! set all to missing in months
        deepwat1(icell,iday) = -9999. ! with less than 31 days so
        deepice1(icell,iday) = -9999. ! days 31, 30, ... are missing
        thawfreezeD1(icell,iday) = -9999.
        snowice(icell,iday) = -9999.
        snowwater(icell,iday) = -9999.
        snowmelt1(icell,iday) = -9999.
      enddo
    enddo
  endif

c   if (iyr .eq. 1999) stop
  if (imon .eq. ifrstmon) then
c     if (iyr .ge. 1950) then ! open thaw depth files for output
c       write(fname,'(''summerthaw.'',i4)') iyr
c       open(98,file=fname)
c     endif
    do i=1, ncells ! zero out max summer thaw
      summerthaw(i) = 0.0d0 ! on Jan 1 each year
    enddo
  endif

c Zero out the monthly runoff accumulation for each of the basins in domain.
c Also zero out variable accumulations for other parameters. These are not
c currently being summed for all the individual basins.
  do i=1, nbasins
    do j=1, navs

```

```

        sumbas(j,i) = 0.0d0
    enddo
enddo

c Call subroutine to read data from files. A two-dimensional array
c (time,gridcell index) is returned.
c Subroutine inputs are:
c   pname(k) - path/filename (39 characters) for input data
c   rmissing - missing value code (real). Values are screened in subr.
c Outputs are:
c   idata     - number of vaild data, ie. days in month, since missing
c               values fill empty spots at end of 31-element series for
c               months having less than 31 days
c   evap, pr0, temp - (idata,ncells) for each day at every grid cell.
c               Note: This is reading all 39926 EASE cells, regardless of
c               how many grids are used based on input drainage table.
    print*, 'Reading data file: ', pname(k)
    call read_data(pname(k),rmissing,idata,pr0)

    print*, 'Reading data file: ', tname(k)
    call read_data(tname(k),rmissing,idata,temp)

    if (read_evapdat) then
        print*, 'Reading data file: ', ename(k)
        call read_data(ename(k),rmissing,idata,evap)
    endif

    if (read_thawdat) then
        print*, 'Reading data file: ', thawname(k)
        call read_data(thawname(k),rmissing,idata,activelayer)
    endif

    if(ievapfunc .eq. 2) then
        print*, 'Reading data files to calculate Penman PET'
        call read_data(tmaxname(k),rmissing,idata,tmaxvals)
        call read_data(tminname(k),rmissing,idata,tminvals)
        call read_data(vaporname(k),rmissing,idata,vaporvals)
        call read_data(windname(k),rmissing,idata,windvals)
        call read_data(radname(k),rmissing,idata,radvals)
        if(imon.eq.1)call read_LAI(lainame(iyrindex),ncells,laivals)
    endif

    ndays = monlastday(imon)
    if (mod(iyr,4) .eq. 0 .and. imon .eq. 2) then
        ndays = 29
    endif

```



```

        if (ndays .lt. 1 .or. ndays .gt. 31) stop 'ndays < 1 or > 31'

c   Call subroutine to repartition precip into N events
c       call precipmod(ndays,rmissing,pr0,pr0_new)

c   Begin daily calculations.
    do iday=1, ndays
        ntotdays = ntotdays + 1 ! a count of total days for model run.
                                ! it's reset for each spinup loop (if any)
                                ! zero out the horizontal flux sum variable
    do m=0, ncells             ! grid ID # went from 62242 to 4446 (geographic)
        disch(m) = 0.0d0      ! changed to 0 to 39926 for EASE drainage
    enddo

    sum_wsnow = 0.0d0
    sum_snowpk = 0.0d0
    sum_p = 0.0d0
    sum_et= 0.0d0
    sum_rootwater= 0.0d0
    sum_rootices = 0.0d0
    sum_deepwater= 0.0d0
    sum_deepices = 0.0d0
    sum_wetlandstore = 0.0d0
    sum_runoff = 0.0d0
    sum_wr = 0.0d0
    sum_snowsubl = 0.0d0
    sum_surfevap = 0.0d0

c   Begin water balance calculations by gridcell.
    do icell = 1, ncells
        if (imon .eq. ifrstmon.and.iday.eq.1) then
            ithawflag(icell) = 0
            nthawdays(icell) = 0

            if (icell .eq. igetcell) then
                sumprecip = 0.0d0 ! these are for annual total
                sumpet = 0.0d0 ! testing now on one cell
                sumsnow = 0.0d0
                sumsubl = 0.0d0
                sumsurfevap = 0.0d0
                sumavailwat = 0.0d0
                sumrunoff = 0.0d0
                sumriver = 0.0d0
            endif
        endif
    endif

```

```

c Initialize monthly runoff to zero and open output file.
  if (iday .eq. 1) then
    monthrunoff(icell,imon) = 0.0d0
    monthevap(icell,imon) = 0.0d0
    monthsub(icell,imon) = 0.0d0
    monthrootwat(icell,imon) = 0.0d0
    monthrootice(icell,imon) = 0.0d0
    monthdeepwat(icell,imon) = 0.0d0
    monthdeepice(icell,imon) = 0.0d0
    monthswc(icell,imon) = 0.0d0
    monthroot2deep(icell,imon) = 0.0d0
    monthmeltwat(icell,imon) = 0.0d0
c     write(runoffname,'(''Grid/pwbn.v1.runoff.'',i4)') iyr
c     open(90,file=runoffname)
  endif

c Set scaler precip, tair, et, ALT from arrays. Read tseries data to get PET.
c Also scale precip if so desired for the run.
  precip = pr0(iday,icell) !put prcp(time,gridcell) into scaler var.
c   precip = pr0_new(iday,icell)
  if (precip .lt. 0.0d0) precip = 0.0d0

  if (temp(iday,icell) .gt. 150.0d0) then
    tair = temp(iday,icell) - 273.16d0 ! set "tair" from array
  else
    tair = temp(iday,icell)
  endif

  active_layer(icell) = activelayer(iday,icell) ! define ALT spatial
  tmin = tminvals(iday,icell) - 273.16d0
  tmax = tmaxvals(iday,icell) - 273.16d0
  vaporpress = vaporvals(iday,icell) * 0.1d0
  windsp = windvals(iday,icell)
  radnet = radvals(iday,icell)
  lai = laivals(imon,iday,icell)

c Set up array to store the last 3 days of tair at each grid cell,
c then check to see if the past three days have been above zero. If yes,
c then set a flag to "1", indicating yes.
c Check for 3 days > 0 will only be done after February.
  ntemp_point = mod(ntotdays-1,3) + 1
  temp_array(ntemp_point,icell) = tair
  if (ithawflag(icell) .eq. 1) goto 50
  if (imon .ge. 3 .and. temp_array(1,icell) .gt. 0.0d0 .and.

```

```

$         temp_array(2,icell) .gt. 0.0d0 .and. temp_array(3,icell)
$         .gt. 0.0d0) then
$           ithawflag(icell) = 1
$         endif
50        if (ithawflag(icell) .eq. 1)
$           nthawdays(icell) = nthawdays(icell) + 1
c  Check for 3 days below 0 in/after August.
$         if (imon .ge. 8 .and. temp_array(1,icell) .le. 0.0d0 .and.
$           temp_array(2,icell) .le. 0.0d0 .and. temp_array(3,icell)
$           .le. 0.0d0) then
$           ithawflag(icell) = 0
$         endif

c  Set air temperature 4 degree C cooler in summer
c         if (ithawflag(icell) .eq. 1) tair = tair - 4.0d0
c         if (ithawflag(icell) .eq. 1) tair = tair + 4.0d0

$         julday = imonday1(imon) + iday      ! set julian day of year
$         if (mod(iyr,4) .eq. 0 .and. imon .gt. 2) julday = julday + 1

c  Set last day of month. Also used as number of days in month
$         if (iday.eq.1.and.icell.eq.1) then
$           lastday = monlastday(imon)
$           if (mod(iyr,4) .eq. 0 .and. imon .eq. 2) then
$             lastday = lastday + 1
$           endif
$         endif

c  ***** Get Potential ET *****
c         ivegcov = ivegitation(icell)

$         ivegcov = inewveg1(icell,iyrindex)
$         if (ivegcov .eq. 0) then
$           print*, icell, imon, iday
$           stop 'Veg = 0'
$         endif

$         if (read_evapdat) then
$           et = evap(iday,icell)      ! set "et" from array
$         else
$           if(ievapfunc.eq.1) call hamon(rlat(icell),julday,tair,et)
$           if(ievapfunc.eq.2) then
$             if (ivegcov .gt. 8) ivegcov = 8
$             FL = 0.5d0 ; sheat = 0.0d0 ; rLAI = 6.0d0
c           write(97,*) julday,rlat(icell),rlon(icell),ivegcov
c           write(97,*) rLAI,FL,windsp,radnet,tair,vaporpress

```

```

        sngl_lat=rlat(icell) ; sngl_lon=rlon(icell)
        sngl_lai=sngl(rLAI) ; sngl_sheat=sngl(sheat)
        sngl_snow=sngl(snowpk1+wsnw1) ; sngl_FL=sngl(FL)
        sngl_wind=sngl(windsp) ; sngl_rad=sngl(radnet)
        sngl_vap=sngl(vaporpress)
        sngl_tmax=sngl(tmax) ; sngl_tmin=sngl(tmin)
        sngl_tair = (sngl_tmax + sngl_tmin) / 2.

        iflag = 0
        et = pmdayf(julday,sngl_lat,sngl_lon,ivegcov,
$         sngl_lai,sngl_snow,sngl_FL,sngl_wind,sngl_rad,
$         sngl_tair,sngl_vap,sngl_sheat,sngl_tmax,
$         sngl_tmin,iflag)
        endif
    endif
    if (et .lt. 0.0) et = 0.0
    potent_et = dble(et)

c   Set k1, k2, k3 equal to cell ID, basin ID, and "next" cell, respectively.
        k1=id(icell)
        k2=ibasin(icell)
        k3=idrain2(icell)

c           ATMOS ROUTINE GOES HERE

        wsnw1=wsnow(icell)
        snowpk1=snowpack(icell)
        rootwatprev=rootwater(icell) !put soilwater, groundwat, and runoff
        deepwatprev=deepwater(icell) ! into scaler variables for input
        rooticeprev=rootices(icell)      ! to subroutine
        deepiceprev=deepices(icell)
        wetlandstoreprev=wetlandwat(icell)
        wr1=wr(icell)
        roi=ro(icell)

c           print*, iday,icell,snowpk1, wsnw1

c   Call subroutine to calculate a snowmelt from solar radiation.
c   *****BYPASSED*****
c           call solarmelt(julday, rlat(icell), rad_2_melt, rad_melt)
        rad_melt = 0.0d0

c   Call snow subroutine.  Need to decide if we run it when no snowpack
        if (tair .lt. tsnow_cutoff) then

```

```

        psnow = precip
        prain=0.0d0
    else
        prain = precip
        psnow = 0.0d0
    endif

c        write(97,'(3i6)') icell, imon, iday

        call snow (snowpk1,wsnw1,snowretain,snowrelease,rad_melt,
$          tair,tsnow_cutoff,precip,potent_et,ivegcov,snowpk2,
$          wsnw2,avail_wat,snowmelt,snow_subl,surf_evap,evap_unmet)
c        write(97,'(3i6,2f7.1)') icell, imon, iday, snowpk2, snowmelt
        et = evap_unmet

    printflag = .false.

        if (printflag) then
        if (icell .eq. igetcell) then
        write(95,111) 'Year = ', iyr
        write(95,111) 'Month = ', imon
        write(95,111) 'DAY = ',iday
        write(95,111) 'Vegcover = ', ivegcov
        write(95,112) 'Snowpack prev = ', snowpk1
        write(95,112) 'Wsnow prev = ', wsnw1
        write(95,112) 'Air temp = ', tair
        write(95,112) 'Psnow = ',psnow
        write(95,112) 'Prain = ',prain
        write(95,112) 'Potential ET = ', potent_et
        write(95,112) 'Radmelt = ', rad_melt
        write(95,112) 'LAI = ', lai
        write(95,112) 'ET not satisfied by snow = ', et
        write(95,112) 'snowpack new = ', snowpk2
        write(95,112) 'Watsnow_new = ', wsnw2
        write(95,112) 'Snowmelt or rain', avail_wat
        write(95,112) 'Snow subl. = ',snow_subl
        write(95,112) 'Surface evap = ',surf_evap ! evap from snowwat
        write(95,*) ' '
        111      format(a8,i4)
        112      format(a23,f10.4)
c          stop
        endif
        endif
        555      continue

```

```

c Reset these at beginning of 4th spinup loop. Won't need this after spinup.
  if (iyr .eq. 2000 .and. julday .eq. 1) then
    zthawmax(icell) = -10000.0d0
  endif
  if (iyr .eq. 2000 .and. julday .eq. 183) then
    zfrzmax(icell) = -10000.0d0
  endif

c Next block executed on first day of simulation only. Same block is
c repeated after call to soil routine.
c Setting previous days thawdepth. These values are input above from spinup.
c Sumtair(icell) and sumtair2(icell) have been read and are available.
c If logical indicates reading ALD from file, then do assignment if ALD
c is non-missing.
  if (read_thawdat .and. active_layer(icell) .ne. -9999.0d0
    $ .and. ntodays .eq. 1) then
    depth_phys_prev = active_layer(icell)
    if (icell .eq. 5842) print*, imon, active_layer(icell)
    depth_space_prev=depth_phys_prev*soil_porosity(icell)
  endif
  if ((read_thawdat .eqv. .false.) .or.
    $ (active_layer(icell) .eq. -9999.0d0)) then
    depth_phys_prev = depth_phys(icell) ! 'depth' on previous day
    depth_space_prev = depth_space(icell)
    sumtair_prev = sumtair(icell)
  endif
c   if (read_thawdat) then
c     active_layer_prev = active_layer(icell)

c Skip next several blocks if TFM is turned off.
  if (no_thaw) goto 700

c Set code to force 10mm/day thaw (10mm PHYSICAL depth) at each grid cell
c after 3 days above zero. The second block can be used to
c 'cap' thaw depth at 1000mm (PHYSICAL depth).
300   if (ctrl_thaw) then
c     if (icell .eq. igetcell) print*, 'here1', imon, iday,
c     $     ithawflag(icell), nthawdays(icell)
    if (ithawflag(icell) .eq. 1) then
      if (nthawdays(icell) .eq. 1) then
        depth_phys_prev = 0.0d0
        sumtair(icell) = 0.0d0
        conduct_sum(icell) = 0.0d0
        conductpeat_sum(icell) = 0.0d0
        ndegdays_summed(icell) = 0
        iseaon(icell) = 1 ! 1 means summer
      endif
    endif
  endif

```

```

        iaccumulate(icell) = 0
    endif
    depth_phys(icell) = depth_phys_prev + 5.0d0
c     if (depth_phys(icell) .gt. 1000.0d0)
c     $         depth_phys(icell) = 1000.0d0
        depth_space(icell) = depth_phys(icell) *
    $         soil_porosity(icell)
    endif
endif
c If both root zone and deep zone ice is gone, reset degree days
c accumulation to zero and set season variable to summer.
    if (rooticeprev .eq. 0.0d0 .and. deepiceprev .eq.0.0d0)then
        sumtair(icell) = 0.0d0
c     summerthaw(icell) = 0.                ! reset to get summer thaw
        conduct_sum(icell) = 0.0d0
        conductpeat_sum(icell) = 0.0d0
        ndegdays_summed(icell) = 0
        izeason(icell) = 1                ! 1 means summer
        iaccumulate(icell) = 0
    endif

c If both root zone and deep zone water is gone, reset degree days
c accumulation to zero and set season variable to winter.
400    if (rootwatprev .eq. 0.0d0 .and. deepwatprev .eq.0.0d0)then
        sumtair(icell) = 0.0d0
        conduct_sum(icell) = 0.0d0
        conductpeat_sum(icell) = 0.0d0
        ndegdays_summed(icell) = 0
        izeason(icell) = 0                ! 0 means winter
        iaccumulate(icell) = 0
    endif

c Set flag to allow for degree day accumulation if 1) it's summer and
c air temp drops below (or equal to) zero or 2) it's winter and air temp
c goes above zero. In either case accumulate both negative and positive air
c temps. Soil routine will freeze or thaw dependant on degree day variable.
c If it is positive, thaw ice. If negative, freeze water
    if (ctrl_thaw .eqv. .true.) then
        if (ithawflag(icell) .eq. 1) goto 500
    endif
    if (izeason(icell) .eq. 1 .and. tair .le. 0.0d0) then
        iaccumulate(icell) = 1
        if (sumtair(icell) .eq. 0.0d0) then
            depth_space_prev = 0.0d0
            depth_phys_prev = 0.0d0
        endif
    endif

```

```

endif
500  if (iseason(icell) .eq. 0 .and. tair .gt. 0.0d0) then
      iaccumulate(icell) = 1
      if (sumtair(icell) .eq. 0.0d0) then
          depth_space_prev = 0.0d0
          depth_phys_prev = 0.0d0
      endif
endif
      if (iaccumulate(icell) .eq. 1) then
          sumtair(icell) = sumtair(icell) + tair
          ndegdays_summed(icell) = ndegdays_summed(icell) + 1
      endif

c Phase is an indicator of positive or negative degree day accumulation.
c When there's positive degree days, phase is 1. When negative DD, it's 0.
c If DD is zero, check the days air temperature to set phase.
c Soil routine looks for phase to compute ET, overland runoff, etc.
      if (sumtair(icell) .lt. 0.0d0) then
          iphase = 0
      else if (sumtair(icell) .gt. 0.0d0) then
          iphase = 1
      else if (sumtair(icell) .eq. 0.0d0) then
          if (tair .gt. 0.0d0) then
              iphase = 1
          else
              iphase = 0
          endif
      endif
endif

c If degree days changes from positive to negative, set previous depth
c to zero.
c If degree days changes from negative to positive, set previous depth
c to zero. NOTE: NEED TO BE SURE THAT THE "EQUAL TO" CASES HERE ARE RIGHT.
c NOTE: BYPASS THESE STATEMENTS IF USING INPUT ACTIVE-LAYER THICKNESSES
      if (read_thawdat) goto 700

      if(sumtair_prev .ge. 0.0d0 .and. sumtair(icell) .lt. 0.0d0
$ .or. sumtair_prev .le. 0.0d0 .and. sumtair(icell) .gt.0.0d0)
$ then
          depth_space_prev = 0.0d0
          depth_phys_prev = 0.0d0
      endif

c Set parameters to turn off thaw/freeze permafrost simulation.
700  if (no_thaw) then
      iseason(icell) = 1      ! season is summer

```



```

        iphase = 1          ! positive accumulation of degree days
        iaccumulate(icell) = 1  ! active mode
        depth_phys(icell) = soildepth(icell)
        depth_space(icell) =soildepth(icell)*soil_porosity(icell)
        sumtair(icell) = 30.0d0
        ndegdays_summed(icell) = ntotdays
    endif

c Set volume of water in soil from previous day's root water and ice, and
c root zone availablr space.
        call bound(0.0d0,(rootwatprev+rooticeprev)/rootdepth(icell),
        $          1.0d0,soilwatvolume)
c          soilwatvolume = 0.4

c Some print statements if soil water is less than 0%.

        if(soilwatvolume .lt. 0.0d0.or.soilwatvolume.gt.1.0d0)then
            print*,'On ',imon,iday,icell,', soilwat out of range'
            if (sumtair(icell) .le. 0.0d0)
        $         print*,'Frozen state ',rootwatprev,deepwatprev
            if(sumtair(icell) .gt. 0.0d0)
        $         print*,'Thawed state ',rooticeprev,deepiceprev
            stop
        endif

c Call routine to interpolate between dry, wet, and saturated
c soil thermal conductivities for mineral and then peat soils

        varjunk=soilwatvolume ! junk variable to write out soilwater
        call conductivity(soilwatvolume,therm_conddry(icell),
        $          therm_condwet(icell),therm_condsat(icell),soilconduct)

        call conductivity(soilwatvolume,therm_condpeatdry,
        $          therm_condpeatwet,therm_condpeatsat,therm_condpeat)

c Define average conductivity since first of year.
        conduct_sum(icell) = conduct_sum(icell) + soilconduct
        conduct_av = conduct_sum(icell) /
        $          real(max(ndegdays_summed(icell),1))
c          if (icell .eq.igetcell)print*,soilconduct,conduct_sum(icell)

        conductpeat_sum(icell)=conductpeat_sum(icell)+therm_condpeat
        conductpeat_av = conductpeat_sum(icell) /
        $          real(max(ndegdays_summed(icell),1))

c          if (read_thawdat) goto 114 ! skip if using other data

```

```

c          if (ctrl_thaw) goto 300          ! skip if creating control thaw

c  Get thaw front, or freeze front depth from Stephan solution.
c  Routine is driven with the accumulated degree day value.
c  "Depth" encompasses, essentially, a thaw or freeze depth.
c  Thaw or freeze depth is non-explicit -- it's implied by looking at
c  accumulated degree days. Positive DD implies thawed state, negative frozen.

c  Skip Stephan calculation if snow is present and it's spring.
c          if(icell.eq.igetcell)print*,snowpk2,imon,iday,sumtair(icell)
c  New version, implemented 2/27/03:
c          if (snowpk2 .gt. 0.0d0 .and. tair .gt. 0.0d0) then
c              depth_phys(icell) = depth_phys_prev
c              depth_space(icell) = depth_space_prev
c              goto 250
c          endif

c  Previously:
c          if (snowpk2 .gt. 0.0d0 .and. imon .lt. 7 .and.
c  $              sumtair(icell) .eq. 0.0d0) then
c              depth_phys(icell) = depth_phys_prev
c              depth_space(icell) = depth_space_prev
c              goto 250
c          endif

c          if (ctrl_thaw .eqv. .true.) then
c              if (ithawflag(icell) .eq. 1) goto 250
c          endif

c          if (no_thaw) goto 250          ! TFM is disabled
c          if (read_thawdat .and.          ! ALT gotten from input files
c  $              active_layer(icell) .ne. -9999.0d0) goto 250

c          if (iaccumulate(icell) .eq. 1) then
c              if (sumtair(icell) .eq. 0.0d0) then
c                  depth_phys(icell) = depth_phys_prev
c                  depth_space(icell) = depth_space_prev
c                  print*, 'Warning: DD = 0'
c                  if(icell.eq.igetcell)
c  $                      write(94,*) 'Sum DD is zero and accumulation is ON!'
c                  goto 250
c              endif

c          abs_sumtair = abs(sumtair(icell))

```

```

        call thaw2layer(abs_suntair,ivegcov,bulk_dens(icell),
$         soilwatvolume,conduct_av,conductpeat_av,
$         soilcarbon(icell),soil_porosity(icell),
$         depth_phys_prev,depthout,iwrite)

c         if(icell.eq.igetcell)print*,snowpk2,iday,tair,depthout
depth_phys(icell) = depthout
depth_space(icell) = depthout * soil_porosity(icell)
c         if(icell.eq.igetcell)print*,depthout

750         if(suntair(icell) .gt. 0.0d0)
$             zthawmax(icell) = max(depthout,zthawmax(icell))
        if(suntair(icell) .le. 0.0d0)
$             zfrzmax(icell) = max(depthout,zfrzmax(icell))
c         if (icell .eq. igetcell)print*,depthout,zthawmax(icell),
c         $             zfrzmax(icell)
c         if(icell.eq.igetcell) then
c             if (suntair(icell) .le. 0.0d0) then
c                 write(94,*)'PDepth from negative DD = ', depthout
c             else
c                 write(94,*)'PDepth from positive DD = ', depthout
c             endif
c         endif
        else
        depth_phys(icell) = depth_phys_prev
        depth_space(icell) = depth_space_prev
c         if(icell.eq.igetcell)
c         $             write(94,*) 'Sum DD is zero and accumulation is off'

        endif

c Set root-zone depth to the thawdepth or rootzone depth from file.
250     root_depth = rootdepth(icell)
        if (root_depth .eq. 0.0d0) root_depth = 100.0d0
        soil_depth = soildepth(icell)

c Set active-layer thickness from file, if so desired.
        if (read_thawdat .and. active_layer(icell) .ne. -9999.0d0)
$             depth_phys(icell) = active_layer(icell)
c         if(icell.eq.igetcell)print*, imon, iday,depth_phys(icell)
        depth_space(icell) = depth_phys(icell) *
$             soil_porosity(icell)

c Make check for maximum summer thaw depth.

```

```

        if (read_thawdat) then
c           summerthaw(icell) = max(summerthaw(icell),
c           $           varjunk)
        else
           summerthaw(icell) = max(summerthaw(icell),
$           depth_phys(icell))
        endif

c           printflag = .false.
           if (printflag) then
           if (icell .eq. igetcell) then
           write(95,112) 'Rootdepth (physical) = ',
$           root_depth / soil_porosity(icell)
           write(95,112) 'soil_depth = ', soil_depth/soil_porosity(icell)
           write(95,112) 'Soil Porosity = ', soil_porosity(icell)
           write(95,112) 'Fieldcapacity(FC/por.) = ',
$           field_capac(icell)
           write(95,112) 'Air temperature = ', tair
           write(95,112) 'Sum degree days thaw = ', sumtair(icell)
           write(95,112) 'Sum degree days freeze = ', rmissing
           write(95,112) 'Soil wat fraction(0-1) = ', varjunk
           write(95,112) 'Soil avg. conduct. = ', conduct_av
           write(95,112) 'Depth physical prev = ',
$           depth_phys_prev
           write(95,112) 'Today's physical depth = ',
$           depth_phys(icell)
           write(95,112) 'Freeze front depth prev = ',
$           rmissing
           write(95,112) 'Freeze front depth = ',
$           rmissing
           write(95,112) 'Infiltration rate = ', infiltration
           write(95,112) 'Wilting point(WP/por.) = ',
$           wilt_point(icell)
           write(95,112) 'Root water previous = ', rootwatprev
           write(95,112) 'Root ice previous = ', rooticeprev
           write(95,112) 'Deep water previous = ', deepwatprev
           write(95,112) 'Deep ice previous = ', deepiceprev
           write(95,*) ' '
           endif
           endif

c Call soil subroutine
           iwrite = 0

c Always call this function. If frozen soil, values will be set to previous
c inside subroutine.

```

```

c Call soil function to thaw or freeze water based on accumulated
c degree day value AND change in "depth", which encompasses, essentially, a
c thaw or freeze depth. Thaw or freeze depth is non-explicit -- it's implied.
    if (ivegcov .ne. 10) then
        call soilzone(root_depth,soil_depth,iwetland(icell),
$           field_capac(icell),
$           wilt_point(icell),et,infiltration,rootbaseflowfact,
$           deepbaseflowfact,depth_space(icell),depth_space_prev,
$           tair,iseason(icell),iphase,avail_wat,rootwatprev,
$           rooticeprev,deepwatprev,deepiceprev,wetlandstoreprev,
$           rootwat,rootice,
$           deepwat,deepice,wetlandstore,ro2,effective_e,
$           overlandRO,rootbaseflow,deepbaseflow,root2deep,iwrite)
    else
        call waterzone(root_depth,soil_depth,et,avail_wat,
$           rootwatprev,rooticeprev,deepwatprev,deepiceprev,
$           rootwat,rootice,deepwat,deepice,ro2,effective_e,iwrite)
        wetlandstore = 0.0d0
    endif
    if (read_thawdat .and.
$       active_layer(icell) .ne. -9999.0d0) then
        depth_phys_prev = active_layer(icell)
c       if (icell .eq. 5842) print*, imon, active_layer(icell)
        depth_space_prev=depth_phys_prev*soil_porosity(icell)
    endif
c       if (icell .eq. igetcell) write(94,*)' '

350    check=(avail_wat+rootwatprev+rooticeprev+
$       deepwatprev + deepiceprev + wetlandstoreprev) -
$       (rootwat+rootice+deepwat+ deepice+ wetlandstore +
$       ro2+effective_e)      ! was + xr after ro2
    if (abs(check) .gt. 1.0d-8) then
        print*,
$       (avail_wat+rootwatprev+rooticeprev+
$       deepwatprev+deepiceprev+wetlandstoreprev),
$       (rootwat+rootice+deepwat+deepice+wetlandstore+
$       ro2+effective_e)
        write(*,*)' '
        write(*,*)'Gridcell water balance check failed'
        write(*,*)'Check should equal 0. Yet, check = ', check
        write(*,*)' '
        write(*,30)icell,avail_wat,precip,rootwatprev,rootwat
$       ,rooticeprev,rootice,deepwatprev,deepwat,
$       wetlandstoreprev,wetlandstore,ro2,effective_e
        stop
    endif

```

```

30      format(i5,10f10.2)

200     snowpack(icell)=snowpk2
        wsnw(icell)=wsnw2
        rootwater(icell)=rootwat      ! put soilwater, groundwater, and runoff
        deepwater(icell)=deepwat      ! into spatial "holding" arrays for
        rootices(icell)=rootice       ! use at next time step.
        deepices(icell)=deepice
        wetlandwat(icell)=wetlandstore
        ro(icell)=ro2
        monthsub(icell,imon) = monthsub(icell,imon) +
$           snow_subl + surf_evap
        monthevap(icell,imon) = monthevap(icell,imon) +
$           effective_e + snow_subl + surf_evap
c       monthevap(icell,imon) = monthevap(icell,imon) + potent_et !for PET
        monthrunoff(icell,imon) = monthrunoff(icell,imon) + ro2
        monthrootwat(icell,imon) = monthrootwat(icell,imon) +rootwat
        monthrootice(icell,imon) = monthrootice(icell,imon) +rootice
        monthdeepwat(icell,imon) = monthdeepwat(icell,imon) +deepwat
        monthdeepice(icell,imon) = monthdeepice(icell,imon) +deepice
        monthswe(icell,imon) = monthswe(icell,imon) + snowpk2 +wsnw2
        monthroot2deep(icell,imon) = monthroot2deep(icell,imon) +
$           root2deep
        monthmeltwat(icell,imon) = monthmeltwat(icell,imon)+snowmelt

c       Write snow for a grid in Greenland to file.
c           if (icell .eq. 33230)
c           $           write(97,'(3i4,f10.1)') iyr,imon,iday,snowpk2

c       Put horiz. discharge for previous time (summed below) into da variable

           da=disch(k1)      ! gridcell horiz. discharge, previous time

c       Call river subroutine.  Inputs are:
c       xr - excess river water (mm)      NOT CURRENTLY USED
c       ro2 - runoff computed in subroutine soil_ground
c       da - gridcell horizontal upstream input
c       wr1 - water in river for previous time step
c       Outputs are:
c       wr2 - water in river output from routine (current time)
c       db2 - gridcell horizontal downstream discharge
c       dr - change in river water

c           print*, iday,icell,xr,ro2,da,wr1      ! TTT!
           call river_discharge(area,km_per_mm,xr,ro2,da,wr1,wr2,
$           db2,dr)

```

```

        wr(icell) = wr2
c      if (wr2 .lt. 0.0d0) idryriv(icell) = idryriv(icell) + 1

c      printflag=.false.
      if (printflag) then
        if (icell .eq. igetcell) then
          write(95,112) 'Evapotranspiration =', effective_e
          write(95,112) 'Root water new = ', rootwat
          write(95,112) 'Root ice new = ', rootice
          write(95,112) 'Deep water new = ', deepwat
          write(95,112) 'Deep ice new = ', deepice
          write(95,112) 'runoff previous = ', ro1
          write(95,112) 'runoff new = ', ro2
          write(95,112) 'river water previous = ', wr1
          write(95,112) 'river water new = ', wr2
          write(95,*) ' '
        endif
      endif

c Next statements check water balance (at each cell) to 10 decimal points

      check=(wr1 + ro2*km_per_mm*area + xr*km_per_mm*area + da) -
$         (wr2 + db2)
      if (abs(check) .ge. 1.0d-10) then
        write(*,*)' '
        write(*,*)'Gridcell river-water balance check failed'
        write(*,*)'Check should equal 0. Yet, check = ', check
        write(*,*)' '
        write(*,'(6f14.10)')wr1,ro2,ro2*km_per_mm*area,da,wr2,db2
        write(*,107) k, icell, avail_wat*km_per_mm*area,
$         rooticeprev*km_per_mm*area,
$         rootwatprev*km_per_mm*area,deepwatprev*km_per_mm*area,
$         deepiceprev*km_per_mm*area,wr1,
$         rootice*km_per_mm*area,rootwat*km_per_mm*area,
$         deepwat*km_per_mm*area,deepice*km_per_mm*area,
$         effective_e*km_per_mm*area,wr2,db2,da
        write(*,*)' '
        stop
      endif
107      format(2i6,14f16.4)

c Accumulate water in "next cell" (k3) grid. Also sum water accumulated at
c each Arctic basin_outlet over time.

      disch(k3) = disch(k3) + db2
      d3 = db2 - da

```

```

c      d3s(icell) = d3s(icell) + d3
c      print*, icell, k3, db2, disch(k3)

      if(k3 .eq. 0) then      ! basin_outlet is sum at each Arctic outlets
        basin_outlet(k2) = basin_outlet(k2) + db2
        ihave_basinout(k2) = 1
      endif

c  Track water in outlets that do not drain in Arctic (they are not k3=0)
c  sum_intrnl is the total stock (accumulated over all time steps) for
c  non_Arctic basin outlets.  NOTE: WAS USED PREVIOUSLY ON GEOGRAPHIC
C  BASIN TABLE.  NOT USING NOW ON EASE TABLE
c      do mm=1, 79
c          if (k3 .eq. intrnl_bas(mm)) then
c              sum_intrnl = sum_intrnl + db2
c              basin_outlet(k2) = basin_outlet(k2) + db2
c              ihave_basinout(k2) = 1
c          endif
c      enddo
c      write(98,*) k3, db2, sum_intrnl
c      if (k3.eq.43030 .or. k3.eq.43029)
c  $          write(98,*) k,j,i,k1,k3,db2,disch(k3)

runoff1(icell,iday) = ro2
evap1(icell,iday) = effective_e + snow_subl + surf_evap
c  evap1(icell,iday) = potent_et
snowwaterq1(icell,iday) = snowpk2 + wsnw2
snowice1(icell,iday) = snowpk2
snowwater1(icell,iday) = wsnw2
rootwat1(icell,iday) = rootwat !snowmelt !rootwat
rootice1(icell,iday) = rootice
deepwat1(icell,iday) = deepwat
deepice1(icell,iday) = deepice
thawfreezeD1(icell,iday) = depth_phys(icell)
snowmelt1(icell,iday) = snowmelt

      if (nspinup .gt. 0 .and. init .eq. nspinup+1 .and.
$          julday .eq. ispinupday) then
          if (icell .eq. 1) write(99,'(a200)') '"ID" "Month" "Day"
$ "rootwater" "rootice" "deepwat" "deepice" "wetlandstore"
$ "snowpk1" "wsnw1" "wr1" "sumtair" "depth_phys" "depth_space"
$ "conduct_sum" "conductpeat_sum" "ndegdays_summed" "iseason"
$ "iaccumulate"'
          write(99,35) icell, imon, iday, rootwat, rootice,
$          deepwat, deepice, wetlandstore, snowpk2, wsnw2, wr2,

```



```

$          sumtair(icell), depth_phys(icell),
$          depth_space(icell), conduct_sum(icell),
$          conductpeat_sum(icell), ndegdays_summed(icell),
$          izeason(icell), iaccumulate(icell)
endif
35      format(i5,2i3,13f16.8,i6,2i2)

c      These sums are temporary for simple checking.  Remove when finished
      if (icell .eq. igetcell.and.iyr.ge.1995) then !sums for Yukon basin
          sumprecip = sumprecip + precip ! * 1.0d-6 * area
          sumpet = sumpet + effective_e ! * 1.0d-6 * area
          sumsnow = sumsnow + snowpk2 * 1.0d-6 * area +
$              wsnw2 * 1.0d-6 * area
          sumsubl = sumsubl + snow_subl ! * 1.0d-6 * area
          sumsurfevap = sumsurfevap + surf_evap ! * 1.0d-6 * area
          sumavailwat = sumavailwat + avail_wat ! * 1.0d-6 * area
          sumrunoff = sumrunoff + ro2 ! * 1.0d-6 * area
          sumriver = sumriver + wr2
          if (k3 .eq. 0) sumatocean = sumatocean + db2
c          print*, imon, iday, sumprecip, sumpet, sumsubl,
c          $          sumsurfevap, sumrunoff
      endif

          ! sum runoff for all basins in domain
          sumbas(1,ibasin(icell)) = sumbas(1,ibasin(icell)) +
$              precip * 1.0d-6 * area
          sumbas(2,ibasin(icell)) = sumbas(2,ibasin(icell)) +
$              effective_e * 1.0d-6 * area + snow_subl * 1.0d-6 * area +
$              surf_evap * 1.0d-6 * area
          sumbas(3,ibasin(icell)) = sumbas(3,ibasin(icell)) +
$              ro2 * 1.0d-6 * area
          if (iday .eq. lastday) then
          sumbas(4,ibasin(icell)) = sumbas(4,ibasin(icell)) +
$              (snowpk2+wsnw2+rootwat+rootice+deepwat+deepice)*1.0d-6*area

          sumbas(5,ibasin(icell)) = sumbas(5,ibasin(icell)) +
$              snowpk2 * 1.0d-6 * area
          sumbas(6,ibasin(icell)) = sumbas(6,ibasin(icell)) +
$              wsnw2 * 1.0d-6 * area
          sumbas(7,ibasin(icell)) = sumbas(7,ibasin(icell)) +
$              rootwat * 1.0d-6 * area
          sumbas(8,ibasin(icell)) = sumbas(8,ibasin(icell)) +
$              rootice * 1.0d-6 * area
          sumbas(9,ibasin(icell)) = sumbas(9,ibasin(icell)) +
$              deepwat * 1.0d-6 * area
          sumbas(10,ibasin(icell)) = sumbas(10,ibasin(icell)) +

```

```

$           deepice * 1.0d-6 * area
      endif
c Sum all land water across all grid cells
      sum_snowpk = sum_snowpk + snowpk2*km_per_mm*area
      sum_wsnow = sum_wsnow + wsnw2*km_per_mm*area
      sum_rootwater = sum_rootwater + rootwat*km_per_mm*area
      sum_rootices = sum_rootices + rootice*km_per_mm*area
      sum_deepwater = sum_deepwater + deepwat*km_per_mm*area
      sum_deepices = sum_deepices + deepice*km_per_mm*area
      sum_wetlandstore = sum_wetlandstore +
$           wetlandstore *km_per_mm*area
      sum_wr = sum_wr + wr2

c Sum runoff
      sum_runoff = sum_runoff + ro2

c Sum the fluxes that will be added/subtracted from the "global cloud"
      sum_p = sum_p + precip*km_per_mm*area
      sum_et = sum_et + effective_e*km_per_mm*area
      sum_snowsubl = sum_snowsubl + snow_subl*km_per_mm*area
      sum_surfevap = sum_surfevap + surf_evap*km_per_mm*area

100      enddo      ! end of drainage cell loop

      PminusE = sum_p - (sum_et + sum_snowsubl + sum_surfevap)
      globe_cloud = globe_cloud - PminusE
      sum2ocean = sum2ocean + disch(0)
      total_land_water = sum_snowpk + sum_wsnow + sum_rootwater +
$           sum_deepwater + sum_rootices + sum_deepices +
$           sum_wetlandstore + sum_wr
      totjunk = totjunk + PminusE

c Initial water plus P-E over time minus current water state
c (soil, snow, river) equals sum of flux to ocean over time
      check = total_initial_water - (globe_cloud +
$           total_land_water + sum_intrnl + sum2ocean)
      if (abs(check) .gt. 1.0d-6) then
        write(*,*)' '
        write(*,*)'Domain water balance check failed'
        write(*,109)'Check should equal 0. Yet, check = ', check
        write(*,*)' '
        write(*,*)' initial water          Globalcloud
$ storage          internal basins          to-ocean          check'
        write(*,108) total_initial_water, globe_cloud,
$           total_land_water, sum_intrnl, sum2ocean, check

```

```

108     format(6f20.10)
109     format(a,f14.10)
        write(*,*)' '
        stop
    endif
  enddo      ! end of day loop
  write(*,110) 'Year ', iyr, ', Month ', imon, ' processed'

110  format(a,i4,a,i2,a)

c  This block writes monthly basin averages to monthly files
    goto 119      ! skip these write statements

    do i=1, nbasins
      write(91,'(i4,f10.1,i2)') i, basin_area(i), ihave_basin(i)
      if (ihave_basin(i) .eq. 0) goto 115
      if (init .eq. 1 .and. k .eq. 1)
        $ write(85,'(f9.1)') (initialstate(i) / basin_area(i)) * 1.0d6
        do j=1, navs
          c      print*, i, j, sumbas(j,i)
          c      basin_av(j,i) = (sumbas(j,i)
            basin_av(j,i) = (sumbas(j,i) / basin_area(i)) * 1.0d6
          enddo
          write(85,116) iyr, imon, i, (basin_av(j,i), j=1, navs)
116     format(i4,i3,i5,3f7.1,2f9.1,5f7.1)

c  Next line writes volume (km^3) of all storage water at each basin each month
c      write(87,122) iyr, imon, i, sumbas(4,i)
c 122  format(i4,i2,i5,f7.1)
115  enddo

119  continue

C*****
c***** OUTPUT SECTION *****
c  Write monthly totals for chosen fields.
c      goto 120
      if (imon .eq. 12 .and. iyr .ge. ioutyr1 .and. imon .ge. ioutmon1
        $ .and. iyr .le. ioutyr2 .and. imon .le. ioutmon2) then
c      write(85,117) sumprecip,sumpet,sumsubl,sumsurfevap,sumrunoff
c 117  format(5f10.2)

c  Set output year string
      write(yearstr, '(i4)') iyr
c  Evapotranspiration

```

```

    if (monthlyout(1) .eq. 1) then
        fname = outpath(1:lengthout)//'pwbm_monthlyevap'//yearstr
        open(90,file=fname)
        write(90,'(i4,a)')
$     iyr,' PWBM v1 monthly total ET(mm); Data: '//headerPfile//'
$ '//headerTfile//' (i6,2f10.4,12f8.1)'
        write(90,'(a)') '"CellID" "Lat" "Long" "01" "02" "03" "04"
118 "$05" "06" "07" "08" "09" "10" "11" "12"'
        do icell = 1, ncells
            if (rlon(icell) .lt. 0.0)
$                 rlon(icell) = 180. + (180. + rlon(icell))
                write(90,118) icell, rlat(icell), rlon(icell),
$                 (monthevap(icell,nn), nn=1,12)
                format(i6,2f9.4,12f8.1)
            enddo
            close(90)
        endif

c  Runoff
    if (monthlyout(2) .eq. 1) then
c        fname = outpath(1:lengthout)//'willmats_monthlyR0'//yearstr
        fname = outpath(1:lengthout)//'pwbm_monthlyrunoff'//yearstr
        open(90,file=fname)
        write(90,'(i4,a)')
$     iyr,' PWBM v1 monthly runoff(mm); Data: '//headerPfile//'
$ '//headerTfile//' (i6,2f10.4,12f8.1)'
        write(90,'(a)') '"CellID" "Lat" "Long" "01" "02" "03" "04"
"$05" "06" "07" "08" "09" "10" "11" "12"'
        do icell = 1, ncells
            if (rlon(icell) .lt. 0.0)
$                 rlon(icell) = 180. + (180. + rlon(icell))
                write(90,118) icell, rlat(icell), rlon(icell),
$                 (monthrunoff(icell,nn), nn=1,12)
            enddo
            close(90)
        endif

c  Root zone water
    if (monthlyout(3) .eq. 1) then
        fname = outpath(1:lengthout)//'pwbm_monthlyrootwat'//yearstr
        open(90,file=fname)
        write(90,'(i4,a)')
$     iyr,' PWBM v1 monthly rootzone water(mm); Data: '//headerPfile//'
$ '//headerTfile//' (i6,2f10.4,12f8.1)'
        write(90,'(a)') '"CellID" "Lat" "Long" "01" "02" "03" "04"
"$05" "06" "07" "08" "09" "10" "11" "12"'

```

```

        do icell = 1, ncells
            if (rlon(icell) .lt. 0.0)
$           rlon(icell) = 180. + (180. + rlon(icell))
            write(90,118) icell, rlat(icell), rlon(icell),
$           (monthrootwat(icell,nn) / real(lastday), nn=1,12)
            enddo
            close(90)
        endif

c Root zone ice
    if (monthlyout(4) .eq. 1) then
        fname = outpath(1:lengthout)//'pwbm_monthlyrootice'//yearstr
        open(90,file=fname)
        write(90,'(i4,a)')
$     iyr,' PWBm v1 monthly rootzone ice(mm); Data: '//headerPfile//'
$     '//headerTfile//' (i6,2f10.4,12f8.1)'
        write(90,'(a)') '"CellID" "Lat" "Long" "01" "02" "03" "04"
$ "05" "06" "07" "08" "09" "10" "11" "12"'
        do icell = 1, ncells
            if (rlon(icell) .lt. 0.0)
$           rlon(icell) = 180. + (180. + rlon(icell))
            write(90,118) icell, rlat(icell), rlon(icell),
$           (monthrootice(icell,nn) / real(lastday), nn=1,12)
            enddo
            close(90)
        endif

c Deep zone water
    if (monthlyout(5) .eq. 1) then
        fname = outpath(1:lengthout)//'pwbm_monthlydeepwat'//yearstr
        open(90,file=fname)
        write(90,'(i4,a)')
$     iyr,' PWBm v1 monthly deepzone water(mm); Data: '//headerPfile//'
$     '//headerTfile//' (i6,2f10.4,12f8.1)'
        write(90,'(a)') '"CellID" "Lat" "Long" "01" "02" "03" "04"
$ "05" "06" "07" "08" "09" "10" "11" "12"'
        do icell = 1, ncells
            if (rlon(icell) .lt. 0.0)
$           rlon(icell) = 180. + (180. + rlon(icell))
            write(90,118) icell, rlat(icell), rlon(icell),
$           (monthdeepwat(icell,nn) / real(lastday), nn=1,12)
            enddo
            close(90)
        endif

c Deep zone ice

```

```

        if (monthlyout(6) .eq. 1) then
            fname = outpath(1:lengthout)//'pwbm_monthlydeepice'//yearstr
            open(90,file=fname)
            write(90,'(i4,a)')
$   iyr,' PWBm v1 monthly rootzone ice(mm); Data: '//headerPfile//'
$   '//headerTfile//' (i6,2f10.4,12f8.1)'
            write(90,'(a)') '"CellID" "Lat" "Long" "01" "02" "03" "04"
$ "05" "06" "07" "08" "09" "10" "11" "12"'
            do icell = 1, ncells
                if (r lon(icell) .lt. 0.0)
$                   r lon(icell) = 180. + (180. + r lon(icell))
                write(90,118) icell, r lat(icell), r lon(icell),
$                   (monthdeepice(icell,nn) / real(lastday), nn=1,12)
            enddo
            close(90)
        endif

c   Snow water equivalent
        if (monthlyout(7) .eq. 1) then
            fname = outpath(1:lengthout)//'pwbm_monthlyswe'//yearstr
            open(90,file=fname)
            write(90,'(i4,a)')
$   iyr,' PWBm v1 monthly snow water eq.(mm); Data: '//headerPfile//'
$   '//headerTfile//' (i6,2f10.4,12f8.1)'
            write(90,'(a)') '"CellID" "Lat" "Long" "01" "02" "03" "04"
$ "05" "06" "07" "08" "09" "10" "11" "12"'
            do icell = 1, ncells
                if (r lon(icell) .lt. 0.0)
$                   r lon(icell) = 180. + (180. + r lon(icell))
                write(90,118) icell, r lat(icell), r lon(icell),
$                   (monthswe(icell,nn) / real(lastday), nn=1,12)
            enddo
            close(90)
        endif

        endif          ! end of if for month 12

120 continue

c   Write daily values for chosen fields.
c       goto 130
        if (iyr .ge. ioutyr1 .and. imon .ge. ioutmon1 .and. iyr .le.
$         ioutyr2 .and. imon .le. ioutmon2) then

c   Set output year/month string
        write(datestring2, '(i4,','.',',i2.2,','.txt')') iyr, imon

```

```

        str2="CellID" "Lat" "Long" "01" "02" "03" "04" "05" "06" "07"
        $"08" "09" "10" "11" "12" "13" "14" "15" "16" "17" "18" "19" "20" "
        $21" "22" "23" "24" "25" "26" "27" "28" "29" "30" "31"
121    format(i6,2f10.4,31f8.1)

c Write chosen daily output fields

c Evaporation
    if (idailyout(1) .eq. 1) then
        fname = outpath(1:lengthout)//'pwbm_dailyevap.'//datestring2
        open(32,file=fname)
        write(str1,'i4,
$    '' PWBM v1 daily evaporation (mm); Data: '' ,a, '' ',
$ a, '' (i6,2f10.4,12f8.1)''')'') iyr, headerPfile, headerTfile
        write(32,'(a140)') str1
        write(32,'(a180)') str2
        do icell = 1, ncells
            if (rlon(icell) .lt. 0.0)
$                rlon(icell) = 180. + (180. + rlon(icell))
                write(32,121) icell, rlat(icell), rlon(icell),
$                (evap1(icell,nn), nn=1,31)
            enddo
        close(32)
    endif

c Runoff
    if (idailyout(2) .eq. 1) then
        fname=outpath(1:lengthout)//'pwbm_dailyrunoff.'//datestring2
        open(32,file=fname)
        write(str1,'i4,
$    '' PWBM v1 daily runoff (mm); Data:'' ,a, '' ',a,
$ a, '' (i6,2f10.4,12f8.1)''')'') iyr, headerPfile, headerTfile
        write(32,'(a140)') str1
        write(32,'(a180)') str2
        do icell = 1, ncells
            if (rlon(icell) .lt. 0.0)
$                rlon(icell) = 180. + (180. + rlon(icell))
                write(32,121) icell, rlat(icell), rlon(icell),
$                (runoff1(icell,nn), nn=1,31)
            enddo
        close(32)
    endif

c Root zone water
    if (idailyout(3) .eq. 1) then
        ! rootwat meltmelt
        fname=outpath(1:lengthout)//'pwbm_dailyrootwat.'//datestring2
        open(32,file=fname)

```

```

        write(str1,'(i4,
$   '' PWBM v1 daily root zone water (mm); Data:'' ,a,'' '' ,a,
$ a,'' (i6,2f10.4,12f8.1)''')') iyr, headerPfile, headerTfile
        write(32,'(a140)') str1 ! root zone water  snowmelt
        write(32,'(a180)') str2
        do icell = 1, ncells
            if (rlon(icell) .lt. 0.0)
$               rlon(icell) = 180. + (180. + rlon(icell))
                write(32,121) icell, rlat(icell), rlon(icell),
$                   (rootwat1(icell,nn), nn=1,31)
            enddo
        close(32)
    endif
c Root zone ice
    if (idailyout(4) .eq. 1) then
        fname=outpath(1:lengthout)//'pwbm_dailyrootice.'//datestring2
        open(32,file=fname)
        write(str1,'(i4,
$   '' PWBM v1 daily root zone ice (mm); Data:'' ,a,'' '' ,a,
$ a,'' (i6,2f10.4,12f8.1)''')') iyr, headerPfile, headerTfile
        write(32,'(a140)') str1
        write(32,'(a180)') str2
        do icell = 1, ncells
            if (rlon(icell) .lt. 0.0)
$               rlon(icell) = 180. + (180. + rlon(icell))
                write(32,121) icell, rlat(icell), rlon(icell),
$                   (rootice1(icell,nn), nn=1,31)
            enddo
        close(32)
    endif
c Deep zone water
    if (idailyout(5) .eq. 1) then
        fname=outpath(1:lengthout)//'pwbm_dailydeepwat.'//datestring2
        open(32,file=fname)
        write(str1,'(i4,
$   '' PWBM v1 daily deep zone water (mm); Data:'' ,a,'' '' ,a,
$ a,'' (i6,2f10.4,12f8.1)''')') iyr, headerPfile, headerTfile
        write(32,'(a140)') str1
        write(32,'(a180)') str2
        do icell = 1, ncells
            if (rlon(icell) .lt. 0.0)
$               rlon(icell) = 180. + (180. + rlon(icell))
                write(32,121) icell, rlat(icell), rlon(icell),
$                   (deepwat1(icell,nn), nn=1,31)
            enddo
        close(32)

```



```

        endif
c   Deep zone ice
    if (idailyout(6) .eq. 1) then
        fname=outpath(1:lengthout)//'pwbm_dailydeepice.'//datestring2
        open(32,file=fname)
        write(str1,'(i4,
$   '' PWBM v1 daily deep zone ice (mm); Data:'' ,a,'' '' ,a,
$ a,'' (i6,2f10.4,12f8.1)''')' ) iyr, headerPfile, headerTfile
        write(32,'(a140)') str1
        write(32,'(a180)') str2
        do icell = 1, ncells
            if (rlon(icell) .lt. 0.0)
$               rlon(icell) = 180. + (180. + rlon(icell))
                write(32,121) icell, rlat(icell), rlon(icell),
$                   (deepice1(icell,nn), nn=1,31)
            enddo
        close(32)
    endif
c   Snow water equivalent
    if (idailyout(7) .eq. 1) then
        fname = outpath(1:lengthout)//'pwbm_dailyswe.'//datestring2
        open(32,file=fname)
        write(str1,'(i4,
$   '' PWBM v1 daily snow water eq. (mm); Data:'' ,a,'' '' ,a,
$ a,'' (i6,2f10.4,12f8.1)''')' ) iyr, headerPfile, headerTfile
        write(32,'(a140)') str1
        write(32,'(a180)') str2
        do icell = 1, ncells
            if (rlon(icell) .lt. 0.0)
$               rlon(icell) = 180. + (180. + rlon(icell))
                write(32,121) icell, rlat(icell), rlon(icell),
$                   (snowwateq1(icell,nn), nn=1,31)
            enddo
        close(32)
    endif
c   Thaw (or freeze) depth
    if (idailyout(8) .eq. 1) then
        fname =outpath(1:lengthout)//'pwbm_dailydepth.'//datestring2
        open(32,file=fname)
        write(str1,'(i4,
$   '' PWBM v1 daily thaw/freeze depth (mm); Data:'' ,a,'' '' ,a,
$ a,'' (i6,2f10.4,12f8.1)''')' ) iyr, headerPfile, headerTfile
        write(32,'(a140)') str1
        write(32,'(a180)') str2
        do icell = 1, ncells

```

```

        if (rlon(icell) .lt. 0.0)
$           rlon(icell) = 180. + (180. + rlon(icell))
           write(32,121) icell, rlat(icell), rlon(icell),
$           (thawfreezeD1(icell,nn), nn=1,31)
        enddo
        close(32)
    endif

c  Snowpack soild portion
c      goto 122
    if (idailyout(9) .eq. 1) then
        fname = outpath(1:lengthout)//'pwbm_dailysnowice.'//datestring2
        open(32,file=fname)
        write(str1,'i4,
$  '' PWBM v1 daily snow frozen portion (mm); Data:'' ,a,'' '' ,a,
$ a,'' (i6,2f10.4,12f8.1)''') iyr, headerPfile, headerTfile
        write(32,'(a140)') str1
        write(32,'(a180)') str2
        do icell = 1, ncells
            if (rlon(icell) .lt. 0.0)
$               rlon(icell) = 180. + (180. + rlon(icell))
                write(32,121) icell, rlat(icell), rlon(icell),
$               (snowice(icell,nn), nn=1,31)
            enddo
        close(32)
    endif

c  Snowpack liquid portion
    if (idailyout(10) .eq. 1) then
        fname = outpath(1:lengthout)//'pwbm_dailysnowwat.'//datestring2
        open(32,file=fname)
        write(str1,'i4,
$  '' PWBM v1 daily snow liquid portion (mm); Data:'' ,a,'' '' ,a,
$ a,'' (i6,2f10.4,12f8.1)''') iyr, headerPfile, headerTfile
        write(32,'(a140)') str1
        write(32,'(a180)') str2
        do icell = 1, ncells
            if (rlon(icell) .lt. 0.0)
$               rlon(icell) = 180. + (180. + rlon(icell))
                write(32,121) icell, rlat(icell), rlon(icell),
$               (snowwater(icell,nn), nn=1,31)
            enddo
        close(32)
    endif

endif          ! end of if for desired years and month to output

```





```

$   radmelt,temp,crittemp,prcp,pet,icovertype,snowpack_new,
$   snowwat_new,water2soil,snowmelt_direct,snowsubl,surface_et,
$   unmet_pet)
c           ! was meltwat where snowmelt_direct is
c
c This routine is a translation of snowpack.c written by R. Lammers
c
  implicit none
  integer icovertype
  real*8  pr_rain,pr_snow,snowpack,snowwatpack,water2soil
  real*8  meltwat,potentmelt,snowsubl,snowpet,snowpackprm
  real*8  snowmelt,crittemp,snowholdfactor,snowdamming,temp,prcp,pet
  real*8  snowpack_new,snowwat_new,meltwat_fact,surface_et,unmet_pet
  real*8  radmelt,diff,snowadj,totalin,totalout,check,potentfreeze
  real*8  snowfreeze,snowmelt_direct

  snowmelt_direct = 0.0d0
  totalin = snowpack + snowwatpack + prcp

c Calculate moisture flux from atmosphere
c if cold -> get snow, if warm -> get rain
  if (temp .lt. crittemp) then
    pr_snow = prcp
    pr_rain = 0.0d0
  else
    pr_snow = 0.0d0
    pr_rain = prcp
  endif

c Determine flux to the atmosphere from snowpack; dependent only on
c existence of snowpack.
c This is something not in original model, which will reduce PET
c when sublimation greater than snowpack. The difference is not put
c into pet.

c !! TT possible numerical errors with using min() then adding to snowpack !!
  if (snowpack .gt. 0.0d0) then
    snowsubl = min(pet, snowpack)
    if (snowsubl .lt. pet) then
      unmet_pet = pet - snowsubl
    else
      unmet_pet = 0.0d0
    endif
  else
    unmet_pet = pet
    snowsubl = 0.0d0
  endif

```

```

endif

c Set new values of snowpack, snowpack water, available water (melt), and
c surface water ET to previous values. Then make adjustments based on inputs.
  snowpack_new = snowpack
  snowwat_new = snowwatpack
  water2soil = 0.0d0
  surface_et = 0.0d0

c Calculate change in snowpack from precipitation
c   if cold, add to snowpack
c   if warm and a snowpack exists, add rain to watpack
c   if warm and no snowpack exists, add rain to available water (to soil)
if (pr_snow .eq. 0.0d0 .and. pr_rain .eq. 0.0d0) goto 200
if (temp .lt. crittemp) then
  snowpack_new = snowpack_new + pr_snow ! add snowfall to snowpack
else
  if (snowpack .gt. 0.0d0) then
    snowwat_new = snowwat_new + pr_rain ! add rain to snowwater
  else
    water2soil = water2soil + pr_rain ! add rain to avail water
  endif
endif
endif
200 continue

c Calculate change in snowpack from sublimation flux to atmosphere
if(snowpack_new .gt. 0.0d0) then
  diff = snowpack_new - snowsubl !was: diff = snowwat_new - snowsubl
  if (diff .ge. 0.0d0) then
    snowpack_new = snowpack_new - snowsubl
  else
    snowsubl = snowpack_new
    snowpack_new = 0.0d0
  endif
endif
endif

c Calculate change from solar radiation melt of snowpack, if a snowpack
c exists. If the potential radiation melt exceeds the snowpack, melt all
c snow and make it snowwater.
if(snowpack_new .gt. 0.0d0) then
  diff = snowpack_new - radmelt
  if (diff .ge. 0.0d0) then
    snowpack_new = snowpack_new - radmelt
    snowwat_new = snowwat_new + radmelt
  else
    snowwat_new = snowwat_new + snowpack_new
  endif
endif

```

```

        snowpack_new = 0.0d0
    endif
endif

c Take unmet PET from snowpack water, if any present
c Check: IS THIS NEEDED? DOES THIS EVER HAPPEN???
    if (unmet_pet .gt. 0.0d0 .and. snowwat_new .gt. 0.0d0) then
        diff = snowwat_new - unmet_pet

        if (diff .ge. 0.0d0) then
            snowwat_new = snowwat_new - unmet_pet
            surface_et = unmet_pet
            unmet_pet = 0.0d0
        else
            unmet_pet = abs(diff)
            surface_et = snowwat_new
            snowwat_new = 0.0d0
        endif
    endif
endif

c Calculate melt from snowpack and add to watpack * OR *
c refreeze some snowwater to solid snow.
c Note: Should this be a check of temp vs. crittemp?????
    if (temp .ge. 0.0d0) then
        snowdamming = snowadj(icovertime)
        potentmelt = snowdamming * (2.63d0 + (2.55d0 * temp)
$           + (0.0912d0 * temp * prcp))

        snowmelt = min(potentmelt, snowpack_new)
        snowpack_new = snowpack_new - snowmelt
        snowwat_new = snowwat_new + snowmelt
    else
        potentfreeze = 2.63d0 + (2.55d0 * abs(temp))
        snowfreeze = min(potentfreeze, snowwat_new)
        snowpack_new = snowpack_new + snowfreeze
        snowwat_new = snowwat_new - snowfreeze
    endif

c Compute meltwat from watpack
    meltwat = 0.0d0
    snowpackprm = snowholdfactor * snowpack_new

    if (snowwat_new .gt. snowpackprm) then
        if (meltwat_fact .eq. 0.0d0) then
            write(*,*) 'Error - - Snowwater meltwat factor = 0'
            stop
        endif
    endif

```





```

c *****
c          THIS SUBROUTINE IS AS MODIFIED IN FEBRUARY 2006
c *****

```

```

c          Finish comments . . . . .

```

```

implicit none
integer ii,iflag,i_season,i_phase,iwrite,iwetland
real*8 soilrootdepth,soilfieldcapacity,soilwiltingpoint
real*8 soilwiltingpoint2,deep_available,downwatfrac,downicefrac
real*8 infiltrationrate,rootbaseflowfactor,deepbaseflowfactor
real*8 soilmaxdepth,dailydepth,prev_depth,soil_surplus1
real*8 airtemp,depthchange,soil_transpiration,soil_pet
real*8 soil_availwater,soil_overlandR0,soil_infiltration
real*8 infiltrate_water,water2water,water2ice,rootzone_excess
real*8 soil_downflux,soil_runoff,deep_capacity,deepzone_excess
real*8 root_maxfieldcapacity,deep_maxfieldcapacity,extra
real*8 root_ice,root_water,root_prev_water,extrawater,a
real*8 root_melt,root_prev_ice,deep_prev_ice,root_waterratio
real*8 root_fieldcapacity,root_baseflow,deep_baseflow,ddiff
real*8 deep_fieldcapacity,deep_water,deep_prev_water,deep_ice
real*8 deep_melt,deep_waterratio,balance,water_in,water_out
real*8 totwatratio,root_freeze,deep_freeze,absval_depthchange
real*8 watvolumn,difference,rmissng,varjunk,rootwatchchange
real*8 infil_watfrac,infil_icefrac,infiltrate_watratio,wat2wetland
real*8 infiltrate_factor,fraction,wetlandstoreprev,wetlandstore
real*8 potential_infiltration,wat2surfacezone
real*8 vartmp1,vartmp2,vartmp3,vartmp4,vartmp5,vartmp6,vartmp7
real*8 vartmp8,vartmp9,rootbaseflowfactor2,deepbaseflowfactor2
parameter (rmissng=-9999.0d0)

```

```

c      root_prev_ice = 200.0d0
c      root_prev_water = 0.0d0
c      soilrootdepth = 200.0d0
c      soilmaxdepth = 600.0d0
c      deep_prev_water = 0.0d0
c      deep_prev_ice = 400.0d0
c      prev_depth = 40.0d0
c      dailydepth = 5.0d0
c      soil_availwater = 0.0d0

```

```

rootwatchchange = 0.0d0
vartmp1 = 0.0d0
vartmp2 = 0.0d0
vartmp3 = 0.0d0

```

```

    vartmp4 = 0.0d0
    vartmp5 = 0.0d0
    vartmp6 = 0.0d0
    vartmp7 = 0.0d0
    vartmp8 = 0.0d0
    vartmp9 = 0.0d0

c          Set some stuff
    ddiff = 0.0d0
    soil_surplus1 = 0.0d0
    rootzone_excess = 0.0d0
    deepzone_excess = 0.0d0
    soil_overlandR0 = 0.0d0
    rootbaseflowfactor2 = rootbaseflowfactor ! dummy local variable
    deepbaseflowfactor2 = deepbaseflowfactor ! dummy local variable

c Determine the thawdepth change from previous day. Can be a negative change
    depthchange = dailydepth - prev_depth

c Calculate field capacity in [mm]. Soilmaxdepth and rootdepth are
c input to subroutine in units of WATER EQUIVALENT DEPTH.

    deep_capacity = max((soilmaxdepth - soilrootdepth), 0.0d0)
    root_maxfieldcapacity = soilrootdepth * soilfieldcapacity
    deep_maxfieldcapacity =
$         max(deep_capacity * soilfieldcapacity, 0.0d0)

c     if (iwrite .eq. 1) write(*,*) i_season, i_phase
C     stop

    water_in = root_prev_water + root_prev_ice + deep_prev_water +
$     deep_prev_ice + wetlandstoreprev + soil_availwater

c *****
c
c Frozen Soil/Unfrozen Soil Calculations
c WHY HAVE INFILTRATION IF LAYER IS FROZEN ???

c Set initial infiltration to lesser of max infiltration rate or the available
c water, provided AIR TEMPERATURE is positive. If it's negative, there's
c no infiltration and only overland runoff (done above)
c Will not allow any infiltration to exceed thawdepth in later checks.
c Overland runoff is excess over max infiltration rate, if any excess.
c (Don't use AvailWater after this - it becomes Infiltration)

    if (root_prev_water .eq. 0.0d0.and.root_prev_ice.eq.0.0d0) then

```

```

        infiltrate_watratio = 0.0d0
c      print*, 'ERROR: Root water and ice equals zero'
c      stop
    else
        infiltrate_watratio = root_prev_water / (root_prev_water +
$      root_prev_ice)
    endif

c This section handles the infiltration into the soil. It also treats
c the wetland storage, if grid has wetland designation. Need to be sure
c of logic for infiltration if a wetland. Same as other grids???
c Double infiltration potential rate if a wetland grid????
c      if (iwetland .eq. 1) infiltrationrate = infiltrationrate * 2.0d0
        infiltrate_factor = min(0.5d0 + infiltrate_watratio, 1.0d0)
        potential_infiltration = min(soil_availwater, ! infiltrate potent same
$      infiltrationrate*infiltrate_factor) ! for wetland and non-wetland

        wat2surfacezone = soil_availwater
        if (iwetland .eq. 0) then                ! *** not a wetland cell ***

            soil_overlandRO = ! drain the surface zone at non-wetland grid
$            max((wat2surfacezone - potential_infiltration), 0.0d0)
            wetlandstore = wetlandstoreprev

        else ! wetlandstore is the same as overlandRO for non-wetland cell
            wetlandstore = wetlandstoreprev + wat2surfacezone
            if (wetlandstore .gt. 1000.0d0) then
                soil_overlandRO = wetlandstore - 1000.0d0
                wetlandstore = 1000.0d0
            endif
c      wat2wetland = max((soil_availwater - potential_infiltration),
c      $                0.0d0)

        endif

        root_melt = 0.0d0
        deep_melt = 0.0d0
        root_freeze = 0.0d0
        deep_freeze = 0.0d0
C Melt ice or freeze water.
        ii = 0
        absval_depthchange = abs(depthchange)
c This next block melts ice.
        if (i_phase .eq. 1 .and. depthchange .gt. 0.0d0 .or.
$      i_phase .eq. 0 .and. depthchange .lt. 0.0d0) then

```

```

ii=ii+1
if (root_prev_ice .gt. 0.0d0) then
  totwatratio = (root_prev_ice + root_prev_water) /
  $      soilrootdepth
  root_melt = min(totwatratio * absval_depthchange,
  $      root_prev_ice)
  if (dailydepth .ge. soilrootdepth.and.i_phase.eq. 1) then
    root_melt = root_prev_ice
  endif
  root_water = root_prev_water + root_melt
  root_ice = root_prev_ice - root_melt
  deep_water = deep_prev_water
  deep_ice = deep_prev_ice
c      if(iwrite.eq.1) write(97,112) 'Rootmelt = ', root_melt
else
  totwatratio = (deep_prev_ice + deep_prev_water) /
  $      deep_capacity
  deep_melt = min(totwatratio * absval_depthchange,
  $      deep_prev_ice)
  if (dailydepth .ge. soilmaxdepth.and.i_phase.eq.1) then
    deep_melt = deep_prev_ice
  endif
  root_water = root_prev_water
  root_ice = root_prev_ice
  deep_water = deep_prev_water + deep_melt
  deep_ice = deep_prev_ice - deep_melt
c      if(iwrite.eq.1) write(97,112) 'Deepmelt = ', deep_melt
endif
c This block freezes water.
  else if (i_phase .eq. 1 .and. depthchange .lt. 0.0d0 .or.
  $      i_phase .eq. 0 .and. depthchange .gt. 0.0d0) then
    ii=ii+1
    if (root_prev_water .gt. 0.0d0) then
      totwatratio = (root_prev_ice + root_prev_water) /
      $      soilrootdepth
      root_freeze = min(totwatratio * absval_depthchange,
      $      root_prev_water)
      if (dailydepth .ge. soilrootdepth.and.i_phase.eq. 0) then
        root_freeze = root_prev_water
      endif
c      if(iwrite.eq.1) write(97,'(3f20.16)') totwatratio *
c      $      absval_depthchange, root_prev_water, root_freeze
      root_water = root_prev_water - root_freeze
      root_ice = root_prev_ice + root_freeze
      deep_water = deep_prev_water
      deep_ice = deep_prev_ice

```

```

c          if(iwrite.eq.1)write(97,112)'Rootfreeze = ',root_freeze
else
    totwatratio = (deep_prev_ice + deep_prev_water) /
$         deep_capacity
    deep_freeze = min(totwatratio * absval_depthchange,
$         deep_prev_water)
    if (dailydepth .ge. soilmaxdepth.and.i_phase.eq. 0) then
        deep_freeze = deep_prev_water
    endif
    root_water = root_prev_water
    root_ice = root_prev_ice
    deep_water = deep_prev_water - deep_freeze
    deep_ice = deep_prev_ice + deep_freeze
c          if(iwrite.eq.1)write(97,*) deep_prev_ice,deep_prev_water,
c $          totwatratio, deep_freeze, deep_water, deep_ice
    endif
c          if(iwrite.eq.1) write(97,112) 'Deepfreeze = ', deep_freeze
else if (depthchange .eq. 0.0d0) then
    ii=ii+1
    totwatratio = 0.0d0
    root_melt = 0.0d0
    root_freeze = 0.0d0
    root_water = root_prev_water
    root_ice = root_prev_ice
    deep_freeze = 0.0d0
    deep_melt = 0.0d0
    deep_water = deep_prev_water
    deep_ice = deep_prev_ice
endif
if (ii .ne. 1) then
    print*, ii, depthchange, i_phase, dailydepth, prev_depth
    stop 'If checks not executed or executed > 1'
endif

vartmp1=root_water+root_ice+deep_water+deep_ice
if(iwrite.eq.1) write(97,112) 'Totwater after frz/melt =',
$     vartmp1
if(iwrite.eq.2) then
    vartmp1 = root_melt
    rootwchange = rootwchange + root_melt
endif

c Calculate ratio of water and ice
c root_waterratio = depth of thawed soil / total root depth
c root_waterratio not currently used.
c     call bound (0.0d0, (dailydepth / soilrootdepth), 1.0d0,

```

```

c      $          root_waterratio)

c          ***** INFILTRATION INTO SOIL *****
c
c Old way.
c      infiltrate_water = potential_infiltration *
c      $          (1.0d0 - (root_ice / soilrootdepth))
c      water2water = min(dailydepth,infiltrate_water)
c      water2ice = potential_infiltration - water2water
c      root_water = root_water + water2water
c      root_ice = root_ice + water2ice

c New way. Put some infiltration to liquid water and some to ice based
c on current amounts of liquid water and ice.
c If root water and root ice are both zero, put half of infiltration to each.
c      write(*,'(2f16.10)')root_water,root_ice
c      if ((root_water + root_ice) .eq. 0.0d0) then
c          infil_watfrac = 0.5d0
c      else
c          infil_watfrac = (root_water / (root_water + root_ice))
c      endif

c      if (iwetland .eq. 0) then

c          root_water = root_water + potential_infiltration*infil_watfrac
c          infil_icefrac = 1.0d0 - infil_watfrac
c          root_ice = root_ice + potential_infiltration * infil_icefrac
c      else
c          root_water = root_water + potential_infiltration*infil_watfrac
c          wetlandstore = wetlandstore -
c          $          potential_infiltration*infil_watfrac
c          infil_icefrac = 1.0d0 - infil_watfrac
c          root_ice = root_ice + potential_infiltration * infil_icefrac
c          wetlandstore = wetlandstore -
c          $          potential_infiltration*infil_icefrac
c      endif

c      $
c      write(*,'(4f16.10)')infil_watfrac,root_water,infil_icefrac,
c      $          root_ice

c      if(iwrite.eq.2) then
c          vartmp2 = water2water
c          rootwatchange = rootwatchange + water2water
c      endif

```

```

    if (iwrite.eq.1) then
      write(97,112) 'Infil as F(ice/rootdepth)=',
    $           potential_infiltration * infil_watfrac
      write(97,112) 'Root water (after infilt.) =', root_water
      write(97,112) 'Root ice (after infilt.) =', root_ice
    endif

c  Ensure that root ice does not exceed root depth. This can occur by way of
c  the section above that partitions infiltration to liquid and frozen parts.
    if (root_ice .gt. soilrootdepth) then
      soil_surplus1 = soil_surplus1 + (root_ice - soilrootdepth)
      root_ice = soilrootdepth
c      write(97,*) soil_surplus1, root_ice, soilrootdepth
      soil_surplus1 = soil_surplus1 + (root_ice - soilrootdepth)
c      write(97,112) 'root_ice > soilrootdepth', soil_surplus1 !remove after
    endif

c          ***** FLUX FROM ROOT ZONE TO DEEP SOIL *****
c  Calculate root to deep water flux, No flux if ice present.
c  TEST THE BOUND FUNCTION HERE !!!
c  Add code to restrict amount going to deep by capacity.
c  if (root_ice .gt. 0.0d0 .or. deep_capacity .eq. 0.0d0) then
    if (deep_capacity .eq. 0.0d0 .or. root_ice .gt. 0.0d0) then
      soil_downflux = 0.0d0
    else
      soil_downflux = max(0.0d0,
    $      (root_water - root_maxfieldcapacity) * rootbaseflowfactor2)
      call bound(0.0d0,deep_capacity-deep_prev_water-
    $      deep_prev_ice,soil_downflux,soil_downflux)
c      if (iwrite .eq. 1)print*,soil_downflux,deep_water, deep_ice,
c      $      deep_capacity
    endif

c  Drain root Zone into deep Soil. The next 4 lines are old way.
c  deep_water = deep_water + soil_downflux * deep_waterratio
c      deep_water = max(deep_water, 0.0d0)
c  deep_ice = deep_ice + soil_downflux * (1.0d0 - deep_waterratio)
c      deep_ice = max(deep_ice, 0.0d0)

c  New way. Put a fraction of downflux to water and some to ice based on
c  proportion of water and ice at this time.
    if (deep_water .eq. 0.0d0 .and. deep_ice .eq. 0.0d0) then
      downwatfrac = soil_downflux * 0.5d0
      downnicefrac = soil_downflux - downwatfrac

```

```

else if (deep_water .eq. 0.0d0) then      ! was no water...all downflux
    downwatfrac = 0.0d0                  ! goes to ice
    downnicefrac = soil_downflux
else if (deep_ice .eq. 0.0d0) then      ! was no ice...all downflux
    downwatfrac = soil_downflux          ! goes to water
    downnicefrac = 0.0d0
else
    downwatfrac = soil_downflux *
$      (deep_water / (deep_water + deep_ice))
    downnicefrac = soil_downflux *
$      (deep_ice / (deep_water + deep_ice))
endif
if(iwrite.eq.1) write(97,112) 'Down Water Frac = ', downwatfrac
if(iwrite.eq.1) write(97,112) 'Down Ice Frac = ', downnicefrac
deep_water = deep_water + downwatfrac
deep_ice = deep_ice + downnicefrac

c Pull the soil "downflux" from root zone.
root_water = root_water - (downwatfrac + downnicefrac)
vartmp8=root_water+root_ice+deep_water+deep_ice
if(iwrite.eq.1) then
    write(97,112) 'Deep water (after downflux) = ', deep_water
    write(97,112) 'Deep ice (after downflux) = ', deep_ice
    write(97,112) 'Soil down flux = ', soil_downflux
    write(97,112) 'Total water after downflux = ', vartmp8
endif

c          ***** SOIL TRANSPIRATION FROM ROOT ZONE *****
c Up to this point PET has had sublimation removed, now remove
c transpiration from root zone water, up to the wilting point.
    soilwiltingpoint2 = max((soilrootdepth - root_ice), 0.0d0)
$      * soilwiltingpoint

c Define field capacity in mm, and water amount above field capacity.
    root_fieldcapacity = max((soilrootdepth - root_ice)
$      * soilfieldcapacity, 0.0d0)
    extrawater = root_water - root_fieldcapacity

if(iwrite.eq.1) then
c    print*, 'here'
    write(98,*) ' '
    write(98,*) 'Field capacity = ', root_fieldcapacity
    write(98,*) 'Wilting point = ', soilwiltingpoint2
    write(98,*) 'Root depth (space) = ', soilrootdepth
    write(98,*) 'Root ice = ', root_ice
    write(98,*) 'Root water = ', root_water

```



```

        write(98,*) 'Root_water - field_capacity = ', extrawater
        write(98,*) 'PET = ', soil_pet
        write(98,*) 'Air Temp = ', airtemp
        write(98,*) 'Wetland storage = ', wetlandstore
    endif

c Handle evapotranspiration. Need to finalize logic.
c Currently not taking ET from the wetland storage, instead just allowing
c PET from the soil
c     **** Check if ET for wetland is OK if PET is zero ****
c
c This block, commented out, will allow evap from the wetland storage zone.
c     if (iwetland .eq. 1 .and. wetlandstore .ge. soil_pet) then
c         soil_transpiration = soil_pet
c         wetlandstore = wetlandstore - soil_transpiration
c         ii=ii+1
c         goto 200
c     else if (iwetland .eq. 1 .and. wetlandstore .gt. 0.0d0) then
c         soil_transpiration = soil_pet      ! is this OK if PET is zero???
c         wetlandstore = wetlandstore - soil_transpiration
c         ii=ii+1
c         goto 200
c     endif
c     ii=0
c     if (airtemp .le. 0.0d0 .or. root_water .le. soilwiltingpoint2 .or.
$     soilwiltingpoint2 .lt. 1.0d-2 .or. root_fieldcapacity .lt.
$     1.0d-2 )then      !checks for wiltpt and fieldcapac added July06
        soil_transpiration = 0.0d0 ! to handle when ice fills porespace
        ii=ii+1
    else
        if (extrawater .ge. soil_pet .or. iwetland .eq. 1) then
            soil_transpiration = soil_pet      ! rootwater is above FC
            ii=ii+1                            ! or grid is a wetland
        else
            ! allow ET at PET rate
            if (root_fieldcapacity .gt. 0.0d0) then
c                 a = dlog(root_fieldcapacity) /
c                 $     (1.1282d0 * root_fieldcapacity) ** 1.2756d0
c                 a = max(a,0.0d0)
                fraction = ((root_water - soilwiltingpoint2) /
$                 (root_fieldcapacity - soilwiltingpoint2))
                if (fraction .gt. 1.0d0) then
                    soil_transpiration = extrawater
                else
                    soil_transpiration = soil_pet * fraction
                    if (soil_transpiration .gt. root_water)

```

```

$           soil_transpiration = max(root_water,soilwiltingpoint2)
           endif
           else
             a = 0.0d0
             soil_transpiration = 0.0d0
           endif
           soil_transpiration = max(soil_transpiration, 0.0d0)

           ii=ii+1
           endif
         endif
       if (ii .ne. 1) stop 'If checks not executed or executed > 1'

c Pull transpiration amount from root water (if air temp > 0).
c Restrict transpiration to interval 0 < transpiration < root_water
c This block is skipped if grid is wetland
       call bound (0.0d0, soil_transpiration, root_water,
$           soil_transpiration)
c       if(iwrite.eq.1) write(98,*) soil_transpiration, root_water
       if (soil_transpiration .gt. root_water) stop 'ET > rootwat' !moved here
       root_water = root_water - soil_transpiration           ! Jul06

200 continue
       if(iwrite.eq.2) then
         vartmp6 = soil_transpiration
         rootwatchange = rootwatchange - soil_transpiration
       endif
       vartmp8=root_water+root_ice+deep_water+deep_ice+soil_transpiration

       if(iwrite.eq.1) then
         write(97,112) 'Soil PET = ', soil_pet
         write(97,112) 'Soil wiltingpoint = ', soilwiltingpoint2
         write(97,112) 'Soil transpiration = ', soil_transpiration
         write(97,112) 'Total water after transpiration = ',vartmp8
       endif

c Thawdepth exceeds soilmaxdepth often. Check why we need soilmaxdepth???
       if (dailydepth .ge. soilmaxdepth) then
         if (i_phase .eq. 1) then
c           print*, 'WARNING ### Thaw depth exceeds soilmaxdepth'
           deep_water = deep_water + deep_ice
           deep_ice = 0.0d0
         else if (i_phase .eq. 0) then
           deep_ice = deep_ice + deep_water
           deep_water = 0.0d0
         else

```

```

        print*, 'ERROR: PHASE IN SOIL ROUTINE IS NOT 0 OR 1'
        stop
    endif
endif

c Here, if root water plus ice exceeds rootdepth, make adjustments.
c Excess in rootzone will be computed as negative. Take the negative
c of it and subtract from root water or ice.

    if(iwrite.eq.2) then
        vartmp7 = soil_downflux
        rootwatchchange = rootwatchchange - soil_downflux
    endif
c    write(97,*) soilrootdepth - root_water - root_ice
    rootzone_excess = min(0.0d0,soilrootdepth-root_water-root_ice)
    if (rootzone_excess .lt. 0.0d0)
$       rootzone_excess = (-1.0d0) * rootzone_excess
        ! the next check occurs often???
c    if (soil_surplus .ne. 0.0d0) print*, 'NOTE: surplus > 0'

    if (rootzone_excess .gt. 0.0d0) then
        if(rootzone_excess.gt.20.0d0) then
            write(*,*) 'Zonewat excess(>20mm) = ', rootzone_excess
        endif
        if(rootzone_excess.gt.40.0d0) print*,'* Soil excess > 40mm *'
        if (root_ice .gt. root_water) then
            root_ice = root_ice - rootzone_excess
        else
            root_water = root_water - rootzone_excess
            if(iwrite.eq.2) then
                vartmp8 = rootzone_excess
                rootwatchchange = rootwatchchange - rootzone_excess
            endif
        endif
    endif
endif

    if(iwrite.eq.1) then
        write(97,112)'Rootzone excess = ', rootzone_excess
    endif

c Adjustments for deepzone excess
    deepzone_excess=min(0.0d0,deep_capacity-deep_water-deep_ice)
    if (deepzone_excess .lt. 0.0d0)
$       deepzone_excess = (-1.0d0) * deepzone_excess

    if (deepzone_excess .gt. 0.0d0) then

```

```

    if (deep_ice .gt. deep_capacity .and. deep_water .gt.
$      deep_capacity) then
      print*, 'Warning: Deepwat&deepice>capacity', deepzone_excess
      deep_ice = deep_capacity
      deep_water = 0.0d0
    else if (deep_ice .gt. deep_capacity) then
      print*, 'Warning: Deep ice > capacity', deepzone_excess
      deep_ice = deep_capacity
      deep_water = 0.0d0
    else if (deep_water .gt. deep_capacity) then
      print*, 'Warning: Deep water > capacity', deepzone_excess
      deep_water = deep_capacity
      deep_ice = 0.0d0
    else
      extra = deep_ice - deepzone_excess
      if (deep_ice - deepzone_excess .gt. 0.0d0) then
        deep_ice = deep_ice - deepzone_excess
      else
        extra = deep_water - deepzone_excess
        deep_water = deep_water - deepzone_excess
      endif
    endif
  endif
  if(iwrite.eq.1)write(97,112)'Deepzone excess = ',deepzone_excess

  root_fieldcapacity = max((soilrootdepth - root_ice)
$    * soilfieldcapacity, 0.0d0)
  deep_fieldcapacity = max((soilmaxdepth - soilrootdepth
$    - deep_ice) * soilfieldcapacity, 0.0d0)

c    TTT add reduction 'a' as per Vorosmarty article
c    BaseFlowFactor is multiplied by water less the current fieldcapacity
c  If grid is wetland, halve the base flow factors.
    if (iwetland .eq. 1) then
      rootbaseflowfactor2 = rootbaseflowfactor * 0.5d0
      deepbaseflowfactor2 = deepbaseflowfactor * 0.5d0
    endif
    root_baseflow = rootbaseflowfactor2
$    * max(0.0d0, root_water - root_fieldcapacity)
    deep_baseflow = deepbaseflowfactor2
$    * max(0.0d0, deep_water - deep_fieldcapacity)

c  Update water levels after baseflow
c    print*, root_water
    root_water = root_water - root_baseflow

```

```

        deep_water = deep_water - deep_baseflow
c      if (iwrite .eq. 1) print*, deep_baseflow, ddiff, deep_water
        if(iwrite.eq.2) then
            vartmp9 = root_baseflow
            rootwatchchange = rootwatchchange - root_baseflow
        endif

c      Don't forget the difference from above
        deep_baseflow = deep_baseflow + deepzone_excess

c      Finally, move any deep water or ice to surplus if deep capacity is 0mm.
c      Can't have any deep water/ice if there is no deep zone....
        if (deep_capacity .eq. 0.0d0) then
            rootzone_excess = rootzone_excess + deep_water + deep_ice
            deep_water = 0.0d0
            deep_ice = 0.0d0
c      print*, deep_capacity, deep_water, deep_ice, soil_surplus
        endif

        if(iwrite.eq.1) then
            write(97,112) 'Overland runoff = ', soil_overlandRO
            write(97,112) 'Soil infiltration = ', potential_infiltration
            write(97,112) 'Soil surplus1 = ', soil_surplus1
            write(97,112) 'Root baseflow = ', root_baseflow
            write(97,112) 'Root wat(after baseflow = ', root_water
            write(97,112) 'Root ice = ', root_ice
            write(97,112) 'Deep baseflow = ',deep_baseflow
            write(97,112) 'Deep wat(after baseflow = ', deep_water
            write(97,112) 'Deep ice = ', deep_ice
            write(97,112) 'Wetland storage = ', wetlandstore
            write(97,*) ' '
        endif

100  soil_runoff = soil_surplus1 + rootzone_excess +
$      soil_overlandRO + root_baseflow + deep_baseflow
water_out = root_water + root_ice + deep_water + deep_ice
$      + wetlandstore + soil_runoff + soil_transpiration
        if (abs(water_in - water_out) .gt. 1.0d-8) then
            print*, 'Water Balance not Maintained in SoilZone routine'
            write(*,*) 'Total input water = ', water_in
            write(*,*) 'Total output water = ', water_out
            write(*,*) 'Root Water = ', root_water
            write(*,*) 'Root Ice = ', root_ice
            write(*,*) 'Deep Water = ', deep_water
            write(*,*) 'Deep Ice = ', deep_ice
            write(*,*) 'Wetlandstore = ', wetlandstore

```



```

runoff_volume = (extra_rivwat + runoff) * kilometer_per_mm * area
tot_water = rivwat_prev + runoff_volume + watupstrm

if (tot_water .gt. 0.0d0) then
  wat2nextgrid = fraction2nextgrid * tot_water
  rivwat_new = tot_water - wat2nextgrid
else
  rivwat_new = rivwat_prev
  wat2nextgrid = 0.0d0
endif

rivwat_change = rivwat_new - rivwat_prev
outwat = rivwat_new + wat2nextgrid

if (outwat .ne. tot_water) then
  write(*,'(a,f14.10)') 'Upstream input = ', watupstrm
  write(*,'(a,f14.10)') 'Previous river water = ', rivwat_prev
  write(*,'(a,f14.10)') 'Extra river water = ', extra_rivwat
  write(*,'(a,f14.10)') 'Runoff input = ', runoff
  write(*,'(a,f14.10)') 'Flux downstream out = ', wat2nextgrid
  write(*,'(a,f14.10)') 'New river water = ', rivwat_new
  write(*,*) 'Water balance failed inside river routine'
  stop
endif

return
end

```

```

real*8 function snowadj(icover)

```

```

c
c Function to return value for snow damming coefficient. This
c coefficient varies with cover type. Cover type is an integer for
c one of the following:

```

c	Cover	Type
c	1	Ice
c	2	Polar Desert
c	3	Tundra
c	4	Forest-Tundra
c	5	Taiga/Boreal
c	6	Grassland/Steppe/Shrubland
c	7	Wetland ----- discontinued -----
c	8	Deciduous/Mixed Forest
c	9	Non-Arctic ----- discontinued -----
c	10	Lakes/Seas













```

real*8 term1,term2,term3,term4,terms,rootterm
real*8 soil_watvolume2
data r_nfactor /0.8d0,0.8d0,0.8d0,0.8d0,0.8d0,0.8d0,
$           0.8d0,0.8d0,1.0d0,1.0d0/
parameter(secperday = 86400.0d0, latentheat = 7.974474d4)
parameter(peatporosity = 0.92d0)

soil_watvolume2 = 1.0d0    ! set water content in denominator of eq. to 1

conduct_ratio = soil_conductivity / peat_conductivity
peatdepth = soil_carbon / 1000.0d0    ! convert depth in mm to meters

c If Ts (daily air temperature) is > 0C, set thaw_depth to previous plus
c value from Stephan solution. If Ts < 0C, thaw_depth is previous minus
c Stephan solution. If Ts=0C, set thaw_depth = previous
c Converting thawdepth in meters to mm.

if (ts .ge. 0.0d0) then
  if (depth_prev .gt. soil_carbon) then
    term1 = peatdepth * (1.0d0 - conduct_ratio)
    term2 = (peatdepth * conduct_ratio) ** 2.0d0
    term3 = (peatdepth**2.0d0) * conduct_ratio *
$         ((soil_watvolume2 * 1000.0d0 * peatporosity) /
$         (soil_watvolume2 * 1000.0d0 * porosity))
    term4 = 2.0d0 * r_nfactor(ivegcov) * ts * secperday /
$         (latentheat * (soil_watvolume2 * 1000.0d0 * porosity) /
$         soil_conductivity)
    terms = term2 - (term3 - term4)
    if (terms .lt. 1.0d-6) terms = 1.0d-6
    rootterm = sqrt(terms)
    if (iwrite .eq. 1) then
      write(93,*)peatdepth,conduct_ratio,porosity,peatporosity,
$         soil_watvolume2,soil_conductivity
      write(93,*)'below peat',term1,term2,term3,term4,rootterm,
$         (term3 - term4), term2 - (term3 - term4)
    endif
    stephandepth = (term1 + rootterm) * 1000.0d0
    if (porosity .eq. 0.0d0) stephandepth = 0.0d0
    if (stephandepth .lt. 0.0d0) then
c      print*, 'Warning: Calculated Stephan Depth < 0'
      stephandepth = 0.0d0
c      write(99,*) 'Thawdepth < 0 in two-layer solution'
    endif
  else
    term1 = 2.0d0 * r_nfactor(ivegcov) * peat_conductivity
$         * secperday * ts

```











```

c 2-broadleaf forest
c 3-savannah
c 4-grassland
c 5-tundra/non-forested wetlands
c 6-cultivated
c 7-desert
c 8-water

c New UAF Vegetation

c 1      Black Spruce
c 2      Coastal Forest
c 3      Deciduous Forest
c 4      Tundra
c 5      White Spruce

c Mapping UAF into the parameters defined for WBM classes.

c UAF -> WBM class
c 1 -> 1
c 2 -> 1
c 3 -> 2
c 4 -> 5
c 5 -> 1

      if (iveg .eq. 1 .or. iveg .eq. 2 .or. iveg .eq. 5) inewveg = 1
      if (iveg .eq. 3) inewveg = 2
      if (iveg .eq. 4) inewveg = 5

      if (iveg .gt. 5) stop 'Vegetation designation > 5'

c*****

      ALB = ALB1(inewveg)
      ALBEDO = ALBEDO1(inewveg)
      CR = CR1(inewveg)
      HEIGHT = HEIGHT1(inewveg)
      LPMAX = LPMAX1(inewveg)
      GLMAX = GLMAX1(inewveg)
      R5 = R51(inewveg)
      CVPD = CVPD1(inewveg)
      LWIDTH = LWIDTH1(inewveg)
      ZOG = ZOG1(inewveg)
      RSS = RSS1(inewveg)
      FETCH = FETCH1(inewveg)
      ZW = ZW1(inewveg)

```



```

INTRINSIC SQRT, EXP
C
SIGMA = 5.67E-08
C
Brutsaert method
EFFEM = 1.24 * (EA * 10. / (TA + 273.15)) ** (1. / 7.)
C
additional methods not used
C
Brunt method
C
    BRUNTA Brunt intercept
C
    BRUNTB Brunt EA coefficient, for kPa (value for mb * 10)
C
BRUNTA = .44
C
BRUNTB = .253
C
EFFEM = BRUNTA + BRUNTB * SQRT(EA)
C
Satterlund method
C
EFFEM = 1.08 * (1 - EXP(-(10. * EA) ** ((TA + 273.15) / 2016.)))
C
Swinbank method
C
EFFEM = .0000092 * (TA + 273.15) ** 2.
C
Idso-Jackson method
C
EFFEM = 1. - .261 * EXP(-.000777 * TA ** 2.)
C
C
NOVERN = (RATIO - C1) / C2
IF (NOVERN .GT. 1.) NOVERN = 1.
IF (NOVERN .LT. 0.) NOVERN = 0.
CLDCOR = C3 + (1. - C3) * NOVERN
NETLONGF = (EFFEM - 1.) * CLDCOR * SIGMA * (TA + 273.15) ** 4

c
print*, 'here 1b', TA, EA, SIGMA, EFFEM
c
print*, 'here 2b', RATIO, C1, C2, C3
c
print*, 'here 3b', NOVERN, CLDCOR, NETLONGF

END
REAL FUNCTION PMF (AA, DD, DELTA, RA, RC)
C
Penman-Monteith evapotranspiration, W/m2
C
input
C
    AA      net energy input, Rn - S, W/m2
C
    DD      vapor pressure deficit, kPa
C
    DELTA   dEsat/dTair, kPa/K
C
    RA      boundary layer resistance, s/m
C
    RC      canopy resistance, s/m
C
local constants
C
    GAMMA   psychrometric constant, kPa/K
C
    CPRHO   volumetric heat capacity of air, J/(K m3)
C
IMPLICIT NONE
REAL AA, DD, DELTA, RA, RC, GAMMA, CPRHO
C

```

```

GAMMA = .067
CPRHO = 1240
PMF = (DELTA * AA + CPRHO * DD / RA) /
*      (DELTA + GAMMA + GAMMA * RC / RA)
END
REAL FUNCTION SRSCF (RAD, TMIN, DD, LAI, SAI, R5, CVPD, RM,
*                  CR, GLMAX, GLMIN)
C      canopy surface resistance, RSC, s/m
C      after Shuttleworth and Gurney (1990) and Stewart (1988)
C      input
C      RS      solar radiation on canopy, W/m2
C      TMIN    minimum air temperature for the day, degC
C      DD      vapor pressure deficit, kPa
C      LAI     projected leaf area index
C      SAI     projected stem area index
C      R5      solar radiation at which conductance is halved, W/m2
C      CVPD    vpd at which conductance is halved, kPa
C      RM      maximum solar radiation, at which FR = 1, W/m2
C      CR      light extinction coefficient for projected LAI
C      GLMAX   maximum leaf surface conductance for all sides of leaf, m/s
C      GLMIN   cuticular leaf surface conductance for all sides of leaf, m/s
C      local
C      FS      correction for stem area
C      RO      a light response parameter
C      FRINT   integral of fR dL over Lp
C      FD      dependence of leaf conductance on vpd, 0 to 1
C      FT      dependence of leaf conductance on temperature, 0 to 1
C      GSC     canopy conductance, m/s
      IMPLICIT NONE
      REAL RAD, TMIN, DD, LAI, SAI, R5, CVPD, RM, CR, GLMAX,
*      GLMIN, FS, RO, FRINT, FD, FT, GSC
      REAL MAX, EXP, LOG
C      INTRINSIC MAX, EXP, LOG - FBM SGI did not like
C
C      solar radiation limitation integrated down through canopy
C      Stewart (1988) and Saugier and Katerji (1991)
      FS = (LAI + SAI) / LAI
      IF (RAD .LE. 1E-10) THEN
        FRINT = 0
      ELSE
        RO = RM * R5 / (RM - 2 * R5)
        FRINT = ((RM + RO) / (RM * CR * FS)) *
*              LOG((RO + CR * RAD) /
*              (RO + CR * RAD * EXP(-CR * FS * LAI)))
      END IF

```





```

CCCCCCCCCCCCCCCCCCCCCCCCCCCCCCCCCCCCCCCCCCCCCCCCCCCCCCCCCCCC
CCCCCCCCCCCCCCCCCCCCCCCCCCCCCCCCCCCCCCCCCCCCCCCCCCCCCCCCCCCC
CCCCCCCCCCCCCCCCCCCCCCCCCCCCCCCCCCCCCCCCCCCCCCCCCCCCCCCCCCCC

```

```

SUBROUTINE ROUGHF (CZS, CZR, HS, HR, LPC, CS, LAI, SAI, HEIGHT,
*                ZOG, ZO, DISP, ZOC, DISPC)
C  roughness parameter and zero-plane displacement
C  input
C    LAI    projected leaf area index
C    SAI    projected stem area index
C    LPC    projected leaf area index for closed canopy
C    CZS    ratio of roughness to height for smooth closed canopies
C    CZR    ratio of roughness to height for rough closed canopies
C    HR     height above which CZR applies, m
C    HS     height below which CZS applies, m
C    HEIGHT canopy height, m
C    ZOG    ground surface roughness, m
C  output
C    ZO     roughness parameter, m
C    DISP   zero-plane displacement, m
C    ZOC    roughness length for closed canopy, m
C    DISPC  zero-plane displacement for closed canopy, m
C  local
C    XX, CDRAG
IMPLICIT NONE
REAL CS,LAI, SAI, LPC, CZS, CZR, HR, HS, HEIGHT, ZOG
REAL ZO, DISP, ZOC, DISPC
REAL XX, CDRAG
REAL MIN, EXP, LOG
C    INTRINSIC MIN, EXP, LOG - FBM SGI did not like
C
IF (HEIGHT .GE. HR) THEN
    ZOC = CZR * HEIGHT
ELSE IF (HEIGHT .LE. HS) THEN
    ZOC = CZS * HEIGHT
ELSE
    ZOC = CZS * HS + (CZR * HR - CZS * HS) *
*    (HEIGHT - HS) / (HR - HS)
END IF

C  Limit ZOC to ZOG 2001-05-23 Tony and FBM
IF (ZOC .LT. ZOG) THEN
    ZOC = ZOG
END IF

DISPC = HEIGHT - ZOC / .3

```





```

c      write(96,*) 'here 1', RADnet,EA,TA,CB,CA,EFFEM,RNETLONGCLEAR
c      write(96,*) C1,C2,C3
c      write(96,*) 10. * EA / ( TA + 273.15),
c      $          (10. * EA / ( TA + 273.15)) ** (0.14285714)
c      write(96,*) 'here 2', 1., ALBEDO, RNETLONGCLEAR, RIOHDAY2
c      write(96,*) 'here 3', RADnet2 - CA * RNETLONGCLEAR
c      write(96,*) 'here 4',((1. - ALBEDO) +
c      $          CB * RNETLONGCLEAR / RIOHDAY2)
c      write(96,*) SOLRAD

c      write(*,*) 'CB = ', CB
c      write(*,*) 'CA = ', CA
c      write(*,*) 'IOHDAY2 = ', RIOHDAY2
c      write(*,*) 'SIGMA = ', SIGMA
c      write(*,*) 'EFFEM = ', EFFEM
c      write(*,*) 'ALBEDO = ', ALBEDO
c      write(*,*) 'RNETLONGCLEAR = ', RNETLONGCLEAR
c      write(*,*) 'SOLRAD (W/m2) = ', SOLRAD
c      write(*,*) ' '
c      endif

return
end

REAL FUNCTION PMDAYF(DOY,LATD,LONGD,iveg,LAI,SNOW,FL,UW,
$          RADNET,TA,EA,SHEAT,TMAX,TMIN,iflag)
C      daily Penman-Monteith PE in mm for day
C      local
C      ALBEDO  albedo
C      DAYLEN  daylength in fraction of day
C      DISP    zero-plane displacement, m
C      DISPC   zero-plane displacement for closed canopy, m
C      IOHDAY  daily potential insolation on horizontal, MJ/m2
C      LAI     projected leaf area index
C      LAT     latitude, radians, south negative
C      SAI     projected stem area index
C      UA      average wind speed for the day, m/s
C      ZA      reference height, m
C      ZO      surface roughness parameter, m
C      ZOC     surface roughness parameter for closed canopy, m
C      SOLNET  average net solar radiation for daytime, W/m2
C      LNGNET  average net longwave radiation for day,-* W/m2
C      AA      available energy, W/m2
C      DD      vapor pressure deficit, kPa
C      RC      canopy or surface resistance, s/m

```



```

ELSE
  SAI = (LPMAX / LPC) * CS * HEIGHT
END IF

c    LAI = FL * LPMAX
c    LAI = MAX(0.001, LAI)

c    LAI is read in input from calling program, instead of calculating it
c    from LPMAX.

    CALL ROUGHF(CZS, CZR, HS, HR, LPC, CS, LAI, SAI, HEIGHT, ZOG,
*             ZO, DISP, ZOC, DISPC)
c    print*, CZS, CZR, HS, HR, LPC, CS, LAI, SAI, HEIGHT, ZOG
c    print*, ZO, DISP, ZOC, DISPC
    ZA = HEIGHT + ZMINH
    IF (UW .LT. 0.2) UW = 0.2
    UA = UW * WNDADJF(ZA, DISP, ZO, FETCH, ZW, ZOW)

c    Call subroutine to get solrad from netrad
    call net2solrad(RADNET,TA,EA,ALBEDO,C1,C2,C3,IOHDAY,SOLRAD,iflag)
c    SOLNET = (1 - ALBEDO) * SOLRAD / IGRATE
c    LNGNET = NETLONGF(TA, EA, SOLRAD / IOHDAY, C1, C2, C3)
c    AA = SOLNET + LNGNET - SHEAT
c    write(96,*) TA, EA, SOLRAD / IOHDAY, C1, C2, C3, LNGNET

c    Using input net radiation.
    AA = RADNET

    CALL ESATF(TA, ES, DELTA)
    DD = ES - EA

c    if (iflag .eq. 1) SOLRAD = 177.23
    RC = SRSCF(SOLRAD, TMIN, DD, LAI, SAI, R5, CVPD, RM,
*           CR, GLMAX, GLMIN)
    RA = (LOG ((ZA - DISP) / ZO)) ** 2 / (0.16 * UA)

    LE = PMF(AA, DD, DELTA, RA, RC)
    PMDAYF = ETOM * IGRATE * LE

END

```